Investigating the Distribution and Source(s) of Lunar Volatiles

Thesis

Investigating the Distribution and Source(s) of Lunar Volatiles

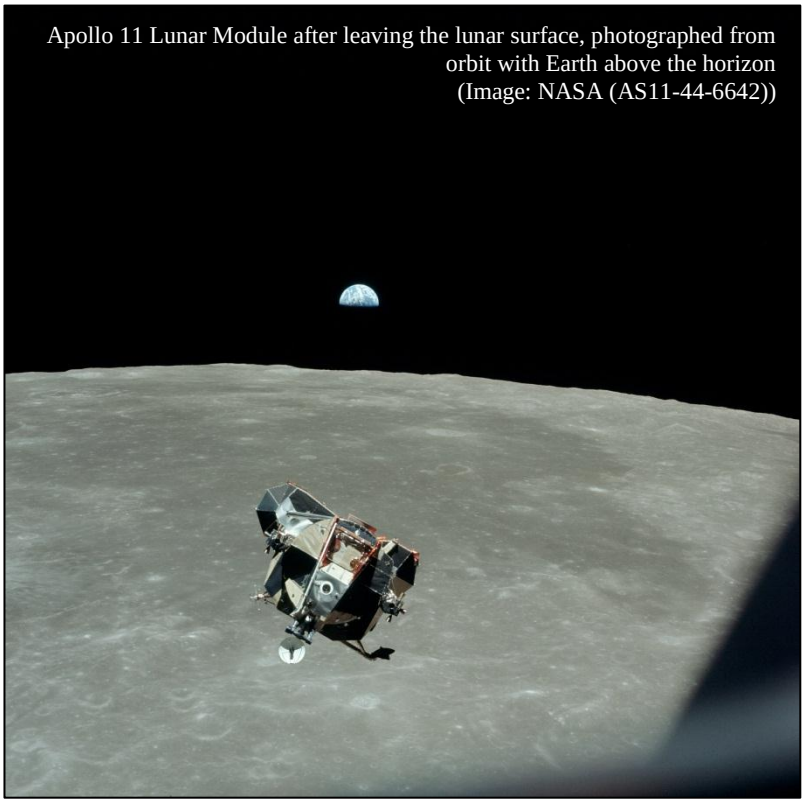

Apollo 11 Lunar Module after leaving the lunar surface, photographed from orbit with Earth above the horizon (Image: NASA (AS11-44-6642))

James Ian Mortimer

(B.Sc. (Hons.) Geoscience, The University of St Andrews)

Department of Physical Sciences, The Open University

Supervisors: Mahesh Anand, Iain Gilmour, Colin Pillinger

This thesis was submitted to The Open University for the degree of Doctor of Philosophy

June 2015

Abstract

Following the renewed interest in the volatile inventory of the Moon witnessed in the last decade, from both sample studies and data from orbital missions, it is timely to reassess the distribution and likely source(s) of light element volatiles (C, N, He, Ne, and Ar) in a diverse suite of lunar mare basalts and soils, providing new insights about volatiles indigenous to the lunar interior, volatiles produced *in situ* at the lunar surface, and volatiles delivered to and implanted into the lunar surface. Simultaneous static-mode mass spectrometric measurements of these key volatiles, extracted from the same aliquot of sample by high-resolution stepped combustion, enable a more detailed identification of the different volatile components present by comparing their varying release patterns across a range of temperature steps. Taken in context with other studies of different volatile elements, this new data contributes towards a greater understanding of the Earth-Moon system, with additional implications for future *in situ* resource utilisation at the lunar surface.

With an average $\delta^{15}N$ value of +0.93 ± 9.39 ‰, the indigenous N component measured in mare basalts is most compatible with a CO carbonaceous chondrite source for nitrogen in the lunar interior, although some caveats exist. Variations in abundance and isotopic composition of indigenous nitrogen imply a heterogeneous lunar mantle. Assuming up to ~50 % loss of solar wind ^{36}Ar from lunar soils, nitrogen trapped in soils can be reconciled with up to 87 % being contributed from a non-solar source with an isotopic composition of between +87 ‰ and +160 ‰.

Noble gases in soils are dominated by solar wind components, with only minor amounts of cosmogenic neon being released at the highest temperature steps. In mare basalts, noble gases are a mixture of trapped, radiogenic, and cosmogenic components (from which cosmogenic production rates can be calculated and exposure ages for previously undated samples suggested.

Acknowledgements

I owe a debt of gratitude to so many people, without whom the completion of this thesis would have been both far more difficult, and much less enjoyable. The following acknowledgements are not exhaustive; if I have missed any names off the list, I apologise unreservedly and I trust that the individuals involved know how grateful I am. *Mea maxima culpa!*

Firstly, I would like to thank my family, who have always supported my education and career choices; I would not have been able to reach this stage without their love and support. In particular, I thank my parents (Pauline and Andrew) and grandparents (Mary, Kathleen, and Alan) for their unwavering moral and financial support, and for providing me with so many invaluable experiences and opportunities.

I also thank my friends and colleagues, old and new, for their companionship and encouragement over the years, including, but not limited to, my fellow St Andrews Geoscience graduates; the Chosen Men, and the many others with whom I shared my time at University Hall; past lecturers (Tony, Stuart, Ruth, Peter, Colin, Ed, Adrian, Jen, and Donald); and especially Tom and Alice.

Most recently, I thank my colleagues in the Department of Physical Sciences at the Open University, in particular Beth, Mohit, Dan D, Adam, Feargus, Jean-David, Kathryn, Pete, Tom, Elliot, Roy, Josh, Axel, Erika, Dan W, Joe, Mike, Jimmy, Calum, Martine, Neil, Ben D, Matt, Phillipa, Natalie, Simon, Andy, Monica, and of course, Ed. To all who have been involved with the DPS House Band, either as performers or audience members- it's been a blast! Thanks are also due to my fellow Cellar and Pavilion regulars, including Karina, Jason, Mariano, Encarni, and Marie-Laure. I thank my fellow UK lunatics for all the fun times shared, including the International Gabling Committee (Katie, Nat, Fran, and Louise), and most of all, Romain and Jess (who has had to endure working alongside me for the past 8 years and deserves a medal for it!).

Finally, words cannot express my gratitude to my supervisors (Mahesh, Colin, and Iain), and to Sasha, for their efforts over the last 3 years, often going above and beyond the call of duty to work through evenings, weekends, and holidays to support this work.

Statement of Original Authorship

The data contained within this thesis are all derived from original research conducted as part of this PhD project; none of this research has been submitted for previous degree courses. Certain data resulting from analyses of some mare basalts have been subject to peer review and subsequently published in a scientific journal; where this is the case, the thesis references the published paper (e.g. Mortimer et al., 2015). Lunar soil data are herein presented in the form of a manuscript which is being submitted for peer review to a scientific journal concurrently with the submission of this thesis; where lunar soil crushing data were obtained by co-authors, this has been acknowledged at the start of the relevant chapter of this thesis.

Table of Contents

Abstract II

Acknowledgements III

Statement of Original Authorship IV

Table of Contents V

List of Figures VIII

List of Tables IX

Chapter One: Introduction 1

1.1: Theories of Lunar Formation 2

1.2: A Brief Overview of Lunar Geological History 5

1.3: The Lunar Surface 7

1.4: Lunar Soil 9

1.5: Apollo Lunar Samples 12

1.6: Previous Laboratory Analyses of Volatiles in Lunar Samples 12

1.7: Research Aims and Objectives 16

Chapter Two: Samples and Methods 18

2.1: Samples 19

2.1.1: Mare Basalts 19

2.1.1.1: Powdered Samples 20

2.1.1.2: Uncrushed Samples (Chips) 21

2.1.2: Soils 21

2.2: Methods 22

2.2.1: Introduction to Stepped Heating Techniques 22

2.2.2: Sample Preparation 24

2.2.2.1: Sample Powdering Protocols 24

2.2.2.2: Sample Preparation for Finesse Analyses 27

2.2.3: 'Finesse' 30

2.2.3.1: Overview of the Finesse Instrument 30

2.2.3.2: Sample Inlet System 31

2.2.3.3: Combustion and Volatile Separation Procedure 33

2.2.3.4: He and Ne analysis 35

2.2.3.5: Carbon analysis 36

2.2.3.6: Nitrogen clean-up and analysis 37

2.2.3.7: Argon analysis 39

Chapter Three: Mare Basalt Analysis Results 40

3.1: Nitrogen 41

3.2: Carbon 51

3.3: Noble Gases 62

3.4: Results (Unpowdered Mare Basalt Chip) 73

Chapter Four: Mare Basalt Analysis Discussion 75

4.1: Indigenous Lunar Nitrogen 76

4.1.1: Indigenous Lunar Nitrogen Isotopic Heterogeneity 79

4.1.1.1: Mineralogy and Lithology 80

4.1.1.2: Crystallisation Age 81

4.1.1.3: CRE Age 83

4.1.1.4: Basaltic Melt Source Regions 85

4.1.1.5: Degassing 87

4.1.1.6: Contamination from Extra-Lunar Sources 92

4.1.1.7: Analytical Factors (date of runs) 94

4.2: C/N Elemental Ratios 96

4.3: Noble Gases 99

4.3.1: Trapped Noble Gases 99

4.3.2: Radiogenic Noble Gases 106

4.3.3: Cosmogenic Volatiles 110

4.3.3.1: Cosmogenic Neon 110

4.3.3.2: Cosmogenic Argon 113

4.3.3.3: Cosmogenic Nitrogen 116

Chapter Five: Lunar Soil Analysis 119

Introduction 120

Samples 122

Methods 123

Stepped Combustion Procedure 125

Crushing Procedure 125

Stepped Combustion Results 127

Crushing Results 137

Discussion 144

Solar vs. non-solar nitrogen 144

Conclusions 152

Chapter Six: Conclusions and Future Considerations 164

6.1: Volatiles in the Moon 165

6.2: Volatiles formed on the Moon 168

6.3: Volatiles delivered to the Moon 171

6.4: Future Considerations 172

References 175

Appendix: Blank Correction and Error Propagation Calculations 191

List of Figures

Figure 2.1: Schematic diagram of 'Finesse' 30
Figure 2.2: Schematic diagram of sample inlet and furnace 32
Figure 2.3: Schematic diagram of gas separation and clean-up section 34
Figure 3.1.1:Step plots of nitrogen in Apollo 11 basalts 42
Figure 3.1.2:Step plots of nitrogen in Apollo 12 basalts 43
Figure 3.1.3:Step plots of nitrogen in Apollo 14 and Apollo 15 basalts 44
Figure 3.1.4:Step plots of nitrogen in Apollo 17 basalts 45
Figure 3.2.1:Step plots of carbon in Apollo 11 basalts 53
Figure 3.2.2:Step plots of carbon in Apollo 12 basalts 54
Figure 3.2.3:Step plots of carbon in Apollo 14 and Apollo 15 basalts 55
Figure 3.2.4:Step plots of carbon in Apollo 17 basalts 56
Figure 3.4.1: Neon isotopic ratios in an unpowdered chip of 12064 73
Figure 4.1.1: Indigenous lunar nitrogen (this study) 78
Figure 4.1.2: Indigenous lunar nitrogen (all studies) 78
Figure 4.1.3: Relationship between crystallisation age and indigenous lunar nitrogen isotopic composition 82
Figure 4.1.4: Relationship between CRE age and indigenous lunar nitrogen isotopic composition 84
Figure 4.1.5: Relationship between TiO_2 content and indigenous lunar nitrogen isotopic composition 87
Figure 4.1.6: Relationship between degassing of hydrogen and indigenous lunar nitrogen isotopic composition 90
Figure 4.1.7: H_2O abundance in the melt at various stages of degassing and fractional crystallisation, vs. hydrogen isotopic composition of the melt 91
Figure 4.1.8: Relationship between distance from the Lunar Module and indigenous lunar nitrogen isotopic composition 94
Figure 4.1.9: Relationship between dates of sample analyses and indigenous lunar nitrogen isotopic composition 95
Figure 4.3.1.1: Correlation between ^{20}Ne and ^{4}He 100
Figure 4.3.1.2: Correlation between ^{20}Ne and ^{21}Ne 101
Figure 4.3.1.3: Neon isotope ratios in powdered sample of 12064 104
Figure 4.3.2.1: Release profiles for radiogenic ^{4}He and ^{40}Ar 107
Figure 4.3.2.2: Correlation between potassium content and ^{40}Ar abundance 109
Figure 4.3.3.1.1: Correlation between CRE ages and $^{21}Ne_{cosm}$ abundances 112
Figure 4.3.3.2.1: Correlation between CRE ages and $^{38}Ar_{cosm}$ abundances 115
Figure 4.3.3.3.1: Correlation between CRE ages and $^{15}N_{cosm}$ abundances 116
Figure 5.1: Diagram of mechanical crusher 124
Figure 5.2: Step plots of nitrogen in lunar soils released by stepped combustion 128
Figure 5.3: Step plots of carbon in lunar soils released by stepped combustion 131
Figure 5.4: Release patterns of nitrogen and ^{40}Ar in lunar soils by stepped combustion 132
Figure 5.5: Release patterns of ^{40}Ar and ^{36}Ar in lunar soils by stepped combustion 133
Figure 5.6: Release profiles of ^{4}He from lunar soils by stepped combustion 134
Figure 5.7: Neon isotope ratios for stepped combustion analyses of lunar soils 136
Figure 5.8: Cumulative release curves for nitrogen released by crushing 138
Figure 5.9: Cumulative release curves for ^{4}He, ^{20}Ne, and ^{36}Ar released by crushing as percentages of the total abundances released by stepped combustion 140
Figure 5.10: Neon isotope ratios for crushing analyses of lunar soils 143
Figure 5.11: Nitrogen isotopic composition of lunar soils vs. $^{36}Ar/N$ ratios normalised to solar ratios (+140 ‰ case) 148
Figure 5.12: Nitrogen isotopic composition of lunar soils vs. $^{36}Ar/N$ ratios normalised to solar ratios (+160 ‰ case) 150

List of Tables

Table 2.1: Summary of powdered basalt samples analysed in this study 20
Table 2.2: Summary of unpowdered basalt samples analysed in this study 21
Table 2.3: Summary of lunar soil samples analysed in this study 21
Table 3.1.1: Percentages of the total nitrogen released in different temperature ranges 41
Table 3.1.2: Nitrogen results for Apollo 11 basalts (Stepped combustion) 47
Table 3.1.3: Nitrogen results for Apollo 12 basalts (Stepped combustion) 48
Table 3.1.4: Nitrogen results for Apollo 14 and Apollo 15 basalts (Stepped combustion) 49
Table 3.1.5: Nitrogen results for Apollo 17 basalts (Stepped combustion) 50
Table 3.2.1: Percentages of the total carbon released in different temperature ranges 52
Table 3.2.2: Carbon results for Apollo 11 basalts (Stepped combustion) 58
Table 3.2.3: Carbon results for Apollo 12 basalts (Stepped combustion) 59
Table 3.2.4: Carbon results for Apollo 14 and Apollo 15 basalts (Stepped combustion) 60
Table 3.2.5: Carbon results for Apollo 17 basalts (Stepped combustion) 61
Table 3.3.1: Helium results for all powdered basalts 64
Table 3.3.2: Neon results for Apollo 11 basalts 65
Table 3.3.3: Neon results for Apollo 12 basalts 66
Table 3.3.4: Neon results for Apollo 14 and Apollo 15 basalts 67
Table 3.3.5: Neon results for Apollo 17 basalts 68
Table 3.3.6: Argon results for Apollo 11 basalts 69
Table 3.3.7: Argon results for Apollo 12 basalts 70
Table 3.3.8: Argon results for Apollo 14 and Apollo 15 basalts 71
Table 3.3.9: Argon results for Apollo 17 basalts 72
Table 3.4.1: All noble gas results for unpowdered chip of 12064 74
Table 4.1.1: Indigenous lunar nitrogen abundances and isotopic compositions 77
Table 4.2.1: C/N ratios of indigenous lunar carbon and nitrogen 97
Table 4.3.3.1: Calculated cosmogenic isotope abundances in basalts 110
Table 5.1: Lunar soil samples chosen for stepped combustion analysis 122
Table 5.2: Total nitrogen abundances released by crushing vs. total nitrogen abundances released by stepped combustion 138
Table 5.3: $^{4}He/^{20}Ne$ and $^{20}Ne/^{36}Ar$ ratios from crushing and stepped combustion analyses 142
Table 5.4: Comparing mixing proportions of solar and non-solar nitrogen in lunar soils in three different scenarios 151
Table 5A: ^{4}He results from stepped combustion analyses of soils 153
Table 5B: ^{40}Ar and ^{36}Ar results from stepped combustion analyses of soils 154
Table 5C: ^{20}Ne and ^{21}Ne results from stepped combustion analyses of soils 155
Table 5D: Carbon in lunar soils released by stepped combustion 156
Table 5E: Nitrogen in lunar soils released by stepped combustion 157
Table 5F: Nitrogen in lunar soils released by crushing 158
Table 5G: 4He, 20Ne, and 36Ar in lunar soils released by crushing 159
Table 5H: Neon isotope ratios in lunar soils analysed by stepped combustion 161
Table 5I: Neon isotope ratios in lunar soils analysed by crushing 163

Chapter One:
Introduction

Earth's only natural satellite has fascinated and inspired countless generations of people through the ages, including authors, poets, artists, philosophers, and even scientists (starting with the first telescopic observations of the cratered lunar surface made by the Italian astronomer, physicist, and mathematician Galileo Galilei, published in his 1610 book 'Sidereus Nuncius'). Interest in the Moon reached a thrilling peak in 1969, when NASA's 'Apollo' programme brought about the first successful manned lunar landing, with the lunar module of Apollo 11 touching down in Mare Tranquillitatis on July 20th. To humanity as a whole, this remarkable feat stood as testimony to mankind's technological achievements, reaching out to a celestial body from our own home planet for the first time. However, to the scientific community, these manned 'Apollo' and unmanned Soviet 'Luna' missions offered a unique opportunity to study the origins of our Earth-Moon system through the analysis of returned samples of lunar rocks and soils. This treasure trove of precious samples is still able to yield ground-breaking results today, after more than four decades of dedicated research by groups all over the world.

One aspect of lunar science that has experienced a true renaissance in recent years has been the field of lunar volatile research, with major implications for how we view not only the Moon's origin, but also that of the Earth (and other terrestrial planets in our Solar System).

1.1: Theories of Lunar Formation

Before samples of the Moon were returned to Earth for analysis, several theories for lunar formation were postulated. The oldest, published by Darwin in 1879, and modified over the years, suggested that the Moon formed from a molten, fast-spinning Earth, with the material that formed the Moon being ejected into space by the speed of Earth's rotation (Darwin, 1879; Ringwood, 1960; Wise, 1969). However, such a rotational fission formation mechanism would have required the angular momentum of the Earth to be

around 73 % greater than it is today (de Meijer et al., 2013), leading some to hypothesise that, assuming a similar angular momentum for the early Earth to that of the present-day Earth-Moon system, the only way to provide the extra energy needed to eject enough silicate material from the Earth to form the Moon is *via* a natural nuclear fission reaction at the terrestrial core-mantle boundary (de Meijer et al., 2013). Although this concept explains the observed compositional similarities between the Earth and Moon, and also removes the need for a major loss of angular momentum in the Earth-Moon system, it requires a very specific set of circumstances and thus is not currently seen as the most likely scenario.

Other early ideas about lunar formation include the suggestion that the gravitational field of the early Earth was strong enough to capture a small planetesimal (which had formed elsewhere in the Solar System and migrated into Earth's orbit) (e.g. Gerstenkorn, 1955; Wood, 1986). However, the compositional similarity of the Earth and Moon is difficult to reconcile with a model which requires the two bodies to be formed in different regions of the Solar System.

Alternatively, it was proposed that the Earth and Moon formed together, at the same time, as a binary planetary system (e.g. Schmidt, 1959), although this idea also fails to account for the current angular momentum of the Earth-Moon system.

The most widely-accepted theory of lunar formation involves the early Earth being hit by a glancing blow from a slow-moving Mars-sized body, at some point around 40 to 62 Ma after the formation of the Solar System (Cameron and Ward, 1976; Canup and Asphaug, 2001; Halliday, 2003, 2004; Hartmann and Davis, 1975; Touboul et al., 2007). Whilst this theory satisfies constraints such as the present angular momentum of the Earth-Moon system and the mass of material required to form the Moon, the resultant Moon in this case

predominantly forms from impactor material (Shearer et al., 2006), and not from material derived from the early Earth, contradicting evidence from a growing number of isotope systems (e.g. tungsten (Touboul et al., 2007), titanium (Zhang et al., 2012), silicon (Armytage et al., 2012), oxygen (Hallis et al., 2010; Wiechert et al., 2001), and chromium (Trinquier et al., 2008)) which all point towards the Earth and Moon forming from a common starting material. The chemical and isotopic similarities between the two bodies can be reconciled with this 'Giant Impact' model if it assumed that such an impact created a proto-lunar disc of vaporised material which underwent equilibration with the outer part of the terrestrial silicate mantle, resulting in homogeneity between the Earth and Moon prior to lunar accretion (Pahlevan and Stevenson, 2007). However, by the time such homogenisation occurred throughout the entire thickness of the vapour disc (~ 100 Ma), the parts of the disc furthest away from the Earth would have begun to accrete (Salmon and Canup, 2012), making an entirely homogenous Earth-Moon system difficult to achieve.

Ultimately, although variations of the canonical Giant Impact model of lunar formation are favoured by a majority of current researchers, no one theory of lunar formation to date completely satisfies all of the various conditions required to produce an Earth-Moon system as observed today.

Whichever theory of lunar formation is adopted, questions still remain about the timing of volatile delivery to the two bodies; the process of planetary accretion is thought to have removed most of the volatile elements from the Earth-Moon system (Albarède, 2009), requiring a so-called 'Late Veneer' of material to be added to both bodies from a chondritic source (with suggestions ranging from an ordinary chondrite (e.g. O'Neill, 1991), a primitive chondrite (e.g. Dale et al., 2012), an H chondrite (e.g. Wood et al., 2010), or a carbonaceous chondrite (e.g. Javoy, 1997) source). A 'Late Veneer' is also

employed to explain the over-abundance of siderophile elements in the terrestrial mantle (Willbold et al., 2011). However, identical tungsten isotopic compositions between the Earth and Moon, for example, place a limit on the amount of material added to the Earth (and, accepting any late accretion occurred in a stochastic manner, place an even lower limit on the amount of material added to the Moon) during a 'Late Veneer' event, with 0.3 ± 0.3 % of Earth's tungsten added from an ordinary chondrite source, or a maximum of 0.5 ± 0.6 % added from a CI carbonaceous chondrite source; such low percentages of material added during a late veneer cannot account for the present abundances of volatiles (such as carbon, sulphur, and water) in the Earth (Halliday, 2008). This implies that, if indeed volatiles were delivered to the Earth-Moon system during a Late Veneer event alongside siderophile elements, such a late accretion did not contribute the entire volatile budget of the two bodies.

Therefore, not only is the formation of the Moon itself still a topic for debate, but so too is the timing of volatile delivery to the Earth-Moon system, whether this was prior to lunar formation, during the lunar forming impact, or delivery after formation as part of a 'Late Veneer' of material to the terrestrial planets.

1.2: A Brief Overview of Lunar Geological History

Following lunar formation, it is thought that the accretionary processes involved resulted in planetary-scale melting, thereby forming a Lunar Magma Ocean (LMO) (Wieczorek et al., 2006), which underwent crystallisation to produce a suite of rocks as differentiation occurred. These products of the LMO include ferroan anorthosites (representing the primary products of crystallisation, forming between 4.29 Ga and 4.56 Ga (Shearer et al., 2006)), Mg- and Fe-rich cumulates (e.g. dunites, nortites, and troctolites, which sank down through the LMO to form cumulate piles (Dymek et al., 1975a; Shearer and Papike, 1999;

Shearer and Papike, 2005)), a plagioclase primary lunar crust (crystallising at around 60 % to 80 % crystallisation, and floating up through the LMO to form the crust (Phinney, 1991)), and the final products of LMO crystallisation, urKREEP (enriched in the incompatible elements potassium (K), phosphorous (P), and Rare Earth Elements (REE)) and ilmenite (crystallised from Fe- and Ti-enriched melts; this dense ilmenite-rich layer is gravitationally unstable, and sinks down through the cumulate pile at the base of the LMO) (Elardo et al., 2011; Hess and Parmentier, 1995; Shearer and Papike, 2005)).

Towards the end of this earliest period of lunar history, at around 3.9 Ga (e.g. Morbidelli et al., 2012), the Earth-Moon system is thought to have experienced a 'late heavy bombardment' from~ 90 % asteroidal and 10 % cometary sources (Bottke et al., 2010; Joy et al., 2012), which formed most of the large basins in the lunar crust (Kring and Cohen, 2002).

Following the supposed 'late heavy bombardment', between ~ 3.95 and 3.1 Ga, basaltic melts were erupted onto the lunar surface, spreading out to fill in basins and form the lunar maria (e.g. Nyquist and Shih, 1992). Displaying wide heterogeneities in terms of their major oxide contents, these mare basalts are thought to be derived from a heterogeneous lunar mantle (Hallis et al., 2014; Ray and Misra, 2014), with source regions varying in estimated depth from 150 km below the lunar surface (Papike et al., 1976), down to 700 km (Hess, 1991). Some mare basalt samples, particularly those collected during the Apollo 15 mission, are enriched in KREEP, suggesting they interacted with urKREEP material at depth to form these KREEP basalts (Lucey et al., 2006).

Mare volcanism also produced fire fountaining, fuelled by the rapid degasing of volatiles as melts rose to the lunar surface (McCubbin et al., *In Press* ; Wilson and Head, 1981). Erupted into the cold vacuum conditions at the lunar surface, these rising magmas rapidly

quenched from temperatures in excess of 1450 ºC (Grove and Krawczynski, 2009) to form glass beads of variable chemical composition (Delano, 1986; Elkins-Tanton et al., 2003); like mare basalts, these volcanic glasses are thought to have formed from melts originating in the lunar upper mantle (Grove and Krawczynski, 2009; Longhi, 1992).

The lunar basaltic meteorite 'Kalahari 009' has been dated to 4.35 Ga (Terada et al., 2007), and is thus thought to represent an earlier phase of basaltic volcanism (forming 'cryptomare' deposits), although such cryptomare basalts have since been blanketed and hidden by subsequent impact ejecta (Antonenko et al., 1995).

1.3: The Lunar Surface

The lunar surface is comprised of layers of debris and brecciated material which vary in thickness laterally, from a few metres thick to several tens of metres thick, dependent upon location. This jumbled coating is known as the 'lunar regolith', and contains rock fragments of varying sizes, from large boulders to extremely fine (μm-sized) grains ('lunar soil') (McKay et al., 1993).

The principal method of formation for the lunar regolith is *via* extra-lunar material impacting the solid lunar anorthositic crustal and mare basaltic bedrock (Langevin and Arnold, 1977). This can take the form of cometary/meteoroid impacts (on the largest scale), which physically fracture and break apart competent bedrock; this is the first stage of regolith formation. Whilst the regolith is still relatively shallow (several cm in depth), fresh impacts can excavate deep enough to regularly break apart new pieces of bedrock. However, once the regolith layer reaches roughly 1 m in depth, only the largest, infrequent impacts can penetrate down to bedrock level (McKay et al., 1993).

Thus begins the secondary phase of regolith evolution, where smaller and more regular impacts mix and 'garden' the existing coarser fraction; at this point, regolith formation rates slow down markedly (McKay et al., 1993), and instead existing fragments are broken down further to form finer particles (comminution) (Langevin and Arnold, 1977).

While exposed at the lunar surface, the grains in the regolith experience bombardment by more than just meteoritic and cometary impacts. Cosmic dust particles can cause pitting (microcraters) on exposed grain surfaces, and solar wind charged atoms interact with grain surfaces in a range of chemical and physical processes. Galactic cosmic rays can penetrate materials to depths of around 1 m, interacting with material at the lunar surface to produce cosmogenic isotopes from target atoms *via* a process known as spallation. These all contribute to the phenomenon of space weathering, and the effects of such space weathering increase with the increase in exposure ages of the lunar regolith (McKay et al., 1993).

Impacts on the lunar regolith have several effects; minerals can undergo shock metamorphism, grains may be fused together (impact breccias), the finest fraction of the lunar soil particles may be melted upon impact and so form either fused 'agglutinates' or agglutinitic glasses (Papike et al., 1982), and some material may be vaporised and either lost to space or recondensed elsewhere on the lunar surface (Langevin and Arnold, 1977; McKay et al., 1993).

Space weathering by ionised radiation can also alter the regolith, in particular when protons and other atoms from the solar wind interact with the finer lunar soil grains. Solar wind protons penetrate the uppermost layers of the soil grains and can either be lost back to space *via* diffusion through the soil (Crider and Vondrak (2002) suggest that 1 % of incident solar wind protons may be backscattered immediately), or trapped chemically by

reactive broken surfaces on soil grains or within the crystal lattice structures of soil grains themselves; this can happen wherever there exist weakened bonds as a result of previous bombardment breaking apart chemical bonds to leave 'dangling' negatively-charged O atoms within mineral structures that readily accumulate incident ions from the solar wind (Crider and Vondrak, 2002; McCord et al., 2011; McKay et al., 1993). This process can form hydrogen, carbon, and nitrogen-bearing volatile species, bonded to the lunar soil particles, which may then be removed by further sputtering by fresh incident solar wind protons at a later date (Crider and Vondrak, 2002).

Also, subsequent impacts which heat the soil and thus release these protons enable them to react with O in FeO in lunar soil impact melts; this reduction produces nanophase Fe particles (np-Fe^0). The abundance of such non-charged Fe microparticles increases with soil maturity and so forms a useful measurement of soil surface exposure age (maturity), when expressed as the ratio of observed ferromagnetic intensity of a soil divided by its total Fe content (Is/FeO) (McCord et al., 2011; McKay et al., 1993). By contrast, Pillinger et al. (1976) suggest that this finely-divided metallic iron (Fe^0) in lunar soils can be formed instead by preferential sputtering of oxygen in lunar soils, reducing ferrous iron to non-charged metallic iron. However, these alternative mechanisms for nanophase iron production in lunar soils still need to be resolved.

1.4: Lunar Soil

Lunar soils can be described as poorly-sorted (well-graded) sandy silts to silty sand, with an average particle size of 70 μm (median lies between 40-130 μm), with between 10-20% of particles being <20 μm (Carrier et al., 1993).

Soil particles display a wide range of shapes, from spherical to extremely angular, although the majority are elongate and subangular/angular (Carrier et al., 1993).

Bulk densities for lunar soils vary slightly; Carrier et al. (1993) state that the 'best estimate' for bulk density of the top 15 cm of soil is 1.50 ± 0.05 g/cm^3, which rises to 1.66 ± 0.05 g/cm^3 when considering the top 60 cm of the lunar soil. However, Vinogradov (1972) states that the bulk density of Luna 20 soil is 1.1 to 1.2 g/cm^3, which reaches 1.7 to 1.8 g/cm^3 upon compaction, which it undergoes readily.

Due to the highly irregular surfaces of lunar soil grains, soil particles undergo mechanical interlocking, making soils highly cohesive (with a high frictional shear strength). Combined with the low gravity conditions present on the Moon, this enabled Apollo astronauts to excavate sample trenches down to around 40 cm depth with near-vertical sides, without the sides collapsing (Carrier, 2005). However, Lindsay (1976) states that the lunar soil at the surface is only weakly cohesive.

Since the optical properties of lunar soils are dominated by the finer fractions (< 45 μm) (Taylor et al., 2010), many mineralogical studies focus on these smaller grain sizes. However, modal mineralogy varies between different size fractions of the same soil sample, with lithic fragments and fused soil particles being more dominant in larger grain size fractions, and the proportion of monomineralic grains and glasses increasing with decreasing grain size (McKay et al., 1993; Papike et al., 1982).

Furthermore, although soil samples typically contain a small amount of exotic material, laterally transported from elsewhere on the lunar surface, soil mineralogy is linked to the bedrock in the immediate vicinity (Lindsay, 1976; McKay et al., 1993); indeed, Shoemaker et al. (1970) estimated that around 95 % of a lunar soil sample at any given location may be derived from bedrock within a 100 km radius. Thus, highland soils have a higher proportion of highland anorthositic lithics and feldspars compared to mare soils, which instead display higher proportions of mare basaltic lithics and mafic minerals (Papike et

al., 1982). In addition, minerals such as plagioclase, which have good cleavage, are readily broken and, alongside any fine-grained crystals in the original bedrock, are preferentially concentrated in the finest grain size fractions of the lunar soil (McKay et al., 1993).

Alongside monomineralic grains, the lunar soil also contains lithic fragments ('mini-rocks', typically in the larger grain size fractions, and including brecciated crystalline rock fragments and soil breccias), agglutinates and glasses (Lindsay, 1976).

Agglutinates are described by Lindsay (1976) as 'intimate mixtures of inhomogeneous dark-brown to black glass and mineral grains, many of which are partially vitrified', being irregular in shape and containing microscopic iron (as Fe^0) droplets and FeS (troilite), most probably formed by micrometeorite bombardments which mix the lunar soil and fuse it together with associated impact melts. Vesicles in agglutinates are thought to form by solar-wind implanted elements and compounds (e.g. H_2, N_2, noble gases, CH_4, and H_2O, which might be produced by H reacting with OH species) being degassed (McKay et al., 1993).

Glasses may be either derived from ejected impact melts, which cool before landing on the lunar surface again (giving rise to spheroidal/rounded rotational shapes, unless subsequently broken up by further comminution); such glasses are largely homogeneous and restricted to smaller grain sizes (larger glass beads do not cool quickly enough and so are broken apart into smaller beads when they land on the lunar surface) (Lindsay, 1976).

Alternatively, glasses in the lunar soil may be derived from volcanic fire-fountaining, as outlined in Section 1.2. Such glasses may be covered by a thin coat of condensates of volatile elements, and can form layers of localised pyroclastic debris, quite unlike the wide distribution across the lunar surface of impact-derived glasses (McKay et al., 1993).

1.5: Apollo Lunar Samples

As part of the six successful NASA Apollo missions that landed on the Moon, a total of around 382 kg of rock and soil samples were returned to Earth, with samples collected from each landing site on the lunar near-side. The Apollo 11 and 12 collections represent lunar mare regions, the Apollo 16 mission collected anorthositic highlands samples, and samples returned by Apollo 14, 15, and 17 come from both mare and highlands areas. The main masses of Apollo samples are identified using five digit numbers, assigned by the Lunar Samples Preliminary Examination Team (LSPET) thus: for Apollo 11 samples, the first two digits are '10___', with Apollo 12, 14, and 15 samples named '12___', '14___', and '15___' respectively. For samples collected by Apollo missions 11 to 14, the remaining three digits assigned to the sample names were generic numbers with no relation to sample location or type. For Apollo 15, 16, and 17, the last digit ('____0' to '____9') refers to sample size, grading upwards from fines to rock samples > 10 mm. For Apollo 16 and 17, the naming scheme was changed slightly, so that the first digit represented the mission number ('6____' and '7____' respectively), and the second digit referenced the sample collection location. Generally, in this present work, samples are referred to using this five digit generic number, although specific subsample numbers of between one and four digits follow the generic five digit name to identify individual allocated subsamples.

1.6: Previous Laboratory Analyses of Volatiles in Lunar Samples

Studies conducted to date of volatiles in both lunar rocks and soil samples have recently been reviewed in detail by McCubbin et al. (*In Press*); whilst a similarly exhaustive overview of previous research is beyond the scope of this introduction, and largely superfluous to the original research discussed in later chapters, it seems necessary at this

point to give a brief outline of prior efforts to characterise some of the volatiles also analysed in this present work.

Carbon abundances and isotopic compositions (expressed as $\delta^{13}C$, or the parts-per-thousand deviation from the terrestrial Vienna Pee Dee Belemnite (vPDB) standard) have long been measured for both lunar rock and soil samples, starting with the return of the first samples by Apollo 11 (e.g. Epstein and Taylor, 1970; Kaplan and Smith, 1970; Moore et al., 1970), and continuing for many decades thereafter (e.g. Becker, 1980; Cadogan et al., 1971; Chang et al., 1974; Des Marais, 1978, 1983; Friedman et al., 1974; Gardiner et al., 1978; Grady and Pillinger, 1990, Kerridge et al., 1978; Norris et al., 1983, Pillinger, 1979). Using a variety of different techniques, it was demonstrated that carbon abundances are typically below 260 ppm (less than 70 ppm in mare basalts (McCubbin et al., *In Press*)), with isotopic compositions ranging from $\delta^{13}C$ values of -40 ‰ to +24 ‰ (McCubbin et al., *In Press*). Lunar soils contain much more carbon than lunar rocks, with carbon in soils dominated by surface-correlated components (Des Marais et al., 1975; Kerridge et al., 1974; Moore et al., 1970). It was also noted that carbon isotopic compositions within a single sample are highly variable, which suggests the presence of several carbon components from different sources within lunar samples (Kaplan and Petrowski, 1971). Mare basalts display a ^{13}C-depleted isotopic composition (with average $\delta^{13}C$ values of around -25 ‰), compared to lunar soils, which have more ^{13}C-enriched signatures of around +10 ‰ (McCubbin et al., *In Press*). This may be explained by the much lower abundances of indigenous lunar carbon present in rock samples compared to soils, making them more susceptible to the effects of terrestrial contamination, thereby masking the true lunar carbon signature. Carbon measured in volcanic glass beads (e.g. Gibson, 1977; Gibson and Moore, 1973; Kaplan and Petrowski, 1971), like carbon in lunar soils, is thought by some to be derived primarily from a solar wind source (e.g. Epstein and

Taylor, 1973). However, others have measured indigenous lunar carbon in melt inclusions inside lunar glasses (0.47 ppm to 5.65 ppm), and calculated lunar mantle carbon abundances up to 0.57 ppm (Wetzel et al., 2014).

Like carbon, nitrogen has been extensively studied in lunar samples, although the low abundances measured in lunar rocks (typically less than 1 ppm of indigenous nitrogen (Becker et al., 1976; Des Marais, 1978, 1983; Mathew and Marti, 2001; Müller, 1974)) have often been below the detection limits of the instruments used, making the measurement of isotopic composition impossible (e.g. Kaplan et al., 1976). Nevertheless, a small number of studies have succeeded in measuring nitrogen thought to be indigenous to the Moon (e.g. Becker et al., 1976; Kerridge et al., 1991; Mathew and Marti, 2001; Murty and Goswami, 1992), deriving $\delta^{15}N$ values (parts-per-thousand deviation from the terrestrial air (AIR) standard) of between +10 ‰ and +16.9 ± 3.4 ‰. A preliminary study involving the crushing of mare basalts obtained a wider range of $\delta^{15}N$ values, from -0.25 ‰ to +22.40 ‰ (Barry et al., 2013).

By contrast, nitrogen in lunar soils is much more abundant than in lunar rocks, and so has been well documented; all lunar soils analysed by stepped heating techniques display a characteristic 'V-shaped' pattern of varying isotopic composition with temperature (Assonov et al., 2002; Becker and Clayton, 1975; Becker et al., 1976; Brilliant et al., 1994; Kerridge, 1993; Thiemens and Clayton, 1980) that was thought to represent either a secular variation in the composition of the solar wind over time (Becker and Clayton, 1975; Clayton and Thiemens, 1980; Kerridge, 1975), or, more recently, a mixing of solar and non-solar nitrogen components delivered to the lunar surface (e.g. Assonov et al., 2002; Wieler et al., 1999). In light of firm measurements of the isotopic composition of the solar wind from the Genesis mission ($\delta^{15}N$ = -407 ± 7 ‰ (Marty et al., 2011)), it has most

recently been suggested that the majority of nitrogen in lunar soils is derived from a non-solar source, enriched in ^{15}N, and most likely contributed by interplanetary dust particles (IDPs) or by CR chondrites (Füri et al., 2012).

Studies of noble gases in lunar samples have been used to derive cosmic-ray exposure ages for samples (e.g. Signer et al., 1977), correlating abundances of cosmogenic isotopes such as $^{21}Ne_{cosm}$ with the amount of time a sample has spent at or close to the lunar surface, whilst measurements of crystallisation ages have relied on Ar-Ar dating techniques (e.g. Stettler et al., 1973). The isotopic composition of the solar wind has also been measured using lunar soil noble gases (e.g. Heber et al., 2003), and noble gas analyses, when conducted in conjunction with other volatile measurements in the same sample, have helped to constrain the origins and proportions of different sources of volatiles being delivered to the Moon (e.g. Füri et al., 2012; Hashizume et al., 2000, 2002; Murty and Goswami, 1992; Ozima et al., 2005; Wieler et al., 1999).

In addition to these sample studies which chart the long-term interest of the scientific community in the field of lunar volatiles, within the last decade/fifteen years, a renewed effort to characterise the volatile inventory of the Moon through sample analysis was spurred on by a number of ground-breaking measurements of water (as water ice, hydroxyl ions, or as molecular hydrogen) all over the lunar surface by orbiting spacecraft and fly-by missions such as Clementine, Lunar Prospector, Cassini, Deep Impact, Chandrayaan-1, LRO (Lunar Reconnaissance Orbiter), and LCROSS (Lunar Crater Observation and Sensing Satellite) (e.g. Clark, 2009; Colaprete et al., 2010; Feldman et al., 1998; Mitrofanov et al., 2010; Nozette et al., 1996; Pieters et al., 2009; Sunshine et al., 2009;). In addition, the LCROSS experiment, through its UV spectrometer, observed light hydrocarbons, carbon dioxide, and sulphur-bearing species within the ejecta plume created

by the impact of a spent rocket section with the regolith inside the south pole crater 'Cabeus'. The estimated water ice content of this crater was calculated to be 5.6 ± 2.9 % by mass (Colaprete et al., 2010). Since then, new analyses of returned samples (lunar glasses and apatite crystals in lunar rocks) have suggested initial magma volatile contents (mainly H, reported as either OH or H_2O) many times higher than previously reported (e.g., Anand et al., 2014; Füri et al., 2014; McCubbin et al., 2010; Saal et al., 2008; Tartèse et al., 2013), some with terrestrial-like volatile abundances (e.g., Barnes et al., 2014; Hauri et al., 2011).

In light of these new data for hydrogen, and given the advances in analytical techniques and understanding made in the decades since the first analyses of other light element volatiles (C, N) and noble gases (He, Ne, Ar) in returned lunar samples, it seems timely to reassess the volatile inventory of the Moon in respect to these particular volatiles, to better constrain their abundances, distribution, and source(s).

1.7: Research Aims and Objectives

This original research has several foci, falling into three main categories:

1. Volatiles in the lunar interior
2. Volatiles produced *in situ* at/on the Moon
3. Volatiles delivered to the lunar surface

For each of these three categories of lunar volatiles, this work aims to answer the following broad questions:

- In what abundance are volatiles (C, N, He, Ne, Ar) present?
- How are these volatiles distributed?
- From which source(s) are these volatiles derived?

and more specifically:

- Can indigenous nitrogen from the lunar interior be identified, and if so, what is its isotopic composition?
- Can cosmogenic isotope production rates be calculated from the results of this work, and if so, can exposure ages for as yet undated samples be suggested?
- Can measurements of trapped nitrogen and implanted solar wind noble gases in lunar soils be used to deconvolute the much-debated sources of nitrogen at the lunar surface?
- How chemically similar are the terrestrial and lunar mantles, and what does this reveal about the starting material from which the Earth-Moon system was formed?

To answer these fundamental research questions, the following objectives will be sought:

- Analyse a wide range of both mare basalt and lunar soil samples, including (where possible) several from each Apollo mission, to fully explore the distribution of volatiles across the different regions of the Moon represented by the Apollo sample collection
- Utilise stepped combustion techniques that permit the separation by release temperature of different volatile components within lunar samples
- Collect abundance and isotopic data for C, N, He, Ne, and Ar simultaneously from the same aliquot of sample material to permit comparisons and cross-checking between different volatile systems and thus aid data interpretation
- Where necessary, take into account the effects of any terrestrial contamination, mass fractionation in the mass spectrometer, and terrestrial system blanks so that true lunar abundances and isotopic data are revealed.

Chapter Two:

Samples and Methods

2.1: Samples

2.1.1: Mare Basalts

A suite of fifteen Apollo mare basalts (powders which were previously prepared: see Section 2.2.2.1) were chosen for stepped combustion analyses, representing five of the six Apollo landing sites, a range of crystallisation ages, cosmic ray exposure (CRE) ages, and chemical compositions. In addition, a fresh chip of one mare basalts (12064) was investigated for the effects of crushing on trapped noble gas inventories. These chips were left uncrushed, and were prepared and analysed using the same protocols as the powdered samples (described in detail in Section 2.2.2.2).

Some samples were analysed multiple times, with time intervals between analyses varying from weeks to months. This was done to monitor data reproducibility, ensuring that results were not anomalous and not affected in any way by other (non-lunar) samples run immediately before each batch of lunar material and associated 'blank' analysis runs.

2.1.1.1: Powdered Samples

Apollo Mission	Sample Number	Sample Weight(s)	Crystallisation Age (Ga)	CRE Age (Ma)	Sample Description
Apollo 11	10017,342	4.670 mg	3.575 ± 0.215[i]	480 ± 25[d]	High Ti, low Al, high K ilmenite basalt (Type A)[l]
Apollo 11	10050,169	5.277 mg	3.75 ± 0.03[h]	480[j]	High Ti, low Al, low K, ilmenite basalt[l]
Apollo 11	10057,285	4.240 mg	3.63 ± 0.02[u]	54.2[f]	High Ti, low Al, high K, ilmenite basalt (Type A)[l]
Apollo 11	10072,173	6.222 mg	3.64 ± 0.05[v]	240[c]	High Ti, low Al, high K, ilmenite basalt (Type A)[l]
Apollo 12	12016,37	4.895 mg	Not known	Not known	Low Ti, low Al, low K, ilmenite basalt[l]
Apollo 12	12040,206	4.656 mg	3.21 ± 0.1[b]	285 ± 50[a]	Low Ti, low Al, low K, olivine basalt[l]
Apollo 12	12047,34	5.146 mg	3.316 ± 0.074[k]	Not known	Low Ti, low Al, low K, ilmenite basalt[l]
Apollo 12	12064,138	5.528 mg; 6.357 mg	3.18 ± 0.01[n]	190 – 220[m]; 255[n]	Low Ti, low Al, low K, ilmenite basalt[l]
Apollo 14	14053,260	5.482 mg	3.94 ± 0.04[x]	21 ± 5[p]	Low Ti, high Al, low K, (Group C)[l]
Apollo 15	15386,54	5.129 mg	3.94 ± 0.01[t]	235 ± 5[x] *	KREEP basalt[l]
Apollo 15	15555,982	4.662 mg	3.32 ± 0.06[y]	81[q]	Low Ti, low Al, low K, olivine basalt[l]
Apollo 17	70017,543	4.252 mg	3.68 ± 0.18[s]	220 ± 20[w]	High Ti, low Al, low K, ilmenite basalt[l]
Apollo 17	70035,194	5.330 mg	3.82 ± 0.06[g]	95 – 100[x]	High Ti, low Al, low K, (unclassified basalt)[l]
Apollo 17	74275,323	5.143 mg	3.85 ± 0.08[r]	32.2 ± 1.4[e]	High Ti, low Al, low K, ilmenite basalt (Type C)[l]
Apollo 17	75055,120	5.426 mg	3.772 ± 0.009[z]	95[o]	High Ti, low Al, low K, ilmenite basalt (Type A)[l]

Table 2.1: Summary of powdered lunar basalt samples analysed in this study, including crystallisation and CRE ages, along with brief sample descriptions, from previous studies. *This is the age of 15382, a related KREEP basalt (no CRE age data exist for15386 itself). Crystallisation ages, CRE ages, and sample descriptions taken from: [a]Burnett et al., 1975; [b]Compston et al, 1971; [c]Eberhardt et al., 1970; [d]Eberhardt et al., 1974, [e]Eugster et al., 1977; [f]Eugster et al., 1984; [g]Evensen et al., 1973; [h]Geiss et al., 1977; [i]Gopalan et al., 1970; [j]Guggisberg et al., 1979; [k]Hallis, 2010; [l]Hallis et al., 2010; [m]Hintenberger et al., 1971; [n]Horn et al., 1975; [o]Huneke et al., 1973; [p]Husain et al., 1972; [q]Marti and Lightner, 1971; [r]Murthy and Coscio, 1977; [s]Nyquist et al., 1974; [t]Nyquist et al., 1975; [u]Papanastassiou et al., 1970; [v]Papanastassiou et al., 1977; [w]Phinney et al., 1975; [x]Stettler et al., 1973; [y]Wasserburg and Papanastassiou, 1971; [z]Tartèse et al., 2013.

2.1.1.2: Unpowdered Samples (Chips)

Apollo Mission	Sample Number	Sample Weight(s)	Crystallisation Age (Ga)	CRE Age (Ma)	Sample Description
Apollo 12	12064,140	5.725 mg	3.18 ± 0.01	190 - 220 Ma; 255 Ma	Low Ti, low Al, low K, ilmenite basalt

Table 2.2: Summary of unpowdered lunar basalt samples analysed in this study (crystallisation ages, CRE ages, and sample descriptions taken from Table 2.1).

2.1.2: Soils

A number of Apollo lunar soils were also chosen for analysis, and were selected to represent a range of Apollo landing and sample collection sites, different soil maturities, and degrees of shielding from extra-lunar processes (i.e. soil sample depth, distance from Lunar Modules (LMs), protected locations underneath boulders etc.). As with the mare basalt samples listed above (Table 2.1), some soil samples were analysed multiple times, using slightly different sample masses (to guard against any potential effect from sample heterogeneity), and heating temperature steps (to provide higher resolution data for temperature ranges of interest in follow-up analyses).

Apollo Mission	Sample Number	Sample Weight(s)	Maturity (I_s/FeO)	Sample Description
Apollo 12	12070,908	5.211 mg	47	Sub-mature contingency soil sample, collected in front of the Lunar Module
Apollo 14	14141,181	7.637 mg	5.7	One of the most immature soil samples
Apollo 15	15040,3	5.662 mg	94	Surface soil from top of trench
Apollo 16	69921,35	5.377 mg	90	Shaded soil collected near a boulder
Apollo 17	72501,32	4.710 mg	81	Reference soil

Table 2.3: Summary of lunar soil samples analysed in this study.

2.2: Methods

2.2.1: Introduction to Stepped Heating Techniques

Heat extraction techniques have been applied to the study of lunar volatiles over the course of the last four decades, from the first return of lunar samples by Apollo 11 and continuing, with periodic improvements and refinements of technique, to the present day.

There are several different forms of this technique that have been used in conjunction with both crystalline rock and soil (bulk and separated fraction) samples; these are described below. However, all are based on the same basic principle; a sample is heated incrementally, and the volatiles liberated from the sample material as gases at each temperature step are then transferred to a mass spectrometer for isotopic analysis (e.g. Epstein and Taylor, 1970; Füri *et al*., 2012; Norris *et al*., 1983).

Samples can be heated in a number of ways. The most widely-applied method utilises a furnace, although there are some variations in furnace design (e.g. Assonov *et al*., 2002; Burnett *et al*., 1975; Epstein and Taylor, 1970, 1971, 1972, 1973, 1974, 1975; Friedman *et al*., 1970; Kaplan *et al*., 1970; Merlivat *et al*., 1974). However, it is also possible to use infrared CO_2 lasers to heat samples in order to extract volatiles from small samples, such as lunar volcanic glasses and lunar soil grains (e.g. Hashizume and Marty, 2004; Wieler *et al*., 1999).

The conditions under which a sample is heated are important variables, particularly for carbon analyses, with two main variations of the stepped heating technique possible: pyrolysis or combustion. Pyrolysis involves the sample being heated under vacuum conditions, without the presence of any oxidising agent (e.g. Epstein and Taylor, 1974; Simoneit *et al*., 1973). Thus, carbon-bearing volatiles released from the sample are

measured in the mass spectrometer as CO, CO_2, and CH_4 (DesMarais *et al*., 1973; Pillinger, 1979), i.e. preserving original speciation.

Combustion requires the sample to be heated in the presence of oxygen, causing the combustion of all released C-bearing species to CO_2 (e.g. Kerridge *et al*., 1977; Norris *et al*., 1983). In combustion analyses, all other volatiles (apart from carbon) are released by pyrolysis; only C compounds are combusted.

Previous lunar studies making use of heat extraction techniques have often employed a mixture of combustion and pyrolysis techniques, depending on the importance of preserving original speciation to each study. In several studies, the first, low temperature step is a combustion step, included to remove terrestrial organic contaminants. Subsequent steps then use pyrolysis to release volatiles (e.g. Mathew and Marti, 2001), although Friedman *et al*. (1970) include one combustion step at 950 °C instead and Becker (1980) at 850 °C, after volatile release by pyrolysis has occurred. However, since it has been shown that isotopic values collected for the same samples using both pyrolysis and combustion methods separately give similar results (Epstein and Taylor, 1971), isotopic data collected using these different forms of the technique can be directly compared.

Although the chosen heating method does not significantly impact the final measured isotopic composition of released volatiles, the type of heating regime chosen for different analyses can have an effect. The number and temperature of heating steps chosen for analyses vary between different studies, and may be pre-determined by sample volatile yields and the detection limits of the instrumentation used, or by the release temperatures of components of interest (e.g. Burnett *et al*., 1975; Epstein and Taylor, 1973). An example of this is the temperature chosen for the first measurement step; below ~ 500 to 600 °C, releases are dominated by terrestrial contamination, and so data from temperatures lower

than this step are often discarded, if collected at all (e.g. Norris *et al*., 1983; Thiemens and Clayton, 1980). Samples can also be heated directly to a final high temperature (e.g. Moore *et al*., 1970; Smith *et al*., 1973), with the measured volatile abundances and isotopic values representing a mixture of all of the volatile components released up to the final temperature.

Such stepped (sometimes known as 'stepwise') heating procedures are similar to the thermal gas analyses carried out by Gibson *et al*. in the 1970s (Gibson and Johnson, 1971; Gibson and Moore, 1972; Gibson and Moore, 1973), although in these analyses, a ramped heating regime was chosen, not stepped heating. Again coupled with a mass spectrometer to record the volatile species released, samples were heated at a rate of either 4 °C or 6 °C per minute, giving 'smooth' volatile release profiles across the whole temperature range up to 1400 °C. However, in these studies, no isotopic data was collected alongside abundance measurements.

Ultimately, whilst the use of different heating regimes between studies allows for the application of the same broad technique to investigate both a whole range of volatile species present in varying abundances, with equipment of different sensitivities, comparison of data collected by different groups can be problematic.

2.2.2: Sample Preparation

2.2.2.1: Sample Powdering Protocols

To produce homogenised bulk powders for multiple analyses, mare basalt chips of approximately 250 mg were powdered using an agate (hydrated SiO_2) mortar and pestle. This was carried out in a Class 1000 clean room (< 1000 particles per cm^3 of air) at The Open University, conditions which keep any possible terrestrial contamination to a

minimum. The agate mortar and pestle used had previously only been used to crush Martian meteorites, and was cleaned before each use with lunar samples using the following protocol:

- Firstly, the mortar and pestle was wiped using acetone and heavy duty synthetic wipes (packed in a clean environment), to remove any visible traces of previously-crushed samples.
- The agate surfaces were then ground for five minutes using pure quartz sand and deionised water to remove any sample material trapped in small imperfections in the agate grinding surfaces, before the quartz sand was washed away using more deionised water.
- The mortar and pestle was again cleaned with acetone and synthetic wipes, followed by further cleaning with an isopropanol (IPA) solution (70 % IPA mixed with 30 % deionised water).
- Pure N_2 was used to visibly dry up any remaining IPA solution on the agate surface, before the mortar and pestle was wrapped in pure aluminium foil and placed in an oven for around 20 minutes at 150 ºC to bake out.
- Upon removal from the oven, the foil-wrapped mortar and pestle was allowed to cool under ambient clean room conditions for another 20 minutes.
- Following standard clean room protocol, the sample preparation work area was also wiped down with IPA solution and covered with a layer of fresh pure aluminium foil before samples were crushed.
- This procedure was repeated before each individual mare basalt chip was powdered to ensure no cross-contamination between lunar samples.

After the agate mortar and pestle had been cleaned in this way, lunar basalt chips were powdered using the following protocol:

- The clean room weighing plate was covered with a piece of pure aluminium foil and zeroed using the 'tare' function.
- The entire sample chip was placed on top of the foil, and weighed to an accuracy of 0.1 g, before being crushed in the cleaned mortar and pestle for between five and fifteen minutes, until a chalky texture was reached. Small fragments were prevented from jumping out of the mortar by a pure aluminium foil wall wrapped around the circumference of the mortar.
- New air-tight sample vials were cleaned with alcohol and baked dry in an oven for several hours. Cleaned vials were then weighed before the crushed lunar sample was transferred into the vial *via* a piece of folded (v-shaped) aluminium foil. The filled vials were then re-weighed and the crushed sample masses compared with the pre-crushed masses to record the loss of material (if any) during the crushing and powder transfer processes.
- The sealed vials were then labelled and stored securely in the clean room suite until preparation for analysis.
- All wipes were used just once before being replaced, and nitrile gloves and foil bench coverings were replaced for each new sample preparation.

Oxygen isotope and bulk rock analyses were subsequently carried out on these homogenised powders (see Hallis *et al*., 2010; 2014), before the first analyses for this project were conducted in April 2013.

2.2.2.2: Sample Preparation for Finesse Analyses

For the purposes of this study, lunar samples (both mare basalts and soils) were prepared in small batches, typically consisting of three or four samples each time, immediately prior to stepped heating analyses using the Finesse mass spectrometer system (which is described in detail in section 2.2.2.3). This ensured that samples were kept under controlled, air-tight conditions in the clean room suite for as long as possible, whilst also enabling analyses to continue without interruption, one sample after another, thus maximising available machine time.

All samples (mare basalt powders, chips, and lunar soils) were prepared for analysis in the same manner, being weighed out and encased in cleaned platinum foil buckets; the Pt foil cleaning procedure is described below:

- Pt foil is cleaned by rolling up small sheets of 25 μm-thick foil and inserting the rolled foil into a quartz tube, along with a foil slug containing CuO.
- This quartz tube is then pumped down to high vacuum (~ 10^{-7} mbar) using an external valve linked to one of the Finesse instrument backline turbo pumps. As the quartz tube/Pt foil is pumped down, it is heated externally using a hydrogen/oxygen torch to start the process of oxidising any contaminants on the Pt foil; any oxidised contaminants are therefore pumped out of the quartz tube at the same time, removing them from the Pt foil.
- After around 30 minutes, the quartz tube, still under vacuum, is sealed and removed from the vacuum line system by torching off the end of the tube containing the Pt foil/CuO slug.
- The sealed quartz tube is then placed in an oven at 900 ºC overnight (at least 12 hours), before being taken out to cool. This sealed tube containing the now-cleaned

Pt foil is then only opened inside a Class 100 clean room when it is needed for the preparation of new samples, minimising any possible re-contamination of the Pt foil before use.

Samples are wrapped in Pt foil for several reasons; the foil helps to hold the small chips or fine powder samples together, ensuring that the entire sample mass reaches the furnace at the same time, and Pt is used because it acts as a catalyst during the combustion of CH_4 and CO to CO_2, and also catalyses the decomposition of nitrous oxides (NO_x; a mixture of NO and NO_2) to N_2 (Boyd *et al*., 1988). This is important, since measurement of N_2 in the mass spectrometer is masked by the presence of CO, both having molecular masses of 28, and the presence of nitrous oxides can cause mass dependant isotopic fractionation to occur between the nitrous oxides and molecular nitrogen, making the isotopic signature of any nitrogen released from the samples impossible to determine (Boyd *et al*., 1988).

Using the cleaned Pt foil, samples were then prepared inside a Class 100 clean room in the following manner:

- Using approximately 8 mm x 8 mm squares of clean Pt foil, sample buckets were made by folding the Pt foil square in half, and turning over two opposite open edges, forming an envelope. This was gently teased open using tweezers to facilitate sample transfer into the bucket.
- The empty bucket was weighed using a balance sensitive to 0.001 mg, and the balance was then zeroed using the ‘tare’ function.
- Holding the empty bucket upright using tweezers in one hand, the sample material was then carefully added either by transfer using a second set of tweezers (in the case of mare basalt chips), a small spatula (in the case of lunar soils), or by

dragging the bucket through a small pile of powdered sample on a separate sheet of pure aluminium foil (for powdered mare basalts).

- The Pt foil bucket containing the sample was weighed again to check that the added sample amount was approximately 5 mg. If not, sample material was either taken out of the bucket, or additional sample material added at this stage.
- Once around 5 mg of sample was inside the bucket, the remaining open edge of the Pt foil bucket was folded over, and using tweezers, the bucket and sample crushed down into a sphere of roughly ≤ 2 mm diameter, sealing the sample inside.
- The crushed bucket was then weighed three more times, with the average mass being taken as the final mass to be analysed.

Prepared samples were wrapped in Al foil and labelled before being taken from the clean room suite into the laboratory, ready for analysis.

2.2.3: 'Finesse'

Lunar samples (prepared as described in Section 2.2.2) were analysed at the Open University, using the custom-built Finesse mass spectrometer system.

2.2.3.1: Overview of the Finesse instrument

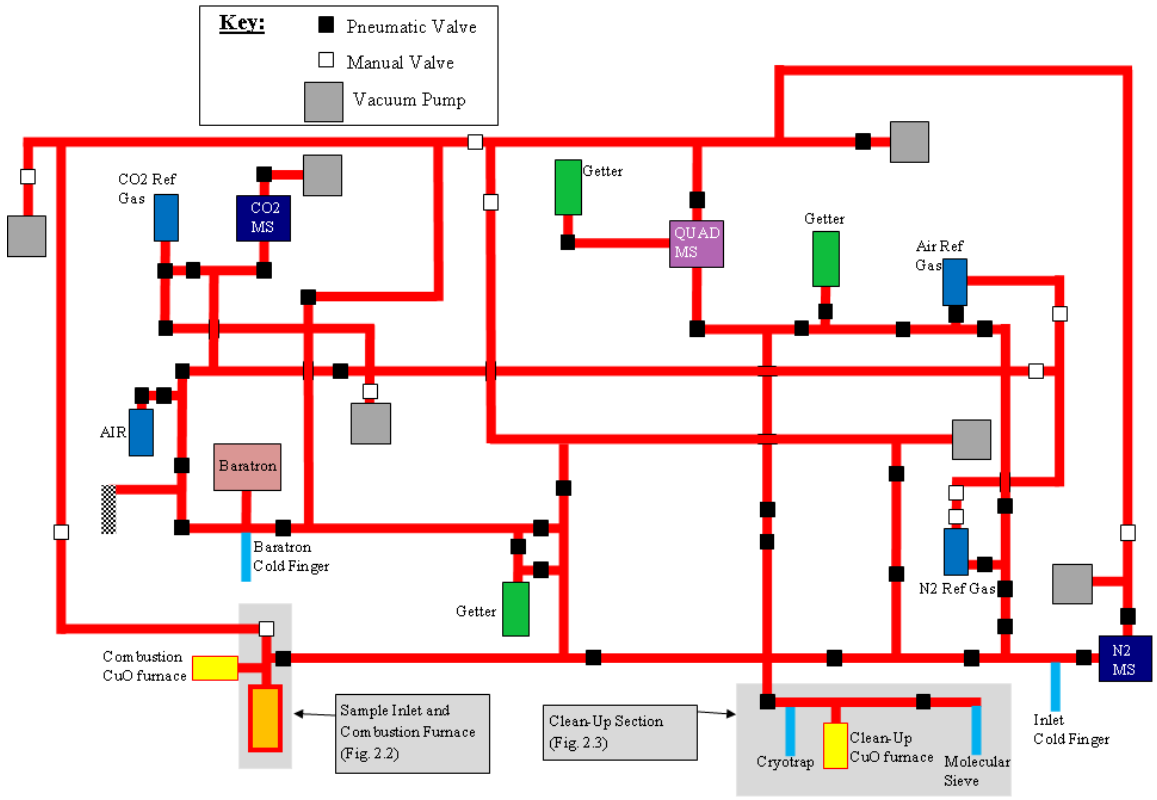

Figure 2.1: Schematic diagram of the entire 'Finesse' triple mass spectrometer instrument. Boxes shaded in grey indicate more detailed close-up diagrams later in this chapter.

The 'Finesse' mass spectrometric instrument consists of three dedicated static-mode mass spectrometers (one for carbon, one for nitrogen and argon, and a quadrupole for helium and neon), all linked *via* high vacuum lines to a common sample inlet, combustion furnace, and clean-up section (Fig. 2.1). Movement of gases around the instrument is controlled by automated pneumatic valves, and the vacuum system operates at around 10^{-7} mbar (see Abernethy *et al*., 2013; Mikhail, 2011: Verchovsky *et al*, 1997; Wright *et al.*, 1988; Wright and Pillinger, 1989 for further details).

For each temperature step, the isotopes of C, N, He, Ne, and Ar were measured sequentially, taking approximately 1.5 hours to complete the cycle for five elements. System blanks were monitored between sample analyses by putting an empty clean Pt foil bucket through the same stepped combustion procedure used for the lunar samples and collecting both abundance and isotopic data. Typical system blank levels were < 10 ng C and < 1 ng of N. Typical system blanks for ^{4}He were < 1 x 10^{-7} cc, for ^{20}Ne were < 6.5 x 10^{-10} cc, and for ^{40}Ar and ^{36}Ar were < 8 x 10^{-9} cc and < 1.2 x 10^{-10}, respectively (Mortimer *et al*., 2015). Before each batch of Pt foil blank and sample analyses, analyses of reference gases were performed, to ensure measurement stability within a single analysis, and to monitor any potential drifting of reference gas isotopic compositions over time due to previous reference gas bleed extractions which may cause fractionation of the remaining reference gas reservoir.

2.2.3.2: Sample Inlet System

The Finesse sample inlet consists of a horizontal glass pipe with an external manual double seal glass valve (V1) for sample loading at one end, with a second manual double seal glass valve (V2) isolating it from a vertical glass pipe, leading down, *via* a manual gate valve, into the quartz pipe inside the combustion furnace (Figure 2.2).

To load Pt-foil-wrapped samples, V2 is closed tightly, to ensure that the main instrument vacuum line is not vented to atmosphere. V1 is removed, and samples transferred into the horizontal glass section using tweezers. V1 is then replaced and mainline ion vacuum pumps are isolated using manual valves before V2 is opened to allow the sample inlet chamber to be pumped down from atmosphere using a turbo pump (taking around fifteen minutes). Once most of the atmosphere has been pumped out from the sample inlet chamber, manual valves are reopened to allow the sample inlet to pump down to the usual

instrument high vacuum baseline (around 10^{-8} mbar) using the Finesse backline pumps. This ensures that the main sample vacuum line is not contaminated by atmospheric gases, and protects the sensitive ion pumps. This second pump-down again takes approximately fifteen minutes to reach high vacuum.

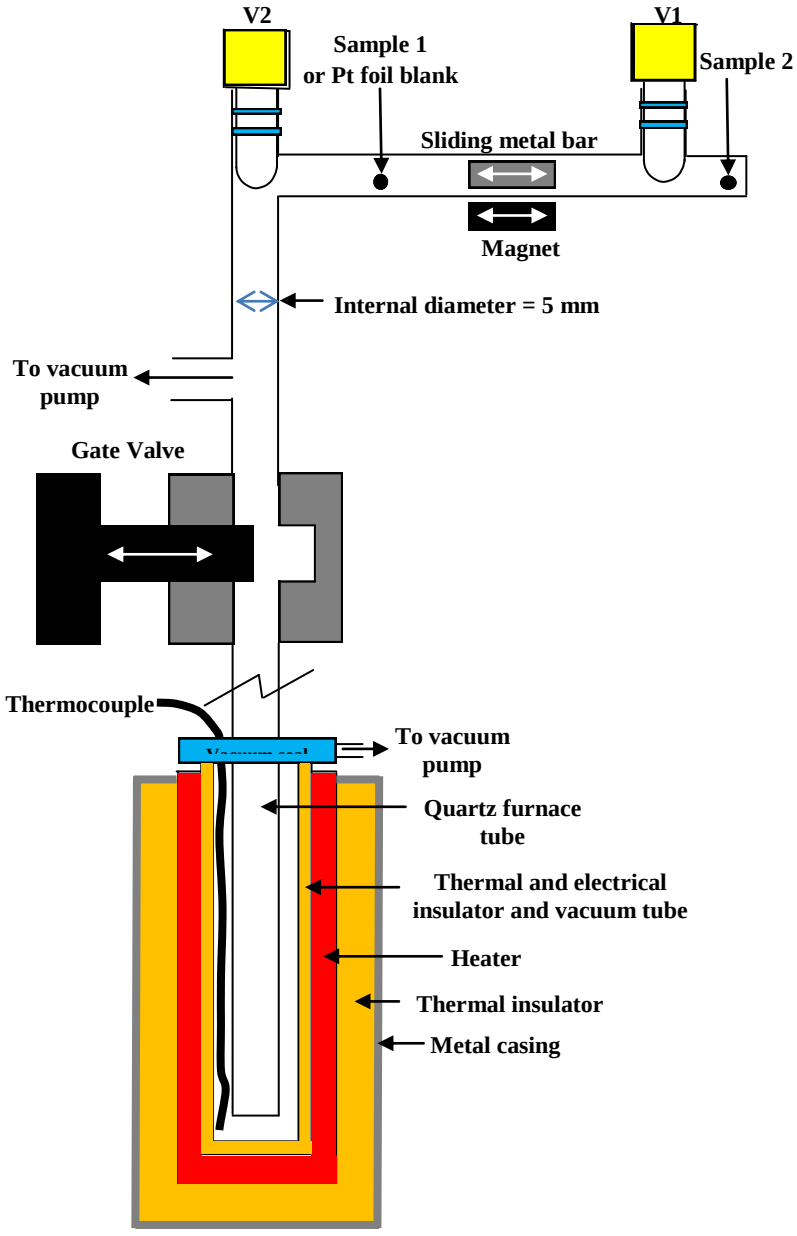

Figure 2.2: Schematic diagram of the Finesse sample inlet section and furnace. N.B. Not to scale. Not shown are the combustion CuO furnace, nor the outlet valve to the analysis sections of the instrument. Adapted from Mikhail (2011).

When samples have been loaded, and the sample inlet has been fully pumped back down to high vacuum, V2 is opened just wide enough to permit the through passage of the crushed sample sphere, and the manual gate valve in the vertical glass section is opened (to a diameter of 5 mm, which is the internal diameter of the quartz combustion tube). The sample is dragged along the horizontal inlet section, using an internal metal bar which is moved along by a manual external magnet, until the sample drops down through V2 and the open gate valve, into the combustion furnace. The pressure reading on the main vacuum line increases shortly after a successful sample drop, indicating that the sample is now in the furnace, and that the manual gate valve can be safely closed, thereby sealing off the main body of the instrument, under high vacuum, from the sample inlet section during analyses.

2.2.3.3: Combustion and Volatile Separation Procedure

Samples are combusted in a double-walled quartz-ceramic furnace for 30 minutes at each temperature step. Oxygen for combustion is supplied from an adjacent furnace containing CuO, which is heated to 930 ºC to liberate oxygen. After combustion, the CuO furnace is allowed to cool to 650 ºC for the resorption of any excess O_2 back onto the CuO (this process taking fifteen minutes), and continues to cool back down to its idling temperature of 350 ºC until the next combustion cycle begins, before transfer of the gases produced to the clean-up section (Fig. 2.3).

Gas fractions are cryogenically separated using liquid nitrogen cooled traps, some of which contain molecular sieves. Liquid nitrogen is automatically pumped (using rotary pumps) to the relevant traps at the required times via plastic pipes from a central 50 L flask. Carbon is trapped down by freezing CO_2 onto a liquid nitrogen-cooled cryotrap (below -160 ºC), before N_2 and Ar are collected on the molecular sieve (also cooled by liquid

nitrogen to < -190 ºC). After this has occurred, the entire clean-up section of the main vacuum line is isolated using V8 whilst the combustion furnace is pumped using the backline vacuum system, and V11, between the cryotrap and the molecular sieve, is also closed. He and Ne, which are not cryogenically trapped, are also held inside the vacuum line of the clean-up section during combustion furnace pumping. Once pumped, the furnace is isolated from the rest of the instrument vacuum lines by closure of a valve; combustion then commences at the next temperature step while the released volatiles from the previous combustion step are analysed.

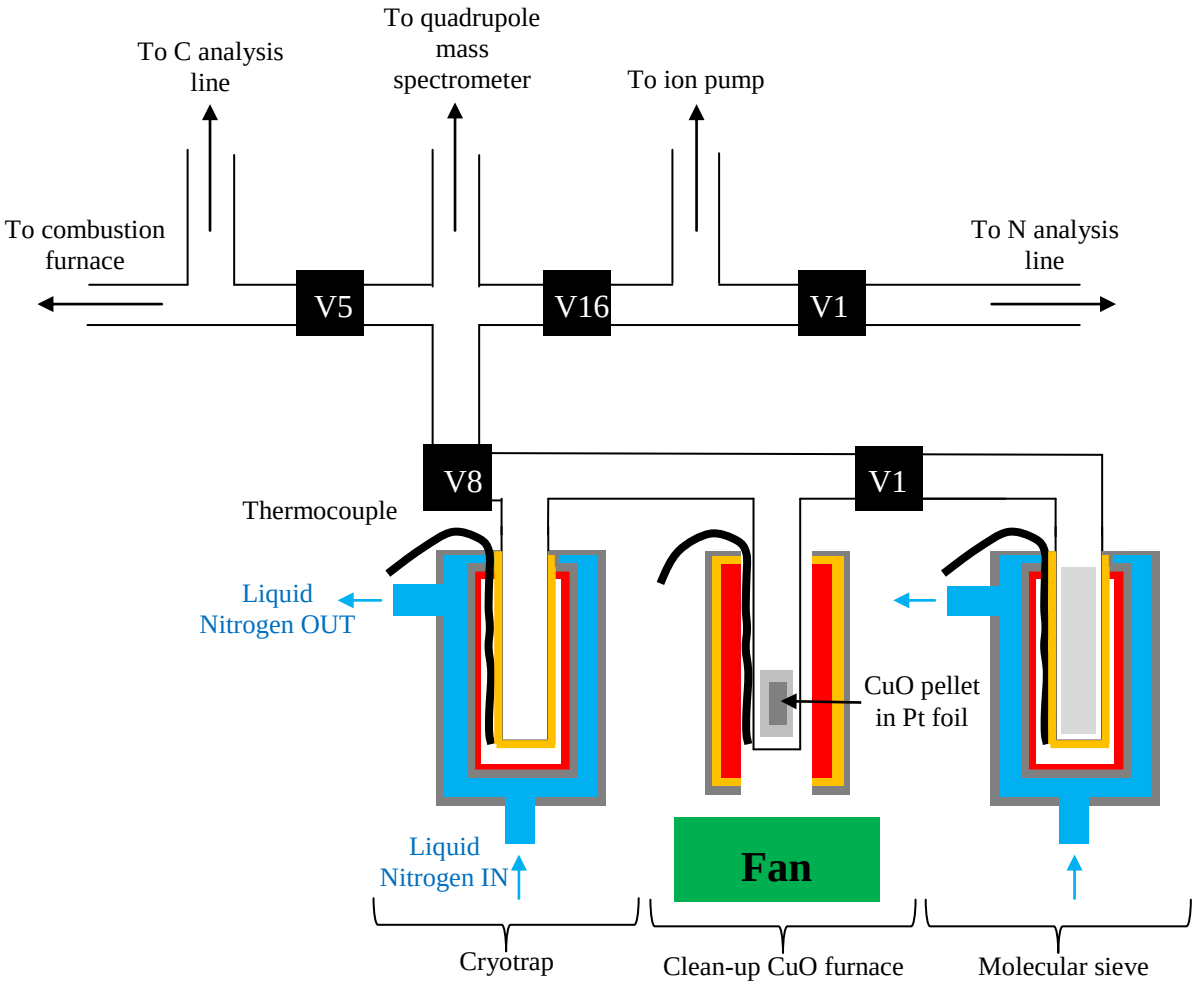

Figure 2.3: Schematic diagram of the Finesse volatile separation and clean-up section. N.B. Not to scale. All valves shown are controlled by an automated pneumatic system. Adapted from Mikhail (2011).

For the initial batch of 5 powdered mare basalt samples, only thirteen combustion steps were used, in 100 °C steps from 200 ºC to 1400 °C. However, for later mare basalt analyses (the remaining powdered basalts plus re-runs of some samples analysed in the initial batch), based on the results of the first several samples (volatile yields and temperature ranges of interest), a higher-resolution combustion regime was chosen; a total of seventeen combustion steps were employed to acquire higher-resolution data across the mid-range temperatures, heating in 100 °C steps from 200 - 600 °C, then in 50 °C steps from 650 - 950 °C, followed by 100 °C steps from 1000 - 1400 °C.

The first lunar soil analysis was conducted using the same thirteen combustion steps as the initial batch of powdered mare basalts, with subsequent soil analyses using fifteen temperature steps (in 100 ºC steps from 200 – 700 ºC, 50 ºC steps from 750 – 850 ºC, and 100 ºC steps from 900 – 1400 ºC).

2.2.3.4: He and Ne analysis

He and Ne are measured in the same procedure using the quadrupole mass spectrometer. With CO_2 still frozen down onto the cryotrap, and N_2 and Ar condensed onto the molecular sieve, the clean-up section is opened up to the main vacuum line, and an aliquot of the non-condensable He and Ne is taken and held in a short section of pipe between two valves. At the same time, a 'zero' measurement is made on the quadrupole to register the base levels of He and Ne isotopes in the mass spectrometer. When this is complete, the aliquot of He and Ne is admitted into the quadrupole, the mass spectrometer is isolated from both the pumps and the rest of the sample main vacuum line by the automated closure of the relevant valves, and the He and Ne measurement is made. He and Ne abundances are determined by calibration of the quadrupole peak intensities at masses 4, 20, 21, and 22.

Because of the relatively low abundances of Ne released from lunar samples, mass interferences in a quadrupole mass spectrometer can be significant; in the case of Ne, contributions from CO_2^{++} and $^{40}Ar^{++}$ can affect measurement of both ^{22}Ne and ^{20}Ne respectively. In order to reduce these contributions, a low ionisation voltage of ~40 V was used in the quadrupole ion source. Also, Ar present in the system was cooled down on the molecular sieves, and an adjacent Ti-Al getter (for Ne purification) was open to the mass spectrometer chamber during Ne measurements. Using this instrument, it has been calculated that mass interference from doubly charged CO_2 during Ne measurements only becomes noticeable when the sample 44/22 ratio is ≥ 100 (Mortimer *et al*., 2015).

2.2.3.5: Carbon analysis

After He and Ne aliquots have been taken, and with V11, separating the cryotrap (containing CO_2) and the molecular sieve (holding N_2 and Ar), still closed, the cryotrap is heated to around -75 ºC (see Figure 2.3). At the same time, a liquid nitrogen cooled cold finger adjacent to a calibrated MKS Baratron™ capacitance manometer is cooled to -160 ºC. As the cryotrap warms up, it releases the trapped CO_2, which is then retrapped down onto the Baratron cold finger. Whilst still at temperatures below 0 ºC, the cryotrap retains any H_2O present in the system, separating it from CO_2. The transfer of CO_2 to the Baratron cold finger is checked by monitoring the pressure recorded in the Baratron itself; as CO_2 is released from the cryotrap, Baratron pressure increases, before decreasing rapidly as the CO_2 is retrapped down onto the cold finger. When all of the CO_2 has been transferred, any non-condensable volatiles in the Baratron section are pumped away. It is then isolated from the rest of the main vacuum line and the cold finger is heated to release the CO_2 into the Baratron for abundance measurements (calculated from the pressure of CO_2 inside the calibrated Baratron, accurate to ± 1 %, and recorded as ng of C).

After the yield of C has been measured, the Baratron section is reopened to the rest of the machine and an aliquot of the sample CO_2 is taken by expanding the gas into a section of the vacuum line between two valves, ready for analysis in the C mass spectrometer. This aliquot is typically around 1 ng of CO_2 (Mikhail, 2011), which provides enough sample gas for an accurate isotopic measurement without flooding the mass spectrometer by admitting the total released C yield.

A 'zero' measurement is carried out in the C mass spectrometer, to measure the instrument background present during sample analysis. Then, the aliquot of sample gas is expanded into the mass spectrometer, and masses 44, 45, and 46 are measured, from which are derived 45/44 and 46/44 isotope ratios. After the measurement has been taken, the mass spectrometer is cleared of sample gas by pumping out with an ion pump attached to the opposite side of the analysis chamber from the chamber inlet. An aliquot of reference CO_2 gas is then taken automatically, replicating the sample CO_2 aliquot size to within 5 % (Mikhail, 2011); if the reference aliquot is not within 5 % of the original sample aliquot, a second reference aliquot is taken later.

After measurement of the reference aliquot, as the reference gas is being pumped away from the mass spectrometer chamber, the $^{13}C/^{12}C$ ratio of the sample C is calculated from the previously measured sample and reference aliquot measurements, and reported using the delta notation ($\delta^{13}C$), as a parts-per-thousand deviation (‰) from the international Vienna Pee Dee Belemnite (VPDB) C standard (where $^{13}C/^{12}C = 0.0112372$).

2.2.3.6: Nitrogen clean-up and analysis

With V11 in the clean-up section still closed, the molecular sieve is allowed to heat up to 250 ºC, releasing N_2 and Ar. At the same time, a second clean-up furnace, next to the molecular sieve, containing CuO is heated to 850 ºC to release oxygen into the clean-up

section. V11 is opened, and this liberated oxygen reacts with any CO (mass 28) present in the sample N_2 (also mass 28), forming CO_2 (mass 44); this then no longer poses the threat of mass interference during N_2 abundance and isotopic measurements. After oxidation of CO to CO_2, the clean-up CuO is cooled back down to 650 ºC (in order to resorb any excess oxygen), then down to 450 ºC (below the temperature at which the CuO powder releases oxygen) using an external fan positioned under the clean-up CuO furnace.

Following this, an aliquot of the purified N_2 and Ar is taken and delivered to a Ti-Al getter; this purifies the Ar, removing N_2, ready for Ar abundance and isotopic analysis. During Ar purification on the getter, with the cryotrap cooled to -160 ºC to minimise background CO_2 levels, a second aliquot of sample N_2 (around 5 % of the total N_2 release) is taken and delivered to the quadrupole mass spectrometer, where a rough nitrogen abundance measurement is taken after a 'zero' measurement, using the intensity of mass 14. Mass 14 is used because it has a low background, and its measurement is not complicated by the presence of any CO at mass 28 (Mikhail, 2011). Total N_2 abundance is measured using another aliquot of sample nitrogen, on the N mass spectrometer; this aliquot is further purified by storing it in a section of vacuum line immediately before the N mass spectrometer inlet, where a liquid nitrogen cooled inlet cold finger traps any condensable gases at around -160 ºC. As this is happening, the N mass spectrometer performs a 'zero' measurement, after which the sample N_2 is admitted into the mass spectrometer chamber for analysis. Nitrogen abundance is measured *via* calibration of the mass spectrometer ion current at mass 28. Masses 28, 29, and 30 are measured, and 28/29 and 30/29 ratios are calculated for the sample gas, after which, the N mass spectrometer is pumped using an ion pump before a reference gas (terrestrial air) aliquot is measured. The aliquot of reference air is taken in the same manner as described above for C; an aliquot of approximately the same size as the sample N aliquot is taken automatically and allowed to expand into the

section of vacuum line immediately in front of the N mass spectrometer inlet. Once the N reference aliquot has equilibrated, this section of vacuum line is isolated, and the inlet cold finger cooled down to -160 ºC (trapping any condensable gases present in the reference gas). When this has occurred, and the N mass spectrometer has been fully pumped so that no sample N remains, the reference aliquot is admitted for analysis, where isotopes and isotopic ratios are measured in the same way as described above for the sample aliquot. After N reference analysis, the N mass spectrometer is again emptied using the ion pump, and the computer programme automatically calculates the isotopic composition (expressed in delta notation as $\delta^{15}N$) of the sample gas as a parts-per-thousand (‰) deviation from the terrestrial standard (AIR), where $^{15}N/^{14}N = 0.003676466$.

2.2.3.7: Argon analysis

Once the Ar aliquot has been purified on the Ti-Al getter to remove N_2 (a process which takes around ten minutes), the cleaned sample Ar aliquot is transferred to the N mass spectrometer inlet section, where it is held whilst the inlet cold finger (at -160 ºC) traps any remaining condensable gases. The sample Ar is then introduced into the N mass spectrometer, where an average value from 50 measurements of masses 36, 37, 38, and 40 is taken. As with the He, Ne, and N, Ar abundance is measured *via* calibration of the mass spectrometer ion peak intensities at the above masses.

By the time the individual clean-up and analysis procedures for the various isotopes have been performed (usually taking approximately 1.5 hours per combustion step for He, Ne, Ar, C, and N), the next combustion step is ready for analysis, and so is transferred from the combustion furnace to the cryotrap and molecular sieve in the clean-up section for the process to begin again.

Chapter Three:

Mare Basalt Analysis Results

3.1: Nitrogen

The stepped combustion results for nitrogen abundance and isotopic composition of the fifteen powdered mare basalts analysed are listed in Tables 3.1.2 to 3.1.5 and displayed in Figs. 3.1.1(Apollo 11); 3.1.2 (Apollo 12); 3.1.3 (Apollo 14 and 15); and 3.1.4 (Apollo 17). All of the samples display the same general release profiles, with 64–94% of the nitrogen being released at temperatures below 500-650 ºC, most likely associated with terrestrial contamination. Between 4% and 26% of the N present is released at mid-temperature steps (between 600 ºC and 900–1000 ºC, the exact temperature range varying slightly between samples), and minor amounts (blank level to 18% of the total N present in the samples) are released at high temperatures, typically above 1000–1100 ºC, which in all samples are associated with a significant enrichment in ^{15}N at these temperature steps (see Table 3.1.1).

Sample	Low Temperature Range (<500 to 600/650 ºC) (% Released)	Mid Temperature Range (600/650 to 1000 ºC) (% Released)	High Temperature Range (>1000 to 1100 ºC) (% Released)
10017	67	16	17
10050	74	8	18
10057	64	24	12
10072	92	4	4
12016	94	5	1
12040	67	26	7
12047	86	7	7
12064	89	10	3
14053	85	12	3
15386	92	6	2
15555	89	4	7
70017	84	7	9
70035	94	6	0 (At blank level)
74275	88	6	6
75055	76	17	7
Min. % Released	64	4	0 (At blank level)
Max. % Released	94	26	18

Table 3.1.1: Percentages of the total sample N released across the low temperature, mid temperature, and high temperature ranges (as outlined in the text above), for each mare basalt sample analysed (see Tables 3.1.2 to 3.1.5 for released N abundances in ng).

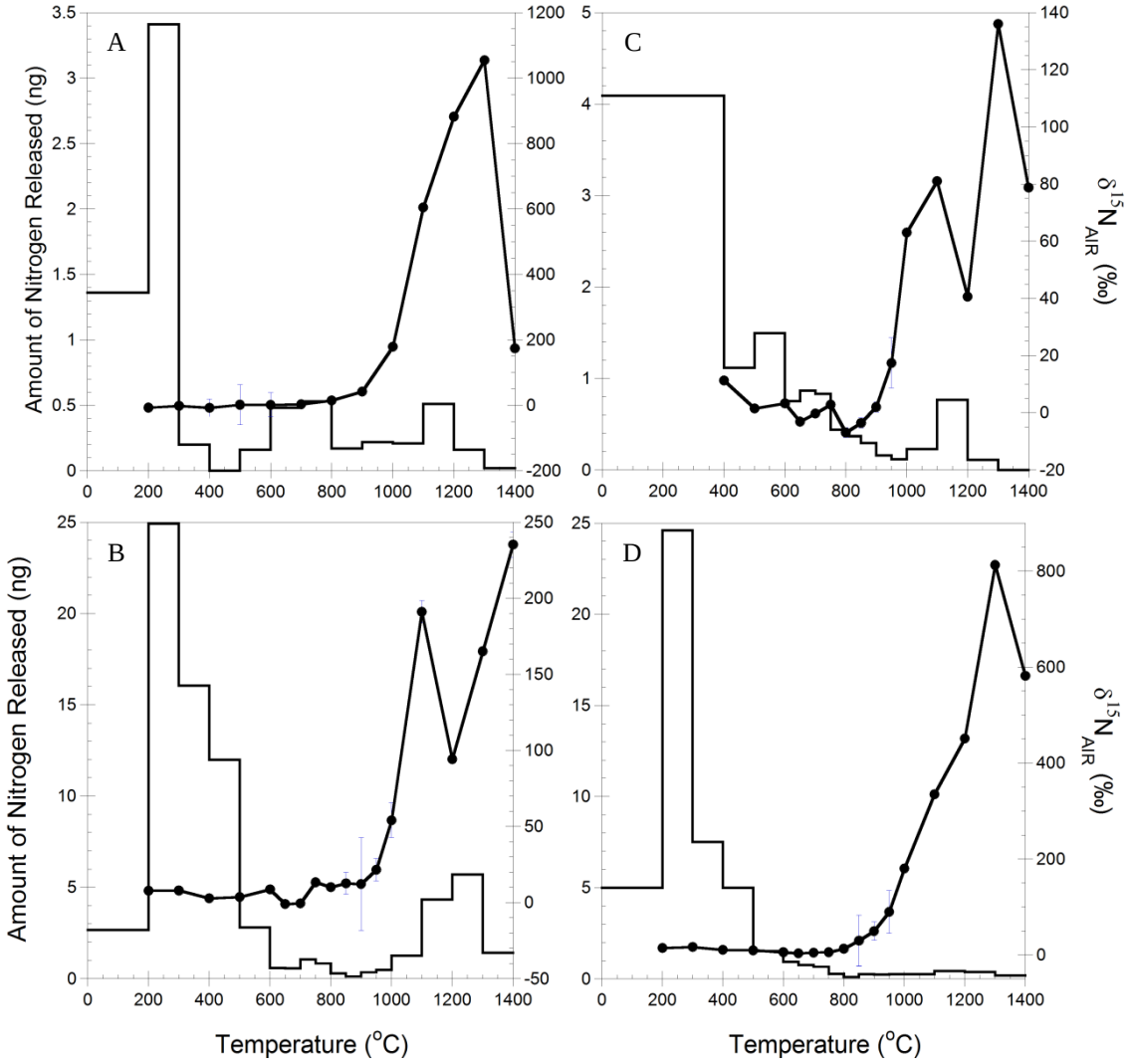

Figure 3.1.1: Step plots of nitrogen abundances and isotopic compositions in Apollo 11 samples, where A = 10017, B = 10050, C = 10057, and D = 10072. The bar chart represents the amount of nitrogen released at each step (left axis), and the line with dots represents the isotopic $\delta^{15}N$ signature of nitrogen released at each step (right axis). N.B.: each plot uses different scales for both the left and right axes. See Table 3.1.2 for data.

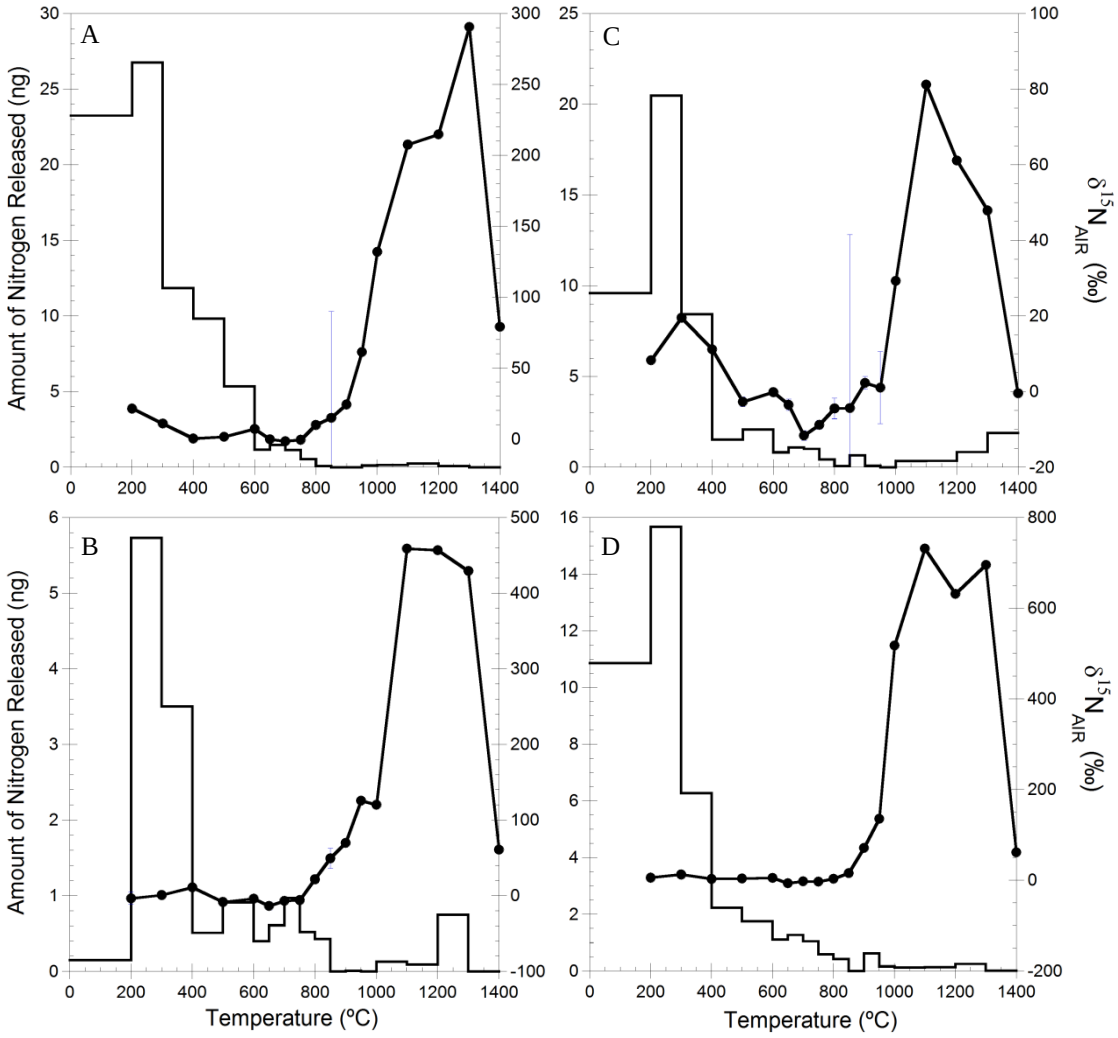

Figure 3.1.2: Step plots of nitrogen abundances and isotopic compositions in Apollo 12 samples, where A = 12016, B = 12040, C = 12047, and D = 12064. The bar chart represents the amount of nitrogen released at each step (left axis), and the line with dots represents the isotopic $\delta^{15}N$ signature of nitrogen released at each step (right axis). N.B.: each plot uses different scales for both the left and right axes. See Table 3.1.3 for data.

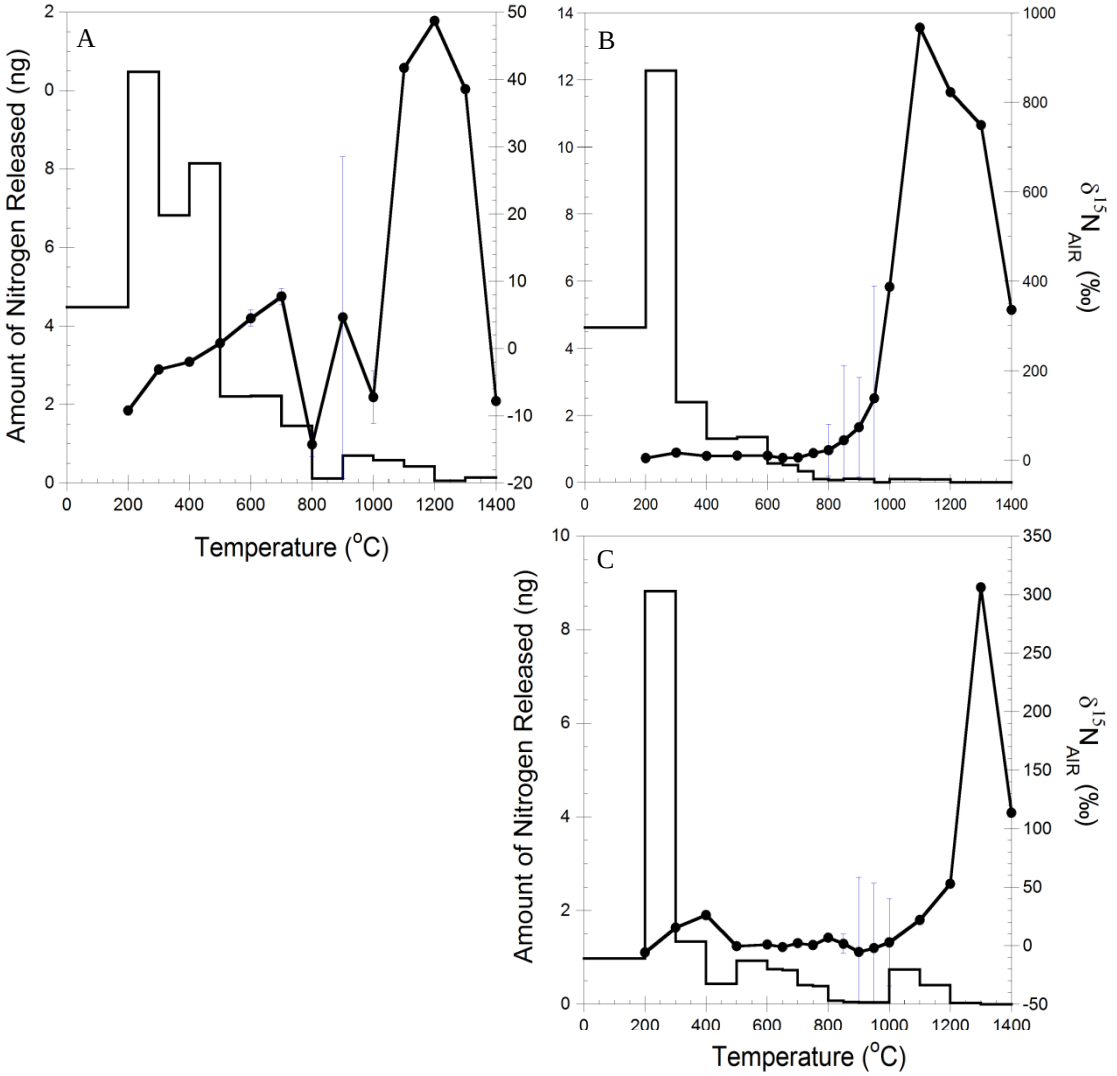

Figure 3.1.3: Step plots of nitrogen abundances and isotopic compositions in Apollo 14 and Apollo 15 samples, where A = 14053, B = 15386, and C = 15555. The bar chart represents the amount of nitrogen released at each step (left axis), and the line with dots represents the isotopic $\delta^{15}N$ signature of nitrogen released at each step (right axis). N.B.: each plot uses different scales for both the left and right axes. See Table 3.1.4 for data.

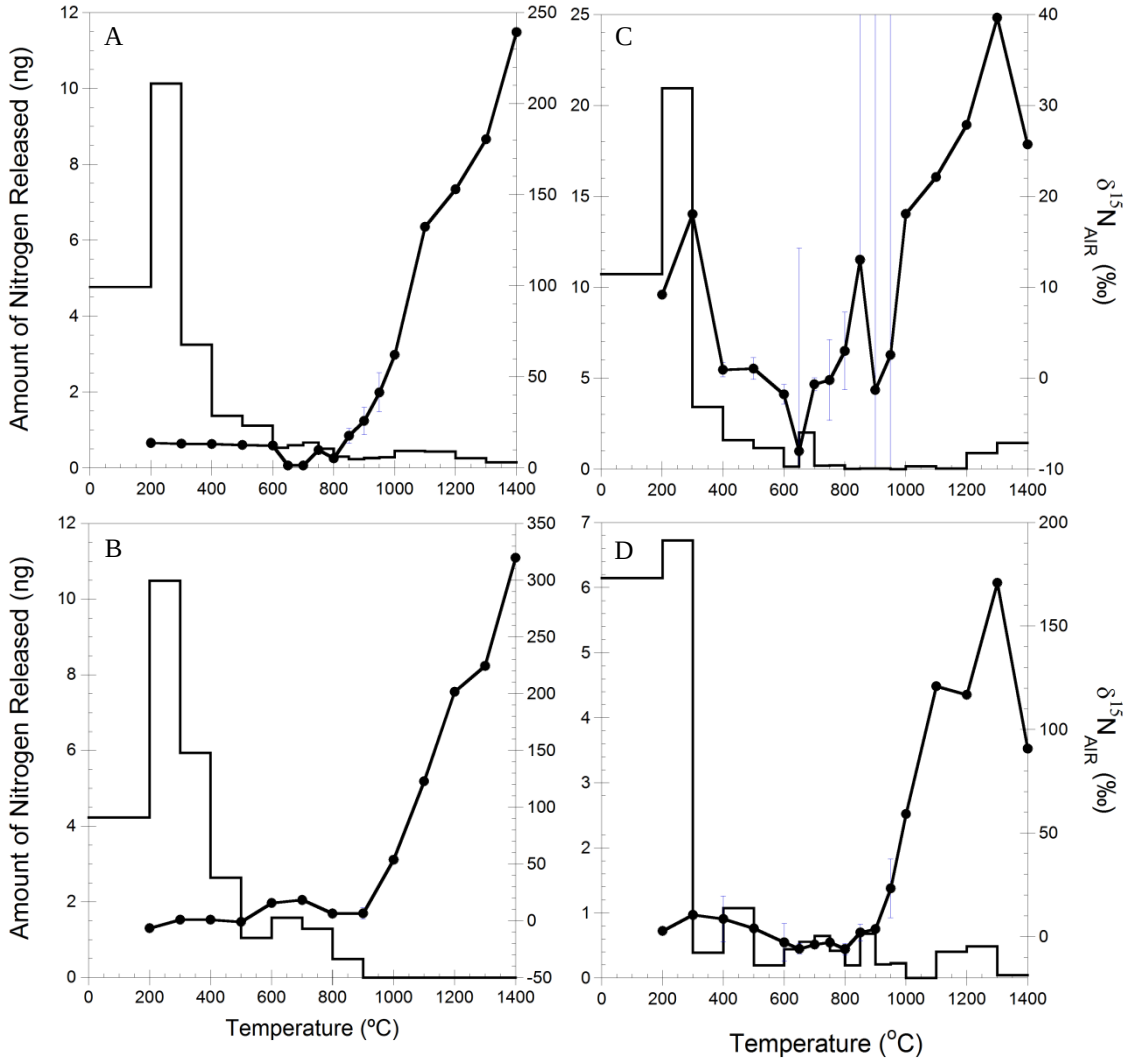

Figure 3.1.4: Step plots of nitrogen abundances and isotopic compositions in Apollo 17 samples, where A = 70017, B = 70035, C = 74275, and D = 75055. The bar chart represents the amount of nitrogen released at each step (left axis), and the line with dots represents the isotopic $\delta^{15}N$ signature of nitrogen released at each step (right axis). N.B.: each plot uses different scales for both the left and right axes. See Table 3.1.5 for data.

In all of the step plots above, both the nitrogen abundance and isotopic data have been corrected for any contributions from the system blank (blank correction methods are outlined in the Appendix). Errors (in pale blue) are not displayed above 1000 ºC since the N abundance from the samples is so close to blank levels at these temperature steps; the error propagation method used to calculate the blank-corrected uncertainties generates extremely large errors that are unsuitable/unrealistic. Indeed, in some samples (see sample 74275/graph C in Fig.3.1.4), even at lower temperature steps, the amount of N released is so close to the blank level that the isotopic measurement for that step is associated with large uncertainties. However, for all samples where error bars are not visible at steps below 1000 ºC, this is because the uncertainties on the isotopic measurements are smaller than the symbol size used in the figures.

Also apparent in the nitrogen step plots above is the release of a high temperature component at 1100-1300 ºC in several samples (e.g. 10050, 10057, 74275 and 75055), associated with a relative depletion in ^{15}N compared to the other high temperature nitrogen releases in these same samples. Both the abundance of this component (up to 5 ng) and its isotopic signature indicate that at these temperature steps, the nitrogen being released is not of purely cosmogenic origin. The nature of this somewhat anomalous component will be addressed in more detail in Chapter 5.

	10017			10050			10057			10072		
Temperature (°C)	N (ng)	$\delta^{15}N$ (‰)	Error (‰)	N (ng)	$\delta^{15}N$ (‰)	Error (‰)	N (ng)	$\delta^{15}N$ (‰)	Error (‰)	N (ng)	$\delta^{15}N$ (‰)	Error (‰)
200	1.36	-7.09	0.66	2.67	7.82	0.32	-	-	-	5.00	14.44	0.37
300	3.41	-1.94	0.51	24.91	8.02	0.16	-	-	-	24.61	16.64	0.32
400	0.20	-7.98	26.84	16.04	2.92	0.21	4.09	11.34	0.33	7.51	10.81	0.43
500	†	1.69	60.90	11.99	3.67	0.24	1.12	1.52	0.61	5.00	9.60	0.46
600	0.16	1.51	36.68	2.81	8.72	0.30	1.50	3.31	0.53	1.53	5.85	0.83
650	-	-	-	0.58	-0.82	1.00	0.75	-3.05	0.90	0.93	3.39	1.10
700	0.48	3.41	5.90	0.57	-0.45	1.00	0.87	-0.24	0.78	0.76	5.02	1.27
750	-	-	-	1.06	13.48	0.82	0.83	2.86	0.73	0.66	5.80	1.50
800	0.53	14.85	10.38	0.84	10.22	1.17	0.44	-6.95	1.70	0.28	12.88	6.21
850	-	-	-	0.30	12.80	7.22	0.37	-3.55	1.76	0.11	30.07	53.01
900	0.17	42.01	29.40	0.13	12.27	30.59	0.30	2.05	1.77	0.26	49.69	18.90
950	-	-	-	0.36	21.66	7.43	0.16	17.48	8.77	0.24	89.69	44.67
1000	0.22	179.08		0.49	54.22		0.12	63.10		0.26	180.52	
1100	0.21	604.83		1.27	191.19		0.23	81.11		0.26	334.84	
1200	0.51	882.24		4.33	94.29		0.77	40.68		0.44	451.38	
1300	0.16	1054.82		5.71	165.17		0.11	136.02		0.37	812.79	
1400	0.02	174.21		1.41	235.26		†	78.79		0.19	581.91	

Table 3.1.2: Nitrogen results for Apollo 11 mare basalts. Note that for 10057, data were not collected below 400 ºC, and for 10017, data was only collected in 100 ºC steps (- = not measured, †= blank level). N.B.: High temperature steps containing cosmogenic N have no error reported, since error propagation on such small abundances gives unrealistic uncertainties. However, these high temperature isotopic signatures have been used to calculate cosmogenic N abundances, and these correlate well with reported exposure ages, suggesting that these isotopic data, although associated with very large errors, are fairly reliable.

	12016			12040			12047			12064		
Temperature (°C)	N (ng)	$\delta^{15}N$ (‰)	Error (‰)	N (ng)	$\delta^{15}N$ (‰)	Error (‰)	N (ng)	$\delta^{15}N$ (‰)	Error (‰)	N (ng)	$\delta^{15}N$ (‰)	Error (‰)
200	23.24	21.41	0.33	0.15	-3.29	7.88	9.60	8.34	0.45	10.86	5.98	0.34
300	26.75	10.91	0.29	5.73	1.03	0.36	20.48	19.53	0.38	15.67	12.77	0.42
400	11.85	0.29	0.34	3.50	11.26	0.53	8.43	11.18	0.51	6.28	3.28	0.45
500	9.84	1.51	0.44	0.51	-8.13	3.18	1.53	-2.66	1.30	2.23	3.95	0.63
600	5.36	7.04	0.38	0.91	-3.66	1.31	2.08	-0.14	0.67	1.75	5.11	0.79
650	1.16	-0.23	0.94	0.40	-13.41	5.67	0.83	-3.47	1.48	1.11	-6.40	0.91
700	1.48	-1.61	0.78	0.61	-6.80	2.09	1.09	-11.59	1.28	1.27	-1.80	0.79
750	1.14	-0.57	1.13	0.97	-5.66	1.34	1.01	-8.78	1.22	1.05	-2.78	0.98
800	0.54	9.88	2.68	0.52	21.90	4.87	0.44	-4.45	2.70	0.59	3.70	1.62
850	0.09	14.93	74.81	0.43	49.43	13.64	0.07	-4.32	45.82	0.42	16.13	3.87
900	†	24.30		†	70.07		0.65	2.33	1.71	†	71.40	
950	†	61.37		0.01	125.81		0.09	1.08	9.52	0.62	135.66	
1000	0.12	131.94		†	120.42		0.01	29.28		0.16	517.78	
1100	0.16	207.55		0.13	458.89		0.35	81.23		0.12	731.58	
1200	0.25	214.75		0.09	456.80		0.36	61.17		0.13	631.58	
1300	0.08	290.60		0.75	429.46		0.84	47.93		0.25	695.70	
1400	†	79.13		†	60.96		1.90	-0.40		0.01	61.77	

Table 3.1.3: Nitrogen results for Apollo 12 mare basalts (- = not measured, †= blank level). N.B.: High temperature steps containing cosmogenic N have no error reported, since error propagation on such small abundances gives unrealistic uncertainties. However, these high temperature isotopic signatures have been used to calculate cosmogenic N abundances, and these correlate well with reported exposure ages, suggesting that these isotopic data, although associated with very large errors, are fairly reliable.

	14053			15386			15555		
Temperature (°C)	N (ng)	$\delta^{15}N$ (‰)	Error (‰)	N (ng)	$\delta^{15}N$ (‰)	Error (‰)	N (ng)	$\delta^{15}N$ (‰)	Error (‰)
200	4.48	-9.20	0.71	4.62	4.42	0.37	0.98	-5.72	0.99
300	10.48	-3.12	0.30	12.27	16.47	0.47	8.82	15.47	0.41
400	6.82	-1.97	0.45	2.39	9.31	0.95	1.34	26.18	0.97
500	8.15	0.80	0.36	1.30	9.91	0.90	0.44	-0.34	1.64
600	2.21	4.50	1.21	1.35	9.62	0.97	0.93	1.05	0.79
650	-	-	-	0.56	4.64	1.72	0.75	-0.94	1.02
700	2.22	7.72	1.21	0.52	5.57	1.95	0.73	2.30	1.02
750	-	-	-	0.33	15.37	5.54	0.41	0.64	1.69
800	1.46	-14.27	1.82	0.10	21.97	58.29	0.39	7.01	2.57
850	-	-	-	0.07	44.26	167.43	0.08	1.73	8.27
900	0.12	4.63	23.91	0.11	73.18	110.96	0.05	-5.30	63.73
950	-	-	-	0.10	137.82	251.40	0.04	-1.93	55.21
1000	0.70	-7.22	3.88	†	387.10		0.04	2.91	37.27
1100	0.58	41.69		0.10	966.89		0.74	22.07	
1200	0.43	48.71		0.09	822.51		0.41	52.88	
1300	0.06	38.56		†	748.88		0.03	306.06	
1400	0.14	-7.82		†	336.04		†	113.64	

Table 3.1.4: Nitrogen results for Apollo 14 and Apollo 15 mare basalts. Note that for 14053, data were only collected in 100 ºC steps (- = not measured, †= blank level). N.B.: High temperature steps containing cosmogenic N have no error reported, since error propagation on such small abundances gives unrealistic uncertainties. However, these high temperature isotopic signatures have been used to calculate cosmogenic N abundances, and these correlate well with reported exposure ages, suggesting that these isotopic data, although associated with very large errors, are fairly reliable.

	70017			70035			74275			75055		
Temperature (°C)	N (ng)	$\delta^{15}N$ (‰)	Error (‰)	N (ng)	$\delta^{15}N$ (‰)	Error (‰)	N (ng)	$\delta^{15}N$ (‰)	Error (‰)	N (ng)	$\delta^{15}N$ (‰)	Error (‰)
200	4.77	13.79	0.39	4.23	-6.44	1.19	10.73	9.20	0.44	6.15	2.80	0.47
300	10.12	13.35	0.06	10.49	1.21	0.29	20.94	18.05	0.38	6.72	10.49	0.41
400	3.25	13.14	0.40	5.94	1.12	0.47	3.41	0.93	0.77	0.39	8.59	11.03
500	1.37	12.67	0.70	2.64	-0.82	1.04	1.59	1.06	1.20	1.08	3.99	1.07
600	1.11	12.36	0.88	1.05	15.76	2.49	1.17	-1.76	1.07	0.19	-2.81	9.06
650	0.54	1.46	1.13	-	-	-	0.14	-8.01	22.31	0.44	-5.92	2.49
700	0.60	1.50	1.06	1.58	18.45	1.68	2.02	-0.66	0.71	0.56	-3.81	1.81
750	0.67	9.92	1.25	-	-	-	0.19	-0.19	4.45	0.65	-2.83	1.48
800	0.51	5.32	1.32	1.29	6.51	2.10	0.21	3.00	4.28	0.42	-6.01	2.78
850	0.30	17.73	4.08	-	-	-	0.02	13.02	742.47	0.20	1.98	4.01
900	0.24	25.91	7.55	0.49	6.57	5.21	0.03	-1.29	71.66	0.68	3.67	1.39
950	0.26	41.54	10.68	-	-	-	0.03	2.57	42.25	0.21	23.31	14.22
1000	0.28	62.14		†	53.83		0.01	18.09		0.23	59.21	
1100	0.45	132.33		†	123.03		0.16	22.13		†	120.93	
1200	0.44	153.02		†	201.81		0.03	27.87		0.40	116.88	
1300	0.26	180.50		†	224.46		0.88	39.66		0.49	170.94	
1400	0.15	239.21		†	319.84		1.44	25.71		0.04	90.83	

Table 3.1.5: Nitrogen results for Apollo 17 mare basalts. Note that for 70035, data were only collected in 100 ºC steps (- = not measured, †= blank level). N.B.: High temperature steps containing cosmogenic N have no error reported, since error propagation on such small abundances gives unrealistic uncertainties. However, these high temperature isotopic signatures have been used to calculate cosmogenic N abundances, and these correlate well with reported exposure ages, suggesting that these isotopic data, although associated with very large errors, are fairly reliable.

3.2: Carbon

The stepped combustion results for carbon abundance and isotopic composition of the six mare basalts are listed in Tables 3.2.2 to 3.2.5 and displayed in Figs. 3.2.1(Apollo 11); 3.2.2 (Apollo 12); 3.2.3 (Apollo 14 and 15); and 3.2.4 (Apollo 17). In each sample, the majority (51–98%) of the carbon present is released below 600 ºC, most likely associated with terrestrial contaminants, with variable $\delta^{13}C$ isotopic signatures. Between 1% and 10% of the carbon present is released from the samples at mid-temperature steps (typically between 650 ºC and 900–1000 ºC), apart from sample 15555, which releases 35% of the total carbon present in the sample between 650 ºC and 950 ºC. In the high temperature combustion steps (typically above 900–1000 ºC), very low amounts of carbon (<5%, down to 0% (blank level)) are released from most of the samples (apart from 15555, which releases 14% of the total C present in this range), and are associated with ^{13}C-enriched isotopic signatures.

Sample	Low Temperature Range (< 600 ºC) (% Released)	Mid Temperature Range (600/650 to 900/1000 ºC) (% Released)	High Temperature Range (> 900 ºC) (% Released)
10017	97	2	1
10050	91	5	4
10057	89	10	1
10072	95	4	1
12016	92	6	2
12040	98	1	0 (At blank level)
12047	89	9	2
12064	97	3	0
14053	98	1	1
15386	98	2	0 (At blank level)
15555	51	35	14
70017	94	5	1
70035	94	1	5
74275	90	9	0 (At blank level)
75055	95	3	2
Min. % Released	51	1	0 (At blank level)
Max. % Released	98	35	14

Table 3.2.1: Percentages of the total sample C released across the low temperature, mid temperature, and high temperature ranges (as outlined in the text above), for each mare basalt sample analysed (see Tables 3.2.2 to 3.2.5 for released C abundances in ng).

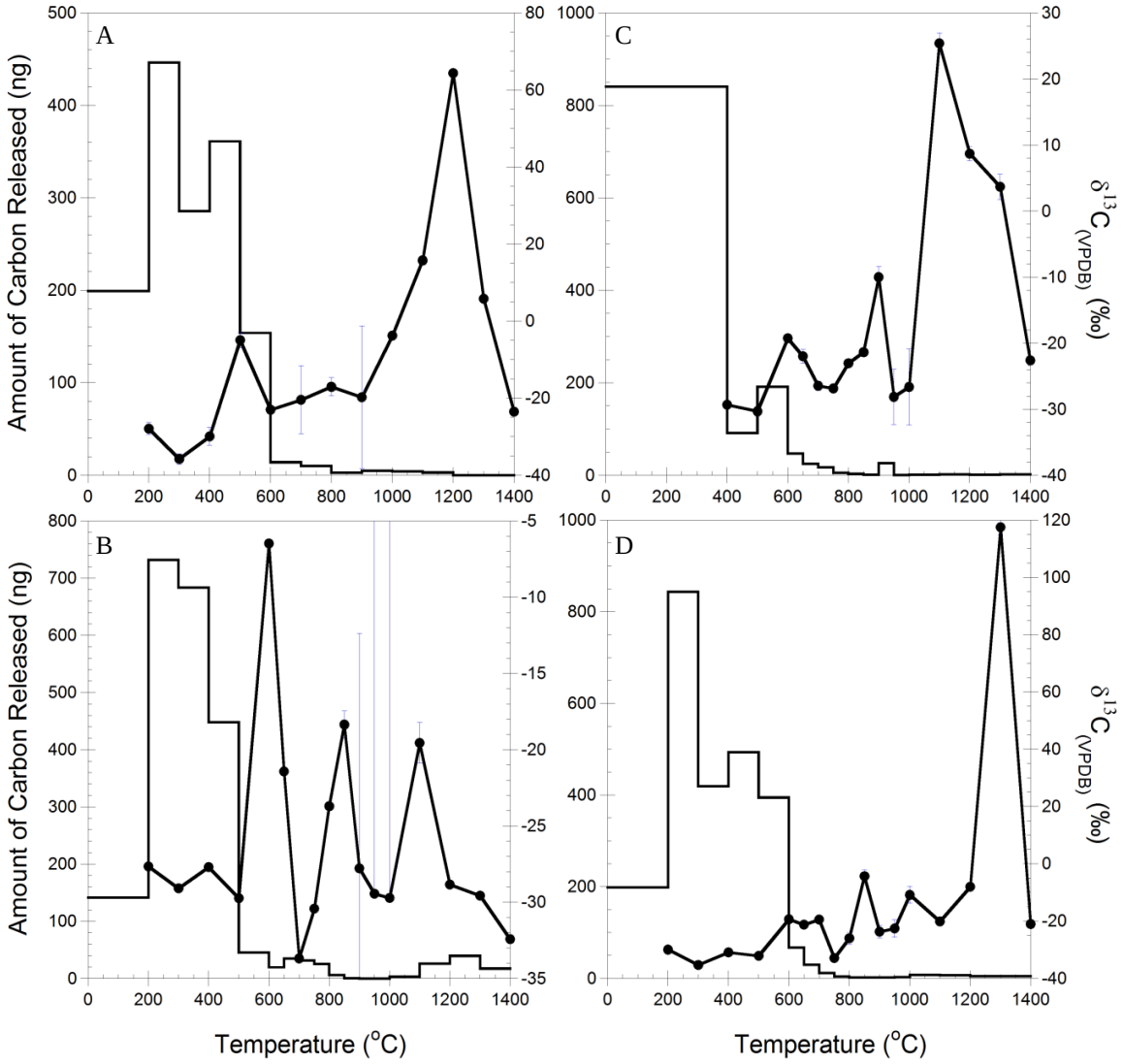

Figure 3.2.1: Step plots of carbon abundances and isotopic compositions in Apollo 11 samples, where A = 10017, B = 10050, C = 10057, and D = 10072. The bar chart represents the amount of carbon released at each step (left axis), and the line with dots represents the isotopic $\delta^{13}C$ signature of carbon released at each step (right axis). N.B.: each plot uses different scales for both the left and right axes. See Table 3.2.2 for data.

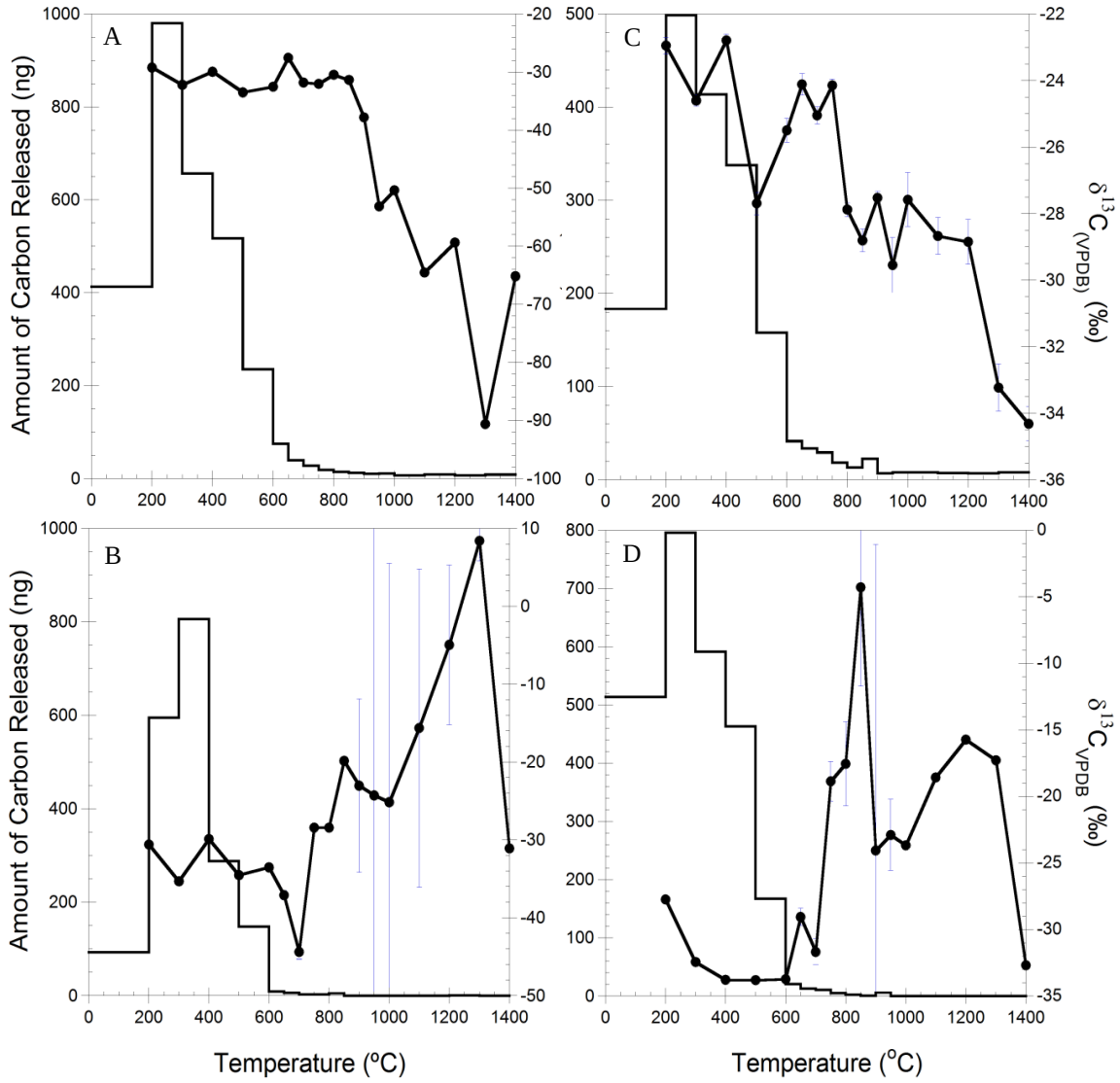

Figure 3.2.2: Step plots of carbon abundances and isotopic compositions in Apollo 12 samples, where A = 12016, B = 12040, C = 12047, and D = 12064. The bar chart represents the amount of carbon released at each step (left axis), and the line with dots represents the isotopic $\delta^{13}C$ signature of carbon released at each step (right axis). N.B.: each plot uses different scales for both the left and right axes. See Table 3.2.3 for data.

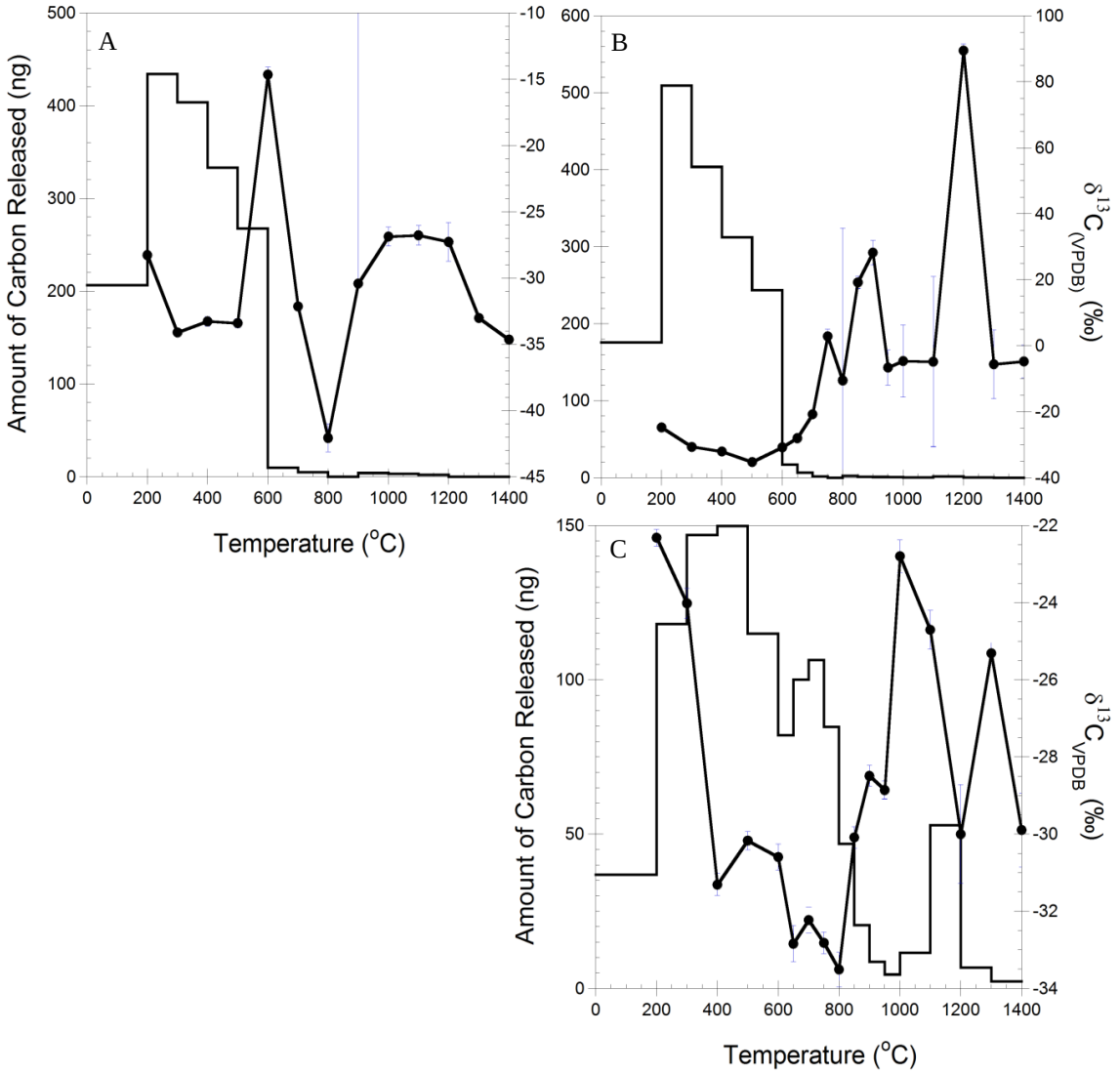

Figure 3.2.3: Step plots of carbon abundances and isotopic compositions in Apollo 14 and Apollo 15 samples, where A = 14053, B = 15386, and C = 15555. The bar chart represents the amount of carbon released at each step (left axis), and the line with dots represents the isotopic $\delta^{13}C$ signature of carbon released at each step (right axis). N.B.: each plot uses different scales for both the left and right axes. See Table 3.2.4 for data.

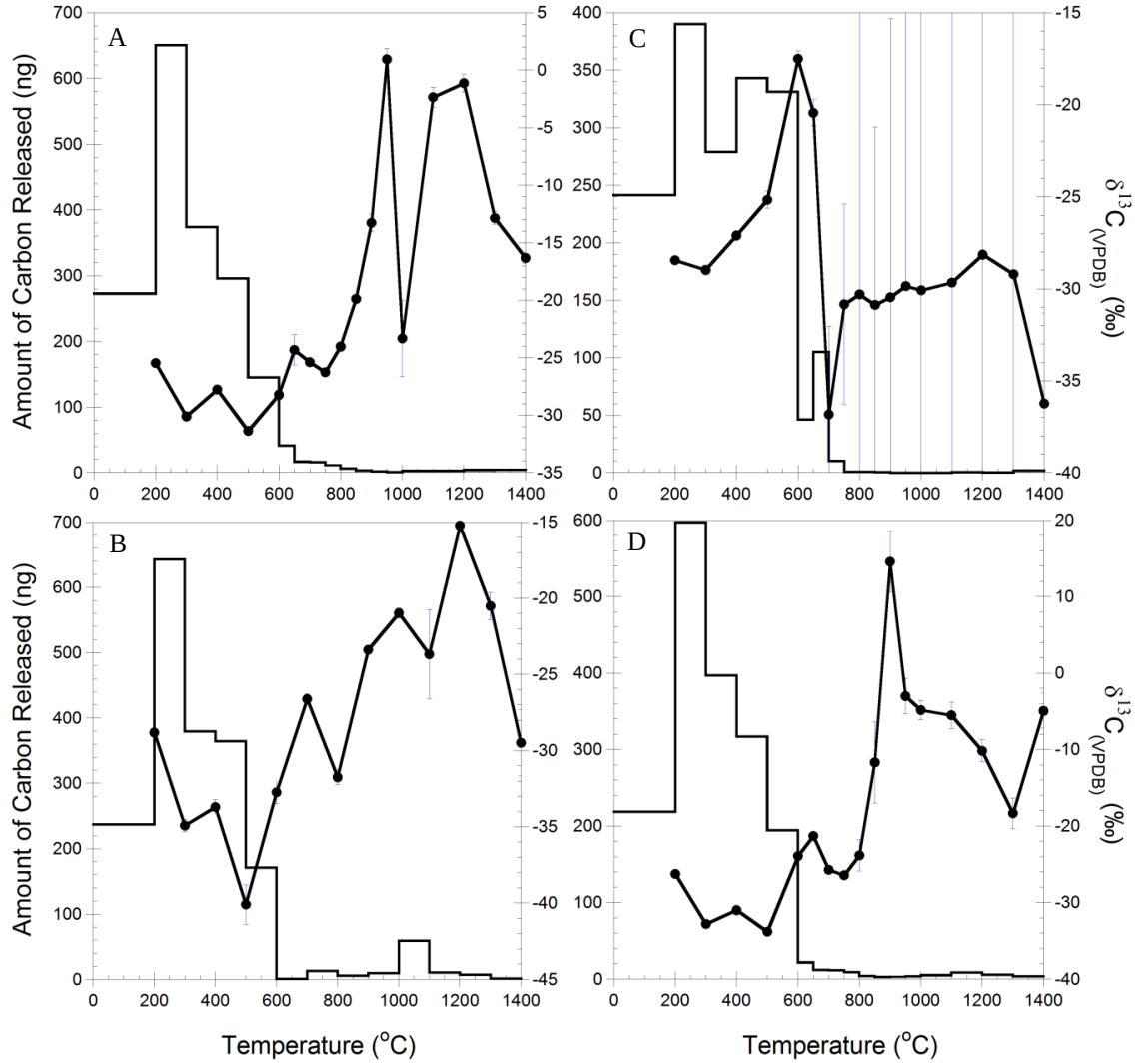

Figure 3.2.4: Step plots of carbon abundances and isotopic compositions in Apollo 17 samples, where A = 70017, B = 70035, C = 74275, and D = 75055. The bar chart represents the amount of carbon released at each step (left axis), and the line with dots represents the isotopic $\delta^{13}C$ signature of carbon released at each step (right axis). N.B.: each plot uses different scales for both the left and right axes. See Table 3.2.5 for data.

Most notably, in basalts 10050, 15555 and 70035 there is a small high temperature release of carbon at 1000–1300 ºC (between 3% and 5% of the total carbon released from these samples), which is relatively ^{13}C-depleted compared to the other high temperature carbon isotope measurements made for the same, and the other powdered mare basalt, samples. Although a similar relative depletion in ^{13}C is seen in several other samples at high temperatures (e.g. 75055), these instances are not found in conjunction with a significantly higher carbon release at the temperature steps in question.

In all of the step plots above, both the carbon abundance and isotopic data have been corrected for any contributions from the system blank (blank correction methods are outlined in the Appendix). Generally, errors (in pale blue) are not displayed for steps where the C abundance from the samples is close to blank levels; due to the error propagation method used to calculate the blank-corrected uncertainties, such a low ratio of sample C to blank abundance generates extremely large errors that are unsuitable/unrealistic. This is illustrated by the inclusion of error bars in the step plot for sample 74275 (graph C in Fig.3.2.4), where errors mostly extend beyond the scale of the graph, despite these errors being several orders of magnitude lower than have been calculated for other samples where sample C abundance is almost identical to blank levels. Therefore, errors are generally not included for other samples where the blank-corrected uncertainties would extend far beyond the scale of the graph.

	10017			10050			10057			10072		
Temperature (°C)	C (ng)	$\delta^{13}C$ (‰)	Error (‰)	C (ng)	$\delta^{13}C$ (‰)	Error (‰)	C (ng)	$\delta^{13}C$ (‰)	Error (‰)	C (ng)	$\delta^{13}C$ (‰)	Error (‰)
200	199.31	-27.88	1.54	141.71	-27.64	0.23	-	-	-	274.21	-29.18	0.24
300	446.39	-35.77	1.33	732.04	-29.08	0.18	-	-	-	919.56	-34.63	0.12
400	285.72	-29.89	2.33	683.47	-27.69	0.18	840.16	-29.30	0.16	508.20	-30.24	0.15
500	361.04	-4.93	1.93	447.99	-29.73	0.19	91.49	-30.31	0.72	582.20	-31.32	0.35
600	153.86	-23.01	0.85	45.35	-6.48	0.19	191.27	-19.26	0.57	423.14	-19.76	0.71
650	-	-	-	19.64	-21.42	0.23	47.11	-21.97	1.04	67.35	-21.18	0.39
700	14.09	-20.40	8.80	35.06	-33.68	0.17	25.01	-26.44	0.69	29.65	-19.43	0.50
750	-	-	-	31.87	-30.42	0.21	17.37	-26.86	0.58	11.77	-32.90	0.51
800	10.10	-17.04	2.39	25.32	-23.70	0.14	5.75	-23.04	0.38	4.42	-25.99	2.06
850	-	-	-	6.14	-18.36	0.90	3.69	-21.36	0.49	2.05	-4.35	2.21
900	2.80	-19.74	18.48	0.49	-27.77	15.39	1.42	-9.99	1.59	2.26	-23.70	2.25
950	-	-	-	0.04	-29.44	768.84	26.28	-28.12	4.16	2.33	-22.55	3.03
1000	4.80	-3.78	3.70	0.07	-29.71	264.48	0.60	-26.61	5.80	3.16	-10.86	2.96
1100	4.08	15.77	1.95	3.42	-19.54	1.34	1.44	25.39	1.58	7.63	-20.08	1.12
1200	2.97	64.36	4.10	26.13	-28.83	0.13	2.10	8.70	1.09	7.07	-7.98	0.66
1300	0.02	5.81		39.64	-29.56	0.16	1.09	3.68	1.93	4.74	117.49	2.71
1400	†	-23.49		17.53	-32.41	0.27	2.35	-22.60	0.77	4.74	-21.02	1.09

Table 3.2.2: Carbon results for Apollo 11 mare basalts. Note that for 10057, data was not collected below 400 ºC, and for 10017, data were only collected in 100 ºC steps (- = not measured, †= blank level). N.B.: Some temperature steps which release carbon only at/close to blank level have no error reported, since error propagation on such small abundances gives unrealistic uncertainties.

	12016			12040			12047			12064		
Temperature (°C)	C (ng)	$\delta^{13}C$ (‰)	Error (‰)	C (ng)	$\delta^{13}C$ (‰)	Error (‰)	C (ng)	$\delta^{13}C$ (‰)	Error (‰)	C (ng)	$\delta^{13}C$ (‰)	Error (‰)
200	413.05	-29.22	0.06	93.09	-30.59	0.16	183.38	-22.95	0.25	513.51	-27.75	0.19
300	980.07	-32.20	0.06	594.65	-35.30	0.30	498.71	-24.61	0.17	795.44	-32.45	0.29
400	656.53	-29.95	0.14	805.40	-29.88	0.21	413.70	-22.79	0.19	591.19	-33.78	0.18
500	517.03	-33.50	0.16	288.02	-34.53	0.46	337.69	-27.69	0.34	463.25	-33.81	0.25
600	235.40	-32.54	0.16	147.77	-33.52	0.47	157.86	-25.50	0.36	166.94	-33.73	0.28
650	74.85	-27.56	0.13	9.33	-37.10	0.60	41.53	-24.11	0.33	20.77	-29.05	0.64
700	39.71	-31.83	0.09	6.39	-44.39	0.90	33.73	-25.05	0.26	12.78	-31.68	0.96
750	27.58	-32.05	0.21	2.65	-28.44	0.29	29.41	-24.15	0.19	10.36	-18.87	1.49
800	18.51	-30.47	0.14	2.65	-28.44	0.29	18.37	-27.88	0.20	4.93	-17.55	3.17
850	14.51	-31.37	0.24	5.15	-19.86	0.50	13.16	-28.81	0.34	2.08	-4.29	7.43
900	12.38	-37.81	0.30	0.32	-23.04	11.12	22.62	-27.52	0.20	0.79	-24.06	22.98
950	10.32	-53.12	0.31	0.11	-24.29	77.95	6.92	-29.55	0.83	5.71	-22.89	2.67
1000	11.00	-50.32	0.25	0.20	-25.15	30.65	8.00	-27.58	0.81	0.15	-23.68	
1100	6.80	-64.52	0.48	0.22	-15.63	20.43	8.06	-28.67	0.55	0.40	-18.59	
1200	9.17	-59.36	0.30	0.24	-4.96	10.24	7.37	-28.85	0.68	0.23	-15.73	
1300	6.70	-90.59	0.44	0.85	8.38	2.54	6.84	-33.22	0.71	0.26	-17.29	
1400	8.67	-65.17	0.30	0.14	-31.09		8.07	-34.32	0.52	0.30	-32.69	

Table 3.2.3: Carbon results for Apollo 12 mare basalts (- = not measured, †= blank level). N.B.: Some temperature steps which release carbon only at/close to blank level have no error reported, since error propagation on such small abundances gives unrealistic uncertainties.

	14053			15386			15555		
Temperature (°C)	C (ng)	$\delta^{13}C$ (‰)	Error (‰)	C (ng)	$\delta^{13}C$ (‰)	Error (‰)	C (ng)	$\delta^{13}C$ (‰)	Error (‰)
200	206.38	-28.28	0.30	175.90	-24.76	0.15	36.85	-22.32	0.21
300	434.21	-34.12	0.21	509.39	-30.60	0.12	118.10	-24.02	0.39
400	403.48	-33.28	0.36	403.72	-32.02	0.23	146.87	-31.31	0.28
500	332.98	-33.41	0.36	312.37	-35.21	0.13	149.84	-30.17	0.24
600	267.54	-14.65	0.56	243.55	-30.77	0.12	114.95	-30.59	0.34
650	-	-	-	17.19	-27.99	0.25	81.98	-32.84	0.46
700	9.86	-32.14	0.29	6.77	-20.74	0.54	100.08	-32.22	0.34
750	-	-	-	1.87	2.86	2.20	106.43	-32.82	0.28
800	4.80	-42.07	1.05	0.18	-10.49	46.16	84.72	-33.51	0.44
850	-	-	-	2.64	19.20	1.86	46.85	-30.08	0.28
900	0.11	-30.42	245.72	1.48	28.22	3.77	20.55	-28.49	0.27
950	-	-	-	0.99	-6.61	5.38	8.61	-28.86	0.23
1000	3.94	-26.88	0.72	0.88	-4.64	10.93	4.53	-22.80	0.42
1100	3.28	-26.77	0.74	0.40	-4.81	25.77	11.53	-24.70	0.50
1200	2.01	-27.27	1.46	1.60	89.41	2.11	52.89	-30.00	1.28
1300	0.02	-33.02		0.40	-5.62	10.44	6.76	-25.31	0.27
1400	0.02	-34.64		†	-4.77	4.96	2.29	-29.89	0.96

Table 3.2.4: Carbon results for Apollo 14 and Apollo 15 mare basalts. Note that for 14053, data were only collected in 100 ºC steps (- = not measured, †= blank level). N.B.: Some temperature steps which release carbon only at/close to blank level have no error reported, since error propagation on such small abundances gives unrealistic uncertainties.

	70017			70035			74275			75055		
Temperature (°C)	C (ng)	$\delta^{13}C$ (‰)	Error (‰)	C (ng)	$\delta^{13}C$ (‰)	Error (‰)	C (ng)	$\delta^{13}C$ (‰)	Error (‰)	C (ng)	$\delta^{13}C$ (‰)	Error (‰)
200	272.87	-25.44	0.36	237.38	-28.81	0.18	241.48	-28.44	0.14	218.49	-26.26	0.39
300	650.68	-30.09	0.23	642.96	-34.92	0.40	390.10	-28.97	0.23	597.33	-32.79	0.12
400	374.16	-27.74	0.16	379.68	-33.70	0.49	278.95	-27.10	0.12	396.99	-30.98	0.19
500	295.85	-31.37	0.34	364.67	-40.09	1.28	343.13	-25.16	0.47	317.04	-33.78	0.15
600	145.41	-28.20	0.40	170.98	-32.72	0.78	331.12	-17.51	0.42	194.39	-23.94	0.28
650	41.39	-24.30	1.31	-	-	-	46.35	-20.44	0.74	21.84	-21.28	0.36
700	16.72	-25.38	0.35	0.81	-26.62	0.35	105.09	-36.83	4.79	12.19	-25.72	0.36
750	16.24	-26.25	0.31	-	-	-	10.21	-30.84	5.45	11.54	-26.43	0.40
800	11.34	-24.01	0.30	12.94	-31.74	0.49	0.91	-30.30	15.97	9.17	-23.82	2.05
850	6.29	-19.87	0.34	-	-	-	0.75	-30.87	9.67	4.11	-11.68	5.30
900	3.22	-13.26	0.73	5.90	-23.38	0.27	0.50	-30.45	15.13	2.92	14.55	4.01
950	2.25	0.94	0.95	-	-	-	†	-29.85	355.34	3.05	-3.01	2.30
1000	0.92	-23.30	3.32	9.59	-20.97	0.33	†	-30.08	18.02	3.86	-4.83	1.24
1100	2.97	-2.35	0.87	59.32	-23.68	2.93	0.18	-29.66	88.64	5.23	-5.52	1.73
1200	3.13	-1.14	0.76	10.77	-15.22	0.51	0.58	-28.14	15.19	8.88	-10.17	1.45
1300	4.23	-12.83	0.57	7.25	-20.51	0.89	0.33	-29.20	42.42	5.72	-18.34	2.02
1400	4.56	-16.31	0.47	1.31	-29.48	2.18	1.86	-36.24	4.93	3.91	-4.95	2.28

Table 3.2.5: Carbon results for Apollo 17 mare basalts. Note that for 70035, data were only collected in 100 ºC steps (- = not measured, †= blank level). Note the large errors present in high temperature steps for sample 74275, which releases carbon only at/close to blank level; this low abundance over blank levels gives rise to large uncertainties during the blank correction calculations.

3.3: Noble Gases

The stepped combustion results for noble gases are provided in Tables 3.3.1 through to 3.3.9. Ne isotope ratios (Table 3.3.10) have been corrected for mass fractionation in the quadrupole mass spectrometer during analyses and for the contribution of a terrestrial atmospheric blank. For most of the powdered mare basalt samples (except 12064,138), the Ne content was so low that its isotopic composition could not be measured with any reasonable precision because of interference with the mas of doubly charged CO_2 at ^{22}Ne. In these cases, only amounts of $^{21}Ne_{(cosmogenic)}$ and $^{20}Ne_{(trapped)}$ have been calculated using the raw data by applying blank corrections for each isotope separately for each temperature step. For that, we used the release pattern of ^{21}Ne and ^{20}Ne, taking the data points outside the release peaks for the isotopes as the blank. Then the temperature steps with the blank level amounts were fitted with a linear of polynomial fit in order to interpolate the data for the temperature steps where the peaks of ^{21}Ne and ^{20}Ne are observed. This same blank correction approach was also used for abundances of isotopes of He and Ar (although a linear trendline (not a polynomial) was used to interpolate the blank contributions for steps containing He peaks). The $^{21}Ne/^{20}Ne$ ratio has been used to take into account the contribution of $^{21}Ne_{(trapped)}$ in order to calculate amounts of $^{21}Ne_{(cosmogenic)}$. The Ne concentration in sample 12064,138 turned out to be high enough in order to measure its isotopic composition and correct it for the blank contribution, since the contribution from doubly charged CO_2 was almost negligible (mass interference due to the presence of doubly charged CO_2 only became significant when the 44/22 ratio was ≥ 100; in both analyses of 12064,138, the 44/22 ratio was ≤ 50). He, Ne, and Ar were only measured in the second run of basalt 10017 (see Table 2.1). Three different noble gas components have been detected in these samples: cosmogenic ^{21}Ne, radiogenic ^{4}He and ^{40}Ar, and trapped

^{20}Ne and ^{36}Ar; in most cases, abundances recorded from these analyses match well with previous noble gas studies of some of these same samples.

	10017	10050	10057	10072	12016	12040	12047	12064	14053	15386	15555	70017	70035	74275	75055
Temperature (°C)	^{4}He (cc/g^{-1})	^{4}He (cc/g^{-1})	^{4}He (cc/g^{-1})	^{4}He (cc/g^{-1})	^{4}He (cc/g^{-1})	^{4}He (cc/g^{-1})	^{4}He (cc/g^{-1})	^{4}He (cc/g^{-1})	^{4}He (cc/g^{-1})	^{4}He (cc/g^{-1})	^{4}He (cc/g^{-1})	^{4}He (cc/g^{-1})	^{4}He (cc/g^{-1})	^{4}He (cc/g^{-1})	^{4}He (cc/g^{-1})
200	7.87E-11	5.06E-06	-	8.18E-09	nd	nd	nd	nd	2.23E-09	1.21E-06	4.12E-08	1.89E-06	nd	4.57E-09	9.41E-10
300	2.15E-05	1.71E-05	1.50E-04	3.38E-05	8.10E-06	3.68E-06	9.35E-06	2.28E-05	1.59E-06	2.98E-05	2.51E-06	3.91E-07	6.77E-06	4.01E-06	3.73E-06
400	1.11E-04	3.07E-05	1.25E-04	1.28E-04	2.92E-05	1.44E-05	2.67E-05	5.32E-05	5.91E-06	1.28E-04	6.77E-06	9.84E-07	2.39E-05	1.73E-05	1.24E-05
500	1.99E-04	3.97E-05	3.62E-05	1.90E-04	4.88E-05	3.67E-05	3.33E-05	6.51E-05	1.12E-05	1.74E-04	1.49E-05	1.89E-06	4.35E-05	4.14E-05	2.37E-05
600	9.41E-05	2.84E-05	4.72E-05	7.77E-05	2.02E-05	2.67E-05	9.08E-06	1.89E-05	3.89E-06	5.16E-05	9.66E-06	1.31E-06	1.89E-05	2.45E-05	9.69E-06
650	1.18E-05	8.09E-06	1.22E-05	2.70E-05	2.66E-06	3.97E-06	2.46E-06	1.62E-06	-	nd	2.27E-06	3.20E-07	-	5.30E-06	2.13E-06
700	6.26E-06	5.69E-06	8.47E-06	1.82E-05	1.00E-06	1.64E-06	9.64E-07	1.45E-07	1.70E-06	nd	1.16E-06	2.56E-07	6.86E-06	2.92E-06	1.31E-06
750	4.68E-06	4.05E-06	6.92E-06	1.31E-05	2.59E-07	8.51E-07	8.57E-07	nd	-	nd	9.53E-07	nd	-	8.23E-07	8.79E-07
800	3.48E-06	5.23E-06	4.75E-06	1.11E-05	3.50E-08	7.37E-07	4.89E-07	nd	8.71E-07	nd	7.10E-07	4.16E-08	4.01E-06	6.62E-07	1.27E-06
850	4.35E-06	1.48E-06	5.54E-06	9.96E-06	2.14E-07	2.36E-06	2.34E-08	7.88E-08	-	nd	6.04E-07	2.76E-08	-	1.13E-06	5.86E-07
900	4.36E-06	8.05E-07	6.06E-06	8.92E-06	nd	4.84E-07	nd	1.37E-08	5.84E-07	nd	2.75E-07	1.44E-08	3.86E-06	7.10E-07	6.84E-07
950	5.37E-06	5.36E-07	2.52E-07	9.64E-06	6.13E-07	9.96E-07	nd	4.38E-06	-	3.29E-06	nd	6.53E-08	-	1.85E-06	7.39E-07
1000	8.86E-06	2.19E-08	9.37E-07	6.35E-06	nd	1.41E-06	nd	nd	8.35E-07	9.09E-06	nd	1.39E-09	5.25E-06	1.12E-06	8.09E-07
1100	1.85E-06	9.02E-09	2.69E-07	1.13E-06	nd	1.24E-07	9.97E-08	nd	1.90E-07	1.91E-06	nd	nd	2.24E-06	2.51E-07	2.27E-08
1200	nd	nd	6.99E-08	nd	nd	nd	nd	nd	nd	nd	nd	nd	3.38E-06	nd	nd
1300	nd	nd	2.15E-10	nd	nd	nd	nd	nd	nd	nd	nd	nd	nd	4.55E-08	1.71E-07
1400	5.52E-10	8.38E-08	2.31E-10	4.10E-08	7.26E-07	nd	7.43E-08	nd	1.45E-08	nd	2.12E-07	nd	nd	6.38E-07	nd
Total	4.76E-04	1.47E-04	4.04E-04	5.34E-04	1.12E-04	9.40E-05	8.34E-05	1.66E-04	2.68E-05	3.99E-04	4.01E-05	7.19E-06	1.19E-04	1.03E-04	5.82E-05
Literature Values	4.91E-04[a] 4.98E-04[b]	8.00E-04[y]	6.00E-04[c]	7.50E-04[y]		7.60E-05[c]		1.81E-04[a]	3.18E-04[d]		8.97E-05[d]			8.80E-05[x]	

Table 3.3.1: Helium results for all powdered mare basalt samples (- = not measured; nd = not detected). Note that data for 10017 were collected during Run 2 (see Table 2.1). [a] Hintenberger et al. (1971); [b] Huneke et al. (1972); [c] Eugster et al. (1984a); [d] Husain et al. (1972); [y] Funkhouser et al. (1970); [x] Eugster et al. (1977).

	10017		10050		10057		10072	
Temperature (°C)	^{20}Ne (cc/g^{-1})	^{21}Ne (cc/g^{-1})	^{20}Ne (cc/g^{-1})	^{21}Ne (cc/g^{-1})	^{20}Ne (cc/g^{-1})	^{21}Ne (cc/g^{-1})	^{20}Ne (cc/g^{-1})	^{21}Ne (cc/g^{-1})
200	nd	nd	nd	9.34E-10	-	-	0	0
300	1.29E-08	3.31E-10	nd	nd	3.25E-07	1.39E-09	0	0
400	3.85E-09	8.68E-10	1.26E-07	nd	5.36E-07	1.05E-09	9.82E-08	1.30E-09
500	2.68E-09	nd	2.38E-07	nd	5.47E-08	2.81E-13	2.03E-07	3.67E-09
600	1.96E-08	4.18E-09	2.26E-07	nd	7.10E-08	1.07E-09	1.32E-07	4.95E-09
650	2.67E-09	nd	3.83E-08	nd	nd	1.27E-09	1.89E-08	4.66E-09
700	nd	5.58E-09	nd	1.25E-09	2.95E-08	1.35E-09	9.07E-10	7.81E-09
750	nd	1.27E-08	nd	1.34E-09	5.65E-10	2.85E-09	0	1.22E-08
800	1.85E-08	1.87E-08	nd	7.50E-09	nd	2.68E-09	1.34E-08	1.72E-08
850	3.59E-08	3.54E-08	nd	6.49E-09	1.08E-09	3.64E-09	1.36E-08	2.39E-08
900	4.16E-08	4.72E-08	nd	7.50E-09	nd	5.35E-09	3.04E-08	2.99E-08
950	3.37E-08	4.82E-08	2.65E-08	1.41E-08	nd	2.35E-10	4.54E-08	3.75E-08
1000	7.03E-08	7.44E-08	3.25E-08	1.81E-08	nd	1.62E-09	3.54E-08	3.62E-08
1100	6.81E-08	7.32E-08	2.33E-08	2.33E-08	nd	2.64E-09	4.04E-08	4.47E-08
1200	1.97E-08	2.70E-08	nd	nd	nd	1.62E-12	3.36E-08	2.61E-08
1300	6.66E-10	7.02E-11	5.03E-08	1.75E-09	nd	1.90E-12	2.78E-08	1.53E-08
1400	nd	nd	nd	nd	nd	nd	0	0
Total	3.30E-07	3.48E-07	7.61E-07	8.23E-08	1.02E-06	2.52E-08	6.93E-07	2.65E-07
Literature Values	7.92E-07[a]	4.66E-07[a] 4.80E-07[b]	9.00E-06[y]	5.10E-07[y]	1.10E-06[y]	5.20E-08[c]	2.35E-06[y]	2.60E-07[y]

Table 3.3.2: Neon results for Apollo 11 powdered mare basalt samples (- = not measured; nd = not detected). Note that data for 10017 were collected during Run 2 (see Table 2.1). [a] Hintenberger et al. (1971); [b] Huneke et al. (1972); [c] Eugster et al. (1984a); [y] Funkhouser et al. (1970).

	12016		12040		12047		12064			
Temperature (°C)	^{20}Ne (cc/g^{-1})	^{21}Ne (cc/g^{-1})	^{20}Ne (cc/g^{-1})	^{21}Ne (cc/g^{-1})	^{20}Ne (cc/g^{-1})	^{21}Ne (cc/g^{-1})	^{20}Ne (cc/g^{-1})	^{21}Ne (cc/g^{-1})	^{21}Ne/^{22}Ne	^{20}Ne/^{22}Ne
200	2.11E-09	1.71E-11	nd	nd	nd	nd	1.52E-11	2.15E-08	0.71 ± 0.04	0.15 ± 0.01
300	nd	nd	nd	nd	4.22E-08	6.26E-11	5.19E-08	4.52E-08	0.69 ± 0.03	0.88 ± 0.04
400	4.20E-08	7.97E-11	nd	3.26E-09	2.30E-08	nd	2.66E-07	1.35E-08	0.33 ± 0.02	6.82 ± 0.34
500	7.80E-08	nd	nd	6.91E-09	3.49E-09	nd	3.98E-07	7.29E-09	0.16 ± 0.01	9.39 ± 0.47
600	7.81E-08	1.54E-09	7.79E-09	1.16E-08	3.71E-08	1.22E-09	2.44E-07	8.62E-09	0.25 ± 0.01	7.54 ± 0.38
650	1.57E-08	5.99E-10	2.74E-09	6.60E-09	3.23E-08	3.03E-10	1.11E-08	7.35E-09	0.59 ± 0.03	1.37 ± 0.07
700	1.95E-08	6.35E-09	8.52E-10	1.19E-08	2.43E-09	nd	nd	1.07E-08	nd	nd
750	1.06E-08	2.36E-08	2.13E-08	3.24E-08	1.93E-08	1.39E-09	nd	1.52E-08	nd	nd
800	nd	3.46E-08	6.14E-08	9.04E-08	4.26E-08	2.21E-09	nd	1.90E-08	nd	nd
850	1.08E-08	2.81E-08	1.01E-07	9.91E-08	6.38E-11	2.26E-09	nd	2.52E-08	nd	nd
900	2.59E-08	2.75E-08	2.96E-08	5.33E-08	nd	2.77E-09	nd	3.05E-08	nd	nd
950	2.32E-08	2.18E-08	2.21E-08	4.41E-08	2.31E-08	3.65E-09	7.03E-08	6.01E-08	0.81 ± 0.04	1.05 ± 0.05
1000	4.73E-08	2.91E-08	4.50E-09	3.43E-08	nd	3.78E-09	nd	4.98E-08	nd	nd
1100	nd	2.22E-08	4.64E-08	7.48E-08	2.39E-08	8.32E-09	2.84E-08	5.54E-08	0.89 ± 0.04	0.49 ± 0.02
1200	3.50E-09	7.20E-12	1.87E-08	3.64E-08	nd	2.14E-09	1.79E-09	3.30E-08	nd	nd
1300	8.61E-09	nd	3.86E-08	2.55E-08	2.53E-08	1.31E-09	nd	1.95E-08	nd	nd
1400	nd	nd	8.17E-09	nd	nd	nd	nd	1.84E-10	nd	nd
Total	3.65E-07	1.96E-07	3.63E-07	5.31E-07	2.75E-07	2.94E-08	1.07E-06	4.22E-07*		
Literature Values			5.40E-08[c]	4.11E-07[c] 4.20E-07[h]			2.95E-07[a]	3.13E-07[a]		

Table 3.3.3: Neon results for Apollo 12 powdered mare basalt samples (- = not measured; nd = not detected). [a] Hintenberger et al. (1971); [c] Eugster et al. (1984a); [h] Bogard et al. (1971). *^{21}Ne $_{(cosmogenic)}$ = 3.18E-07 cc/g^{-1}.

	14053		15386		15555	
Temperature (°C)	^{20}Ne (cc/g^{-1})	^{21}Ne (cc/g^{-1})	^{20}Ne (cc/g^{-1})	^{21}Ne (cc/g^{-1})	^{20}Ne (cc/g^{-1})	^{21}Ne (cc/g^{-1})
200	nd	nd	nd	2.62E-09	nd	nd
300	1.89E-08	5.81E-12	2.61E-08	1.84E-08	nd	nd
400	2.92E-08	nd	8.89E-08	1.72E-08	nd	nd
500	6.78E-08	7.95E-10	1.15E-07	1.59E-08	nd	nd
600	3.87E-08	6.09E-10	5.68E-08	9.25E-09	nd	nd
650	-	-	nd	7.10E-09	nd	nd
700	1.25E-08	1.13E-09	nd	1.05E-08	nd	nd
750	-	-	1.26E-08	1.60E-08	nd	nd
800	1.34E-08	2.44E-09	4.40E-09	2.47E-08	nd	nd
850	-	-	1.38E-08	3.48E-08	nd	6.42E-10
900	nd	3.83E-09	2.05E-08	4.39E-08	nd	5.02E-09
950	-	-	2.42E-08	4.82E-08	nd	9.35E-09
1000	1.82E-09	6.99E-09	2.36E-08	4.51E-08	nd	6.87E-09
1100	2.41E-08	7.21E-09	2.63E-08	4.91E-08	nd	9.07E-09
1200	1.53E-08	2.66E-09	nd	2.93E-08	nd	nd
1300	5.78E-10	2.66E-10	3.85E-09	2.27E-08	nd	nd
1400	2.26E-09	nd	nd	1.15E-10	nd	nd
Total	2.25E-07	2.59E-08	4.16E-07	3.95E-07	nd	3.10E-08
Literature Values	1.20E-07[d]	2.21E-08[d]			7.97E-07[d]	1.15E-07[d]

Table 3.3.4: Neon results for Apollo 14 and Apollo 15 powdered mare basalt samples (- = not measured; nd = not detected). Note that data for 14053 were only collected in 100 ºC steps. [d] Husain et al. (1972).

	70017		70035		74275		75055	
Temperature (°C)	^{20}Ne (cc/g^{-1})	^{21}Ne (cc/g^{-1})	^{20}Ne (cc/g^{-1})	^{21}Ne (cc/g^{-1})	^{20}Ne (cc/g^{-1})	^{21}Ne (cc/g^{-1})	^{20}Ne (cc/g^{-1})	^{21}Ne (cc/g^{-1})
200	nd	nd	nd	nd	nd	nd	nd	1.47E-14
300	nd	nd	nd	nd	1.65E-09	nd	1.73E-09	4.55E-10
400	nd	3.29E-10	nd	nd	nd	2.76E-10	2.59E-08	8.14E-10
500	nd	2.07E-11	nd	nd	6.57E-09	6.99E-10	nd	1.14E-09
600	nd	2.82E-10	4.23E-10	7.30E-10	2.29E-08	1.57E-10	1.59E-08	2.08E-09
650	nd	4.57E-10	-	-	nd	nd	1.72E-08	2.50E-09
700	nd	1.53E-10	nd	5.99E-09	7.69E-09	1.04E-11	3.20E-09	3.99E-09
750	nd	nd	-	-	1.34E-08	nd	1.75E-08	5.11E-09
800	nd	1.74E-09	1.17E-08	1.16E-08	nd	1.44E-09	2.22E-08	8.57E-09
850	nd	2.66E-09	-	-	5.35E-08	3.04E-09	nd	8.73E-09
900	nd	3.44E-09	3.24E-08	2.06E-08	8.15E-09	3.27E-09	1.27E-09	1.23E-08
950	nd	3.91E-09	-	-	6.95E-08	4.76E-09	nd	1.57E-08
1000	nd	5.13E-09	4.81E-08	3.02E-08	nd	2.96E-09	nd	1.74E-08
1100	nd	6.42E-09	5.46E-08	2.57E-08	3.96E-08	4.28E-09	nd	2.03E-08
1200	nd	3.86E-09	1.23E-07	1.02E-08	nd	2.71E-09	4.38E-09	1.49E-08
1300	nd	1.28E-12	nd	nd	1.03E-08	5.33E-10	3.89E-09	8.91E-09
1400	nd	nd	2.00E-09	2.79E-09	nd	1.12E-12	nd	1.03E-13
Total	0	2.84E-08	2.72E-07	1.08E-07	2.33E-07	2.41E-08	1.13E-07	1.23E-07
Literature Values					3.44E-08[x]	3.49E-08[x]		

Table 3.3.5: Neon results for Apollo 17 powdered mare basalt samples (- = not measured; nd = not detected). Note that data for 70035 were only collected in 100 ºC steps. [x] Eugster et al. (1977).

	10017		10050		10057		10072	
Temperature (°C)	^{40}Ar (cc/g^{-1})	^{36}Ar (cc/g^{-1})	^{40}Ar (cc/g^{-1})	^{36}Ar (cc/g^{-1})	^{40}Ar (cc/g^{-1})	^{36}Ar (cc/g^{-1})	^{40}Ar (cc/g^{-1})	^{36}Ar (cc/g^{-1})
200	nd	nd	nd	1.15E-12	-	-	nd	1.51E-10
300	1.44E-06	nd	3.38E-07	3.88E-12	-	-	4.97E-06	nd
400	4.29E-06	2.93E-09	7.22E-07	5.37E-09	2.76E-05	6.26E-08	1.22E-05	nd
500	5.57E-06	6.21E-09	1.21E-06	2.20E-08	2.23E-06	nd	1.53E-05	4.02E-09
600	7.90E-06	1.42E-08	1.73E-06	5.32E-08	9.40E-06	1.20E-08	1.42E-05	1.32E-08
650	2.91E-06	8.43E-09	1.05E-06	4.99E-08	4.97E-06	7.56E-09	6.74E-06	1.23E-08
700	2.86E-06	1.15E-08	1.17E-06	5.43E-08	4.70E-06	9.85E-09	5.15E-06	1.94E-08
750	2.21E-06	8.71E-09	8.18E-07	4.56E-08	4.29E-06	9.58E-09	4.22E-06	2.53E-08
800	1.79E-06	5.68E-09	7.88E-07	3.68E-08	3.05E-06	5.10E-09	2.89E-06	2.03E-08
850	1.20E-06	4.75E-09	3.97E-07	1.48E-08	2.17E-06	1.96E-09	1.95E-06	1.32E-08
900	9.05E-07	nd	3.87E-07	9.18E-09	1.59E-06	nd	1.43E-06	3.39E-09
950	7.67E-07	nd	4.62E-07	4.08E-09	1.81E-06	4.58E-09	1.11E-06	nd
1000	1.39E-06	9.49E-09	4.31E-07	1.44E-10	3.23E-07	nd	7.11E-07	nd
1100	1.34E-06	2.21E-08	3.38E-07	nd	4.50E-07	2.19E-11	1.00E-06	3.06E-09
1200	4.58E-07	4.11E-08	2.44E-08	nd	3.49E-07	1.93E-09	5.17E-07	2.55E-09
1300	nd	5.83E-08	nd	3.16E-10	nd	7.08E-10	nd	nd
1400	nd	nd	2.03E-08	nd	nd	nd	nd	nd
Total	3.50E-05	1.93E-07	9.89E-06	2.96E-07	6.29E-05	1.16E-07	7.24E-05	1.17E-07
Literature Values	4.95E-05[a] 4.79E-05[b]	4.65E-07[a]	2.50E-05[y]	1.50E-06[y]	4.30E-05[c] 4.72E-05[z]	1.90E-07[y]	7.60E-05[y]	4.10E-07[y]

Table 3.3.6: Argon results for Apollo 11 powdered mare basalt samples (- = not measured; nd = not detected). Note that data for 10017 were collected during Run 2 (see Table 2.1). [a] Hintenberger et al. (1971); [b] Huneke et al. (1972); [c] Eugster et al. (1984a); [z] Marti et al. (1970); [y] Funkhouser et al. (1970).

	12016		12040		12047		12064	
Temperature (°C)	^{40}Ar (cc/g^{-1})	^{36}Ar (cc/g^{-1})	^{40}Ar (cc/g^{-1})	^{36}Ar (cc/g^{-1})	^{40}Ar (cc/g^{-1})	^{36}Ar (cc/g^{-1})	^{40}Ar (cc/g^{-1})	^{36}Ar (cc/g^{-1})
200	nd	nd	nd	8.56E-12	nd	nd	3.99E-07	7.39E-11
300	4.73E-09	nd	2.48E-07	3.12E-10	5.21E-07	nd	6.43E-07	nd
400	nd	nd	8.53E-07	2.01E-10	1.06E-06	9.20E-10	1.39E-06	2.85E-09
500	6.90E-07	3.69E-09	1.52E-06	6.32E-09	1.92E-06	3.54E-09	2.27E-06	1.41E-08
600	1.81E-06	1.22E-08	2.06E-06	1.07E-08	3.18E-06	6.08E-09	3.03E-06	2.98E-08
650	3.82E-07	7.45E-09	1.49E-06	5.84E-09	2.47E-06	4.57E-09	2.14E-06	2.24E-08
700	1.39E-06	1.56E-08	1.82E-06	7.91E-09	2.48E-06	5.29E-09	2.02E-06	2.96E-08
750	1.02E-06	1.61E-08	1.82E-06	8.08E-09	2.23E-06	4.47E-09	1.70E-06	3.60E-08
800	5.08E-07	1.06E-08	1.36E-06	5.39E-09	1.60E-06	2.77E-09	1.21E-06	2.46E-08
850	1.68E-07	4.91E-09	1.06E-06	3.88E-09	9.91E-07	2.27E-10	6.74E-07	1.15E-08
900	2.67E-08	2.93E-09	2.00E-07	nd	5.85E-07	nd	*	*
950	2.13E-08	3.04E-09	9.39E-08	nd	2.14E-07	nd	4.15E-07	5.34E-09
1000	nd	5.00E-09	8.59E-09	nd	1.23E-07	nd	nd	nd
1100	nd	7.39E-09	nd	3.37E-09	nd	2.33E-09	2.76E-08	9.91E-09
1200	nd	9.06E-09	nd	nd	nd	nd	2.61E-08	8.01E-09
1300	1.91E-08	8.20E-09	nd	nd	nd	nd	nd	nd
1400	5.48E-07	nd	8.34E-08	nd	4.20E-07	5.20E-10	2.18E-08	nd
Total	6.59E-06	1.06E-07	1.26E-05	5.20E-08	1.78E-05	3.07E-08	1.60E-05	1.94E-07
Literature Values			9.90E-06[c]	1.48E-07[c] 2.20E-07[h]			1.65E-05[a]	1.91E-07[a]

Table 3.3.7: Argon results for Apollo 12 powdered mare basalt samples (- = not measured; nd = not detected; * = data not collected). [a] Hintenberger et al. (1971); [c] Eugster et al. (1984a); [h] Bogard et al. (1971).

	14053		15386		15555	
Temperature (°C)	^{40}Ar (cc/g^{-1})	^{36}Ar (cc/g^{-1})	^{40}Ar (cc/g^{-1})	^{36}Ar (cc/g^{-1})	^{40}Ar (cc/g^{-1})	^{36}Ar (cc/g^{-1})
200	nd	nd	nd	nd	nd	1.39E-10
300	1.45E-06	7.38E-09	8.09E-06	1.59E-09	2.64E-07	nd
400	3.87E-06	1.30E-08	1.85E-05	8.11E-09	3.57E-07	3.02E-10
500	7.47E-06	1.70E-08	1.98E-05	1.60E-08	6.27E-07	1.10E-09
600	1.18E-05	2.52E-08	1.47E-05	2.72E-08	1.02E-06	5.19E-09
650	-	-	5.30E-06	2.02E-08	7.72E-07	4.00E-09
700	1.36E-05	3.32E-08	4.91E-06	2.30E-08	7.75E-07	2.48E-09
750	-	-	4.22E-06	2.20E-08	7.79E-07	3.73E-09
800	9.99E-06	2.93E-08	3.44E-06	1.64E-08	6.51E-07	3.39E-09
850	-	-	2.23E-06	1.01E-08	5.36E-07	2.80E-09
900	5.18E-06	1.56E-08	8.90E-07	2.31E-09	3.34E-07	5.71E-10
950	-	-	2.69E-07	nd	1.32E-07	1.05E-10
1000	3.58E-06	6.45E-09	nd	nd	nd	6.15E-10
1100	2.47E-06	5.72E-09	nd	1.04E-09	nd	4.77E-09
1200	1.61E-06	nd	nd	nd	nd	9.92E-09
1300	nd	nd	nd	nd	6.12E-09	2.08E-08
1400	nd	nd	nd	nd	6.55E-08	1.10E-09
Total	6.10E-05	1.53E-07	8.23E-05	1.48E-07	6.32E-06	6.10E-08
Literature Values	6.42E-05[d]	4.98E-08[d] 3.00E-08[f]			9.13E-06[d] 7.32E-06[e]	1.85E-07[d] 9.11E-08[e]

Table 3.3.8: Argon results for Apollo 14 and Apollo 15 powdered mare basalt samples (- = not measured; nd = not detected). [d] Husain et al. (1972); [e] York et al. (1972); [f] Eugster et al. (1984b).

	70017		70035		74275		75055	
Temperature (°C)	^{40}Ar (cc/g^{-1})	^{36}Ar (cc/g^{-1})	^{40}Ar (cc/g^{-1})	^{36}Ar (cc/g^{-1})	^{40}Ar (cc/g^{-1})	^{36}Ar (cc/g^{-1})	^{40}Ar (cc/g^{-1})	^{36}Ar (cc/g^{-1})
200	nd	nd	8.73E-11	2.42E-09	nd	2.67E-11	nd	nd
300	8.87E-09	5.86E-11	1.15E-06	nd	7.83E-07	nd	5.55E-08	4.58E-09
400	1.84E-06	1.86E-08	2.18E-06	4.19E-09	1.63E-06	9.35E-11	2.84E-07	2.16E-10
500	1.36E-06	2.13E-08	3.68E-06	3.38E-09	2.58E-06	1.73E-09	1.08E-06	3.10E-09
600	1.99E-06	3.00E-08	5.24E-06	5.64E-09	3.42E-06	1.96E-09	2.31E-06	5.62E-09
650	1.07E-06	2.15E-08	-	-	2.41E-06	2.13E-09	1.52E-06	3.77E-09
700	9.52E-07	2.03E-08	5.96E-06	5.78E-09	1.76E-06	1.44E-09	1.38E-06	3.92E-09
750	9.29E-07	1.88E-08	-	-	1.09E-06	8.64E-10	1.21E-06	3.90E-09
800	7.04E-07	1.48E-08	3.94E-06	3.42E-09	1.04E-06	7.65E-10	9.22E-07	3.04E-09
850	3.89E-07	8.04E-09	-	-	8.45E-07	1.44E-09	2.91E-07	9.86E-10
900	3.18E-07	6.77E-09	2.10E-06	2.46E-09	4.74E-07	9.71E-10	1.10E-07	9.58E-11
950	8.48E-09	nd	-	-	2.02E-07	4.34E-10	1.78E-08	nd
1000	7.05E-08	nd	6.73E-07	nd	7.82E-08	3.49E-10	nd	nd
1100	1.62E-07	9.82E-10	6.12E-07	5.37E-09	nd	1.34E-09	4.08E-08	3.71E-10
1200	1.94E-07	1.56E-09	1.26E-09	1.99E-10	nd	9.10E-10	9.66E-08	9.26E-10
1300	4.82E-09	nd	5.16E-09	nd	nd	2.37E-08	1.24E-09	nd
1400	2.52E-08	nd	2.37E-09	nd	nd	nd	nd	nd
Total	1.00E-05	1.63E-07	2.55E-05	3.29E-08	1.63E-05	3.81E-08	9.31E-06	3.05E-08
Literature Values			1.53E-05[g]	8.41E-08[g]	1.98E-05[x]			

Table 3.3.9: Argon results for Apollo 17 powdered mare basalt samples (- = not measured; nd = not detected). Note that data for 70035 were only collected in 100 ºC steps. [g] Stettler et al. (1973); [x] Eugster et al. (1977).

3.4: Results (Unpowdered Mare Basalt Chip)

In addition to the fifteen powdered mare basalt samples above, a chip of 12064 was also analysed for noble gases (He, Ne, and Ar), to evaluate any potential modifications in the indigenous elemental or isotopic signatures of mare basalts through sample preparation procedures (e.g. powdering), in response to the measurement of terrestrial atmospheric-like neon ratios in the powdered aliquot of 12064 (see Table 3.3.3, and Section 4.3.1). In summary, a 5.725 mg chip of 12064,140 yielded almost identical results (for ^{4}He, $^{21}Ne_{cosm}$, and total ^{21}Ne and ^{40}Ar abundances (Table 3.4.1)) as analyses of the powdered aliquot of 12064,138. However, this chip of 12064 released an order of magnitude less trapped ^{20}Ne than the powdered sample, and neon isotopic ratios (after corrections for mass fractionation in the mass spectrometer and for the presence of a system blank of terrestrial atmospheric composition) suggest that most of the neon in the chip is cosmogenic in origin ($^{21}Ne_{cosm}$ = 3.65E-07 cc/g^{-1}, or 98.5 % of the total ^{21}Ne abundance released) (Fig. 3.4.1).

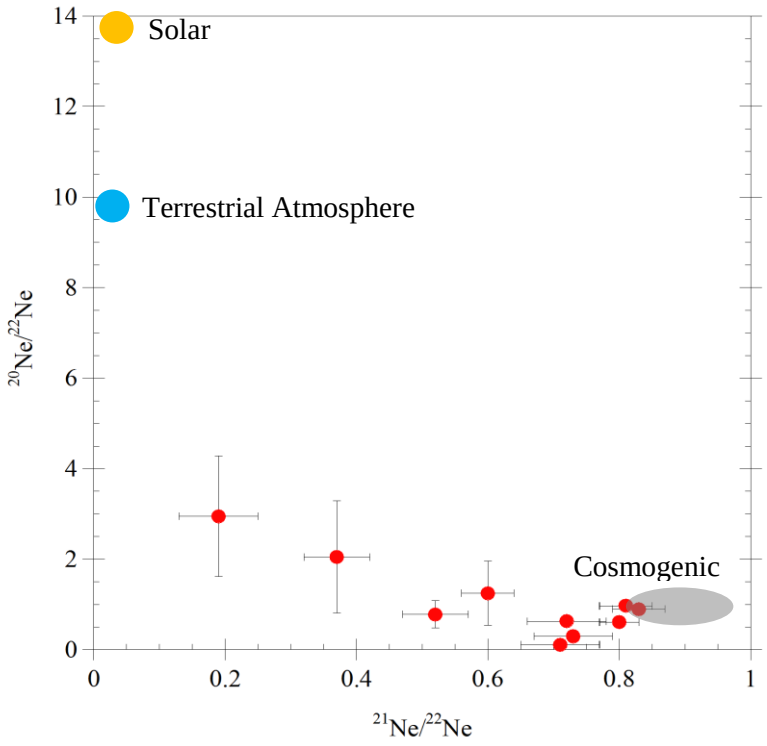

Figure 3.4.1: Neon isotopic ratios in an unpowdered chip of 12064,140. Unlike the powdered sample (see Sections 3.3 and 4.3.1), here, neon is predominantly cosmogenic.

Temperature (°C)	^{4}He (cc/g^{-1})	^{20}Ne (cc/g^{-1})	^{21}Ne (cc/g^{-1})	$^{21}Ne/^{22}Ne$	$^{20}Ne/^{22}Ne$	^{40}Ar (cc/g^{-1})	^{36}Ar (cc/g^{-1})
200	1.23E-08	nd	nd	nd	nd	3.72E-08	2.62E-10
300	2.82E-06	nd	5.65E-09	nd	nd	nd	nd
400	2.50E-05	5.72E-08	2.55E-08	0.60 ± 0.04	1.25 ± 0.71	2.59E-07	nd
500	5.10E-05	3.08E-08	1.83E-08	0.52 ± 0.05	0.78 ± 0.30	1.27E-06	1.01E-09
600	3.17E-05	4.05E-08	6.76E-09	0.37 ± 0.05	2.05 ± 1.24	2.09E-06	9.65E-09
650	1.17E-05	nd	1.64E-09	nd	nd	1.35E-06	4.23E-09
700	7.34E-06	3.08E-08	1.89E-09	0.19 ± 0.06	2.95 ± 1.33	1.48E-06	1.22E-08
750	4.72E-06	nd	4.02E-09	nd	nd	1.55E-06	2.60E-08
800	4.35E-06	nd	7.84E-09	nd	nd	1.97E-06	1.63E-08
850	3.61E-06	nd	1.87E-08	nd	nd	1.46E-06	6.07E-09
900	3.21E-06	9.17E-09	2.48E-08	0.73 ± 0.06	0.30 ± 0.07	9.98E-07	2.24E-09
950	4.71E-06	1.43E-09	2.02E-08	0.71 ± 0.06	0.11 ± 0.03	5.37E-07	nd
1000	6.52E-06	1.89E-08	2.45E-08	0.72 ± 0.06	0.63 ± 0.07	6.01E-08	nd
1100	1.76E-05	5.27E-08	4.76E-08	0.81 ± 0.04	0.97 ± 0.05	9.91E-07	2.91E-08
1200	4.00E-06	5.17E-08	7.58E-08	0.80 ± 0.03	0.61 ± 0.03	1.45E-06	1.25E-07
1300	nd	8.48E-08	8.59E-08	0.83 ± 0.04	0.90 ± 0.04	nd	9.44E-08
1400	1.36E-07	nd	1.19E-09	nd	nd	5.40E-09	1.82E-10
Total	1.79E-04	3.78E-07	3.70E-07*			1.55E-05	3.27E-07

Table 3.4.1: Noble gas results for the unpowdered chip of 12064,140 (nd = not detected). *of which 3.65E-07 cc/g^{-1} or 98.5 % is of cosmogenic origin.

Chapter Four:
Mare Basalt Analysis Discussion

4.1: Indigenous Lunar Nitrogen

The release of terrestrial nitrogen from the samples at temperatures below 500 ºC is associated with variable $\delta^{15}N$ values (ranging from -9.2 ‰ to +26.2 ‰). At the highest temperatures, very low amounts of nitrogen are released (see Table 3.1.1) with a very distinct isotopic signature, which is extremely ^{15}N-enriched. This suggests that at high temperatures, nitrogen release is dominated by a cosmogenic N component (cosmogenic nitrogen containing a high proportion of ^{15}N relative to ^{14}N). The most ^{15}N-enriched signature measured was +1054.8 ‰ in sample 10017; this basalt also has one of the highest calculated cosmic ray exposure (CRE) ages on the lunar surface, at 480 Ma (Table 2.1). Note that sample 10050 also has a CRE age of around 480 Ma, but, as described in the preceding chapter (Chapter 3), the presence of a high-temperature component with a much more ^{15}N-depleted isotopic signature in this sample serves to mask the extreme ^{15}N-enrichment caused by the release of cosmogenic nitrogen, when compared to 10017. By contrast, the least ^{15}N-enriched high temperature step with a cosmogenic $\delta^{15}N$ signature (again discounting those samples which display a non-cosmogenic high-temperature nitrogen release, as outlined in Chapter 3) is observed in sample 14053, with a $\delta^{15}N$ value of +48.7 ‰. This sample also has the lowest CRE age, at 21 Ma (Table 2.1).

The presence of terrestrial contaminants (adsorbed atmospheric nitrogen, terrestrial organics etc.) serves to mask any indigenous lunar nitrogen signature at low temperature steps, and so too does the release of cosmogenic nitrogen at the higher temperature steps. Thus, in attempting to characterise the abundance and isotopic signature of any indigenous lunar nitrogen, the mid-temperature range (variable between different samples, based on analysis of each sample's individual release profiles, but typically between 600–700 ºC to 1000 ºC) offers the best opportunity to do this. For the fifteen powdered mare basalt samples analysed in this study, $\delta^{15}N$ values in the mid temperature range varied among

samples, from a maximum of +8.3 ± 12.4 ‰, down to -6.6 ± 2.7 ‰) (Table 4.1.1 and Fig.4.1.1).

Sample	Temperature Range (°C)	Nitrogen Abundance (ng)	$\delta^{15}N$ (‰)	Error (‰)
10017	600-800	1.17	8.33	12.44
10050	650-900	3.49	7.91	2.60
10057	700-900	2.80	-0.57	1.14
10072	700-800	1.70	6.60	2.16
12016	650-850	4.41	0.75	2.63
12040	600-800	3.41	-2.04	2.51
12047	700-950	3.36	-6.61	2.69
12064	650-850	4.44	-0.75	1.27
14053	700-1000	4.50	-1.82	2.43
15386	650-750	1.41	7.51	2.70
15555	800-1000	0.60	4.41	14.25
70017	700-800	1.78	5.77	1.08
70035	800-900	1.78	6.53	2.96
74275	700-950	2.50	-0.18	8.40
75055	600-900	3.13	-2.15	2.46
Average			0.93	9.39 (2σ)

Table 4.1.1: Indigenous lunar nitrogen abundance and isotopic composition for all fifteen powdered mare basalt samples. Individual sample isotopic compositions and errors are weighted averages. The average isotopic composition is weighted according to sample indigenous nitrogen abundance, and its associated error is 2σ.

This small release (typically between 0.6 and 4.5 ng of N) is attributed to a minor indigenous N component in lunar basalts. This range of indigenous $\delta^{15}N$ values, although quite broad, yields a weighted average value of +0.93 ‰ (± 9.39 ‰ (2σ)), which is slightly lower than previous measurements of +13.0 ± 1.2 ‰ across the same temperature range, as measured by Mathew and Marti (2001). A $\delta^{15}N$ value of ~ +13‰ has also been reported by Becker et al. (1976), Kerridge et al. (1991) and Murty and Goswami (1992). Barry et al. (2013) reported indigenous lunar nitrogen values between ~ 0 ‰ and ~ +20 ‰ for three lunar basalt samples with low CRE ages (Fig. 4.1.2).

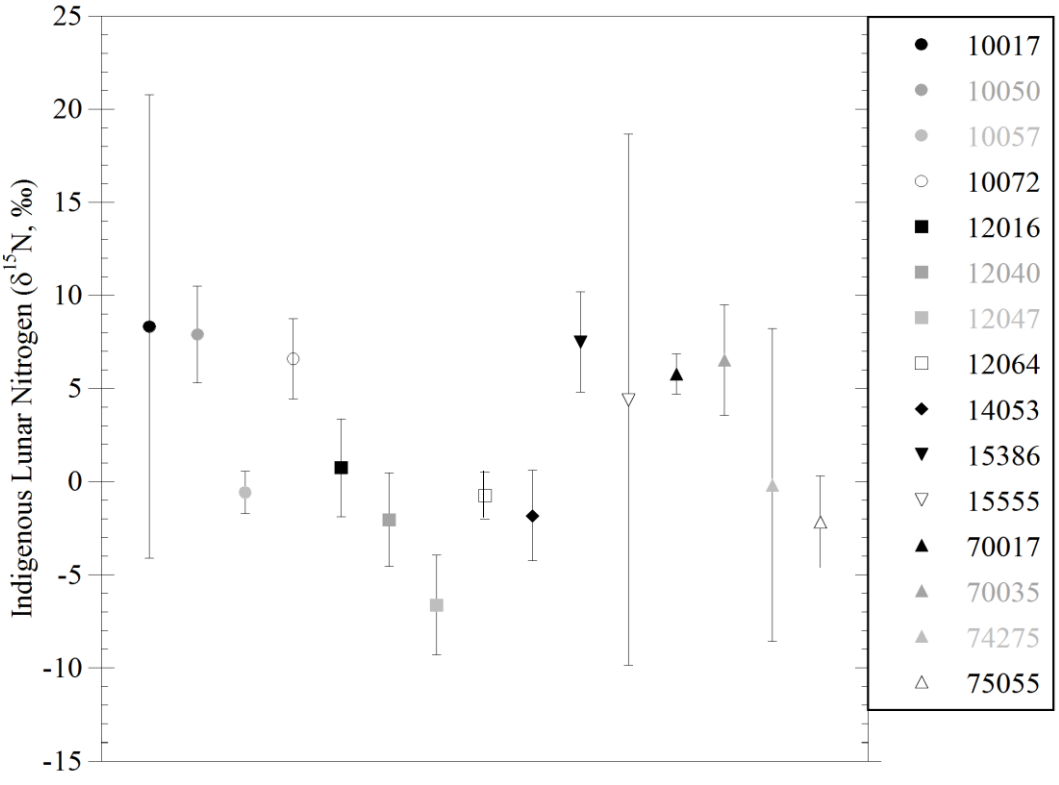

Figure 4.1.1: Indigenous lunar nitrogen isotopic signature (powdered mare basalt samples).

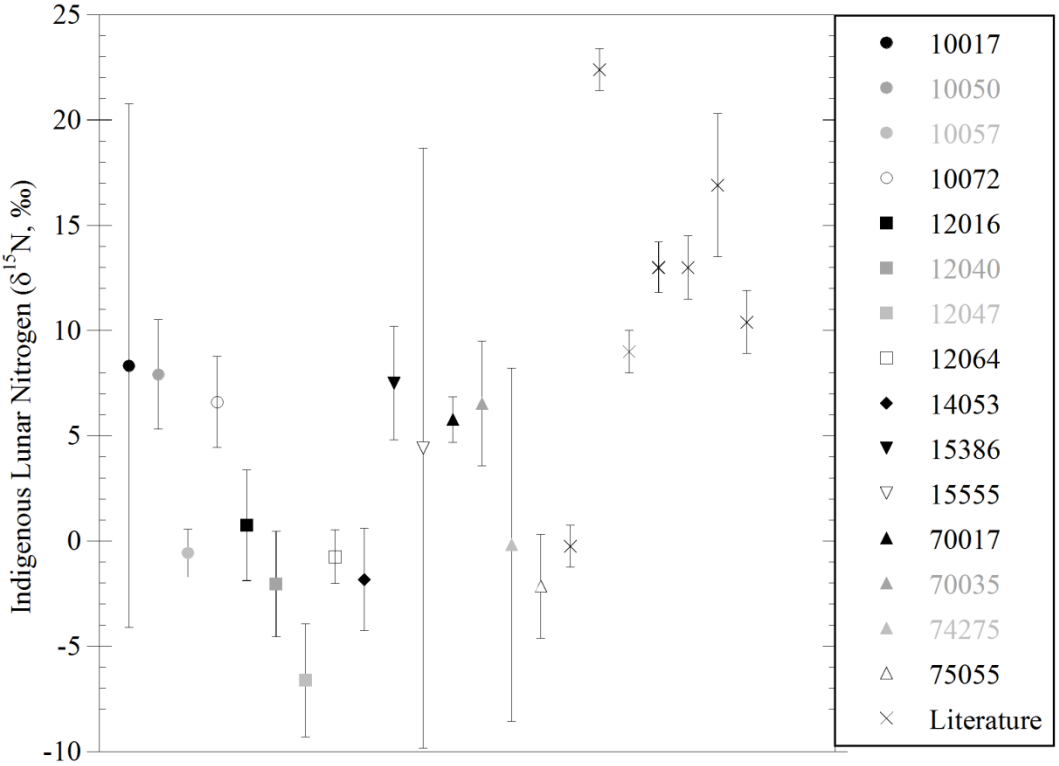

Figure 4.1.2: Indigenous lunar nitrogen isotopic signatures from this study, plus data from several previous studies of lunar nitrogen (including data from other mare basalt samples, lunar soil drill cores, breccias, and lunar meteorite MAC88105).

Although two of the samples in this study (10017 and 15555) have $\delta^{15}N$ values similar (within error) to these previously-reported heavy N signatures, these are the two samples with the greatest errors, caused in large part by several individual temperature steps within their indigenous nitrogen ranges releasing N in abundances close to system blank levels. In these instances, the error propagation calculations used during the blank correction procedure (see Appendix) introduce large uncertainties, which are then carried over into the average values for these samples. Nevertheless, there is also good agreement (within error) between data collected by Becker et al. (1976) and Barry et al. (2013) for breccia 68815 and basalt 71557 (respectively) and basalts 10050, 10072, 15386, and 70035 from this study (all of these samples being associated with much smaller uncertainties than 10017 and 15555 mentioned above), with indigenous lunar N signatures between +5 ‰ and +10 ‰. Likewise, the isotopic measurement by Barry et al. (2013) for 12008 agrees with measurements in this study for other Apollo 12 basalts (12016, 12040, and 12064), plus 10057, 74275, and 75055, suggesting an indigenous lunar N signature of ~ 0 ‰.

Given the range of abundances and $\delta^{15}N$ values measured in the fifteen powdered mare basalt samples analysed in this study, coupled with the (albeit limited) previous measurements of indigenous lunar N described above and shown in Fig. 4.1.2, it appears that nitrogen within the mare basalts (and by extension, inside the Moon) is both heterogeneously distributed, and also isotopically heterogeneous, with an almost bimodal distribution of isotopic signatures, including a group of measurements around 0 ‰, and a more ^{15}N-enriched grouping between +5 ‰ and +10 ‰ (and possibly higher).

4.1.1: Indigenous Lunar Nitrogen Isotopic Heterogeneity

Even taking into account the error-propagated uncertainties associated with these data, with such a clear distribution in isotopic measurements, it is necessary to consider possible

reasons for this spread of values; factors which could potentially influence the N isotopic compositions of these samples are discussed and evaluated in this section.

4.1.1.1: Mineralogy and Lithology

Since the indigenous lunar nitrogen measured in this study is released at temperatures up to 1000 ºC, and from powdered samples as well as a chip of basalt, it can be assumed that lunar N is located within the crystal lattice structure of the main rock-forming minerals in these samples, and not in the interstices between minerals or in vesicles. Thus, it is possible that changes in modal mineralogy between samples may be driving the N isotopic heterogeneity observed in the fifteen basalts analysed in this study.

However, taking into account the modal mineralogy (taken from James and Jackson (1970) for 10017, and Dungan and Brown (1977) for 12047) for the two samples at both extremes of the N isotopic range measured (10017 at +8.33 ‰, and 12047 at -6.61 ‰), it is clear that, despite their differing N isotopic compositions, they have very similar modal mineralogies. Both 10017 and 12047 are ilmenite basalts, containing 47.6 % and 48.4 % pyroxene (respectively), 26.9 % and 38 % plagioclase (respectively), 14.2 % and 5.3 % ilmenite (respectively), and 8.5 % and 2 % mesostasis areas (respectively). Admittedly, while pyroxene content is the same between these two samples, there are small differences in plagioclase and ilmenite abundances. Sample 75055 is also an ilmenite basalt with a modal mineralogy almost identical to 10017, with 50.2 % pyroxene, 28.6 % plagioclase, 15.9 % ilmenite, and 0.8 % mesostasis (Brown et al., 1975). However, whereas indigenous N in 10017 is measured at +8.33 ‰, $\delta^{15}N$ for 75055 is -2.15 ‰. Therefore, difference in modal mineralogy between samples does not seem to be an explanation for variations in N isotopic compositions.

Considering lithological differences as a potential reason for N heterogeneity, it must be noted that most measurements of indigenous lunar nitrogen have been made using basalts; indeed, all of the samples in this study are basalts, as are samples in Barry et al. (2013), and yet these samples still display considerable heterogeneity in terms of N abundance and isotopic composition. However, sample 68815 (Becker et al., 1976) is a breccia, and gives a nitrogen isotopic composition identical within error to the more ^{15}N-enriched group of basaltic samples in this study. Similarly, clast W-1 in MAC88105 (Murty and Goswami, 1992) is a granulitic anorthosite, and yields a δ^{15}N value identical (within error) to the value measured in black and orange glass beads from the lunar regolith double-drive core 74001/74002 (Kerridge et al., 1991) and to ferroan anorthosite 60025 and basalt 75075 (Mathew and Marti, 2001). This all suggests that lithological differences are not driving N isotopic heterogeneities in the lunar interior.

4.1.1.2: Crystallisation Age

It is possible that nitrogen isotopes underwent fractionation throughout the significant time period during which basaltic melts were being generated and erupted to form mare basalts on the lunar surface; nitrogen remaining in the lunar interior could potentially fractionate as subsequent basaltic melts containing N are erupted, changing the isotopic signature of any N remaining in the lunar interior and also reducing the abundance available for incorporation into future basaltic melts. This scenario assumes that all mare basalts were derived from a common source region which underwent fractional crystallisation over time (see Section 4.1.1.4).

Taking just the N isotopic data from this study alone, it is obvious that crystallisation age has no correlation with isotopic composition (Fig.4.1.3). Sample 10050 is one of the older mare basalts in this study, and crystallised at 3.75 ± 0.03 Ga, with an indigenous lunar

$\delta^{15}N$ value of +7.91 ‰. Sample 14053 is the oldest basalt in this study, crystallising at 3.94 ± 0.04 Ga, and yet has one of the most ^{15}N-depleted indigenous lunar N isotopic signatures, at -1.82 ‰. By contrast, the youngest sample in this study (12064, which crystallised at 3.18 ± 0.01 Ga) has an indigenous N signature of -0.75 ‰, and thus also falls into the same ^{15}N-depleted grouping as the oldest mare basalt in this study.

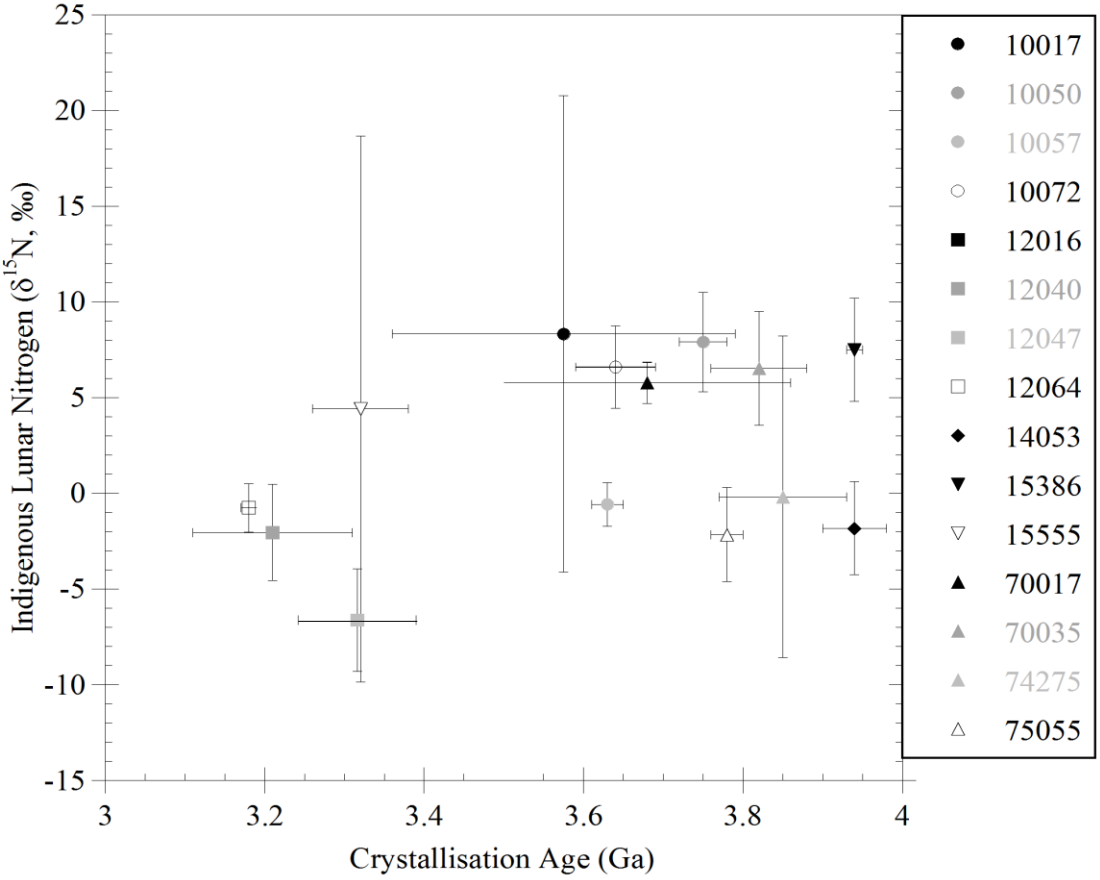

Figure 4.1.3: Relationship between crystallisation age and indigenous lunar nitrogen isotopic signature. Crystallisation age data taken from Table 2.1 and references therein.

There is a similar lack of correlation between indigenous N abundance and crystallisation age, with the oldest sample (14053) releasing 4.50 ng of N, and the youngest sample (12054) also releasing a comparable 4.44 ng of N across the mid-temperature range taken as representing the release of indigenous N.

4.1.1.3: CRE Age

Although care has been taken to exclude from assessments of indigenous lunar N those temperature steps which display evidence of contributions to N isotopic signatures from cosmic-ray induced spallation reactions, it may be the case that, with indigenous N temperature ranges extending up to 1000 ºC in some samples, a small contribution from cosmogenic sources to a largely indigenous lunar N release could result in small variations in N isotopic composition. As discussed previously, since spallation reactions produce a high proportion of ^{15}N relative to ^{14}N, even a small input from cosmogenic N would increase the $\delta^{15}N$ signature of the indigenous N in a sample to a more ^{15}N-enriched value.

Comparing the N data for the fifteen basalts in this study (Table 4.1.1) with CRE ages taken from the literature (Table 2.1 and references therein), it is immediately apparent that no temperature steps including a cosmogenic N input have been included in the characterisations of indigenous lunar N. Indigenous N in basalt 14053 was determined to be released between 700-1000 ºC, the upper limit of this being a temperature which in other samples already displays evidence for the presence of cosmogenic N. However, in 14053, a $\delta^{15}N$ signature of -1.82 ± 2.43 ‰ shows that this N release is relatively depleted in ^{15}N and thus does not contain any cosmogenic N contribution. Alternatively, some of the samples with the most ^{15}N-enriched indigenous N signatures are associated with a temperature range only extending up to 750-850 ºC, well below the temperatures at which cosmogenic components begin to be released.

Finally, samples 10072, 12040, 12064, 15386, and 70017 all have similar CRE ages (of around 240 Ma on average), and yet still display considerable isotopic heterogeneity, with isotopic signatures of +6.60 ‰, -2.04 ‰, -0.75 ‰, +7.51 ‰, and +5.77 ‰, respectively. Furthermore, 12040 and 75055 both have identical indigenous N signatures of -2.04 ± 2.51

‰ and -2.15 ± 2.46 ‰, respectively, but very different CRE ages of 285 Ma and 95 Ma, respectively.

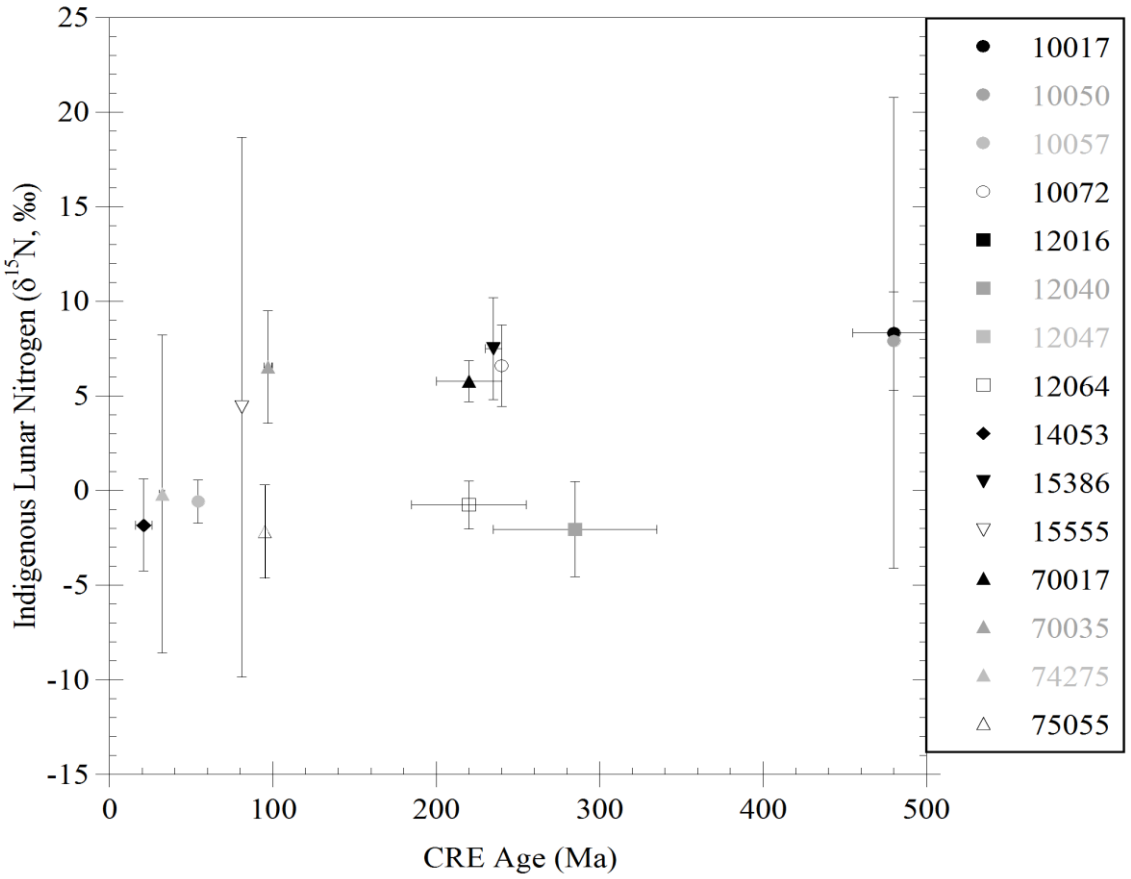

Figure 4.1.4: Relationship between cosmic ray exposure age and indigenous lunar nitrogen signature. CRE age data taken from Table 2.1 and references therein.

4.1.1.4: Basaltic Melt Source Regions

As shown in Table 2.1, mare basalts can be divided into several different groups based on their major element geochemical characteristics, as well as by their modal mineralogy. One of the main geochemical differences between basalts is in their Ti content, which can range from 1to14 wt.%, with low-Ti basalts at 1-5 wt.% TiO_2, and high-Ti basalts containing 9-14 wt.% TiO_2 (Papike et al., 1976). In general, high-Ti basalts form a grouping of older samples, with crystallisation ages from 3.85 ± 0.08 Ga to 3.575 ± 0.215 Ga. Low-Ti basalts tend to be younger in age, with crystallisation ages from 3.32 ± 0.06 Ga to 3.18 ± 0.01 Ga. However, 14053 is an unusual sample, being a low-Ti basalt (2.93 wt.% TiO2 (Papike et al., 1976)) that crystallised at 3.94 ± 0.04 Ga, making it one of the oldest mare basalt samples (See Table 2.1 and references therein). Where earlier (Section 4.1.1.2) it was suggested that, in a scenario where crystallisation age has an impact on indigenous lunar N isotopic heterogeneity, a common source (undergoing progressive partial melting/fractional crystallisation) for all mare basalts was required, major and trace element geochemical data suggest that in fact, the scale of Ti content differences between mare basalt samples is evidence for multiple source regions, both laterally and in terms of depth, giving rise to basaltic melts of different starting compositions (Hallis et al., 2014; Papike et al., 1976; Ray and Misra, 2014). Through assessment of trace element contents, and via experimental high-pressure phase equilibria studies, it has been suggested that high-Ti and low-Ti basalts are derived from different depths within the lunar interior, although there is some disagreement about the exact depths these separate basaltic melts were generated at. Papike et al. (1976) propose that low-Ti basalts may be derived from an olivine-pyroxene source at a depth ranging between 500 km, up to 200 km below the lunar surface. They also found that high-Ti basalts were likely to have come from olivine-pyroxene-ilmenite cumulate sources within the outermost 150 km of the Moon. Ray and

Misra (2014) assume a pressure gradient of 20 km/kbar in the outer portion of the Moon, and from this suggest that high-Ti basaltic glasses were derived from melts forming at depths of around 300 km, with low-Ti mare basaltic melts being generated at shallower lunar mantle depths of between 200 km and 300 km (a similar range to Papike et al., 1976). The disagreement about the depth of high-Ti basalt melt generation is further complicated by Hess (1991), whose thermodynamic and phase equilibria studies suggest that high-Ti picritic mare glasses are derived from melting of cumulate sources 'only modestly endowed with ilmenite-enriched crystallisation products', with the partial melt rising adiabatically as diapirs from initial mantle depths below 700 km. As the source diapirs rise, they experience pressure-release melting and incorporate significant amounts of surrounding (shallower) mantle material. Thus, the final high-Ti basaltic melts represent material sampled from different depths within the lunar mantle.

However complex the melt generation history for these samples may be, a simple observation is that high-Ti and low-Ti basalts are derived from different depths within the lunar mantle, and so, if a correlation between source depth and indigenous lunar N is sought, nitrogen isotopic signatures should be compared to Ti content (Fig. 4.1.5). As this scatter plot shows, both the low-Ti and high-Ti basalt groups (from different depths within the lunar mantle) display considerable indigenous N isotopic heterogeneity; therefore, this heterogeneity cannot be caused by different melts being generated at different depths.

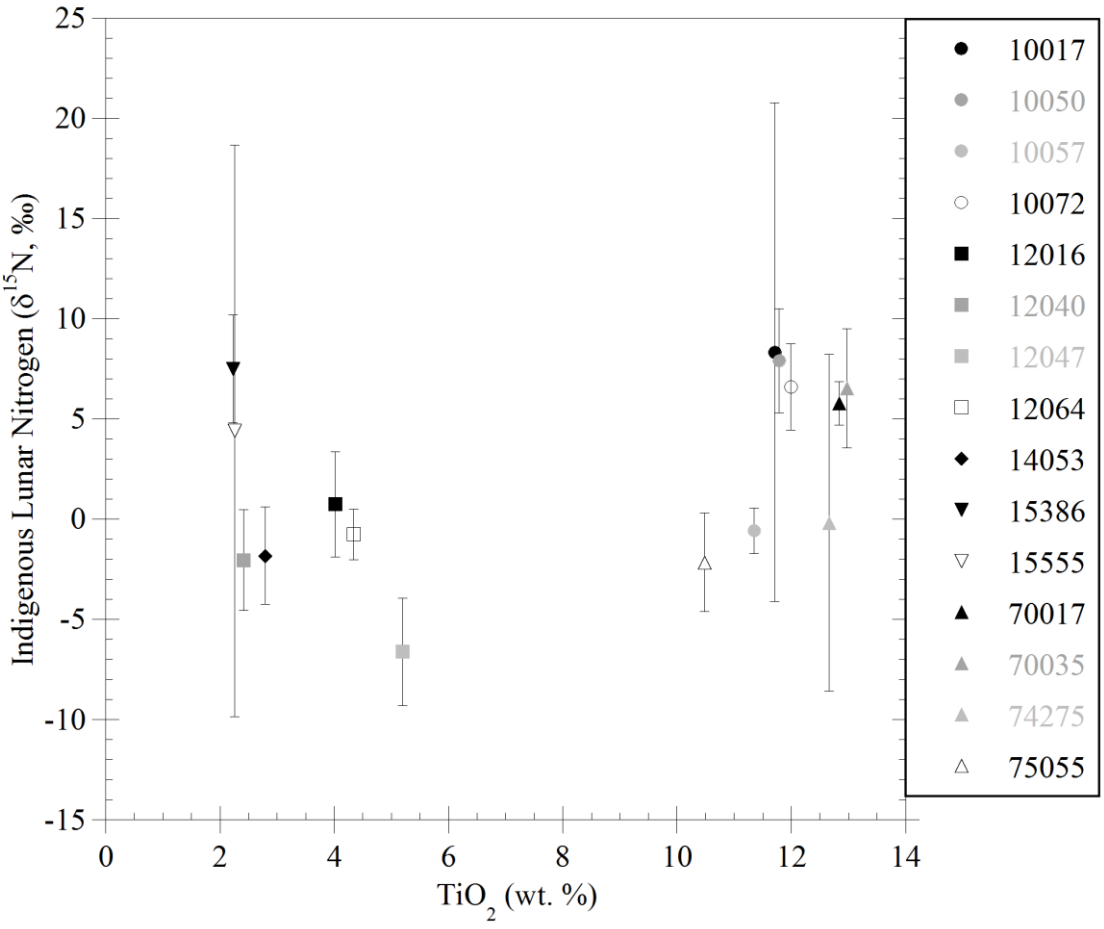

Figure 4.1.5: Correlation between TiO_2 content (as a proxy for depth of melt generation) and indigenous lunar N isotopic composition. TiO_2 data taken from Compston et al., 1970; Compston et al., 1971; Duncan et al., 1974; Duncan et al., 1976; Dymek et al., 1975b; Hubbard et al., 1972; Maxwell et al., 1970; Rhodes et al., 1973; Rhodes et al., 1976; Rhodes et al., 1977; Rhodes et al., 1980; and Wänke et al., 1971.

4.1.1.5: Degassing

The degree of degassing a melt undergoes is affected by the solubility of the element in question under the P-T-$f0_2$ conditions specific to each planetary body. Solubility in the melt under mantle conditions is itself controlled by speciation, which is dependent upon oxygen fugacity. Under the oxidising conditions of the terrestrial mantle, carbon dissolves into the melt as carbonate ions, and degasses as CO_2. Upon degassing, C in the melt fractionates and gradually becomes more ^{13}C-depleted, leading to lower δ^{13}C values in degassed melts. By contrast, N in the terrestrial mantle is much less soluble, and so is

more readily degassed from melts than C. When degassing occurs, N isotopes are fractionated in the opposite sense to those of C, such that ^{14}N is preferentially degassed over ^{15}N, leading to higher $\delta^{15}N$ values in the degassed melt (Cartigny et al., 2001).

However, under the reducing conditions of the lunar mantle, relative solubilities of C and N are very different, meaning so too is the expected degassing (and associated isotopic fractionation) behaviour of these two elements. Under reducing conditions, N solubility is greatly increased by dissolution into the melt as N^{3-} species, which then bond with atoms in the silicate melt network (Libourel et al., 2003). At the same time, under reducing conditions (fO_2 lower than -0.55 relative to the iron wüstite buffer), carbon dissolves in the melt as Fe-pentacarbonyl and (to a lesser degree) methane. This change in speciation (from dissolving as carbonate under oxidising conditions) decreases carbon solubility by a factor of two (Wetzel et al., 2013). Therefore, under the reducing conditions of the lunar mantle, carbon is expected to preferentially degas compared to nitrogen. Under such conditions, taking into account the bonding of dissolved N^{3-} species into the silicate melt network, it is reasonable to suggest that relatively little nitrogen degassed from lunar basaltic melts prior to/during crystallisation, and therefore, should not have played a major role in driving the observed N isotopic heterogeneities in lunar rocks.

Although there are no estimates for the amount of N degassing lunar samples may or may not have experienced, degassing of H and its associated isotopic fractionation effect on final measured H isotopic compositions has been modelled using H isotopic measurements of the late-forming mineral apatite in mare basalts (e.g.: Tartèse et al., 2013; Tartèse et al., 2014). In contrast to N, hydrogen is readily degassed from lunar magmas as H_2 under reducing conditions (Tartèse et al., 2013), and during degassing, significantly fractionates

hydrogen from deuterium, leaving the residual H in the melt enriched in ^{2}H (deuterium, or D) (Anand et al., 2014).

If it is assumed that any degassing of N is occurring at the same time as H degassing, since much less N is expected to degas from lunar basaltic melts compared to H, comparing the amount of H degassing a sample has undergone against its N isotopic composition should result in a very weak/no correlation. That is, more degassed samples should show similar N isotopic compositions to less degassed samples (See Fig. 4.1.6).

Taking H degassing data for 15386 and 15555 from Tartèse et al. (2014) and Tartèse et al. (2013) (80-90 % degassed and 98 % degassed, respectively), and plotting these against $\delta^{15}N$ values (from this study), it appears that basalts with a ^{15}N-enriched indigenous N signature (+7.51 ‰ and +4.41 ‰) are also highly degassed. However, 12064 experienced 99 % degassing (Tartèse et al., 2013), and yet has a ^{15}N-depleted signature of -0.75 ‰.

Several additional basalt samples can be added to this comparison, using the equations for H_2 degassing in Tartèse et al. (2014), and calculations for the enrichment of H left in the melt caused by incompatibility with crystallising phases during fractional crystallisation (Tartèse et al., 2013), plus H_2O abundance data for apatites in 12040, 14053, and 75055 (measured by Greenwood et al., 2011). Making these calculations for 75055 (starting from a hypothetical source region with a δD value of -100 ‰ relative to Vienna Standard Mean Ocean Water (VSMOW) (following the conclusions of Barnes et al., 2014), and an H_2O abundance of between 1000-3000 ppm), it seems that this basalt most likely experienced 95- 98 % degassing (Fig.4.1.7), and yet has a N isotopic signature of -2.15 ‰. 12040, with a similar N isotopic composition, is likely to have experienced very little degassing; even after the H-abundance enriching effects of fractional crystallisation, apatite in this sample contains no more water than the detection limit of Greenwood et al.

(2011). 14053 is another sample which probably experienced very little degassing, based on its apatite water content and measured δD values, and yet also has a ^{15}N-depleted indigenous N signature of -1.82 ‰.

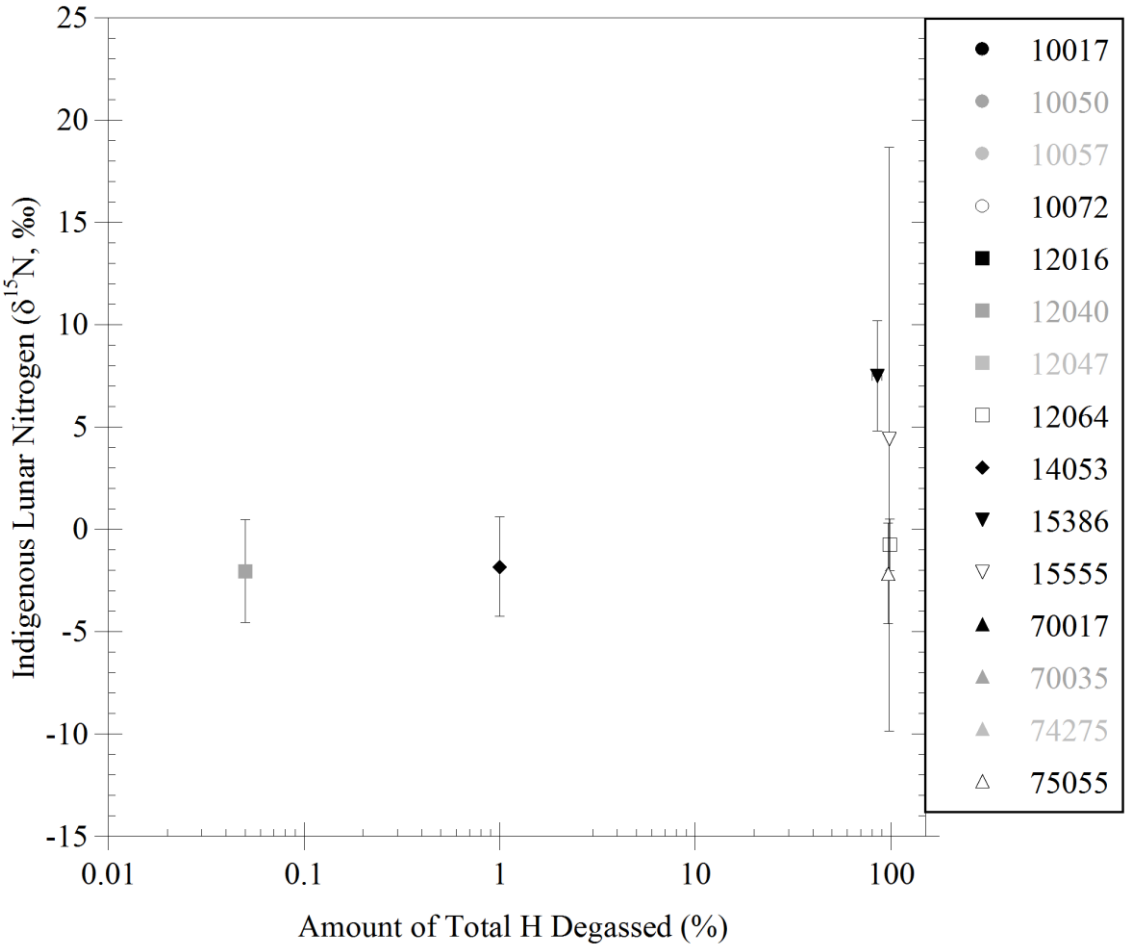

Figure 4.1.6: Relationship between amount of degassing a sample has experienced (assuming that a sample highly degassed in H will also be degassed to a relative degree in N) and indigenous lunar N isotopic composition. H degassing values taken from Tartèse et al., 2013; Tartèse et al., 2014, and calculated from H abundance and isotopic data in Greenwood et al., 2011.

Although this comparison does seem to suggest that degassing of lunar melts has no impact on N isotopic heterogeneity, a rather large caveat is that this assumes that N degassing (if indeed any significant N degassing does occur, given the bonding into the silicate melt network that N species experience under reducing lunar mantle conditions) occurs to the same degree as H degassing in the same samples. Also, H data is collected from the mineral apatite, which crystallises at >95 % crystallisation (Greenwood et al., 2011); since the N-hosting phase(s) in mare basalts are unknown, it is possible that N is incorporated into minerals much earlier in the crystallisation sequence, whilst degassing is still taking place, making the degree of H degassing incomparable with any N degassing that may have occurred.

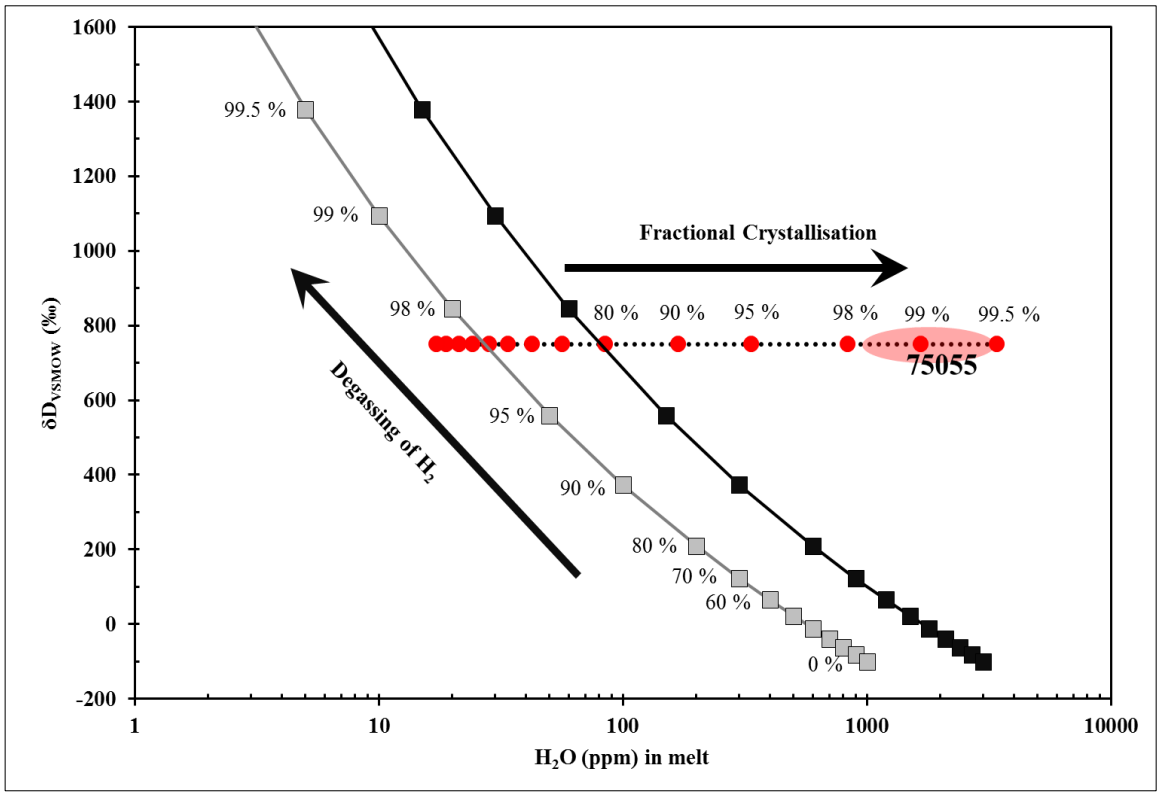

Figure 4.1.7: H_2O abundance in the melt at various stages of degassing and fractional crystallisation versus H isotopic composition of the degassing/crystallising melt. The grey degassing curve assumes a starting δD value of -100 ‰ and an initial melt abundance of 1000 ppm. The black degassing curve represents a starting δD value of -100 ‰ and an initial melt abundance of 3000 ppm. The red crystallisation sequence illustrates increasing H_2O abundance in the remaining melt (at constant δD) as crystallisation progresses. The red oval indicates the point during crystallisation at which apatite crystallised, and the δD value of these apatites (from Greenwood et al., 2011).

4.1.1.6: Contamination from Extra-Lunar Sources

Another possible explanation for such heterogeneity in both N abundances and isotopic composition between samples could involve the addition of non-lunar sources of N to the indigenous lunar N component, differing amounts of which would cause varying degrees of departure from the true indigenous lunar abundance and isotopic composition.

Firstly, as already stated, only N releases in the mid-temperature steps are used in this study to characterise the indigenous lunar N component; these temperatures are safely above the low temperature steps where any adsorbed terrestrial atmospheric N may be released.

Secondly, fuel used by the Lunar Module (LM) descent rockets was a mixture of N_2H_4 and $(CH_3)_2N_2H_2$ in equal parts by weight, with N_2O_4 as an oxidiser. Therefore, the LM exhaust gases contained appreciable amounts of N_2 (which, along with water, H_2, and CO constituted up to ~ 90 mole % of the total LM fuel combustion products. N_2 alone accounted for 32 mole % of the LM exhaust gases) (Aronowitz et al., 1968). Estimated desorption rates for these exhaust gases indicate that chemically adsorbed H_2O, N_2, and OH will have undergone such minimal desorption over the timescale of sample collection on the lunar surface that returned samples should contain detectable abundances of these exhaust gases. Furthermore, modelling suggested that exhaust gas N_2 abundances of up to several $\mu g/cm^2$ could be expected even several hundred metres away from the LM landing site (Aronowitz et al., 1968). However, adsorbed LM exhaust gases would be surface-correlated contaminants, and the samples used in this study were taken from the interiors of the returned mare basalts upon sample splitting back on Earth; thus, contamination from LM exhaust gases is not expected in these basalt samples. A simple check for this involves comparing the $\delta^{15}N$ values of these samples with the distances from the LM at which they

were collected. Samples collected closest to the LM landing sites should have experienced the greatest degree of contamination from exhaust gases, and samples collected several km away should have experienced minimal contamination. All of the Apollo 11 basalt samples in this study were collected in an area immediately to the SSW of the LM, within approximately 20 m of the landing site, and while three samples display an elevated isotopic signature, 10057 falls into the lower, ^{15}N-depleted grouping (Fig. 4.1.8). At the Apollo 17 landing site, samples 70017 and 70035 were collected close to the LM (within tens to hundreds of metres away), and both have ^{15}N-enriched signatures. However, at the Apollo 15 landing site, similarly ^{15}N-enriched signatures occur in samples collected both 2 km to the west of the LM, and 4-5 km to the south of the LM. Measuring similar isotopic signatures at different distances from the LM (Fig. 4.1.8), and in different directions away from the LM at the same site (which eliminates the possibility of the distal ^{15}N-enriched values being caused by the LM landing trajectory flying over that sampling site) all suggests that the N isotopic heterogeneity seen in these samples is not a result of varying amounts of contamination from LM exhaust gases.

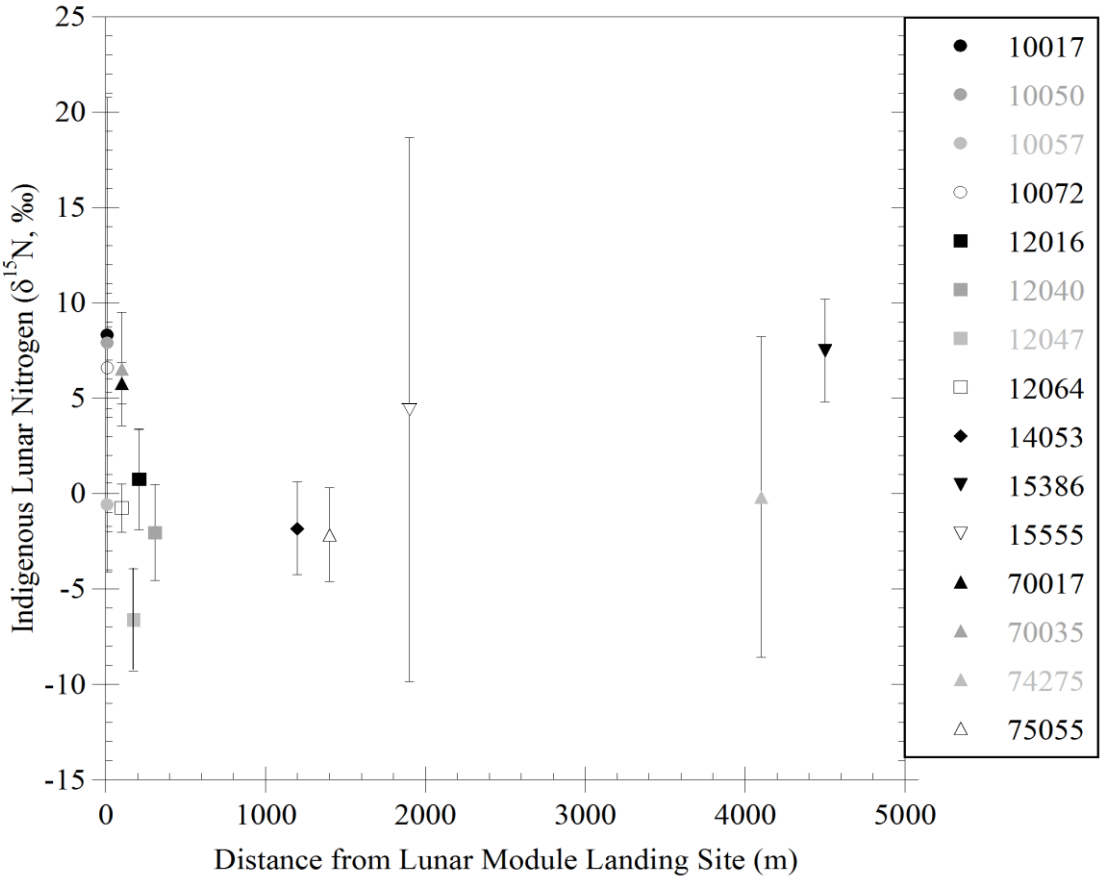

Figure 4.1.8: Relationship between distance from the LM at which samples were collected and indigenous lunar N isotopic composition. Collection site locations were taken from Apollo Sample Catalogs and Sample Information documents.

4.1.1.7: Analytical Factors (date of runs)

A final possibility is that the observed isotopic heterogeneity is merely an artefact of small-scale variations in the analytical conditions over time. The Finesse mass spectrometer instrument has low, stable system blank levels (e.g. Mikhail, 2011), and furthermore, instrument blank levels were monitored regularly, before each sample batch was analysed. In this way, even if there was a small, temporary anomaly in system blank levels and isotopic composition, the sample data collected at these times would be corrected for the presence of this anomalous blank. The mare basalt samples used for this study were processed and analysed in several batches spread out over more than twelve months; it is

striking that there is no correlation between the dates of analyses and the indigenous N isotopic composition (Fig. 4.1.9), which strongly suggests that the observed N heterogeneity has nothing to do with any analytical factors.

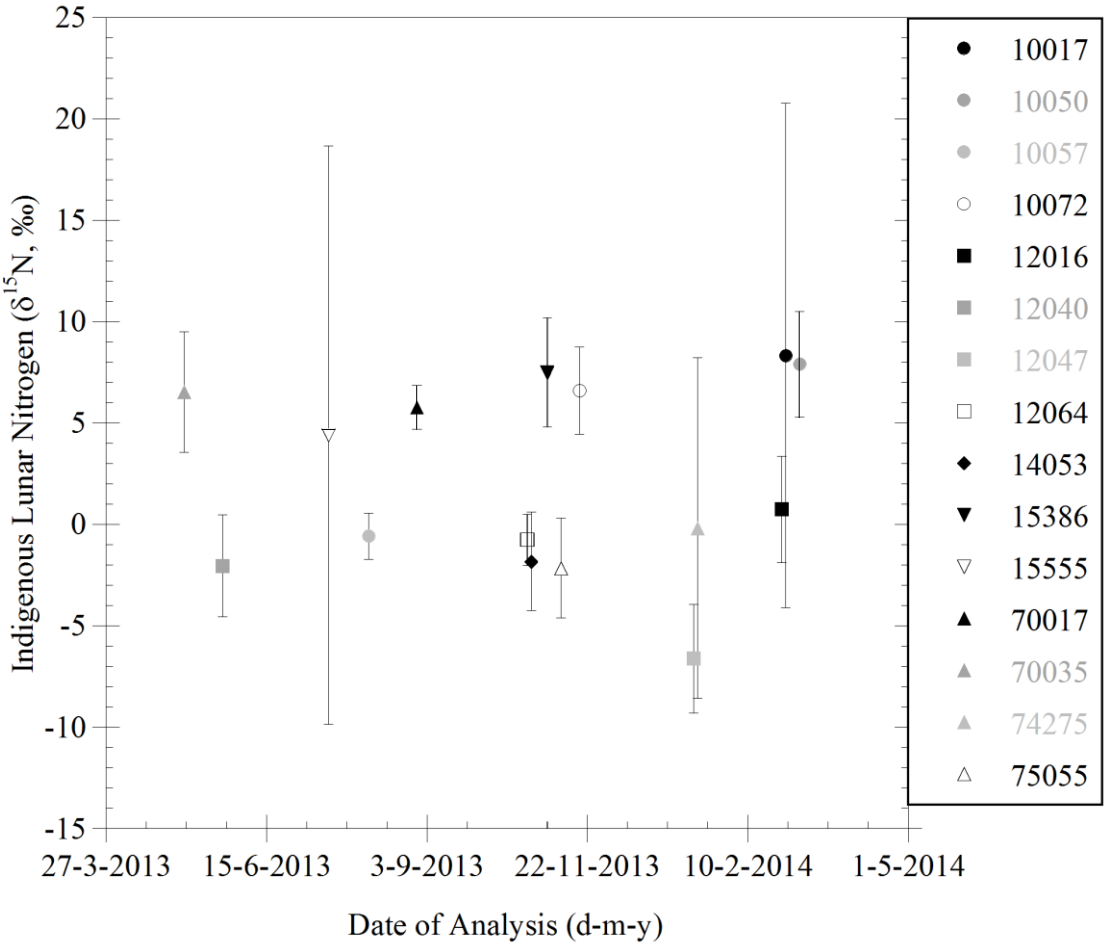

Figure 4.1.9: Relationship between dates of sample analyses and indigenous lunar N isotopic composition.

After exhausting possible reasons to explain the observed N heterogeneity in lunar basalts, the only conclusion that may be drawn is that N within the Moon is innately heterogeneously distributed and of heterogeneous isotopic composition. Perhaps this is not unexpected, given recent data collected for other volatiles in the lunar interior (e.g. H abundance and isotopic composition (Robinson and Taylor, 2014, and references therein)).

4.2: C/N Elemental Ratios

As outlined for indigenous N in Section 4.1, using the stepped combustion method, it is possible to identify the temperature ranges where indigenous lunar volatile signatures are overprinted by terrestrial contamination, and an extra-lunar addition from cosmogenic spallation processes. This leaves a 'window' at mid temperatures (typically between 650–700 ºC and 1000–1100 ºC) where it is feasible to quantify the amount and isotopic composition of indigenous volatile components in lunar basalts. By comparing the release profiles of C and N in the six basalt samples studied, it is possible to identify several samples where the C and N are most likely co-located in the same phase, although the exact nature of this phase remains unidentified on the basis of release temperature alone. Since C and N do seem to be located in the same phase, it is possible to use the calculated C/N ratios for these indigenous volatile components (released at mid temperatures) as a means of characterising the C and N properties of the lunar mantle, from which these samples are derived. However, degassing during magma eruption and emplacement on the lunar surface may have caused some degree of elemental fractionation, modifying the true lunar mantle ratio, and, therefore, a range of lunar mantle C/N ratios may be expected (discussed in greater detail later in this section).

The average blank-corrected C/N ratios of the mid temperature indigenous components (Table 4.2.1, including several C/N ratios previously reported in Mortimer et al., 2014) for fourteen out of the fifteen samples analysed are relatively tightly constrained, between 4 and 40, with an average C/N ratio of 20. The exception to this is sample 15555, which has a much higher C/N ratio of 275, probably owing to the greater release of low temperature carbon contamination still being released at mid-temperature steps in this sample. Since this extra C release is not associated with N, the ratio of C to N increases. Excluding the data for sample 15555, average C/N ratios measured among the basalts in this study, over

the temperature interval interpreted as representing indigenous volatile components, are much smaller than those measured for the terrestrial depleted mantle (C/N_{mantle} = 535 ± 224 (Halliday, 2013; Marty, 2012)), or even for bulk silicate Earth (BSE) (C/N_{BSE} = ~ 40– 50 (calculated from data in Halliday, 2013)), although 12016 and 12047 C/N ratios approach the lower end of this BSE range, potentially through the inclusion of C releases at 650-700 ºC, which in these samples may still be affected by the last remnants of terrestrial contamination release.

Sample	**C/N Ratio**	**$\delta^{15}N_{AIR}$ (‰)**
10017	21	8.33
10050	34	7.91
10057	19	-0.57
10072	27	6.6
12016	40	0.75
12040	8	-2.04
12047	37	-6.61
12064	11	-0.75
14053	4	-1.82
15386	18	7.51
15555	275	4.41
70017	25	5.77
70035	11	6.53
74275	5	-0.18
75055	20	-2.15
Lunar Average	**20**	**0.93 ± 9.39**
Terrestrial Depleted Mantle	535 ± 224[a]	-5 to -30[c]
Bulk Silicate Earth (BSE)	40 to 50[e]	
Enstatite Chondrites	4.5 to 15[b]	-29.2 ± 0.6[b]
CI Chondrites	16[d]	~33[c]
CM Chondrites	24[d]	~15 to 50[c]
CO Chondrites	14[d]	~-20 to 12[c]

Table 4.2.1: C/N ratios of mid-temperature indigenous lunar C and N. (N.B. 15555 has a higher C/N ratio than the other samples in this study (see text for further discussion)). [a] Taken from Marty and Zimmermann (1999). [b] Calculated from data in Wasson and Kallemeyn (1988) and Thiemens and Clayton (1983). [c] Taken and calculated from Marty (2012). [d] Calculated from average C and N abundances in Pearson et al. (2006). [e]calculated using data in Halliday (2013).

The large difference in average C/N ratios between the terrestrial depleted mantle and indigenous lunar values may be explained by the significant influence of subducted biological organics greatly increasing the C content of the Earth's mantle relative to N, compared to that of the Moon. Without active plate tectonics, any C added from extra-lunar sources or processes remains at the lunar surface, and is not incorporated into the lunar mantle, from which these basalt samples were derived. Therefore, a more relevant comparison might be made between primordial terrestrial mantle C and N values and this indigenous lunar C and N data, although no direct measurements of the primordial terrestrial mantle are available. Taking an enstatite chondrite composition as a proxy for the primordial terrestrial mantle (Javoy et al., 2010), and using carbon values averaging 3800 ppm (Wasson and Kallemeyn, 1988) and the extremes of the nitrogen values proposed by Thiemens and Clayton (1983) (254–850 ppm), a C/N ratio of between 4.5 and 15 is obtained. Both of these C/N ratios for enstatite chondrites fall within the range found in this study for indigenous C and N in lunar basalts. However, there is a difference between the indigenous $\delta^{15}N$ signatures for these lunar basalts, and the values measured for enstatite chondrites (-29.2 ± 0.6 ‰ (Thiemens and Clayton, 1983)), suggesting that indigenous lunar N does not share a common source with that of enstatite chondrites. Considering carbonaceous chondrites as a possible source for volatiles in the Earth–Moon system (e.g. Marty, 2012), CI and CM chondrites have elemental C/N ratios within/similar to the range calculated for lunar samples. However, N isotopic signatures for these two primitive chondrite groups are heavier than lunar values (Table 4.2.1), with an average of around +40 ‰. CO chondrites, by contrast, not only have C/N ratios within the same range as lunar samples, but also have comparable $\delta^{15}N$ values, supporting the theory that volatiles in the Earth and lunar interior may have a carbonaceous chondrite heritage (e.g. Saal et al., 2013).

A complicating factor regarding the use of C/N ratios is the varying solubility of both C and N between different Solar System bodies (as discussed in Section 4.1.1.5), which can have an impact on the C/N elemental ratios measured in mantle-derived samples. Within the Earth, CO_2 solubility is much greater than that of N_2, and hence during degassing, C/N ratios can greatly increase in the residual melt (Cartigny et al., 2001), giving rise to the much higher C/N ratios for the terrestrial mantle as listed in Table 4.2.1. Because of this link between solubility and elemental fractionation, the degree of elemental fractionation depends on the speciation of C and N within the mantle melts. Thus, in the reducing conditions of the lunar mantle, N solubility is greatly increased (Libourel et al., 2003), whilst C solubility is decreased by a factor of two (Wetzel et al., 2013). Therefore, with C being preferentially degassed compared to N, elemental C/N ratios decrease in the residual melts from which lunar mare basalts were formed. These differences between C and N solubilities in the lunar and terrestrial mantles may also explain the observed disparity between elemental C/N ratios in these two bodies.

4.3: Noble Gases

4.3.1: Trapped Noble Gases

The release of radiogenic ^{4}He is correlated with a low-temperature release of a trapped ^{20}Ne component in most samples (10050, 10057, 10072, 12016, 12047, 12064, 14053, 15386, and 75055 (e.g. Fig. 4.3.1.1), although interestingly, in samples 10017, 12040, 70035, and 74275 which do not show co-release of ^{20}Ne with ^{4}He, the main release of ^{20}Ne is at higher temperatures and correlated with the release of cosmogenic ^{21}Ne instead (e.g. Fig. 4.3.1.2). No trapped ^{20}Ne was released above blank levels in 15555 and 70017.

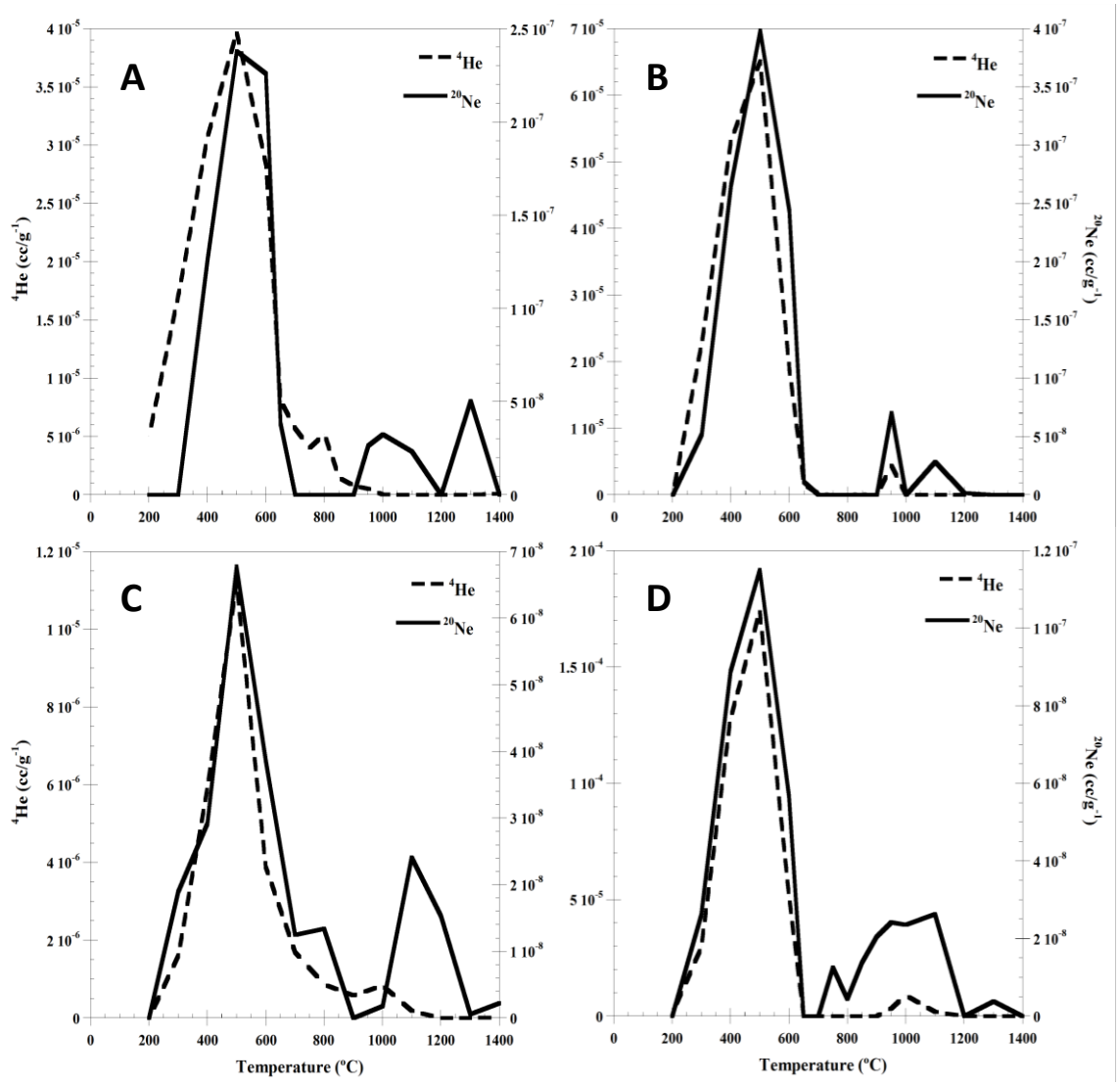

Figure 4.3.1.1: Correlation between release profiles of trapped ^{20}Ne with radiogenic ^{4}He in mare basalts A) 10050, B) 12064, C) 14053, and D) 15386.

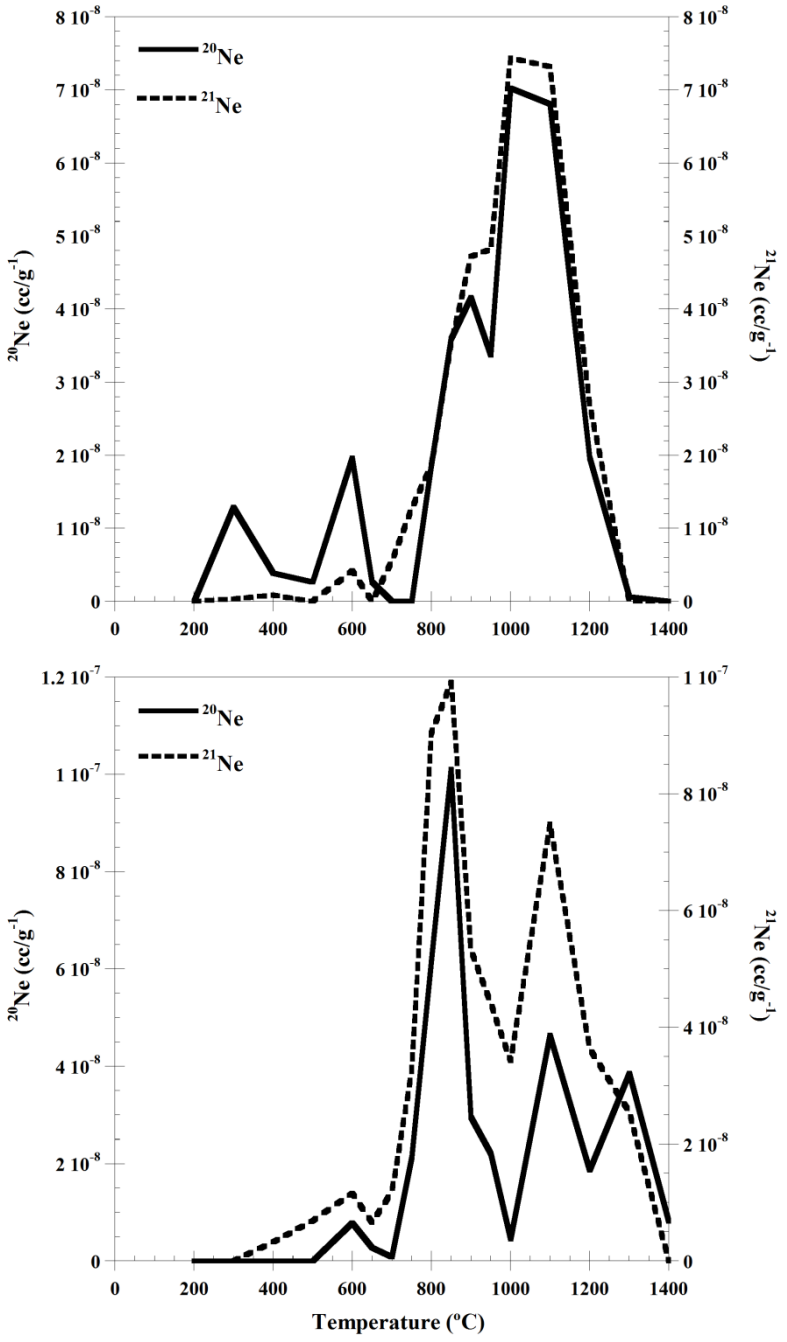

Figure 4.3.1.2: Correlation between release profiles of ^{20}Ne with ^{21}Ne in mare basalts A) 10017, and B) 12040, suggesting that for samples which show a high temperature maximum release of ^{20}Ne, the released ^{20}Ne is predominantly of cosmogenic origin.

One possible explanation for this unexpected variation in ^{20}Ne release profiles could be that the trapped ^{20}Ne component is introduced during sample preparation, when highly reactive fresh mineral surfaces are created during powdering, which can attract any atmospheric gases present. Any such terrestrial contaminant gases would be only weakly bound to the mineral surface and could be expected to be released at low temperature steps during analysis. Alternatively, the friction generated during sample powdering may cause local atomic level heating, and thus some grain surfaces may be annealed, trapping the weakly-bonded gases in the mineral sub-surface as an 'inclusion'; such pseudo-inclusions would then release the trapped gas only at higher temperatures, as the trapped component begins to diffuse out of the sample. Thus, it may be possible to release a terrestrial trapped Ne component at the same high temperature steps as cosmogenic ^{21}Ne. A similar explanation is proposed by Niedermann and Eugster (1992), who observed over 75% of the terrestrial noble gases incorporated during crushing of lunar anorthositic samples being released at temperatures above 600 ºC. In their study, they attribute these high-release temperatures with noble gas fixing by strong chemisorptive bonding, or by trapping beneath the sample surface, due to mechanical and thermal energy supplied during the crushing process.

Although in most samples, significant interference from doubly-charged CO_2 during ^{22}Ne measurements was observed (where $CO_2^{++}/^{22}Ne \geq 100$), in 12064, this interference was minimal ($CO_2^{++}/^{22}Ne < 50$) (Mortimer et al., 2014). This means that the measured Ne isotopic ratios ($^{20}Ne/^{22}Ne$ and $^{21}Ne/^{22}Ne$), after correction for both the presence of a system blank of terrestrial atmospheric composition and for any mass fractionation in the mass spectrometer during analysis, can be used to characterise both the low and high temperature ^{20}Ne releases. In 12064, even after correcting both the ratios of $^{21}Ne/^{22}Ne$ and $^{20}Ne/^{22}Ne$ for these contributions/effects, a mixing trend between cosmogenic Ne and

terrestrial atmospheric Ne is observed (Fig. 4.3.1.3). Comparing the isotope ratios for the steps at which the low-temperature maximum ^{20}Ne release is observed in this sample reveals that this release is of a composition close to terrestrial atmospheric Ne, indicating that in 12064, maximum ^{20}Ne release comes from a predominantly terrestrial atmospheric source mixing with a more minor cosmogenic component. This is certainly in keeping with the suggestions outlined above that atmospheric Ne could be incorporated into the sample during the powdering procedure prior to analysis. Whilst this confirms a low temperature release for terrestrial trapped Ne, suggesting that Ne added during crushing is only relatively weakly bound to the sample, and not trapped via the strong chemisorptive bonding mechanism proposed by Niedermann and Eugster (1992), it does not explain why this trapping of terrestrial Ne is only seen as a major effect in some samples and not others (i.e. samples where maximum ^{20}Ne release occurs at much higher temperatures, correlated with cosmogenic ^{21}Ne releases (Figure 4.3.1.2)), since all samples underwent the same crushing procedures in the same clean room suite.

For the other mare basalts which also show this abundant low temperature release of ^{20}Ne, although similar comparisons with their Ne isotopic compositions cannot be made due to the presence of doubly-charged CO_2 (which has the effect of offsetting the points plotted on a three-isotope diagram down towards the origin), it is plausible to suggest a similar explanation, invoking the trapping of terrestrial atmospheric Ne which is being released from the powdered samples at 500 ºC (maximum release).

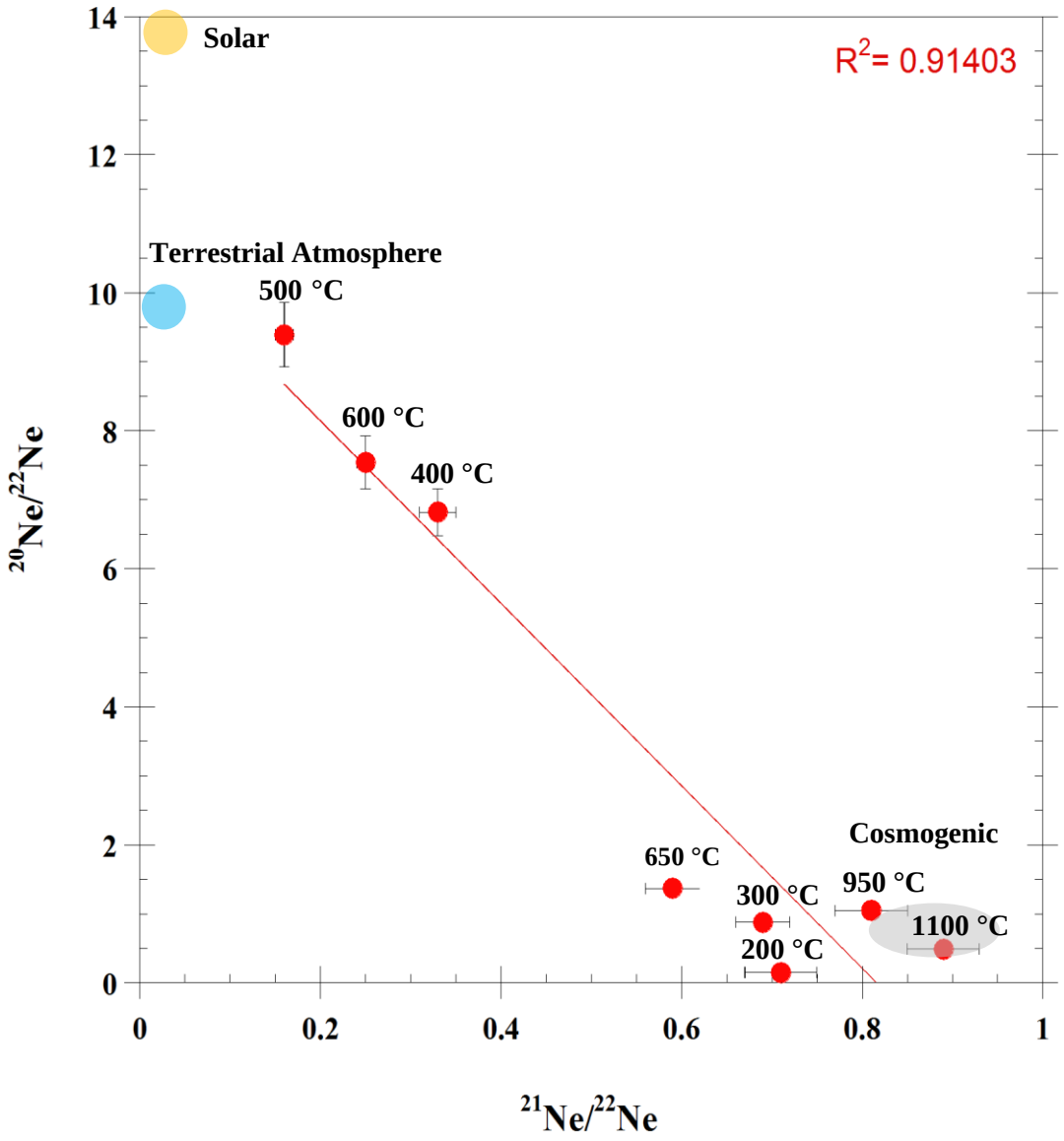

Figure 4.3.1.3: Ne isotopes in 12064 (powdered sample), with the release temperatures for individual points annotated. Note that the low temperature peak release of ^{20}Ne in this sample is at 500 ºC (panel B, Fig. 4.3.1.1), and is associated with the most terrestrial-like Ne isotopic composition on this plot. The less abundant high temperature release of ^{20}Ne is associated with almost purely cosmogenic Ne compositions.

The other trapped noble gas for which data were collected is ^{36}Ar; as with any trapped atmospheric Ne, a higher abundance of ^{36}Ar might be expected if additional terrestrial atmospheric gases were introduced during sample crushing for this study. However, whilst a higher abundance of ^{36}Ar is observed in sample 14053 compared to published values, in most other samples in this study there is good agreement between these data and literature

values, and in several samples, the amount of ^{36}Ar observed is lower than that measured in previous studies (See Tables 3.3.6 to 3.3.9), suggesting that Ar is not incorporated into the powdered mare basalts during the crushing procedure alongside terrestrial atmospheric Ne.

Similarly, assuming that all of the trapped ^{20}Ne in 12064 was introduced during sample crushing and is therefore from the terrestrial atmosphere, a high abundance of N may also be expected, since N is many orders of magnitude more abundant in the terrestrial atmosphere than either Ne or Ar. By taking the relative abundances of N and Ne in the current terrestrial atmosphere ($N_2/^{20}Ne$ = 65902.39 (by mass)), and applying that to the total abundance of trapped ^{20}Ne in sample 12064, the expected abundance of any trapped terrestrial N can be calculated (62960.52 ng of N). However, basalt 12064 releases only 42.52 ng of N in total, (almost 1500 times lower than the calculated expected abundance) and therefore, does not seem to show any evidence of significant trapped terrestrial atmospheric N, especially considering the fact that the majority of the N released in 12064 can be attributed (based on its C/N ratios (average C/N = 100, across the temperature range where the majority of N in 12064 is released) and release temperatures) to terrestrial organic material and not the terrestrial atmosphere. Discounting the terrestrial organic N contribution, the measured abundance of N in 12064 is significantly lower than the expected contribution from contamination by terrestrial atmospheric N.

4.3.2: Radiogenic Noble Gases

Radiogenic ^{4}He is found in all of the basalts for which helium data were collected. In every sample (apart from 10057, which contains higher ^{4}He abundances in low temperature steps caused by the sample being held in the furnace for longer than usual as a result of cooling failures), the peak release is at 500 ºC. Radiogenic ^{40}Ar is also released from the basalt samples across a wide temperature range, but with peak releases between 600 and 700 ºC, the slightly higher release temperature for ^{40}Ar being a function of the slower diffusion rate of the larger Ar atom compared to that of He (Fig. 4.3.2.1).

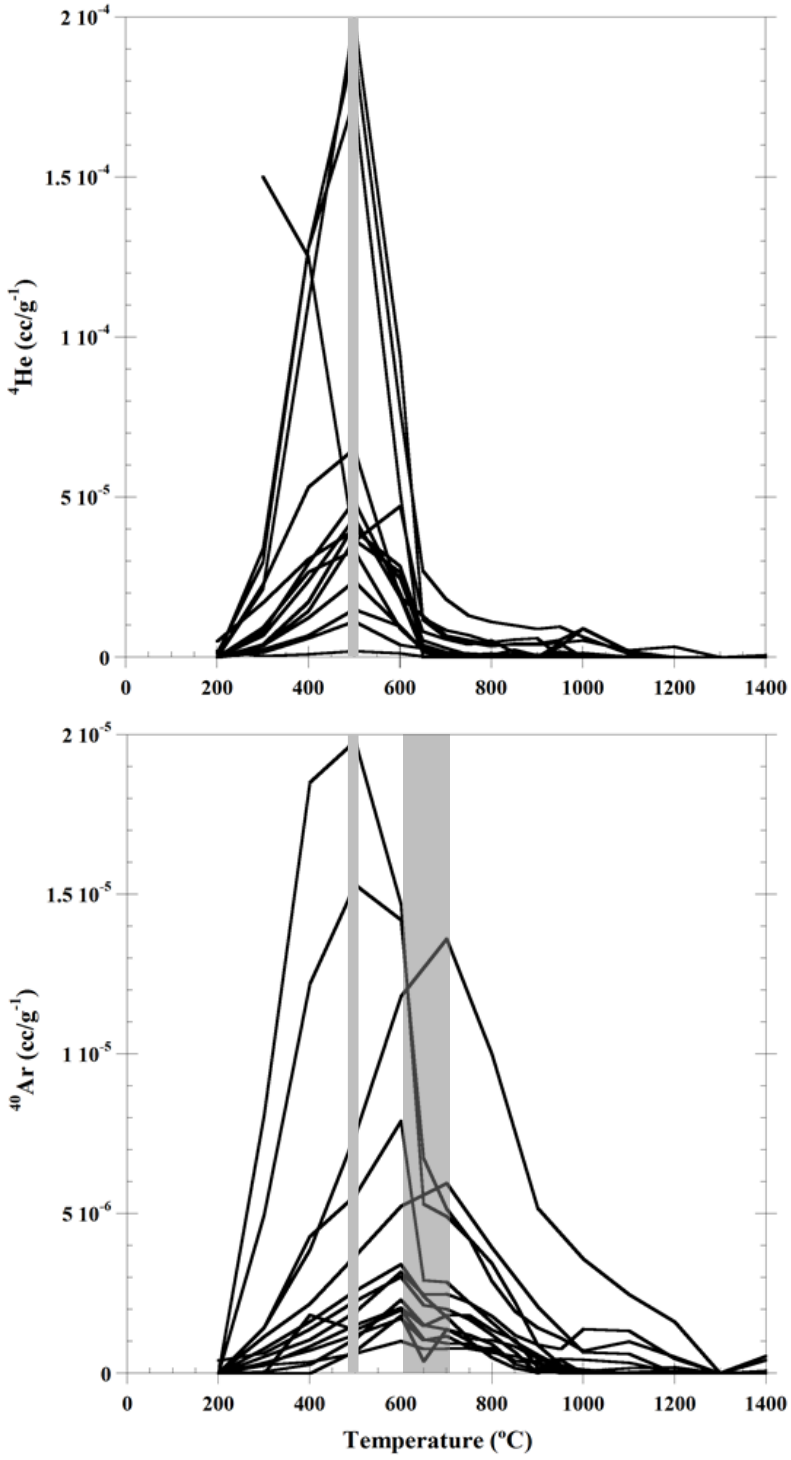

Figure 4.3.2.1: Release profiles for radiogenic noble gases ^{4}He and ^{40}Ar. Note that ^{4}He peak release is at 500 ºC (thin grey line), and peak release for ^{40}Ar is often between 600 ºC and 700 ºC (thick grey box), these temperatures being a function of differing diffusion rates out of the samples. However, in two samples, 10072 and 15386, peak ^{40}Ar release occurs at 500 ºC, alongside ^{4}He peak release.

It is worth noting that the actual amounts of radiogenic He and Ar vary across the samples; ^{4}He and ^{40}Ar are formed in situ by the radioactive decay of U and Th, and K, respectively. Because of a correlation between the known chemical compositions of the samples with radiogenic isotope abundances, samples of the same age with greater initial U and Th, and K can be expected to release greater abundances of radiogenic ^{4}He and ^{40}Ar. Using literature values, sample 15386 has the highest K abundance, at ~ 0.67 wt.% (Rhodes, 1973) and based on the results of this study, it also releases the most ^{40}Ar (Table 3.3.8). This is to be expected, since 15386 is a KREEP basalt, enriched in K compared to other mare basalts. Conversely, basalt 15555 has one of the lowest K contents represented in this sample set, at ~ 0.04 wt.% (Chappell and Green, 1973), corresponding with the lowest ^{40}Ar value measured in this study (Fig. 4.3.2.2).

The abundances of radiogenic He and Ar are also related to the formation age of their host rocks. Out of the fourteen non-KREEP basalts, the sample which releases the most ^{40}Ar (totalled across all temperature steps) is 10072, with a crystallisation age of 3.64 Ga (Papanastassiou et al., 1977). By comparison, out of the 2 samples with the lowest ^{40}Ar releases (12016 and 15555), 15555 has a younger crystallisation age of 3.32 Ga (Wasserburg and Papanastassiou, 1971), although 12016 has not yet been dated.

Besides these expected correlations between released ^{40}Ar abundance, sample composition (K abundance) and crystallisation ages for the samples analysed in this study, comparisons with previously published values from different laboratories show a close agreement in the case of ^{40}Ar, and a good general agreement for ^{4}He values, demonstrating the effectiveness of the extraction technique used in this study.

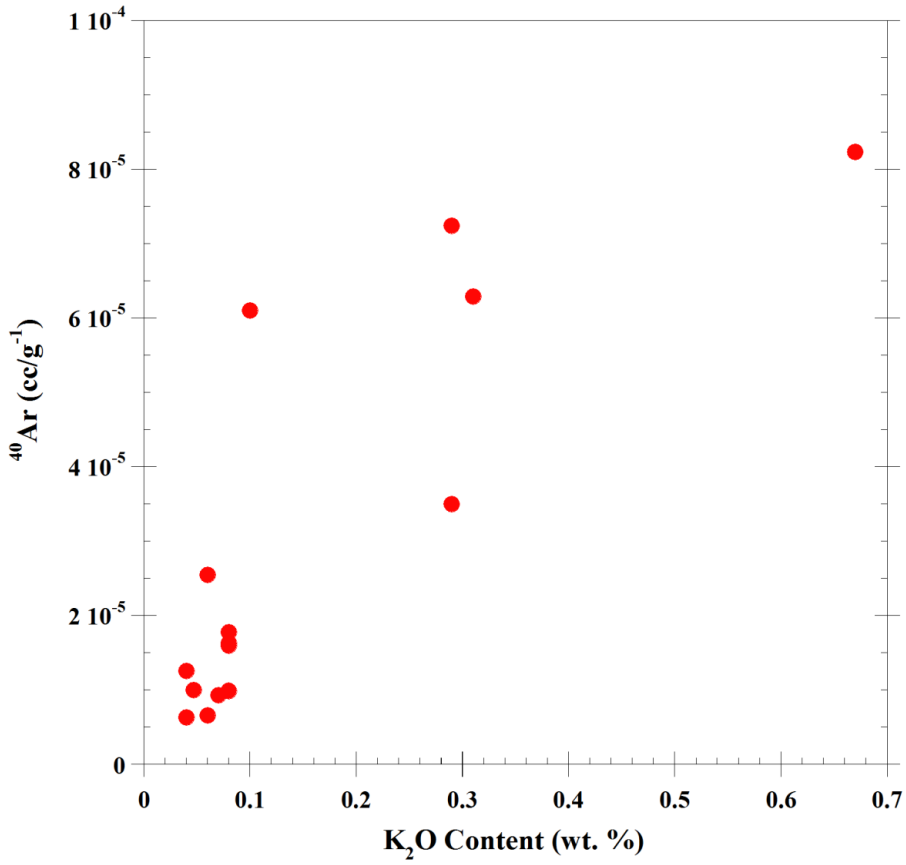

Figure 4.3.2.2: Correlation between K content of basalts with the total ^{40}Ar abundance released across all temperature steps. K_2O data taken from: Chappell et al., 1972; Compston et al., 1970; Compston et al., 1971; Duncan et al., 1974; Dymek et al., 1975b; Hubbard et al., 1972; O'Kelley et al., 1970; Rhodes and Hubbard, 1973; Rhodes et al., 1976; Rhodes et al., 1977; Rhodes and Blanchard, 1980; Wänke et al., 1971; Wänke et al., 1974.

4.3.3: Cosmogenic Volatiles

The following table outlines the calculated abundances of cosmogenic isotopes present in each sample:

Sample	CRE Age	$^{21}Ne_{cosm}$ (cc/g)	$^{38}Ar_{cosm}$ (cc/g)	$^{15}N_{cosm}$ (ng)
10017	480 ± 25	3.38E-07	2.68E-07	2.90E-03
10050	480	1.63E-07	1.48E-07	7.18E-03
10057	54.2	1.18E-08	1.99E-08	4.58E-04
10072	240	2.46E-07	1.78E-07	2.86E-03
12016		1.63E-07	8.90E-08	4.64E-04
12040	285 ± 50	3.68E-07	7.36E-08	1.76E-03
12047		1.30E-08	3.10E-08	3.34E-04
12064	220 ± 30	3.18E-07	9.14E-08	1.88E-03
14053	21 ± 5	2.59E-08	1.96E-08	1.74E-04
15386	235 ± 5	3.61E-07	1.60E-07	1.76E-03
15555	81	3.10E-08	4.62E-08	8.01E-04
70017	220 ± 20	2.72E-08	1.26E-08	1.97E-03
70035	97.5 ± 2.5	1.08E-07	3.82E-08	1.77E-04
74275	32.2 ± 1.4	8.35E-09	8.86E-09	2.81E-04
75055	95	9.47E-08	4.63E-08	8.87E-04

Table 4.3.3.1: Calculated abundances of cosmogenic isotopes in powdered mare basalts.

4.3.3.1: Cosmogenic Neon

Cosmogenic ^{21}Ne is also released from all the mare basalt samples in this study. To calculate the abundance of cosmogenic ^{21}Ne, the following equation was used:

$$^{21}Ne_{cosm} = {}^{22}Ne_{meas} * (^{21}Ne/^{22}Ne)_{cosm} * \frac{(^{21}Ne/^{22}Ne)_{tr} - (^{21}Ne/^{22}Ne)_{meas}}{(^{21}Ne/^{22}Ne)_{tr} - (^{21}Ne/^{22}Ne)_{cosm}}$$

(where $^{21}Ne_{cosm}$=cosmogenic ^{21}Ne abundance, $^{22}Ne_{meas}$=measured ^{22}Ne abundance, $(^{21}Ne/^{22}Ne)_{cosm}$=cosmogenic end-member ratio, $(^{21}Ne/^{22}Ne)_{tr}$=terrestrial atmospheric ratio, $(^{21}Ne/^{22}Ne)_{meas}$=measured sample ratio).

Generally, between 70 % and 98 % of the total ^{21}Ne released from the powdered mare basalts was of cosmogenic origin, and plotting these cosmogenic ^{21}Ne abundances against published exposure ages reveals a positive correlation (Fig. 4.3.3.1). For example,

Hintenberger et al. (1971) measured 3.13E-07 cc/g^{-1} of cosmogenic ^{21}Ne being released from 12064, from which they calculated a CRE age of 220 Ma for this sample. By comparison, analyses from this study recorded a total ^{21}Ne release for sample 12064 of 4.22E-07 cc/g^{-1}, of which around 75% (3.18E-07 cc/g^{-1}) is of cosmogenic origin, almost identical to the published abundance data.

Cosmogenic ^{21}Ne is produced via spallation of major elements (Na, Mg, Al, Si, Ca, and Fe) within a sample (Hohenberg et al., 1978). Using the predicted production rates for ^{21}Ne from each of these principle targets in Hohenberg et al. (1978) and applying these to the major element compositions of individual samples, and using the calculated cosmogenic ^{21}Ne abundances from the present study, an average production rate (P_{21}) of 1.42E-09 cc/g rock/Ma is calculated. However, taking the $^{21}Ne_{cosm}$ abundances from this study, and using the published CRE ages for these samples, a slightly lower production rate is calculated (P_{21} = 9.50E-10 cc/g rock/Ma, excluding samples 10017, 10050, and 70017 which plot below the main trend). Although this is a fairly small difference in production rate, especially taking into account errors in measurements and calculations of cosmogenic isotope abundances and major element abundances, and errors placed on published CRE ages, it is in keeping with the findings of Hohenberg et al. (1978), who found that their predicted production rates for $^{21}Ne_{cosm}$ were around 25-30 % higher than their observed production rate (which, at 8.50E-10 cc/g rock/Ma, is in agreement with the observed production rate for cosmogenic ^{21}Ne in this present study). Whilst there is a good general correlation for most samples, there are three samples which plot far away from the main trend. 97.3 % of the total ^{21}Ne abundance in 10017 is of cosmogenic origin, and yet this sample, despite being the longest-exposed (480 Ma) in this present study sample set, contains a similar abundance of cosmogenic Ne as samples exposed for only 230-240 Ma. This may be caused by several factors: either, as with 10050 and 70017, an unusually low

abundance of total ^{21}Ne was measured in this sample for some reason, or alternatively, samples exposed for longer than approximately 250 Ma reach a plateau in cosmogenic Ne production, representing a saturation in the amount of cosmogenic Ne that a sample can produce.

Samples 12016 and 12047 have no published exposure ages and so cannot be added to Fig.4.3.3.1. However, using the same calculations to work out the percentage of total ^{21}Ne that is of cosmogenic origin, rough CRE ages of around 150 Ma and 70 Ma (respectively) can be tentatively suggested, based on the correlation observed in Fig.4.3.3.1 (excluding anomalous samples 10050 and 70017). Using the calculated value for P_{21} from this study, CRE ages of 170 Ma and 15 Ma (respectively) can be calculated.

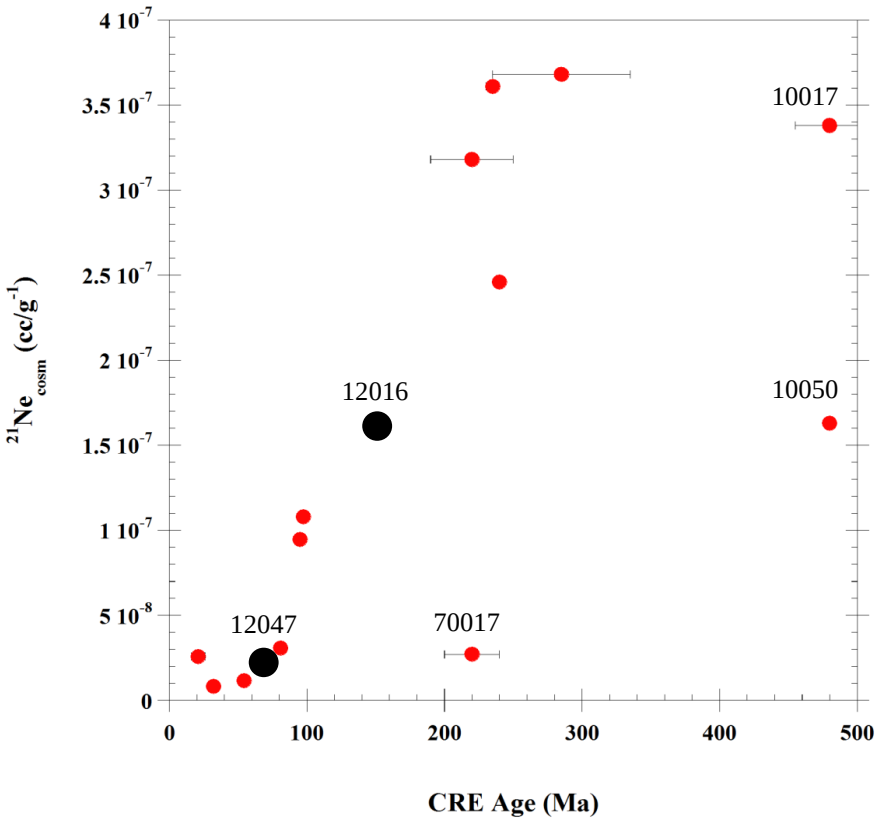

Figure 4.3.3.1.1: Correlation between CRE age and calculated abundances of cosmogenic ^{21}Ne in powdered mare basalt samples. CRE ages are taken from Table 2.1 and references therein. Three samples which do not fit the correlation displayed by the other basalts are labelled (10017, 10050, and 70017). Samples 12016 and 12047 (which do not have published CRE ages) are shown in black circles, positioned along the main correlation line according to their calculated cosmogenic ^{21}Ne abundances.

4.3.3.2: Cosmogenic Argon

Cosmogenic ^{38}Ar is also released from all the mare basalt samples in this study. To calculate the abundance of cosmogenic ^{38}Ar, the following equation was used:

$$^{38}Ar_{cosm} = {}^{38}Ar_{meas} * \frac{(^{36}Ar/^{38}Ar)_{meas} - (^{36}Ar/^{38}Ar)_{tr}}{(^{36}Ar/^{38}Ar)_{cosm} - (^{36}Ar/^{38}Ar)_{tr}}$$

(where $^{38}Ar_{cosm}$=cosmogenic ^{38}Ar abundance, $^{38}Ar_{meas}$=measured ^{38}Ar abundance, $(^{36}Ar/^{38}Ar)_{cosm}$=cosmogenic end-member ratio, $(^{36}Ar/^{38}Ar)_{tr}$=terrestrial atmospheric ratio, $(^{36}Ar/^{38}Ar)_{meas}$=measured sample ratio).

Generally, around 80% to 95 % of the total ^{38}Ar released from the powdered mare basalts was of cosmogenic origin. As with cosmogenic ^{21}Ne, plotting cosmogenic ^{38}Ar abundances against published CRE ages reveals a good positive correlation (Fig. 4.3.3.2.1).

However, three samples plot below the main trend (these being 70017, 12040, and 10050). Taking into account the large error on the CRE age of 12040, and assuming that this sample could be from the lower end of this age range instead (e.g. 235 Ma), then this sample does not plot too far from the trend established by the other samples. Nevertheless, 70017 and 10050 contain significantly lower cosmogenic ^{38}Ar abundances than might be expected based on their published CRE ages. It is interesting to note that these samples are also anomalous in terms of their cosmogenic ^{21}Ne abundances too, indicating that these basalts have had an eventful exposure history at the lunar surface.

It is reasonable to suggest that perhaps these anomalously low cosmogenic abundances may reflect some analytical issue such as a valve failing to close fully, resulting in the loss of some of the released gases. However, since neon and argon are measured in two different processes on two separate mass spectrometers, it is highly unlikely that a problem of this kind could occur in two different parts of the machine at the same time, especially

considering these two samples were analysed six months apart. Rather, the agreement between cosmogenic noble gas abundances in these samples suggests that they may have much younger CRE ages than previous studies have concluded.

Assuming that the published CRE ages for these samples are correct, using the calculated abundances of cosmogenic ^{38}Ar (excluding abundances for samples which plot below the main correlation), an average production rate for cosmogenic ^{38}Ar (P_{38}) of 5.56E-10 cc/g rock/Ma is calculated. There is some variation in calculated P_{38} values between samples, but all are within the same order of magnitude (2.75E-10 to 9.35E-10 cc/g rock/Ma), and in agreement with a production rate (P_{38} = 8.14E-10 cc/g rock/Ma) calculated using cosmogenic ^{38}Ar abundances and a ^{81}Kr-Kr age for an ilmenite concentrate of 10071 reported by Eberhardt et al. (1974). However, Hashizume et al. (2002) suggested that P_{38} for samples within the lunar regolith could be as little as half of this absolute rate, and therefore in even closer agreement with the cosmogenic ^{38}Ar production rate calculated in this study. Using the P_{38} value derived from data in this present study, samples 12016 and 12047, which have no published CRE ages, are calculated to have exposure ages of around 160 Ma and 60 Ma (respectively), in good agreement with the ages suggested by cosmogenic ^{21}Ne abundances.

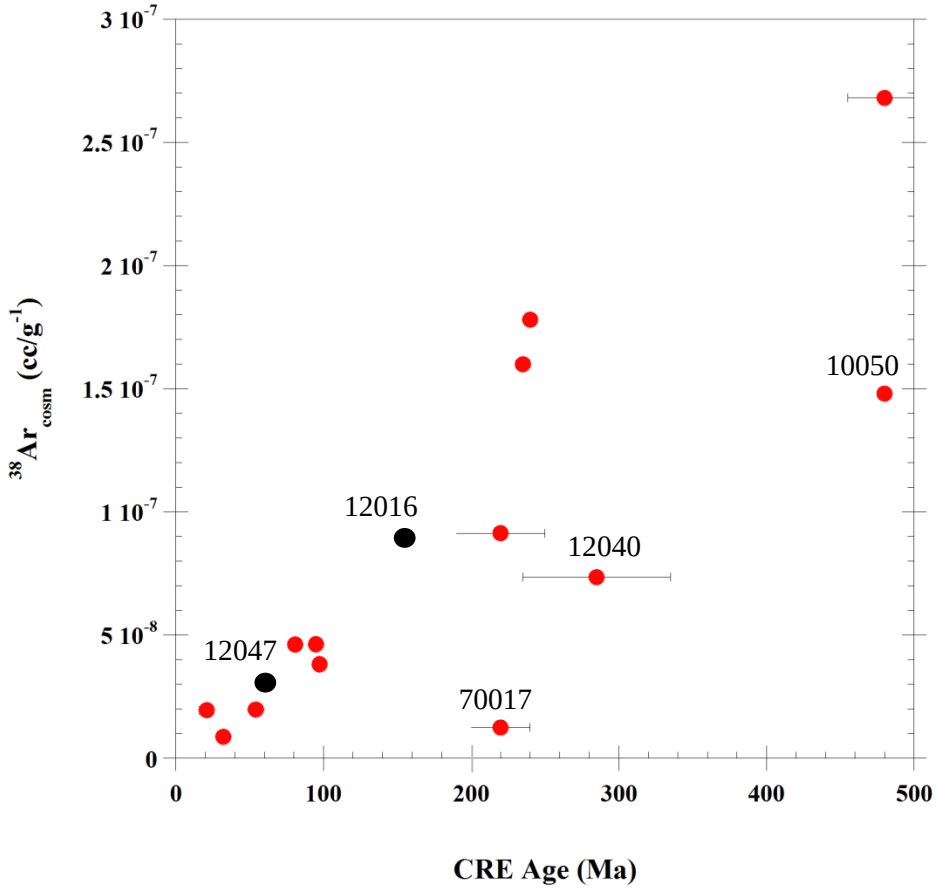

Figure 4.3.3.2.1: Correlation between CRE age and calculated abundances of cosmogenic ^{38}Ar in powdered mare basalt samples. CRE ages are taken from Table 2.1 and references therein. Three samples which do not fit the correlation displayed by the other basalts are labelled (10050, 12040, and 70017). Samples 12016 and 12047 (which do not have published CRE ages) are shown in black circles, positioned along the main correlation line according to their calculated cosmogenic ^{38}Ar abundances.

4.3.3.3: Cosmogenic Nitrogen

In addition to the correlations observed between cosmogenic ^{21}Ne abundance, cosmogenic ^{38}Ar abundance, and published exposure ages for mare basalts, the abundance of cosmogenic ^{15}N is well-correlated with published exposure ages (excepting 70035, which has a much lower abundance of cosmogenic ^{15}N than expected compared to other samples of a similar exposure age) (Fig. 4.3.3.3.1). Since cosmogenic ^{15}N is produced via spallation from target ^{16}O atoms (Mathew and Marti, 2001), which are ubiquitous in silicate samples such as basalts, final measured abundances of cosmogenic ^{15}N ought to be unaffected by compositional variations.

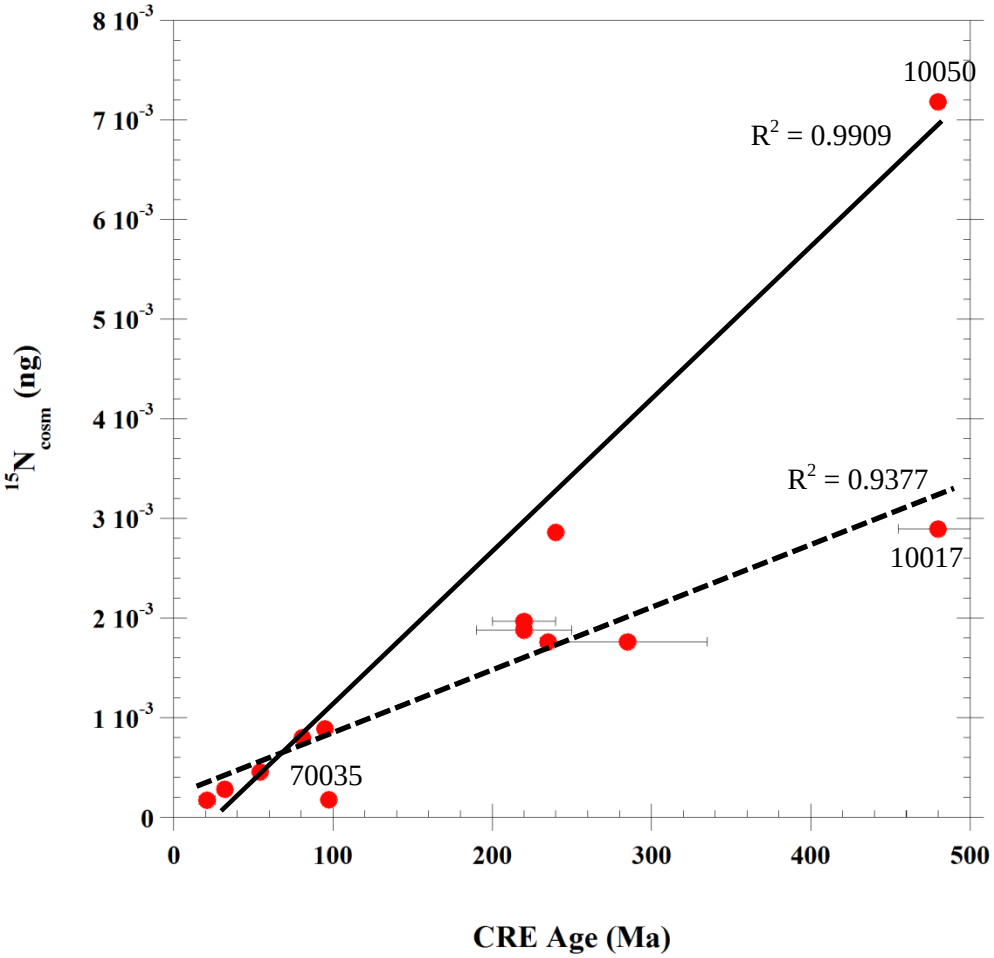

Figure 4.3.3.3.1: Correlation between CRE age and abundances of cosmogenic ^{15}N in powdered mare basalt samples. CRE ages are taken from Table 2.1 and references therein. 70035 does not fit the otherwise excellent correlation seen for the group of samples exposed for the shortest time.

Interestingly, discounting 70035, there seems to be two separate trends observed in the data; a steeper trendline (shown in solid black in Fig. 4.3.3.3.1), passing through samples up to 95 Ma, and including 10072 (at 240 Ma) and 10050 (at 480 Ma) with an R^2 value of 0.9909, and a slightly shallower trendline (in dashed black in Fig. 4.3.3.3.1) passing through the same samples up to 95 Ma, and including 12064 and 70017 (at 220 Ma), 15386 (at 235 Ma), 12040 (at 285 Ma), and 10017 (at 480 Ma), with an R^2 value of 0.9377. Perhaps this reflects the fact that these aliquots were taken from samples collected from different locations on the lunar surface, none of which were in situ outcrops, and so separate samples will have experienced very different exposure histories, with some sitting at the top of the regolith, undisturbed for the entire duration of their exposure, and others experiencing more frequent burial/re-exposure cycles caused by the bombardment of the lunar surface by impactors; such burial/turnover of individual samples would provide varying degrees of shielding from incident cosmic rays and so have an effect on the production of cosmogenic ^{15}N. Also, these aliquots were subsampled from the interiors of the original collected sample masses, and so could have experienced different levels of shielding depending upon the location of the subsampling area relative to the exterior of the main sample mass, and its original orientation on the lunar surface.

Assuming that published CRE ages for these samples are correct, using these abundances of cosmogenic ^{15}N, an average production rate for cosmogenic ^{15}N (P_{15}) of 1.67E-12 g ^{15}N/g rock/Ma is calculated. There is considerable variation in calculated P_{15} values between samples, with one sample giving a production rate an order of magnitude lower than the rate calculated for shielding at 225g/cm^2 (P_{15} = 3.2E-12 g ^{15}N/g rock/Ma (Mathew and Murty, 1993)). Perhaps this variation in production rates may be an artefact of very little N being released above system blank levels at temperature steps over 1000 ºC,

thereby introducing large errors on $\delta^{15}N$ values for these releases, from which cosmogenic ^{15}N abundances are then calculated.

However, taking into account either or both of these correlations, it seems that the abundance of cosmogenic ^{15}N (released at temperatures above ~ 1000 ºC) may also be a useful exposure parameter, alongside cosmogenic noble gases.

While abundances of cosmogenic ^{21}Ne suggest CRE ages for 12016 and 12047 of 150 Ma and 70 Ma (respectively), and abundances of cosmogenic ^{38}Ar suggest CRE ages of 160 Ma and 60 Ma (respectively), abundances of cosmogenic ^{15}N suggest slightly shorter exposure ages of ~ 50 Ma and 40 Ma respectively.

Chapter Five:
Lunar Soil Analysis

The following chapter is written as a manuscript and is being submitted to Meteoritics and Planetary Science for peer review. Stepped combustion work was conducted by J. Mortimer. Stepped crushing was performed by A. B. Verchovsky and A. Buikin (Vernadsky Institute of Geochemistry and Analytical Chemistry, Moscow, Russia); the crushing results were processed and interpreted by J. Mortimer.

Volatiles in Lunar Soils

Introduction

For decades, there has been debate about the source(s) of nitrogen in lunar soil samples; since noble gases in lunar soils are predominantly solar, and nitrogen is both well correlated with these solar components, and likewise, co-located on soil grain surfaces (Wieler et al, 1999), a predominantly solar source for nitrogen was expected. However, stepped heating analyses of lunar regolith have consistently revealed a similar release profile across all Apollo and Luna soils, with low temperature, ^{15}N-enriched nitrogen preceding a mid-temperature, ^{15}N-depleted component, which is then followed at the highest temperature steps by a second ^{15}N-enriched release (e.g. Assonov et al, 2002; Brilliant et al, 1994). This pattern of heavy-light-heavy ('V-shaped') nitrogen, with large-scale variations in nitrogen isotopic composition of around 300 ‰ (Assonov et al, 2002; Becker and Clayton, 1975; Brilliant et al, 1994; Clayton and Thiemens, 1980; Frick et al, 1988; Füri et al, 2012; Kerridge, 1975, 1993; Wieler et al, 1999), coupled with the observation that N isotopic variations correlate with ^{40}Ar/^{36}Ar ratios (which are taken as a proxy for soil antiquity, or when in the past a soil was exposed at the lunar surface) (Furi et al, 2012), led many to suggest that the composition of the solar wind must have changed over time, becoming relatively more enriched in ^{15}N (Becker and Clayton, 1975; Clayton and Thiemens, 1980; Kerridge, 1975).

In contrast, solar noble gases as measured in soils display very minor variations in comparison to nitrogen isotopic compositions (e.g. Kerridge, 1989, 1993), casting doubt on a predominantly solar source of nitrogen in soils. Further, N/^{36}Ar ratios measured in soils (Assonov et al, 2002; Frick et al., 1988; Kerridge, 1993; Wieler et al, 1999) are around ten times greater than the solar elemental abundance ratio of 37 (Anders and Grevesse, 1989),

and, whilst ^{15}N-depleted ('light') nitrogen is correlated with the release of solar wind D-depleted hydrogen from the outer rims of lunar soil grains, ^{15}N-enriched ('heavy') nitrogen correlates with the release of D-enriched hydrogen from a planetary source (Hashizume et al, 2000). Thus, the observed trend of higher average δ^{15}N values with decreasing soil antiquity may not be caused by a secular variation in solar wind composition, but instead may be recording a change in the relative contribution of a planetary nitrogen source to the lunar surface (Hashizume et al, 2002). Therefore, many now agree that nitrogen in lunar soils represents mixing between a 'heavy' planetary nitrogen component with a solar wind component of 'light' composition (Assonov et al, 2002; Furi et al, 2012; Geiss and Bochsler, 1982; Hashizume et al., 2000, 2002; Marty et al., 2003; Ozima et al., 2005; Wieler et al., 1999). This has been supported by recent direct measurements of solar wind nitrogen implanted into the Genesis Solar Wind Concentrator target, which gave a modern-day δ^{15}N value for solar wind of -407 ± 7 ‰ (Marty et al, 2011), comparable to the composition of protosolar nitrogen (-383 ± 8 ‰ (Marty et al, 2011)), and to that of the Jovian atmosphere (Owen et al., 2001).

In light of this, Furi et al (2012) calculated that most of the nitrogen released from Luna 24 soil grains is from a non-solar source with a planetary composition of between +100 ‰ and +160 ‰, assuming binary mixing with ^{15}N-depleted solar wind, with the highest proportion contribution from a non-solar source being found in recently exposed Apollo soils (with ^{40}Ar/^{36}Ar ratios ≤ 1.5).

In this study, a diverse set of Apollo lunar soils have been analysed both by stepped combustion and by mechanical crushing *in vacuo*. With both methods, gases released were simultaneously analysed for nitrogen and noble gases (He, Ne, and Ar).

Samples

Five Apollo lunar soils, representing both extremely mature (e.g. $I_s/FeO = 94$) and immature (e.g. $I_s/FeO = 5.7$) samples, and covering a range of collection locations, from Apollo 12, 14, 15, 16, and 17, and including both shaded soils and samples collected at the surface of the regolith in unshaded locations, were chosen for stepped combustion analyses (with 12070 analysed twice) (Table 1). Of these, further aliquots of the same allocated sample material were taken for three of the lunar soils, for the purposes of crushing under vacuum conditions (Table 2). All samples, regardless of volatile extraction method, were analysed using the same gas clean-up and separation sections, and mass spectrometers (as outlined in Methods).

Apollo Sample	Weight (mg) (Combustion)	Weight (mg) (Crushing)	Maturity (I_s/FeO)	Description
12070	Run 1: 2.063 Run 2: 5.211	22.2	47[a]	Collected as part of the contingency sample, taken from a location in front of the Lunar Module (LM)
14141	7.637	21.7	5.7[a]	Coarse soil, collected from near the rim of Cone Crater
15040	5.662	-	94[a]	Collected at Station 8, from the surface at the top of a trench
69921	5.377	24.7	90[a]	Skim soil, collected from top 1 cm of regolith in shaded area next to a small (0.5 m) boulder at Station 9
72501	4.710	-	81[a]	Collected from landslide at Station 2, at the base of the slope of the South Massif, close to Nansen Crater

Table 5.1: List of five lunar soil samples chosen for stepped combustion analysis, with the weights of three of these soils that were chosen for crushing analysis. ([a] Morris, 1978).

Methods

For stepped combustion analyses, samples were weighed out and transferred into 4 mm x 4 mm clean platinum foil buckets in a Class 100 clean room (Pt foil cleaning methods are as described in Abernethy et al., 2013). Tweezers and spatulas used to transfer the sample fines from their respective vials to the platinum buckets were cleaned before use, and wiped with acetone using lint-free cloths between uses with separate samples. For crushing analyses, soil samples were weighed out in the same Class 100 clean room, and transferred to the laboratory in vials for introduction into the crushing tube.

The 'Finesse' mass spectrometric instrument used in this study is a custom-built mass spectrometer system, consisting of three dedicated static-mode mass spectrometers (one for carbon, one for nitrogen and argon, and a quadrupole for helium and neon), all linked *via* high vacuum lines to a common sample inlet and gas clean-up sections, and combustion furnace (see Verchovsky et al., 1997 ; Wright et al., 1988; and Wright and Pillinger, 1989 for further details, and Boyd et al., 1997, for a review of the stepped-heating method). The custom-built small volume mechanical crusher (Figure 1) is also attached to this triple mass spectrometer and gas clean-up system, and consists of a vertical stainless steel tube mounted on a 34 mm flange, with a concave stainless steel end piece at the bottom (into which the sample is loaded). A magnetic metal rod of a slightly smaller diameter than the inside of the crushing tube is then inserted; this crushing rod has a convex lower end designed to fit the curve of the concave sample holding depression at the base of the crushing tube. The top of the crushing tube is attached, *via* a stainless steel vacuum line and computer-controlled pneumatic valve, to the main gas handling and analysis sections of 'Finesse', allowing the crusher to be pumped down to vacuum and baked out at ~ 200 ºC for 12 hours before crushing begins, and for immediate transfer of released gases to the

mass spectrometers at predetermined steps during the crushing procedure. A series of five computer-controlled solenoids on the outside of the crushing tube work in sequence to raise the magnetic crushing rod inside, before it is allowed to drop back down onto the sample. Gases released during crushing are held in the crushing tube until transfer into the rest of the mass spectrometer system for cleaning, separation, and measurements. The crusher is cleaned after every sample with fine sandpaper (to remove any ingrained material from internal surfaces), and washed with acetone before being sonicated overnight.

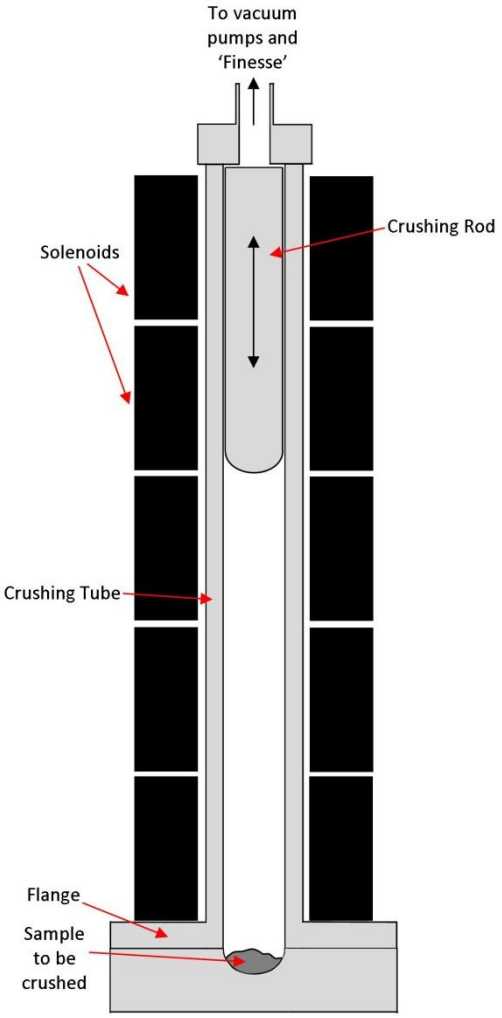

Figure 5.1: Diagram of the mechanical crusher used in this study.

Stepped Combustion Procedure

Samples were combusted in oxygen, supplied from CuO, in a double-walled quartz-ceramic furnace for 30 minutes at each temperature step, followed by 15 min for oxygen resorption, before transfer

of the gases produced to the clean-up section. For Run 1 of soil 12070, twelve combustion steps were used, in 100 ºC steps from 300 to 1400 ºC. However, for Run 2 of soil 12070, fifteen combustion steps were employed to acquire higher-resolution data, heating in 100 ºC steps from 200 to 700 ºC, then in 50 ºC steps from 750 to 850 ºC, followed by 100 ºC steps from 900 to 1400 ºC. All other soil samples were combusted in seventeen temperature steps, in increments of 100 ºC from 200 to 600 ºC, then in 50 ºC steps from 650 to 850 ºC, followed by 100 ºC steps from 900 to 1400 ºC. During stepped combustion analyses, C, N, He, Ne, and Ar data were collected.

Crushing Procedure

Samples were crushed in steps under vacuum conditions, with the released gases being transferred to the clean-up and analysis sections of 'Finesse' after a predetermined number of strokes had been completed. The number of strokes between transfers of gases out of the crusher was increased during the analyses, from an initial ten strokes, up to durations of 2000 to 3000 strokes each time. Cumulatively, the number of crushing strokes performed on a sample totalled 14280 strokes for 12070, 13880 strokes for 14141, and 18880 strokes for 69921. The cumulative numbers of strokes a sample experienced varied based on the measured release of gases; for each sample, crushing ended when the abundance of gas released per stroke had decreased to almost negligible amounts. Unlike stepped combustion analyses, C was not measured during the crushing experiments, only N and noble gases (He, Ne, and Ar).

Gas fractions released from both stepped combustion and crushing extraction procedures were processed in the same way. First, the released gases were cryogenically separated using liquid nitrogen cooled traps, one of which was filled with a molecular sieve. Argon and neon were purified using Ti–Al getters, and nitrogen was purified using a CuO furnace to ensure no CO was present. Carbon yields (recorded as ng of C) were calculated using the pressure of CO_2 measured on a calibrated MKS Baratron™ capacitance manometer. Nitrogen yields (also recorded as ng) were measured *via* calibration of the mass spectrometer ion current at $m/z = 28$, with yields of noble gases also determined by calibration of mass spectrometer peak intensities at the appropriate *m/z* values. Gases were transferred to different parts of the machine using a system of computer-controlled pneumatic valves. For each temperature step, the isotopes of C, N, He, Ne, and Ar were measured sequentially, taking approximately 1.5 hours to complete the cycle for five elements. Once all measurements were complete, the high vacuum line was pumped before the next temperature step.

In order to reduce the contributions from CO_2^{++} and $^{40}Ar^{++}$ on Ne masses (22 and 20), a low ionisation voltage of ~ 40 V was used in the quadrupole ion source. Also, Ar present in the system was cooled down on the molecular sieves and the Ti–Al getter was open to the mass spectrometer chamber during Ne measurements.

Isotopic data are expressed using the delta (δ) notation, as parts per thousand (‰) deviations from standards (Vienna Peedee Belemnite ($_{VPDB}$) for C, and terrestrial air ($_{AIR}$) for N). System blanks

were monitored between sample analyses by putting an empty clean Pt foil bucket through the same stepped combustion procedure used for the lunar samples and collecting both abundance and isotopic data. Typical system blank levels for stepped combustion were < 10 ng of C and < 1 ng of N. Typical system blanks for ^{4}He were < 1E-7 cc, for ^{20}Ne were <

6.5E-10 cc, and for ^{40}Ar and ^{36}Ar were < 8E-9 cc and < 1.2E-10, respectively. For crushing analyses, system blanks were monitored at several stages during the total sample crushing runs by stopping crushing and closing off the crushing tube for a length of time comparable to the next crushing step duration, and typically these were < 0.76 ng of N, < 6E-9 cc for ^{20}Ne, < 8.5E-6 cc for ^{4}He, and for ^{40}Ar and ^{36}Ar were < 1.65E-8 cc and < 3.7E-10 cc, respectively.

All data presented in this manuscript have been corrected for the contribution of system blanks (unless otherwise stated), and any isotopic averages presented are calculated as weighted averages.

Stepped Combustion Results

Stepped combustion analyses in this study reveal volatile releases that are in excellent agreement with previous combustion work. For all soil samples, N is released in the characteristic heavy-light-heavy isotopic profile (as previously observed by Assonov et al, 2002; Brilliant et al, 1994 etc) (Table E; Figure 2).

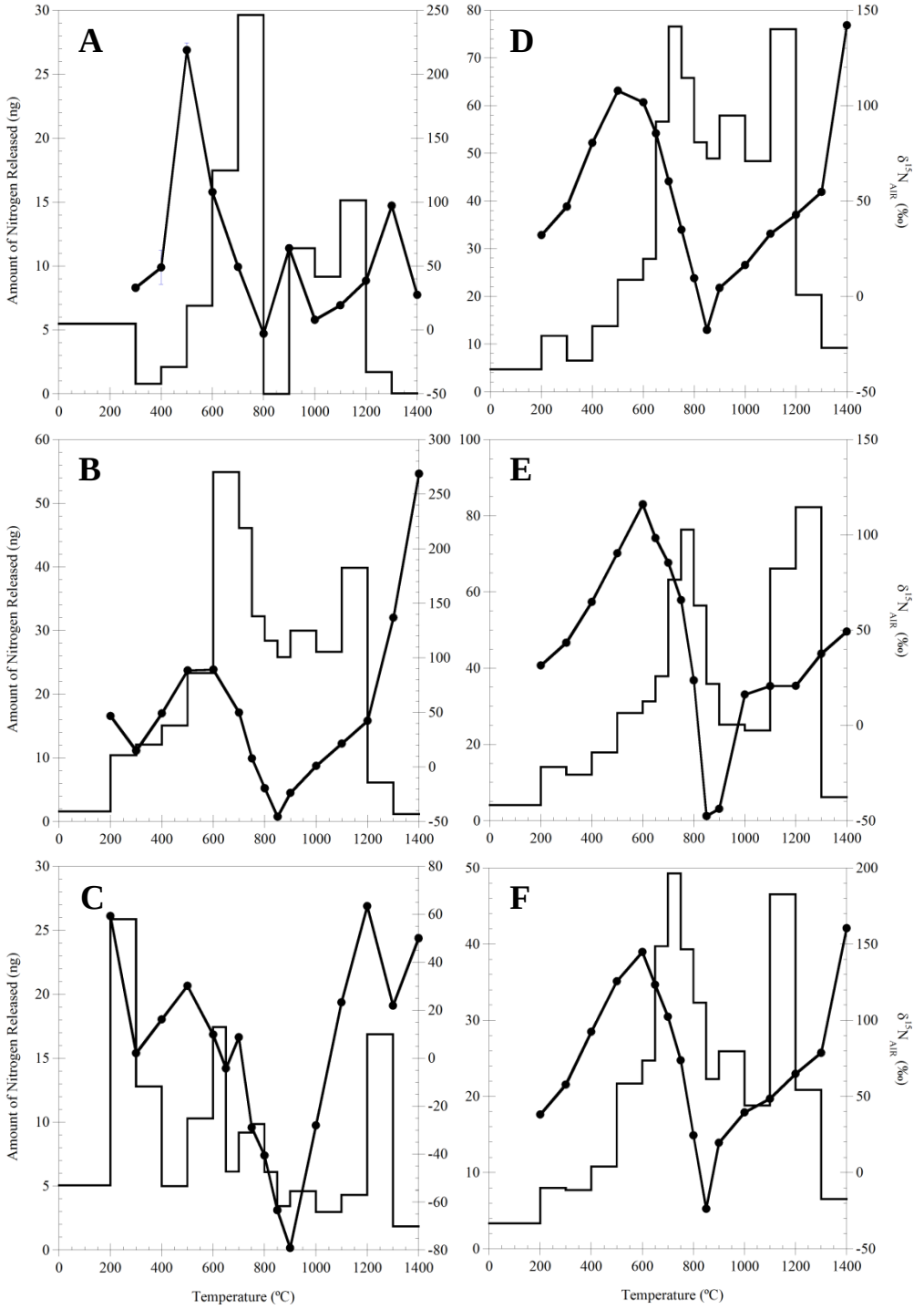

Figure 5.2: Step plots showing nitrogen release profiles for all soils analysed by stepped combustion. Abundances, measured on left-hand axis, are displayed as a histogram, and isotopic compositions, measured on the right-hand axis, are displayed as a line graph. (A = 12070 Run 1; B = 12070 Run 2; C = 14141; D = 15040; E = 69921; F = 72501).

For each soil, the most ^{15}N-depleted ('lightest') isotopic signature is measured at 850-900 ºC (apart from 12070 Run 1 (Panel A, Figure 2), where the 900 ºC step released N at little over the system blank level). It must be noted that the combustion steps releasing the lightest nitrogen component are not coincident with the maximum N abundances, but instead are associated with some of the lower released abundances (relative to combustion steps at temperatures either side of 850-900 ºC), which, given a solar wind N isotopic signature of around -400 ‰ (Marty et al, 2011), indicates that the main contributor to N abundances in lunar soils must be from a non-solar source with a much more ^{15}N-enriched ('heavier') isotopic composition (see Discussion section).

In contrast to N releases, hundreds of ng of C are released from the first few temperature steps, up to 500-600 ºC. This is associated with the release of terrestrial contaminants from the samples. However, above this temperature, two further releases of C are observed in all soils; one at roughly 600-900 ºC, and a second at temperatures above 1000 ºC (Table D; Figure 3). Although large uncertainties are associated with some of these C releases, C isotopic composition varies considerably; in some samples (14141, 15040, and 72501) there is an apparent relative depletion in ^{13}C associated with the 600-900 ºC release peak of C, but in general, despite variations in isotopic composition, δ^{13}C values for C released above around 600 ºC are positive (i.e. ^{13}C-enriched). The exception to this observation is 14141, which is the least mature soil included in this sample set. Whilst this soil shows similar relative patterns of varying isotopic composition to the other, more mature, soils, in this case, δ^{13}C values remain between -35 ‰ and -20 ‰.

Again, as previously noted by others (e.g. Assonov et al, 2002; Brilliant et al, 1994; Hohenberg et al, 1970), ^{40}Ar, ^{36}Ar, and N are co-released in all samples (Figures 4 and 5), albeit with an additional release peak of ^{40}Ar at lower temperatures (typically between 400

ºC and 600 ºC) that is not observed in releases of ^{36}Ar, which gives rise to the elevated $^{40}Ar/^{36}Ar$ ratios at these lower temperatures (Table B). Assonov et al (2002) explain this low temperature ^{40}Ar release as being attributable to terrestrial atmospheric contamination and/or re-implantation of ^{40}Ar liberated to the lunar atmosphere during regolith reworking events (this re-implanted ^{40}Ar being much more loosely fixed at the surfaces of grains which have experienced little or no reworking than the bulk of the argon contained in the soils, which, after soil reworking, is immured deeper within grains; thus re-implanted ^{40}Ar is liberated at lower temperatures during analysis). As noted in previous studies (e.g. Assonov et al, 2002), atomic $N/^{36}Ar$ ratios above ~650 ºC are relatively constant, at around ten times the solar ratio (as estimated by Anders and Grevesse, 1989).

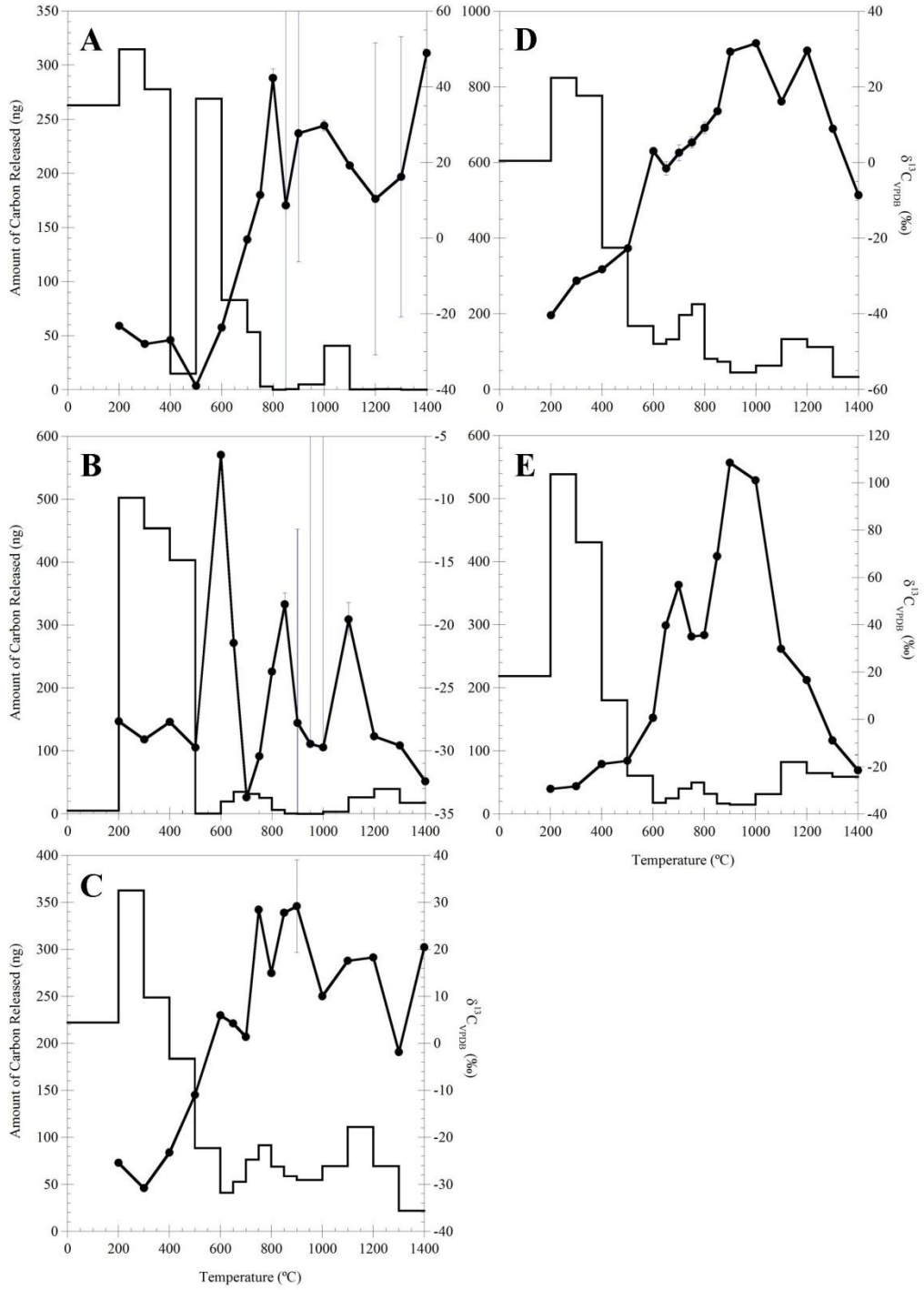

Figure 5.3: Step plots showing carbon release profiles for soils analysed by stepped combustion. N.B: No carbon data was collected for 12070 Run 1. Abundances, measured on left-hand axis, are displayed as a histogram, and isotopic compositions, measured on the right-hand axis, are displayed as a line graph. (A = 12070 Run 2; B = 14141; C = 15040; D = 69921; E = 72501).

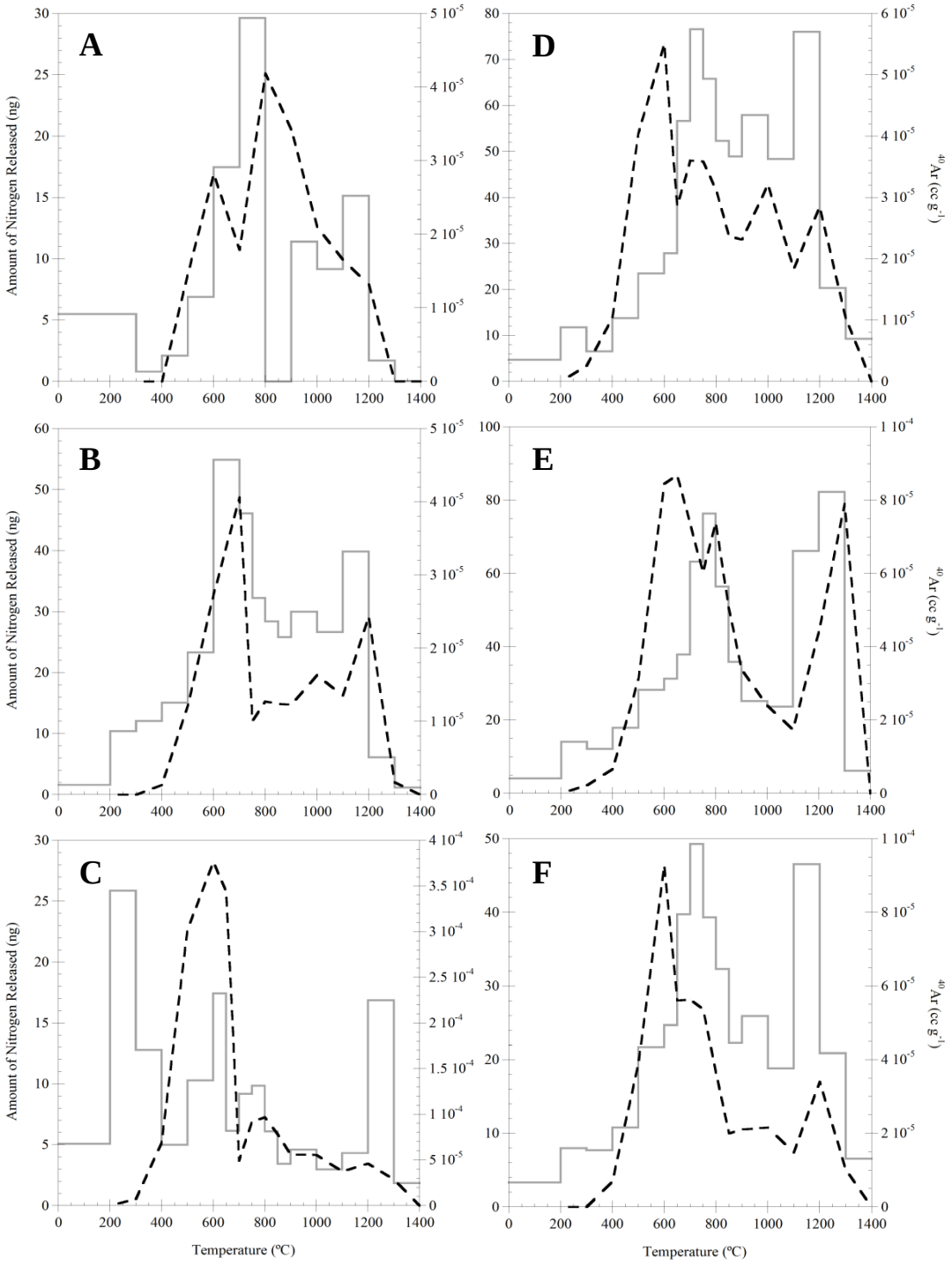

Figure 5.4: Release patterns for nitrogen (grey histogram, with values corresponding to the left-hand axis) and ^{40}Ar (dotted black lines, with values corresponding to the right-hand axis) abundances, showing the co-release of ^{40}Ar and N at temperatures above ~ 650 ºC, plus the additional low temperature (400-600 ºC) release of ^{40}Ar, attributable to terrestrial atmospheric contamination and/or re-implanted ^{40}Ar liberated into the lunar atmosphere by impact reworking of the lunar regolith (Assonov et al, 2002). (A = 12070 Run 1; B = 12070 Run 2; C = 14141; D = 15040; E = 69921; F = 72501).

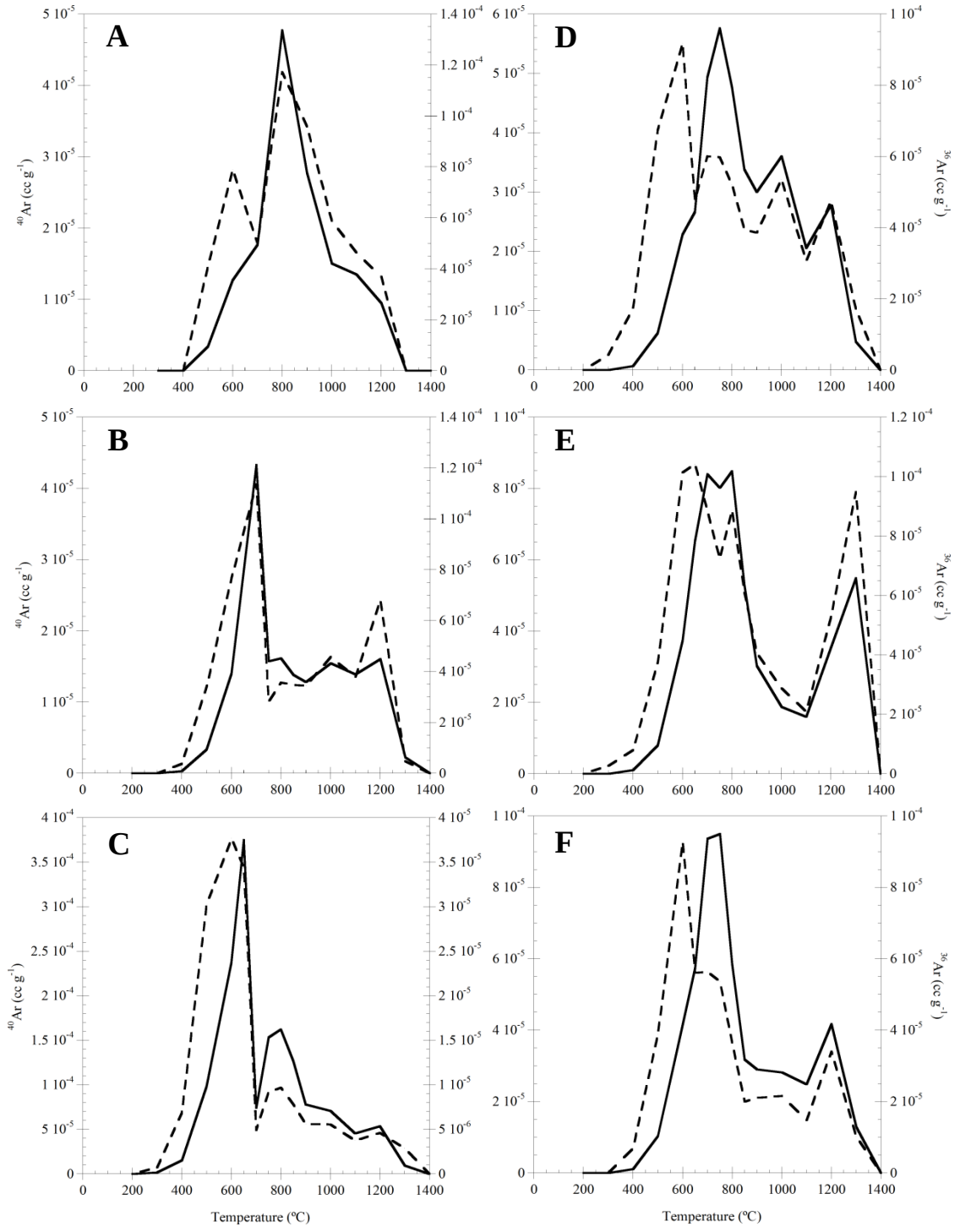

Figure 5.5: Release patterns of ^{40}Ar (black dotted lines, with values corresponding to the left-hand axis) and ^{36}Ar (solid black lines, with values corresponding to the right-hand axis), showing co-release of both isotopes at temperatures over approximately 650 ºC. (A = 12070 Run 1; B = 12070 Run 2; C = 14141; D = 15040; E = 69921; F = 72501).

^{4}He is released from all soil samples by stepped combustion (Figure 6), and is present in much greater abundances than in lunar basalts (Mortimer et al, 2015). However, unlike ^{4}He in mare basalts, which is of radiogenic origin, ^{4}He in soils is from a solar wind source (e.g. Wieler, 1998).

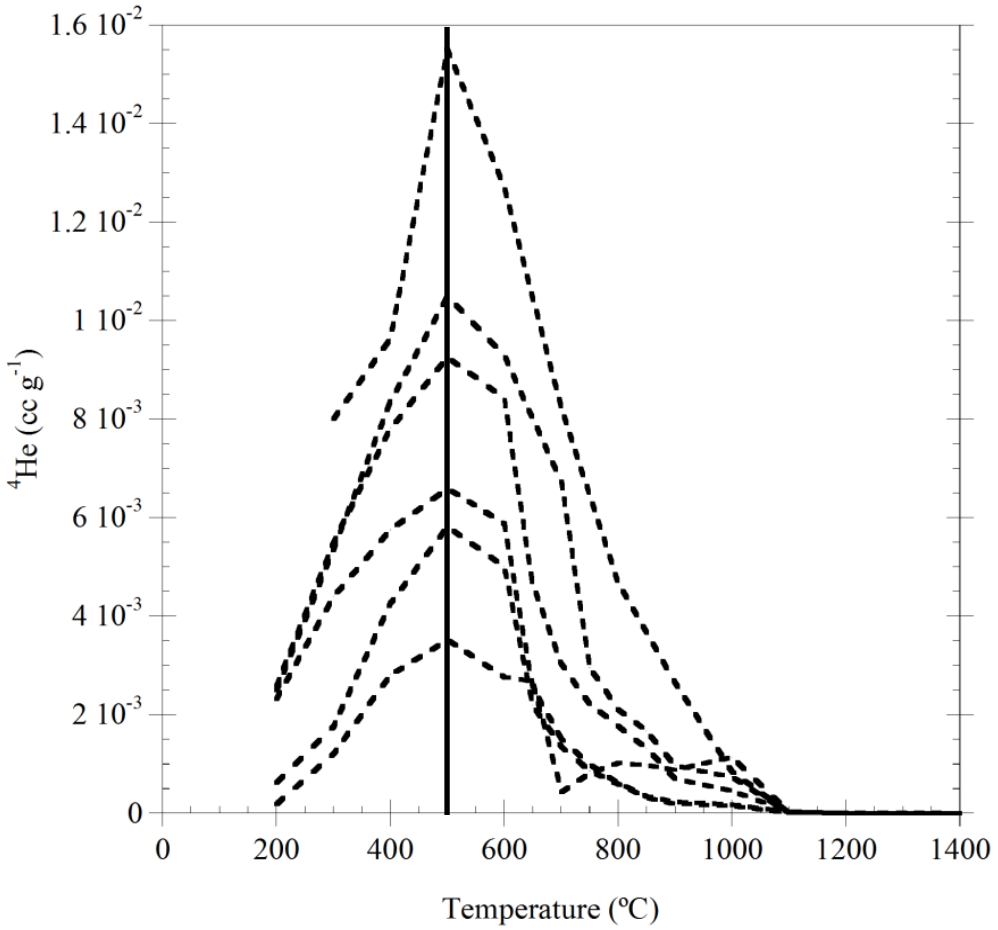

Figure 5.6: Stepped combustion releases of ^{4}He from all soil samples in this study, showing varying abundances between samples, but the common peak release temperature of 500 ºC (vertical black line).

Neon is also released from all soil samples by stepped combustion (Table C); after correcting Ne isotope ratios for both the contribution of a system blank of atmospheric composition, and for the effects of fractionation in the mass spectrometer during analysis, the majority of the Ne released by combustion appears to be from a solar source, which is

fractionated away from the pure solar values upon implantation into the lunar surface. This dominant solar Ne component is also mixed with a much less abundant cosmogenic Ne component in some samples, although even the highest temperature steps still appear to be a mixture of solar and cosmogenic Ne (Table H; Figure 7).

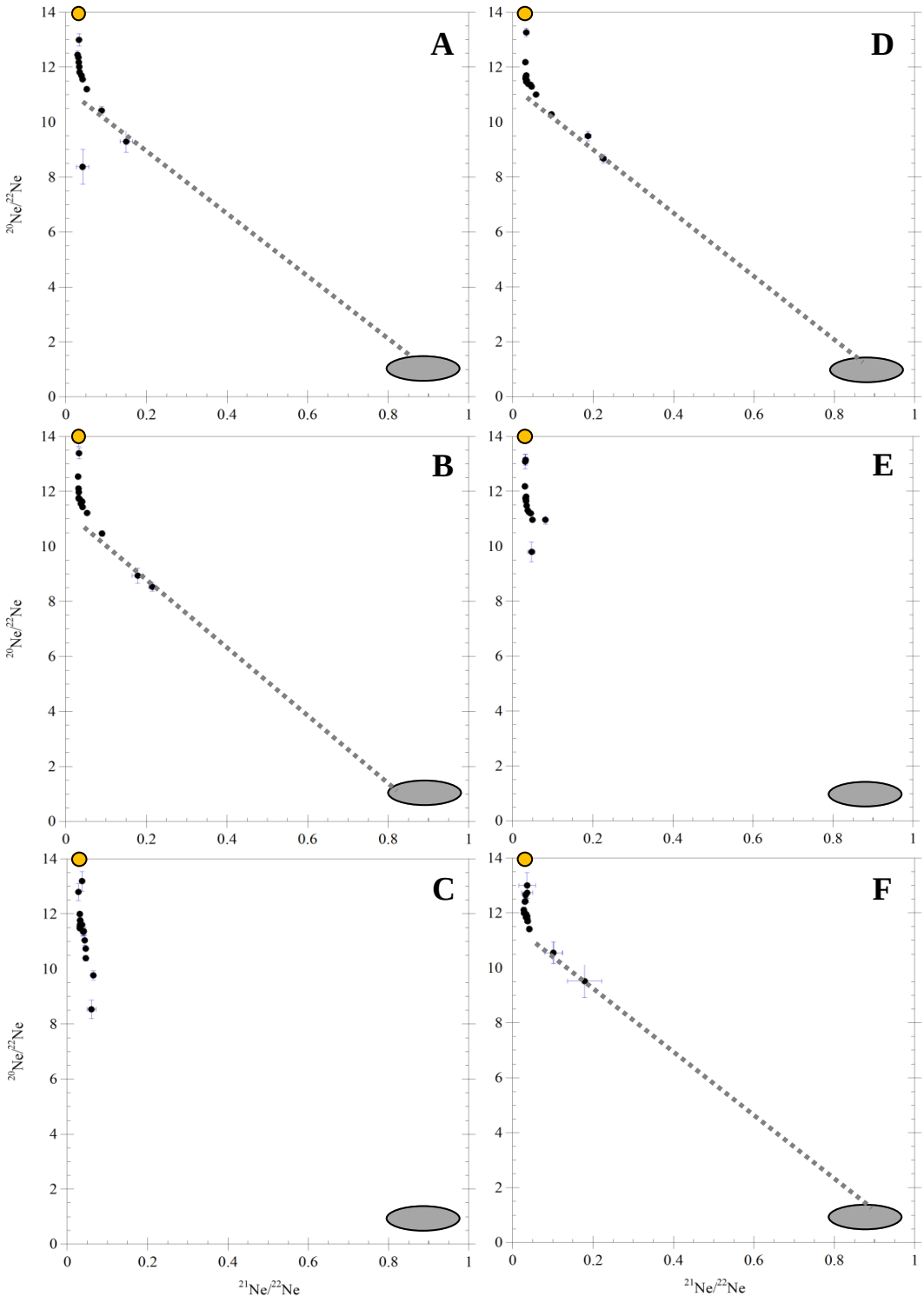

Figure 5.7: Neon isotopic compositions for stepped combustion analyses of lunar soils. Most of the neon released is from a solar source, fractionated away from true solar values during implantation. In some soils, this fractionated solar neon component is mixed with a minor cosmogenic neon component (grey dotted lines indicate mixing trend). Solar and cosmogenic end-member compositions are represented by orange circles and grey ellipses (respectively). Instrument errors are 5 %. (A = 12070 Run 1; B = 12070 Run 2; C = 14141; D = 15040; E = 69921; F = 72501).

Crushing Results

Noble gas (He, Ne, and Ar) and nitrogen data were collected for soils 12070, 14141, and 69921. Carbon data were not collected during crushing analyses.

Crushing in vacuum released much lower abundances of nitrogen from the samples than stepped combustion, ranging from 0.2 % of the total combustion release to 1.8 % (Table 3). Most of the nitrogen that was released by crushing was liberated within the first few tens to hundreds of strokes (Table F; Figure 8), with a marked decrease in the amount of N being released as crushing progressed. The fact that crushing only releases a few percent of the total N known to be liberated by stepped combustion suggests that the mechanism of nitrogen release is different to that of noble gases. Being highly reactive, nitrogen may be more strongly bound to molecules within minerals than unreactive noble gases, making it much less likely to be released. Also, if nitrogen is bound up in crystal lattices, and not weakly implanted into grain surfaces (as solar noble gases are), then it will require longer timescales to diffuse out from these deeper depths into void spaces in sample material, from where it can be released when these voids are cracked open during crushing. There may also be a kinetic effect at work, with any frictional heating caused by crushing happening in a highly localised and transient way (i.e. not equilibrium heating, as with stepped combustion). In this case, soil grains may not experience heating for long enough to aid the release of bound nitrogen and its diffusion into void spaces within the sample. Interestingly, despite the low abundances of N released by crushing, there is a positive correlation between the total N abundance (from crushing) and soil maturity.

Sample	Total N from Combustion (ng/g)	Total N from Crushing (ng/g)	% of Combustion Total Released by Crushing
12070	254.24 (Run2)	0.60	0.2
14141	18.56	0.34	1.8
69921	108.04	1.51	1.4

Table 5.2: Total N abundances released by stepped combustion, compared with total N abundances released from lunar soils by crushing.

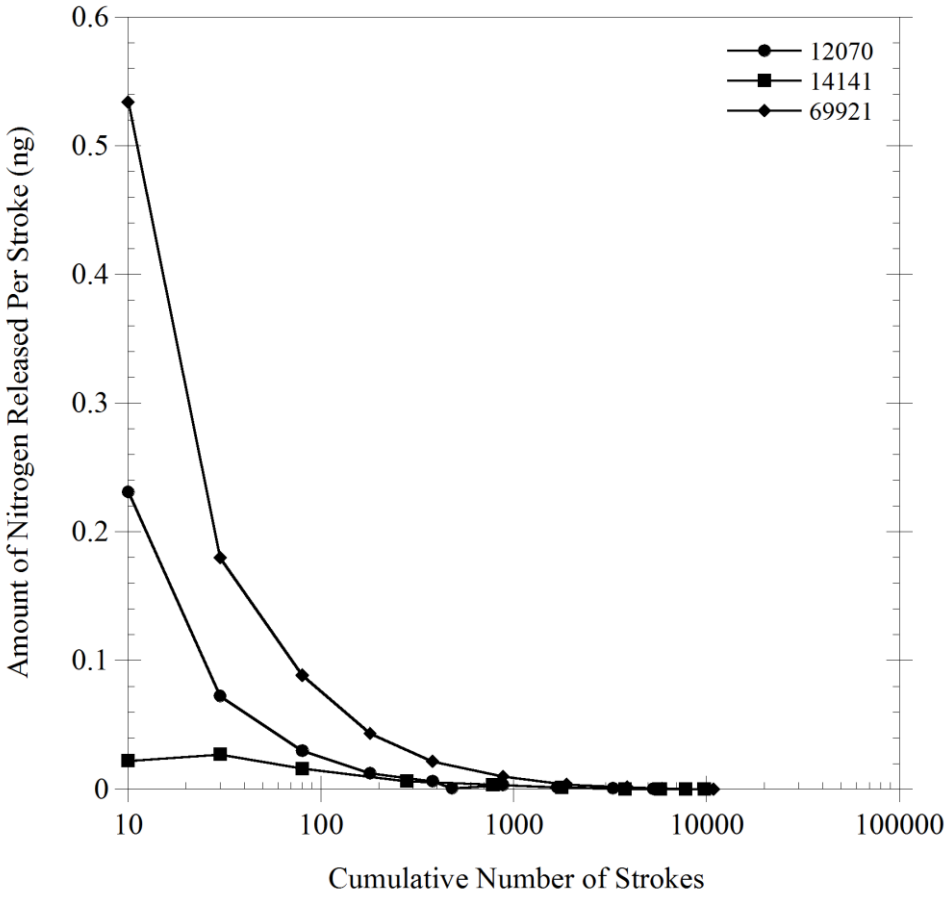

Figure 5.8: Cumulative release curves for nitrogen released by crushing, showing the rate at which N is released slowing down considerably after the first few hundred strokes.

Noble gases released by crushing display some unusual trends. During stepped combustion analyses, ^{4}He reaches maximum release first, followed by ^{20}Ne, and then ^{36}Ar; this is true for all samples in this study. However, when crushed, only the least mature soil (14141) shows this trend, with ^{20}Ne released from 12070 and 69921overtaking that of ^{4}He after

several hundred crushing strokes and reaching maximum release first (Table G; Figure 9). Whilst this is unexpected, a possible explanation may be that frictional heating caused by the crushing process is highly localised and affects grain surfaces more than grain interiors. Although both ^{4}He and ^{20}Ne in lunar soils are of solar origin, studies have shown that ^{4}He is implanted to greater depths into grains of target material than neon or argon (e.g. Verchovsky et al., 2003). If this is the case for solar wind implantation into lunar soil grains, it follows that ^{20}Ne would be located closer to the grain surface, and so would be expected to be released first, compared to other ^{4}He.

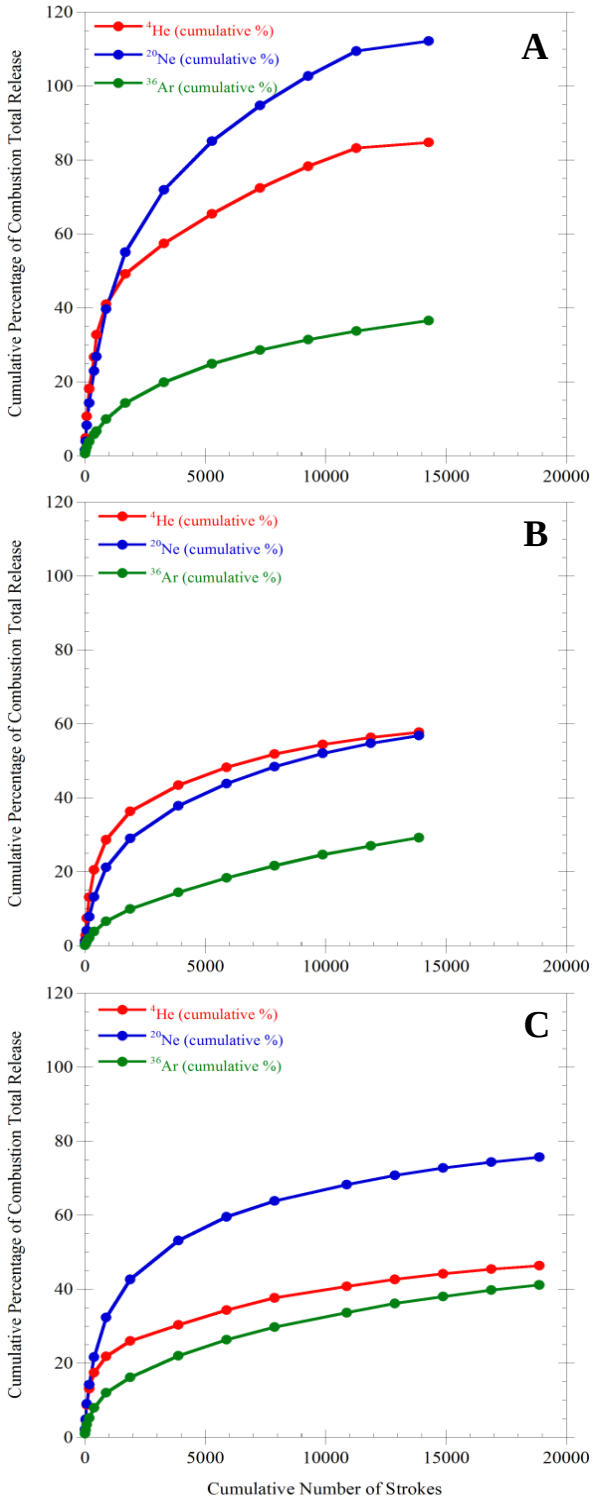

Figure 5.9: Cumulative release curves for ^{4}He, ^{20}Ne, and ^{36}Ar (expressed as percentages of the total abundances released by combustion) for A) 12070, B) 14141, and C) 69921. Note that for A and C (12070 and 69921), release of ^{20}Ne overtakes that of ^{4}He, unlike B (14141), which displays the trend expected based on stepped combustion releases of the same isotopes. Note also that 12070 releases more than 100 % of the total released by combustion.

For most noble gases, total released abundances from crushing appear to be much lower than abundances released by combustion (between 20 % and 40 % of the combustion total for ^{36}Ar, and 40 % to 80 % of the combustion totals for ^{4}He (Table G)), indicating that mechanical crushing is a less efficient method for volatile extraction than combustion techniques. Relative variations in the yield of certain isotopes between samples (in comparison to yields from combustion analyses), including the release of ^{20}Ne from 12070 at 112 % of the abundance released by combustion, are likely caused by sample heterogeneity, with the aliquots used for crushing having a slightly different modal compositions to those taken from the same bulk samples for combustion analyses.

Crushing of lunar soils yields variable ^{4}He/^{20}Ne and ^{20}Ne/^{36}Ar ratios (Table 4), although the range of ratios measured for 12070 and 14141 are comparable in both cases. Ratios measured during crushing of 69921, however, show a much tighter range of values for both ^{4}He/^{20}Ne and ^{20}Ne/^{36}Ar, and the ratios themselves are lower. Nevertheless, when these ranges of ratio values from crushing are compared with the ratios derived from each temperature step of the relevant combustion analyses, some similarities emerge. In the case of ^{4}He/^{20}Ne, crushing ratios match combustion ratios over a wide range of temperatures, from 400 ºC up to 900 ºC. ^{20}Ne/^{36}Ar crushing ratios agree with combustion ratios over a much smaller temperature window, from 600 ºC up to 700 ºC. For both ratios, the average combustion temperature of the range that agrees with the crushing ratios is 650 ºC, and thus we tentatively suggest that during mechanical crushing in vacuum, individual soil grain surfaces are frictionally heated to similar temperatures locally, which facilitates the release of volatiles.

Sample	$^{4}He/^{20}Ne$ range (crushing)	Corresponding Combustion Temperature Range		$^{20}Ne/^{36}Ar$ range (crushing)	Corresponding Combustion Temperature Range
12070	18.2 to 57.1	500-900 °C		3.9 to 18.4	600-700 °C
14141	19.7 to 61.3	400-800 °C		4.0 to 15.9	600 °C
69921	10.0 to 26.2	500-750 °C		1.7 to 5.4	650 °C
		Min. Temp. = 400 °C Max. Temp. = 900 °C Av. Temp. = 650 °C			Min. Temp. = 600 °C Max. Temp. = 700 °C Av. Temp. = 650 °C

Table 5.3: $^{4}He/^{20}Ne$ and $^{20}Ne/^{36}Ar$ ratios measured during soil crushing analyses, with combustion temperatures which yield matching ratios.

If crushing does cause the samples to be heated to between 400 ºC and 900 ºC, this helps to explain the Ne isotope ratios measured in crushing analyses. Both combustion runs of 12070 show mixing of mostly implanted (and therefore fractionated) solar Ne with a cosmogenic Ne component, which is only released at temperatures of 900-1000 ºC and over. Ne isotope ratios from crushing analysis of 12070 (Table I; Figure 10) do not show any significant cosmogenic Ne input, and so must have been released at temperatures lower than 900 ºC.

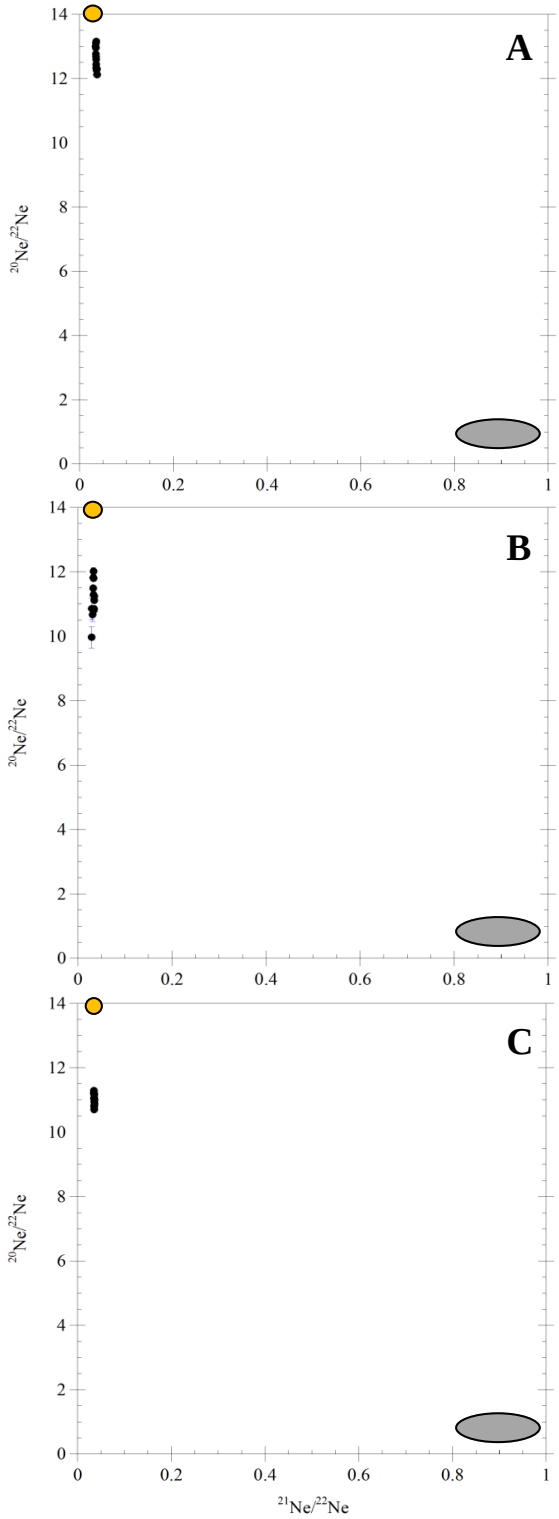

Figure 5.10: Neon isotopic compositions for crushing analyses of lunar soils. Neon released by crushing is from a solar source, fractionated away from true solar values during implantation. Unlike in stepped combustion analyses (Fig.7), solar Ne is not mixed with cosmogenic Ne in these crushing data. Solar and cosmogenic end-member compositions are represented by orange circles and grey ellipses (respectively). Instrument errors are 5 %. (A = 12070; B = 14141; C = 69921).

Discussion

Solar vs non-solar nitrogen

Although spallation processes generated by incoming cosmic rays lead to a significant enrichment in ^{15}N progressively over time as a sample resides at or near to the lunar surface, stepped combustion analyses of lunar basalts demonstrate that such cosmogenic N is only present in very low abundances (between 0.20 ppm and 0.25 ppm) (e.g. Mortimer et al. 2015). Lunar soils contain much greater abundances of total N (ranging from 18.56 ppm N in immature soil 14141, up to 108.04 ppm N in mature soil 69921), and so the effect of a cosmogenic N component on measured isotopic compositions of lunar soils will be negligible. Similarly, stepped combustion analyses of lunar basalts reveal a minor indigenous lunar nitrogen component (at +0.35 ± 9.11 ‰, and present in abundances of between 0.13 ppm and 0.83 ppm (Mortimer et al., 2015)); this is volume-correlated, and as with any cosmogenic N, is several orders of magnitude less abundant than the total N released from lunar soils, which is mostly surface-correlated anyway (e.g. Hashizume et al., 2000). Therefore, for the purposes of the following calculations, it is assumed that inputs from both cosmogenic and indigenous lunar N are so low in relation to the total N release from lunar soils that they have essentially no impact on weighted average (across all temperature steps) N isotopic compositions for each soil sample.

Assuming instead that the total N released from lunar soils represents a binary mixture of solar and non-solar nitrogen components, and taking into account the isotopic composition of the solar wind as measured by Genesis (at -400 ‰ (Marty et al., 2011), it is possible to recreate the calculations of Furi et al., 2012 using data from this study, working backwards from the measured (mixed) N values to derive estimates for both the percentage

contribution from a non-solar source of N to the lunar surface, and the likely isotopic composition of this non-solar contributor.

Weighted average $\delta^{15}N_{tr}$ values (the average value for all the nitrogen trapped in a soil sample) for the soils in this study vary between +1.0 ‰ and +65.7 ‰, with average atomic $^{36}Ar/N$ ratios (normalised to the solar $^{36}Ar/N$ value of 0.02714, taken from Anders and Grevesse, 1989) varying between 0.12 and 0.17 times the solar value (Table 5). The relative proportions of solar and non-solar N are calculated using the following equation:

$$\delta^{15}N_{tr} = \frac{\delta^{15}N_{SW} + f_P\,\delta^{15}N_P}{1 + f_P}$$

where $\delta^{15}N_{tr}$ is the abundance-weighted average value off all the nitrogen trapped in the soil sample, $\delta^{15}N_{SW}$ and $\delta^{15}N_P$ are the end-member isotopic compositions of solar wind nitrogen and non-solar ('planetary') nitrogen, respectively. f_P is the mixing proportion of non-solar to solar nitrogen, and is defined thus:

$$f_P = \frac{N_P}{N_{SW}}$$

Clearly, with $^{36}Ar/N_{tr}$ values varying between $1/9^{th}$ and $1/6^{th}$ of the solar ratio, either $^{36}Ar_{SW}$ has been lost as a result of impact and gardening processes at the lunar surface (with N being preferentially retained as a result of chemisorption onto activated grain surfaces), or a significant proportion of non-solar nitrogen (N_P) has been added to that derived from a solar source (negligible amounts of ^{36}Ar are added from the non-solar source, as evidenced by the majority of other noble gases (i.e. Ne) being derived from solar and not planetary sources). Whilst the preferential loss of solar noble gases over solar nitrogen is certainly an important factor, as evidenced by the relatively easy and abundant releases of noble gases from soils during *in vacuo* crushing compared to the miniscule N

crushing yields, average $\delta^{15}N_{tr}$ values measured in lunar soils by stepped combustion methods display considerable enrichment in ^{15}N relative to the solar end-member value, which strongly suggests that the majority of the N measured in lunar soils comes from a non-solar source. Therefore, when calculating the relative contributions from both solar and non-solar sources of N, assuming that no loss of $^{36}Ar_{SW}$ has taken place, and that all of the difference between measured and solar $^{36}Ar/N$ values is caused by the addition of non-solar N, will give an upper limit to the proportion of non-solar N present, or alternatively, provide the lower limit of the isotopic composition of the non-solar end-member.

Thus, to calculate the mixing proportion (f_P) of non-solar to solar N (N_P/N_{SW}), the following equation is used:

$$\frac{(^{36}Ar/N)_{tr}}{(^{36}Ar/N)_{SW}} = \frac{1 - f_R}{1 + f_P}$$

where $(^{36}Ar/N)_{tr}$ is the average measured ratio for the soil sample, $(^{36}Ar/N)_{SW}$ is the solar ratio taken from Anders and Grevesse (1989), and f_R is the fraction of solar gas lost (which here will be taken to be 0).

Assuming no loss of $^{36}Ar_{SW}$ means that a range of N_P end-member isotopic compositions are required, from +87 ‰ for 12070 (Run 2), up to +140 ‰ for 72501 (Figure 11). However, this range of isotopic compositions results in a much tighter range of mixing proportions between N_P and N_{SW}, with the non-solar nitrogen source contributing 77.15 % of the total N in soil 14141, up to 87.25 % of the total N in soil 15040 (Table 5.4). It is interesting to note that, although most sub-mature and mature soils have a similar relative contribution from a non-solar source (at approximately 86 % to 87 % of the total N in the soils), the sample with the lowest maturity, 14141, also has the lowest relative contribution from non-solar sources of N, at 77.15 %. Therefore, it seems that N contributions from

non-solar sources are increasingly dominant as a soil matures at the lunar surface. Furthermore, despite slight differences in the mixing proportions of solar and non-solar nitrogen sources between samples, it is clear that in all lunar soils, solar N only accounts for a small proportion of the total N present (< 23 % solar N). This conclusion is in agreement with those of Furi et al. (2012), who state that between 60 % and 83 % of the N present in low-antiquity ($^{40}Ar/^{36}Ar$ ratios ≤ 1.5) Apollo soils comes from a non-solar source. All of the Apollo soils used in this study have $^{40}Ar/^{36}Ar$ ratios ≤ 1.5, except 14141, which has a $^{40}Ar/^{36}Ar$ ratio of 10.92. The range of N_P isotopic compositions suggested here is also in close agreement with values (+90 ‰ to +130 ‰) proposed by Furi et al., 2012.

If, however, we assume that some degree of $^{36}Ar_{SW}$ loss is also occurring alongside addition of non-solar N, theoretical mixing lines can be constructed between a solar N end-member (at ~ -400 ‰) and a non-solar (N_P) end-member composition of +140 ‰ (the value suggested by negligible loss of $^{36}Ar_{SW}$ from the most ^{15}N-enriched soil) (Figure 5.11). In this case, 12070 (Run 2) has experienced the largest loss of $^{36}Ar_{SW}$, at ~ 40 % loss (f_R = 0.42) (Table 5.4).

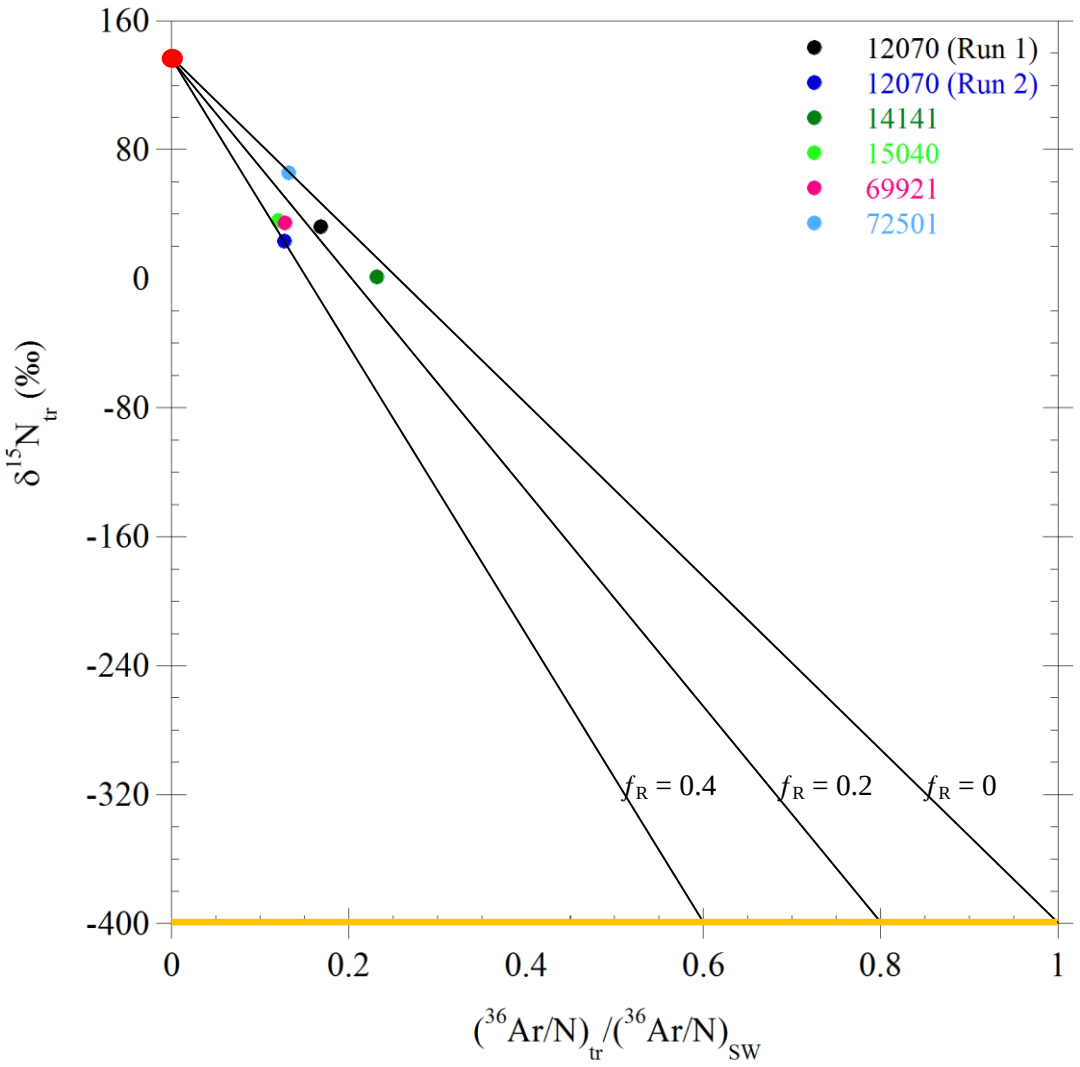

Figure 5.11: Isotopic composition of nitrogen released from lunar soils (weighted average across all temperature steps) versus measured $^{36}Ar/N$ ratios in samples, normalised to the solar ratio (taken from Anders and Grevesse, 1989). The large red circle at +140 ‰ on the y-axis indicates the end-member isotopic composition of the non-solar N contribution, assuming no loss ($f_R = 0$) of $^{36}Ar_{SW}$ from the most ^{15}N-enriched sample (72501), and a maximum of 40 % loss ($f_R = 0.4$) of $^{36}Ar_{SW}$ from the least ^{15}N-enriched sample (12070 run 2). The yellow bar at -400 ‰ represents the composition of solar nitrogen. Solid black lines are theoretical mixing lines between solar and non-solar N end-members, assuming different fractions of $^{36}Ar_{SW}$ loss. The grey dotted line represents the mixing line between solar and non-solar N (with a minimum isotopic composition of +87 ‰), assuming 0 % loss of $^{36}Ar_{SW}$ from the least ^{15}N-enriched sample, and so by extension, the lower limit for the isotopic composition of the non-solar end-member for all soils in this study.

Soil maturity (I_s/FeO) is positively correlated ($R^2 = 0.58$) with weighted average $\delta^{15}N$ values, indicating that, as a soil undergoes progressive processing at the lunar surface, this

seems to be driving the variations observed in $\delta^{15}N$ values. Further, whilst relative percentage contributions to the total N present in lunar soils from a non-solar source are positively correlated with both weighted average $\delta^{15}N$ values ($R^2 = 0.47$), and with soil maturity ($R^2 = 0.77$), indicating that relatively more N comes from non-solar sources as a soil is processed and matured at the lunar surface, the weaker correlation with average N isotopic compositions suggests that the addition of non-solar N is not the only factor which determines the overall isotopic composition of soils.

If, therefore, the potential loss of $^{36}Ar_{SW}$ from all soil samples is also taken into account , and a non-solar end-member isotopic composition of +160 ‰ is assumed (as proposed by Furi et al. (2012)), then the range of relative contributions from a non-solar N source remains largely the same (71.6 %, up to 83 % non-solar N) (Table 5.4), confirming that non-solar N is the major contributor to the total N present in lunar soils, and that solar N contributes only around a quarter of the N total abundance. A non-solar composition of +160 ‰ requires losses of $^{36}Ar_{SW}$ of between 18 % and 48 %, which again fits well with the calculations of Furi et al. (2012) (Figure 5.12).

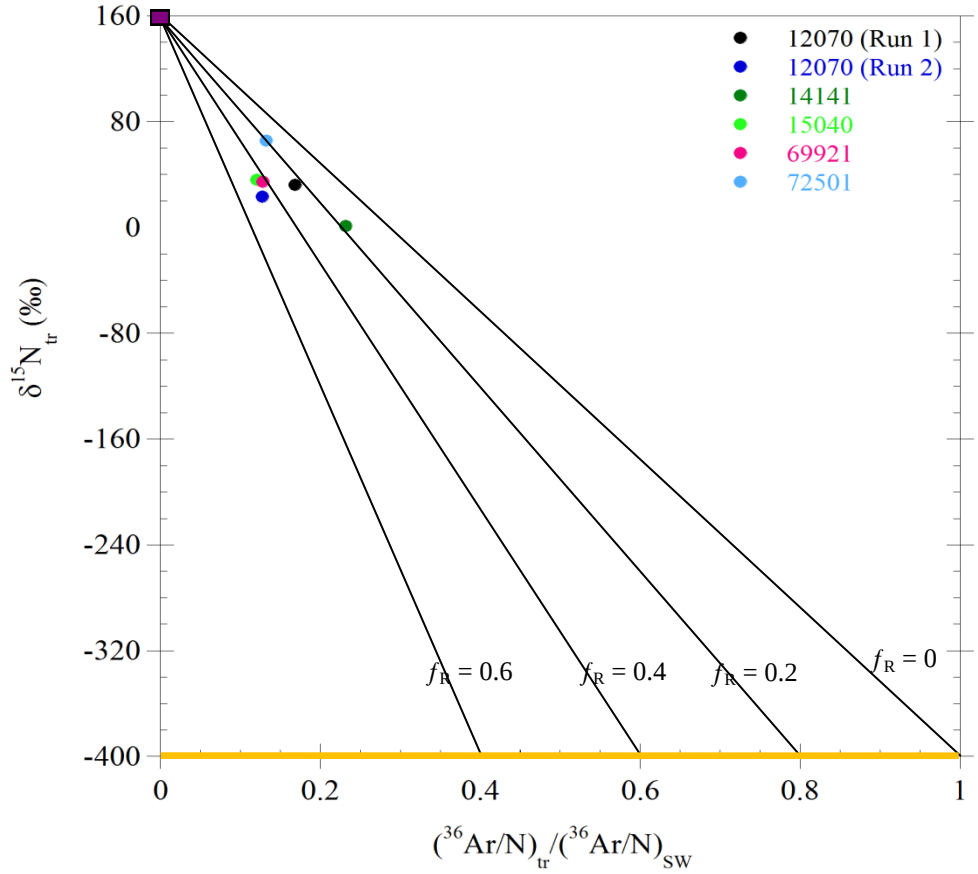

Figure 5.12: Isotopic composition versus $(^{36}Ar/N)_{tr}/(^{36}Ar/N)_{SW}$ ratios. The purple square at +160 ‰ on the y-axis indicates the end-member isotopic composition of N_P, taken from Furi et al, 2012. The yellow bar at -400 ‰ represents the composition of solar nitrogen. Solid black lines are theoretical mixing lines between solar and non-solar N end-members, assuming different fractions of $^{36}Ar_{SW}$ loss.

Assuming 0 % loss of $^{36}Ar_{SW}$						
	12070 Run 1	**12070 Run 2**	**14141**	**15040**	**69921**	**72501**
Weighted Average Isotopic Composition ($\delta^{15}N$, ‰)	32.3	23.3	1.0	36.2	34.6	65.7
Non-Solar End-Member Isotopic Composition ($\delta^{15}N$, ‰)	120	87	120	100	100	140
Contribution of Non-Solar Nitrogen (%)	83.15	86.90	77.15	87.25	86.90	86.25
Contribution of Solar Nitrogen (%)	16.85	13.10	22.85	12.75	13.10	13.75
Loss of Solar Wind ^{36}Ar (%)	0	0	0	0	0	0
f_R	0	0	0	0	0	0
f_P	4.935	6.634	3.376	6.843	6.634	6.273
$(1-f_R)/(1+f_P)$	0.1685	0.1310	0.2285	0.1275	0.1310	0.1375
$(^{36}Ar/N)_{tr}/(^{36}Ar/N)_{SW}$	0.1685	0.1270	0.2319	0.1206	0.1282	0.1325
Assuming N_P = +140 ‰						
	12070 Run 1	**12070 Run 2**	**14141**	**15040**	**69921**	**72501**
Weighted Average Isotopic Composition ($\delta^{15}N$, ‰)	32.3	23.3	1.0	36.2	34.6	65.7
Non-Solar End-Member Isotopic Composition ($\delta^{15}N$, ‰)	140	140	140	140	140	140
Contribution of Non-Solar Nitrogen (%)	80.05	78.40	74.26	80.80	80.15	86.20
Contribution of Solar Nitrogen (%)	19.95	21.60	25.74	19.20	19.85	13.80
Loss of Solar Wind ^{36}Ar (%)	15	42	10	37	35	4
f_R	0.15	0.42	0.10	0.37	0.35	0.04
f_P	4.013	3.630	2.885	4.208	4.038	6.246
$(1-f_R)/(1+f_P)$	0.1696	0.1253	0.2317	0.1210	0.1290	0.1325
$(^{36}Ar/N)_{tr}/(^{36}Ar/N)_{SW}$	0.1685	0.1270	0.2319	0.1206	0.1282	0.1325
Assuming N_P = +160 ‰						
	12070 Run 1	**12070 Run 2**	**14141**	**15040**	**69921**	**72501**
Weighted Average Isotopic Composition ($\delta^{15}N$, ‰)	32.3	23.3	1.0	36.2	34.6	65.7
Non-Solar End-Member Isotopic Composition ($\delta^{15}N$, ‰)	160	160	160	160	160	160
Contribution of Non-Solar Nitrogen (%)	77.2	75.6	71.6	77.9	77.6	83
Contribution of Solar Nitrogen (%)	22.8	24.4	28.4	22.1	22.4	17
Loss of Solar Wind ^{36}Ar (%)	25	48	18	45	42	20
f_R	0.25	0.48	0.18	0.45	0.42	0.2
f_P	3.386	3.098	2.521	3.525	3.464	4.882
$(1-f_R)/(1+f_P)$	0.1710	0.1269	0.2329	0.1215	0.1299	0.1360
$(^{36}Ar/N)_{tr}/(^{36}Ar/N)_{SW}$	0.1685	0.1270	0.2319	0.1206	0.1282	0.1325

Table 5.4: Comparing mixing proportions of solar and non-solar N end-members in 3 different scenarios (no loss of $^{36}Ar_{SW}$ and variable N_P compositions; variable loss of $^{36}Ar_{SW}$ and N_P = +140 ‰; variable loss of $^{36}Ar_{SW}$ and N_P = +160 ‰).

Conclusions

Simultaneous measurements of carbon, nitrogen, and noble gases in lunar soils by stepped combustion analysis reveal the characteristic release pattern of heavy-light-heavy nitrogen, as well as reconfirming that ^{40}Ar, ^{36}Ar, and N releases are well-correlated (above 650 ºC). An excess of ^{40}Ar (relative to releases of ^{36}Ar) at low temperatures is most likely caused by the re-implantation of liberated ^{40}Ar from the lunar atmosphere and/or terrestrial atmospheric contamination. The correlation between argon and nitrogen releases perhaps implies a common source for these volatiles. Neon isotopes measured by stepped combustion reveal that the majority of neon in lunar soils comes from a solar source, with a minor cosmogenic component released at only the highest temperature steps. However, the release of ^{15}N-enriched nitrogen from soils shows that it is not purely solar in origin (given solar wind nitrogen signatures of around -400 ‰), and calculations reveal that up to 87 % of the nitrogen measured in lunar soils could come from a non-solar/planetary source, with an isotopic signature of between +87 ‰, up to +160 ‰.

Mechanical crushing of lunar soils under vacuum conditions suggests that any liberated nitrogen is almost instantly retrapped down onto freshly created grain surfaces, and so is only released in negligible amounts, especially compared to noble gases, which are readily released by crushing. Comparing noble gas ratios obtained by crushing with those obtained at different temperatures during stepped combustion analyses indicates that localised frictional heating during the crushing process results in temperatures of between 400 ºC and 900 ºC, with solar neon isotopes showing no evidence of mixing with cosmogenic neon in crushed samples, which also supports the conclusion that crushing does not produce temperatures above around 1000 ºC.

Temperature Step (°C)	12070 (Run 1) ^{4}He (cc g^{-1})	12070 (Run 2) ^{4}He (cc g^{-1})	14141 ^{4}He (cc g^{-1})	15040 ^{4}He (cc g^{-1})	69921 ^{4}He (cc g^{-1})	72501 ^{4}He (cc g^{-1})
200	-	2.50E-03	1.89E-04	2.59E-03	2.32E-03	6.22E-04
300	8.01E-03	5.35E-03	1.21E-03	5.50E-03	4.40E-03	1.76E-03
400	9.64E-03	8.36E-03	2.81E-03	7.81E-03	5.75E-03	4.26E-03
500	1.55E-02	1.05E-02	3.52E-03	9.26E-03	6.60E-03	5.82E-03
600	1.27E-02	9.30E-03	2.77E-03	8.43E-03	5.88E-03	5.01E-03
650	-	-	2.68E-03	4.65E-03	2.56E-03	2.19E-03
700	8.22E-03	6.73E-03	4.40E-04	3.03E-03	1.51E-03	1.35E-03
750	-	2.96E-03	8.09E-04	2.22E-03	9.91E-04	8.64E-04
800	4.68E-03	2.11E-03	1.02E-03	1.77E-03	6.21E-04	5.96E-04
850	-	1.67E-03	9.85E-04	1.32E-03	3.46E-04	3.27E-04
900	2.65E-03	9.68E-04	8.83E-04	7.00E-04	2.31E-04	1.95E-04
1000	8.45E-04	7.38E-04	1.14E-03	4.60E-04	1.81E-04	1.54E-04
1100	1.33E-05	1.40E-05	3.48E-05	3.67E-05	2.99E-05	1.13E-05
1200	4.02E-06	4.00E-06	5.47E-06	5.90E-06	8.72E-06	2.15E-06
1300	nd	2.05E-06	1.21E-05	5.49E-06	6.46E-07	nd
1400	nd	1.72E-06	nd	9.61E-07	9.35E-10	nd
Total	6.23E-02	5.13E-02	1.85E-02	4.78E-02	3.14E-02	2.32E-02

Table 5A: Releases of ^{4}He from lunar soils by stepped combustion analysis. (- = not measured; nd = not detected).

	12070 (Run 1)		12070 (Run 2)		14141		15040		69921		72501	
Temperature Step (ºC)	^{40}Ar (cc g^{-1})	^{36}Ar (cc g^{-1})	^{40}Ar (cc g^{-1})	^{36}Ar (cc g^{-1})	^{40}Ar (cc g^{-1})	^{36}Ar (cc g^{-1})	^{40}Ar (cc g^{-1})	^{36}Ar (cc g^{-1})	^{40}Ar (cc g^{-1})	^{36}Ar (cc g^{-1})	^{40}Ar (cc g^{-1})	^{36}Ar (cc g^{-1})
200	-	-	2.16E-10	1.64E-10	nd	7.86E-12	nd	nd	nd	9.47E-12	nd	nd
300	1.34E-09	nd	4.87E-10	3.69E-10	7.33E-06	1.63E-07	2.56E-06	nd	2.27E-06	2.06E-11	1.12E-08	nd
400	nd	nd	1.34E-06	8.69E-07	6.88E-05	1.52E-06	1.03E-05	1.09E-06	6.65E-06	1.24E-06	6.88E-06	1.13E-06
500	1.46E-05	9.46E-06	1.21E-05	9.33E-06	3.02E-04	9.82E-06	4.04E-05	1.03E-05	3.12E-05	9.60E-06	3.88E-05	1.03E-05
600	2.82E-05	3.56E-05	2.74E-05	3.91E-05	3.76E-04	2.37E-05	5.50E-05	3.80E-05	8.44E-05	4.48E-05	9.27E-05	4.15E-05
650	-	-	-	-	3.44E-04	3.75E-05	2.87E-05	4.44E-05	8.68E-05	7.83E-05	5.61E-05	5.74E-05
700	1.79E-05	4.94E-05	4.06E-05	1.21E-04	4.92E-05	7.41E-06	3.60E-05	8.22E-05	7.38E-05	1.01E-04	5.63E-05	9.36E-05
750	-	-	1.01E-05	4.40E-05	9.19E-05	1.53E-05	3.59E-05	9.60E-05	6.03E-05	9.62E-05	5.37E-05	9.49E-05
800	4.18E-05	1.34E-04	1.27E-05	4.52E-05	9.68E-05	1.62E-05	3.13E-05	7.96E-05	7.38E-05	1.02E-04	3.64E-05	5.84E-05
850	-	-	1.24E-05	3.87E-05	7.84E-05	1.27E-05	2.37E-05	5.63E-05	5.07E-05	6.35E-05	2.00E-05	3.18E-05
900	3.42E-05	7.76E-05	1.23E-05	3.58E-05	5.59E-05	7.81E-06	2.31E-05	4.99E-05	3.39E-05	3.63E-05	2.11E-05	2.90E-05
1000	2.10E-05	4.21E-05	1.63E-05	4.33E-05	5.56E-05	7.09E-06	3.21E-05	6.01E-05	2.40E-05	2.25E-05	2.15E-05	2.82E-05
1100	1.66E-05	3.79E-05	1.35E-05	3.88E-05	3.75E-05	4.55E-06	1.84E-05	3.43E-05	1.74E-05	1.91E-05	1.48E-05	2.48E-05
1200	1.32E-05	2.66E-05	2.43E-05	4.49E-05	4.60E-05	5.35E-06	2.85E-05	4.63E-05	4.40E-05	4.26E-05	3.40E-05	4.17E-05
1300	nd	nd	1.71E-06	6.27E-06	2.89E-05	9.57E-07	1.03E-05	7.95E-06	7.90E-05	6.58E-05	1.02E-05	1.29E-05
1400	nd	nd	1.06E-08	8.06E-09	nd	5.76E-11	nd	nd	nd	4.26E-10	nd	nd
Total	1.87E-04	4.12E-04	1.85E-04	4.68E-04	1.64E-03	1.50E-04	3.76E-04	6.06E-04	6.68E-04	6.82E-04	4.62E-04	5.26E-04

Table 5B: Releases of ^{40}Ar and ^{36}Ar from lunar soils by stepped combustion analysis. (- = not measured; nd = not detected).

	12070 (Run 1)		12070 (Run 2)		14141		15040		69921		72501	
Temperature Step (ºC)	^{20}Ne (cc g^{-1})	^{21}Ne (cc g^{-1})	^{20}Ne (cc g^{-1})	^{21}Ne (cc g^{-1})	^{20}Ne (cc g^{-1})	^{21}Ne (cc g^{-1})	^{20}Ne (cc g^{-1})	^{21}Ne (cc g^{-1})	^{20}Ne (cc g^{-1})	^{21}Ne (cc g^{-1})	^{20}Ne (cc g^{-1})	^{21}Ne (cc g^{-1})
200	-	-	1.19E-05	2.82E-08	7.75E-07	2.41E-12	1.50E-05	3.97E-08	9.78E-06	2.48E-08	2.58E-06	1.66E-08
300	4.22E-05	1.12E-07	2.69E-05	6.95E-08	5.58E-06	5.40E-12	3.52E-05	9.31E-08	2.22E-05	5.77E-08	8.26E-06	2.49E-08
400	1.09E-04	2.70E-07	1.26E-04	3.27E-07	5.96E-05	1.49E-07	1.96E-04	5.34E-07	9.81E-05	2.58E-07	7.48E-05	2.02E-07
500	3.60E-04	9.53E-07	3.64E-04	1.01E-06	1.54E-04	4.29E-07	5.74E-04	1.66E-06	2.67E-04	7.69E-07	1.77E-04	4.74E-07
600	3.72E-04	1.05E-06	3.79E-04	1.08E-06	1.50E-04	4.13E-07	5.64E-04	1.66E-06	2.88E-04	8.58E-07	1.64E-04	4.32E-07
650	-	-	-	-	1.13E-04	3.06E-07	2.43E-04	7.12E-07	1.35E-04	4.05E-07	7.24E-05	1.78E-07
700	3.25E-04	9.43E-07	3.22E-04	9.27E-07	1.41E-05	7.27E-08	1.88E-04	5.68E-07	1.06E-04	3.14E-07	5.97E-05	1.95E-07
750	-	-	1.45E-04	4.22E-07	2.09E-05	5.35E-08	1.48E-04	4.60E-07	9.10E-05	3.36E-07	5.12E-05	2.89E-07
800	2.14E-04	6.59E-07	8.82E-05	2.80E-07	1.74E-05	3.63E-08	1.10E-04	3.54E-07	6.69E-05	4.80E-07	3.95E-05	2.69E-07
850	-	-	6.27E-05	2.17E-07	1.27E-05	2.27E-08	7.98E-05	2.83E-07	4.70E-05	8.55E-07	2.92E-05	4.47E-07
900	1.09E-04	8.57E-07	4.74E-05	3.92E-07	1.02E-05	2.59E-08	5.67E-05	5.17E-07	3.81E-05	7.49E-07	2.32E-05	3.92E-07
1000	9.18E-05	1.80E-06	9.51E-05	8.24E-07	2.48E-05	6.41E-08	9.90E-05	9.62E-07	5.27E-05	1.13E-06	4.03E-05	6.67E-07
1100	3.92E-05	9.98E-07	4.09E-05	1.07E-06	1.22E-05	2.56E-07	5.10E-05	1.46E-06	3.17E-05	7.02E-07	2.02E-05	3.54E-07
1200	9.50E-06	4.50E-07	1.13E-05	5.37E-07	6.21E-06	1.17E-07	1.32E-05	6.83E-07	1.59E-05	3.98E-07	9.82E-06	1.99E-07
1300	1.09E-06	1.19E-07	1.95E-06	2.83E-07	9.52E-07	1.01E-10	1.54E-06	1.84E-07	3.10E-06	1.34E-07	4.53E-07	3.46E-08
1400	3.38E-08	1.00E-08	6.63E-07	8.63E-08	nd	nd	1.26E-06	2.05E-07	2.56E-07	1.19E-08	7.53E-08	3.12E-08
Total	1.67E-03	8.22E-06	1.72E-03	7.55E-06	6.02E-04	1.95E-06	2.38E-03	1.04E-05	1.27E-03	7.48E-06	7.72E-04	4.21E-06

Table 5C: Releases of ^{20}Ne and ^{21}Ne from lunar soils by stepped combustion analysis. (- = not measured; nd = not detected).

	12070 (Run 1)			12070 (Run 2)			14141			15040			69921			72501		
Temperature Step (ºC)	C (ng)	$\delta^{13}C_{VPDB}$ (‰)	Error (‰)	C (ng)	$\delta^{13}C_{VPDB}$ (‰)	Error (‰)	C (ng)	$\delta^{13}C_{VPDB}$ (‰)	Error (‰)	C (ng)	$\delta^{13}C_{VPDB}$ (‰)	Error (‰)	C (ng)	$\delta^{13}C_{VPDB}$ (‰)	Error (‰)	C (ng)	$\delta^{13}C_{VPDB}$ (‰)	Error (‰)
200	-	-	-	262.92	-23.10	0.83	4.99	-27.64	0.23	222.10	-25.41	0.69	604.66	-40.35	0.85	218.74	-29.29	0.23
300	-	-	-	314.70	-27.92	0.55	502.23	-29.08	0.18	362.58	-30.78	0.65	823.52	-31.23	0.55	538.20	-28.20	0.19
400	-	-	-	277.62	-26.89	0.63	453.67	-27.69	0.18	248.88	-23.19	0.20	776.31	-28.19	0.40	430.60	-18.79	1.12
500	-	-	-	14.80	-38.97	0.43	402.99	-29.73	0.19	183.71	-10.97	0.58	375.04	-22.63	0.19	180.33	-17.42	0.38
600	-	-	-	269.03	-23.57	0.60	0.35	-6.48	0.19	88.56	5.97	0.56	168.02	3.02	1.01	60.95	0.70	0.53
650	-	-	-	-	-	-	19.64	-21.42	0.23	41.10	4.26	0.23	121.18	-1.54	1.78	17.90	39.78	0.65
700	-	-	-	82.78	-0.32	0.57	35.06	-33.68	0.17	52.67	1.40	0.79	132.34	2.60	2.10	25.21	56.87	1.04
750	-	-	-	53.27	11.45	0.51	31.87	-30.42	0.21	76.43	28.43	0.66	197.22	5.35	1.44	40.55	35.04	0.30
800	-	-	-	2.88	42.31	2.40	25.32	-23.70	0.14	91.65	14.96	0.20	225.66	9.22	1.48	50.27	35.67	0.96
850	-	-	-	0.01	8.70	462.23	6.14	-18.36	0.90	68.95	27.78	0.23	81.30	13.61	0.26	32.00	68.96	1.72
900	-	-	-	0.36	27.72	33.91	0.49	-27.77	15.39	58.70	29.17	9.85	73.92	29.31	0.23	16.68	108.47	0.80
1000	-	-	-	4.91	29.74	1.37	0.07	-29.71	264.48	54.83	10.08	0.87	45.40	31.57	0.45	15.27	101.09	0.86
1100	-	-	-	40.63	19.22	0.56	3.42	-19.54	1.34	69.38	17.58	0.30	63.20	16.18	0.34	31.71	29.93	0.29
1200	-	-	-	0.26	10.39	41.19	26.13	-28.83	0.13	111.01	18.29	0.22	133.11	29.62	0.86	82.71	16.66	0.36
1300	-	-	-	0.46	16.22	37.05	39.64	-29.56	0.16	69.46	-1.82	0.37	112.16	8.98	0.17	65.07	-8.81	0.46
1400	-	-	-	0.17	48.88	94.55	17.53	-32.41	0.27	22.12	20.46	0.42	33.39	-8.59	0.29	58.96	-21.46	0.49

Table 5D: Releases of carbon from lunar soils by stepped combustion analysis. (- = not measured; nd = not detected).

	12070 (Run 1)			12070 (Run 2)			14141			15040			69921			72501		
Temperature Step (ºC)	N (ng)	$\delta^{15}N_{AIR}$ (‰)	Error (‰)	N (ng)	$\delta^{15}N_{AIR}$ (‰)	Error (‰)	N (ng)	$\delta^{15}N_{AIR}$ (‰)	Error (‰)	N (ng)	$\delta^{15}N_{AIR}$ (‰)	Error (‰)	N (ng)	$\delta^{15}N_{AIR}$ (‰)	Error (‰)	N (ng)	$\delta^{15}N_{AIR}$ (‰)	Error (‰)
200	-	-	-	1.59	46.66	2.58	5.07	59.25	0.70	4.74	32.25	0.51	4.07	31.52	0.56	3.34	38.21	0.63
300	5.49	32.98	1.25	10.41	14.89	0.80	25.85	2.09	0.24	11.75	47.10	0.38	14.10	43.39	0.35	7.98	57.79	0.41
400	0.80	48.98	13.31	12.07	49.24	0.82	12.78	16.24	0.36	6.54	80.47	0.67	12.10	64.76	0.43	7.70	92.55	0.66
500	2.10	218.90	5.69	15.06	88.56	0.78	4.99	30.14	0.56	13.78	107.87	0.48	17.89	90.32	0.39	10.79	125.69	0.61
600	6.89	107.81	1.15	23.32	89.36	0.72	10.29	9.87	0.36	23.48	101.73	0.32	28.26	116.01	0.36	21.70	144.88	0.40
650	-	-	-	-	-	-	17.42	-4.26	0.31	27.88	85.54	0.24	31.31	98.30	0.30	24.69	123.39	0.32
700	17.47	49.36	0.85	54.89	49.82	0.78	6.13	8.71	0.32	56.66	60.40	0.20	37.90	85.35	0.25	39.71	102.38	0.21
750	-	-	-	46.10	7.93	0.92	9.18	-28.91	0.48	76.59	34.96	0.26	63.21	65.78	0.37	49.29	73.77	0.19
800	29.63	-2.88	0.80	32.23	-19.46	0.79	9.85	-40.53	0.50	65.79	9.58	0.28	76.34	23.67	0.36	39.31	24.43	0.17
850	-	-	-	28.40	-45.67	0.76	6.11	-63.36	0.73	52.33	-17.53	0.21	56.41	-47.55	0.38	32.31	-23.70	0.18
900	†	63.91	3.07	25.81	-23.65	0.76	3.43	-79.14	1.34	48.95	4.54	0.23	35.88	-43.78	0.36	22.28	19.58	0.25
1000	11.40	8.02	0.81	29.99	1.14	0.79	4.61	-28.00	0.51	57.91	16.42	0.29	25.22	16.30	0.32	25.92	39.52	0.23
1100	9.16	19.34	0.93	26.65	21.35	0.82	2.97	23.34	0.81	48.37	32.93	0.24	23.65	20.67	0.40	18.81	48.50	0.28
1200	15.14	38.56	0.90	39.86	42.43	0.91	4.32	63.40	0.84	76.00	42.85	0.28	66.16	20.76	0.37	46.55	64.93	0.20
1300	1.71	97.15	2.96	6.13	136.88	1.48	16.87	21.93	0.36	20.32	54.76	0.36	82.25	37.64	0.36	20.87	78.72	0.32
1400	0.04	27.55	284.81	1.17	268.63	11.42	1.85	50.01	1.61	9.24	142.07	0.85	6.19	49.26	0.55	6.55	160.44	1.25

Table 5E: Releases of nitrogen from lunar soils by stepped combustion analysis. (- = not measured; † = blank level).

12070			
Number of Strokes	Cumulative Number of Strokes	N (ng)	Cumulative %
10	10	2.31	17.42
20	30	1.45	28.36
50	80	1.50	39.67
100	180	1.25	49.12
200	380	1.28	58.75
100	480	0.08	59.38
400	880	1.31	69.24
800	1680	1.36	79.50
1600	3280	1.56	91.24
2000	5280	1.16	100.00
Total		13.26	
14141			
Number of Strokes	Cumulative Number of Strokes	N (ng)	Cumulative %
10	10	0.22	3.05
20	30	0.54	10.52
50	80	0.81	21.65
200	280	1.25	38.88
500	780	1.89	64.84
1000	1780	1.50	85.43
2000	3780	0.86	97.24
2000	5780	0.14	99.10
2000	7780	†	99.10
2000	9780	0.07	100.00
Total		7.28	
69921			
Number of Strokes	Cumulative Number of Strokes	N (ng)	Cumulative %
10	10	5.34	14.28
20	30	3.60	23.90
50	80	4.44	35.77
100	180	4.35	47.41
200	380	4.35	59.04
500	880	5.02	72.48
1000	1880	3.89	82.88
2000	3880	3.73	92.86
2000	5880	1.62	97.19
2000	7880	0.79	99.29
3000	10880	0.27	100.00
Total		37.40	

Table 5F: Releases of nitrogen from lunar soils by *in vacuo* crushing. († = blank level).

12070						
Cumulative Number of Strokes	^{4}He (cc g^{-1})	Cumulative % of Combustion Total	^{20}Ne (cc g^{-1})	Cumulative % of Combustion Total	^{36}Ar (cc g^{-1})	Cumulative % of Combustion Total
10	1.05E-03	1.68	2.71E-05	1.62	2.63E-06	0.64
30	2.00E-03	4.89	4.04E-05	4.04	5.76E-06	1.40
80	3.66E-03	10.77	7.25E-05	8.37	1.05E-05	2.54
180	4.63E-03	18.20	9.93E-05	14.31	1.63E-05	3.95
380	5.33E-03	26.75	1.45E-04	22.97	2.42E-05	5.86
480	3.78E-03	32.82	6.62E-05	26.93	2.78E-05	6.74
880	5.13E-03	41.04	2.15E-04	39.78	4.12E-05	9.98
1680	5.12E-03	49.25	2.57E-04	55.11	5.91E-05	14.33
3280	5.13E-03	57.48	2.82E-04	71.97	8.23E-05	19.95
5280	4.97E-03	65.46	2.20E-04	85.15	1.03E-04	24.95
7280	4.37E-03	72.47	1.61E-04	94.80	1.18E-04	28.64
9280	3.66E-03	78.34	1.33E-04	102.73	1.30E-04	31.49
11280	3.06E-03	83.26	1.13E-04	109.50	1.39E-04	33.80
14280	9.76E-04	84.82	4.53E-05	112.21	1.51E-04	36.64
Total	5.29E-02		1.88E-03		9.11E-04	
14141						
Cumulative Number of Strokes	^{4}He (cc g^{-1})	Cumulative % of Combustion Total	^{20}Ne (cc g^{-1})	Cumulative % of Combustion Total	^{36}Ar (cc g^{-1})	Cumulative % of Combustion Total
10	2.65E-04	1.43	4.95E-06	0.82	3.43E-07	0.23
30	2.64E-04	2.86	4.30E-06	1.54	4.60E-07	0.53
80	8.64E-04	7.53	1.58E-05	4.16	9.93E-07	1.20
180	1.05E-03	13.20	2.22E-05	7.85	1.55E-06	2.23
380	1.36E-03	20.56	3.30E-05	13.33	2.49E-06	3.89
880	1.50E-03	28.67	4.82E-05	21.33	4.27E-06	6.73
1880	1.42E-03	36.35	4.70E-05	29.13	4.87E-06	9.98
3880	1.32E-03	43.49	5.25E-05	37.86	6.79E-06	14.50
5880	8.98E-04	48.34	3.64E-05	43.90	5.81E-06	18.37
7880	6.65E-04	51.93	2.76E-05	48.49	4.98E-06	21.69
9880	4.80E-04	54.53	2.15E-05	52.05	4.47E-06	24.66
11880	3.46E-04	56.40	1.66E-05	54.81	3.68E-06	27.12
13880	2.51E-04	57.76	1.28E-05	56.93	3.20E-06	29.25
Total	1.07E-02		3.43E-04		4.39E-05	

Table 5G: Releases of ^{4}He, ^{20}Ne, and ^{36}Ar from lunar soils by *in vacuo* crushing.

69921						
Cumulative Number of Strokes	^{4}He (cc g^{-1})	Cumulative % of Combustion Total	^{20}Ne (cc g^{-1})	Cumulative % of Combustion Total	^{36}Ar (cc g^{-1})	Cumulative % of Combustion Total
10	6.15E-04	1.96	2.84E-05	2.23	6.84E-06	1.00
30	8.88E-04	4.78	3.39E-05	4.89	6.99E-06	2.03
80	1.26E-03	8.80	5.31E-05	9.07	1.03E-05	3.54
180	1.37E-03	13.17	6.72E-05	14.34	1.24E-05	5.35
380	1.37E-03	17.53	9.40E-05	21.73	1.80E-05	7.98
880	1.37E-03	21.87	1.36E-04	32.43	2.81E-05	12.09
1880	1.33E-03	26.11	1.31E-04	42.71	2.90E-05	16.34
3880	1.33E-03	30.35	1.33E-04	53.17	3.90E-05	22.06
5880	1.28E-03	34.42	8.13E-05	59.56	2.98E-05	26.43
7880	1.03E-03	37.69	5.55E-05	63.92	2.33E-05	29.84
10880	9.70E-04	40.78	5.64E-05	68.35	2.66E-05	33.74
12880	5.94E-04	42.67	3.09E-05	70.78	1.65E-05	36.16
14880	4.87E-04	44.22	2.52E-05	72.75	1.35E-05	38.14
16880	3.97E-04	45.48	2.10E-05	74.41	1.16E-05	39.84
18880	2.96E-04	46.42	1.62E-05	75.68	9.34E-06	41.21
Total	1.46E-02		9.63E-04		2.81E-04	

Table 5G (cont.): Releases of ^{4}He, ^{20}Ne, and ^{36}Ar from lunar soils by *in vacuo* crushing.

	12070 (Run 1)				12070 (Run 2)				14141			
Temperature Step (ºC)	$^{21}Ne/^{22}Ne$	Error (±)	$^{20}Ne/^{22}Ne$	Error (±)	$^{21}Ne/^{22}Ne$	Error (±)	$^{20}Ne/^{22}Ne$	Error (±)	$^{21}Ne/^{22}Ne$	Error (±)	$^{20}Ne/^{22}Ne$	Error (±)
200	-	-	-	-	0.0317	0.0039	13.9432	0.3030	0.0368	0.0050	13.1912	0.3546
300	0.0329	0.0036	12.9908	0.2316	0.0329	0.0026	13.3869	0.2027	0.0280	0.0042	12.8005	0.3036
400	0.0292	0.0020	12.4468	0.1396	0.0308	0.0011	12.5431	0.0777	0.0311	0.0012	11.9979	0.0812
500	0.0311	0.0010	12.3546	0.0820	0.0317	0.0006	12.1025	0.0461	0.0313	0.0007	11.4805	0.0512
600	0.0325	0.0011	12.1765	0.0732	0.0323	0.0006	11.9674	0.0400	0.0313	0.0008	11.5426	0.0497
650	-	-	-	-	-	-	-	-	0.0319	0.0008	11.7679	0.0618
700	0.0331	0.0012	12.0164	0.0791	0.0321	0.0007	11.7561	0.0453	0.0321	0.0016	11.7598	0.0993
750	-	-	-	-	0.0323	0.0011	11.7355	0.0726	0.0318	0.0018	11.6132	0.1275
800	0.0344	0.0012	11.8148	0.0938	0.0351	0.0011	11.7060	0.0891	0.0368	0.0025	11.6100	0.1469
850	-	-	-	-	0.0377	0.0016	11.5506	0.1036	0.0395	0.0027	11.3531	0.1569
900	0.0392	0.0014	11.6882	0.0897	0.0408	0.0013	11.6273	0.0831	0.0435	0.0029	11.0401	0.1754
1000	0.0416	0.0011	11.5566	0.0579	0.0420	0.0009	11.4326	0.0495	0.0412	0.0020	11.3683	0.1166
1100	0.0521	0.0016	11.1987	0.0852	0.0532	0.0011	11.2154	0.0588	0.0460	0.0012	10.7347	0.0672
1200	0.0887	0.0044	10.4186	0.1518	0.0899	0.0026	10.4679	0.0962	0.0465	0.0019	10.3887	0.0940
1300	0.1502	0.0156	9.2922	0.3850	0.2147	0.0089	8.5298	0.1548	0.0651	0.0043	9.7657	0.1691
1400	0.0420	0.0158	8.3728	0.6291	0.1788	0.0140	8.9350	0.2722	nd	nd	nd	nd

Table 5H: Neon isotope ratios for lunar soils analysed by stepped combustion. All ratios have been corrected for contributions from a system blank of terrestrial atmospheric composition, and for the effects of mass fractionation in the mass spectrometer. (- = not measured; nd = not detected).

	15040				69921				72501			
Temperature Step (ºC)	$^{21}Ne/^{22}Ne$	Error (±)	$^{20}Ne/^{22}Ne$	Error (±)	$^{21}Ne/^{22}Ne$	Error (±)	$^{20}Ne/^{22}Ne$	Error (±)	$^{21}Ne/^{22}Ne$	Error (±)	$^{20}Ne/^{22}Ne$	Error (±)
200	0.0364	0.0035	14.4355	0.2610	0.0316	0.0038	13.0858	0.2643	0.0363	0.0208	13.0008	0.4653
300	0.0334	0.0020	13.2645	0.1582	0.0325	0.0026	13.1427	0.1955	0.0365	0.0141	12.7339	0.3473
400	0.0315	0.0008	12.1819	0.0513	0.0304	0.0011	12.1821	0.0837	0.0324	0.0021	12.6579	0.1064
500	0.0318	0.0004	11.6039	0.0282	0.0320	0.0006	11.7555	0.0430	0.0316	0.0011	12.4311	0.0716
600	0.0323	0.0005	11.5717	0.0294	0.0333	0.0007	11.8054	0.0463	0.0310	0.0011	12.4042	0.0712
650	0.0324	0.0007	11.6494	0.0464	0.0331	0.0009	11.6975	0.0656	0.0282	0.0019	12.1077	0.0976
700	0.0333	0.0008	11.6966	0.0507	0.0329	0.0010	11.7163	0.0725	0.0303	0.0019	11.9916	0.0974
750	0.0338	0.0009	11.4700	0.0565	0.0333	0.0011	11.6437	0.0711	0.0287	0.0014	11.9935	0.0717
800	0.0349	0.0011	11.5078	0.0620	0.0350	0.0009	11.4754	0.0565	0.0345	0.0017	11.9388	0.0896
850	0.0382	0.0013	11.3899	0.0758	0.0377	0.0007	11.3015	0.0435	0.0331	0.0011	11.8354	0.0642
900	0.0437	0.0011	11.3559	0.0609	0.0404	0.0008	11.2470	0.0516	0.0363	0.0014	11.7939	0.0815
1000	0.0466	0.0009	11.2915	0.0467	0.0440	0.0008	11.2048	0.0430	0.0359	0.0010	11.8796	0.0526
1100	0.0577	0.0008	10.9996	0.0424	0.0452	0.0010	11.1941	0.0549	0.0372	0.0015	11.6955	0.0744
1200	0.0964	0.0021	10.2822	0.0754	0.0497	0.0015	10.9629	0.0739	0.0415	0.0026	11.4133	0.0970
1300	0.1871	0.0081	9.4899	0.1746	0.0817	0.0044	10.9617	0.1643	0.1016	0.0222	10.5483	0.3945
1400	0.2250	0.0087	8.6669	0.1570	0.0471	0.0088	9.7901	0.3647	0.1791	0.0432	9.5149	0.6011

Table 5H (cont.): Neon isotope ratios for lunar soils analysed by stepped combustion. All ratios have been corrected for contributions from a system blank of terrestrial atmospheric composition, and for the effects of mass fractionation in the mass spectrometer. (- = not measured; nd = not detected).

12070				14141				69921			
$^{21}Ne/^{22}Ne$	Error (±)	$^{20}Ne/^{22}Ne$	Error (±)	$^{21}Ne/^{22}Ne$	Error (±)	$^{20}Ne/^{22}Ne$	Error (±)	$^{21}Ne/^{22}Ne$	Error (±)	$^{20}Ne/^{22}Ne$	Error (±)
0.0347	0.0014	13.1155	0.0965	0.0331	0.0016	11.8173	0.1021	0.0366	0.0006	10.8714	0.0368
0.0352	0.0012	13.1138	0.0816	0.0333	0.0017	12.0156	0.1130	0.0355	0.0005	10.9488	0.0343
0.0340	0.0009	13.0065	0.0608	0.0331	0.0010	11.8014	0.0576	0.0355	0.0005	10.9582	0.0287
0.0350	0.0007	12.9561	0.0515	0.0314	0.0039	10.6727	0.2176	0.0350	0.0004	11.0482	0.0246
0.0350	0.0006	12.7644	0.0452	0.0331	0.0006	11.4916	0.0404	0.0346	0.0003	11.2104	0.0203
0.0356	0.0009	13.1572	0.0617	0.0334	0.0004	11.2852	0.0304	0.0348	0.0003	11.2941	0.0179
0.0352	0.0005	12.6808	0.0369	0.0347	0.0005	11.1125	0.0305	0.0349	0.0003	11.1923	0.0181
0.0356	0.0004	12.5997	0.0303	0.0345	0.0005	10.8509	0.0269	0.0355	0.0003	11.0572	0.0160
0.0355	0.0004	12.4429	0.0327	0.0342	0.0006	10.8081	0.0357	0.0352	0.0004	10.8129	0.0216
0.0356	0.0005	12.3328	0.0327	0.0298	0.0049	10.8544	0.3250	0.0355	0.0005	10.7321	0.0239
0.0362	0.0006	12.2621	0.0404	0.0291	0.0052	9.9670	0.3297	0.0354	0.0004	10.7017	0.0248
0.0362	0.0007	12.2915	0.0387	0.0347	0.0010	11.2447	0.0587	0.0354	0.0006	10.8164	0.0367
0.0370	0.0007	12.3021	0.0446					0.0360	0.0007	11.0049	0.0401
0.0373	0.0006	12.1170	0.0360					0.0357	0.0008	11.1476	0.0418
								0.0355	0.0008	11.2027	0.0506

Table 5I: Neon isotope ratios for lunar soils analysed by *in vacuo* crushing. All ratios have been corrected for contributions from a system blank of terrestrial atmospheric composition, and for the effects of mass fractionation in the mass spectrometer.

Chapter Six:

Conclusions and Future Considerations

The simultaneous collection of abundance and isotopic data for a number of different volatiles (carbon, nitrogen, helium, neon, and argon), across a very varied sample set, encompassing both mare basalts and soils collected from diverse locations at every Apollo landing site, enables several narratives about lunar volatiles to be constructed. These can be categorised into three broad themes: volatiles **in** the Moon (by which is meant any volatiles indigenous to the lunar interior); volatiles formed **on** the Moon (produced through radioactive decay, spallation etc.); and volatiles delivered **to** the Moon (located at the lunar surface and including contributions from solar wind, meteoritic and/or cometary sources). This chapter summarises the findings of this study in relation to these three themes, and concludes by considering what future steps can be taken to build upon this work to date.

6.1: Volatiles in the Moon

When considering volatiles indigenous to the lunar interior, it is necessary to think carefully about the types of samples that might contain components from such a source. Samples derived from melts generated in the lunar mantle, such as mare basalts, are viable options for characterising any indigenous volatiles, since they will inherit such volatiles directly from the mantle source regions. However, the degassing of volatiles from lunar melts is also an important process (e.g. Tartèse et al., 2013), leading to some modifications of indigenous volatile signatures, such as those proposed for the lunar volcanic glasses (e.g. Füri et al., 2014; Hauri et al., 2015). When making bulk sample measurements (as used in this study), the *in situ* production of cosmogenic volatile species at/near to the lunar surface will mask the indigenous volatile signatures to some degree in both basalt and volcanic glass samples, but in the case of lunar volcanic glasses, the relatively large surface area to volume ratio introduces further masking of the indigenous signatures by the presence of surface-correlated non-indigenous volatiles. Further, the allocated aliquots of

mare basalts used in this study came from the interiors of the main sample masses, removing the possibility of any surface-correlated volatile contributions to the volume-correlated indigenous components measured. Thus, mare basalts here represent the best available sample type for assessing the indigenous volatile inventory of the lunar interior.

Using the abundance and isotopic composition data for individual temperature steps, it is possible to identify nitrogen releases that represent terrestrial contamination (between 200 ºC and 600 ºC), and also those which show contributions from cosmogenic nitrogen production (released at temperatures over 1000 ºC). Eliminating these two complicating nitrogen components leaves behind a release of nitrogen in the mid-temperature range (between 650 ºC and 950 ºC), which is considered to be indigenous to the mare basalts and therefore to the lunar interior.

Average isotopic compositions (weighted by the abundance of the nitrogen releases at each temperature step) for these basalts reveal a range of $\delta^{15}N$ values, from -6.61 ‰ to +8.33 ‰, with an average value for all samples of +0.93 ± 9.39 ‰, close to, but distinct from, terrestrial mantle nitrogen values (which vary between -5 ‰ and -30 ‰ (Marty and Zimmermann, 1999)). Indigenous lunar nitrogen values do fall within the range of values measured in most carbonaceous chondrite groups, most closely matching the isotopic signatures of CO chondrites (+13 ‰ to -30 ‰ (Kerridge, 1985; Pearson et al., 2006)).

Using the measured abundances of carbon and nitrogen across this mid-temperature window (taken to represent indigenous lunar volatile components), elemental C/N ratios of lunar basalts appear to be lower (i.e. relatively enriched in nitrogen compared to carbon) than C/N ratios of the terrestrial depleted mantle (e.g. Halliday, 2013), and fall within the range of C/N ratios measured in CO and CI carbonaceous chondrites, and also enstatite chondrites (Mortimer et al., 2015). However, C/N ratios as measured in lunar basalt

samples are likely to have been modified by the preferential degassing of carbon compared to nitrogen under reducing conditions in the lunar mantle (i.e. lowering the C/N ratios), thus explaining the differences in lunar and terrestrial ratios (the terrestrial mantle being more oxidising than that of the Moon, thereby preferentially degassing nitrogen compared to carbon instead).

Whilst C/N ratios may not represent true lunar mantle values, both the range and average isotopic composition of indigenous lunar nitrogen measured in this study point to a likely CO chondrite source for nitrogen in the lunar interior. This is slightly different from the suggested source for water in the lunar interior (mainly CI chondrites, with some CM and/or CO chondrite input, as concluded by Barnes, 2014), although CO chondrites are required to satisfy both lunar water and nitrogen sources. Furthermore, to place this into a wider context of Earth-Moon system formation, the CO chondrite source for indigenous lunar nitrogen suggested by these data is in agreement with many other studies which propose a carbonaceous chondrite source for volatiles delivered to the Earth and Moon, although the timing of this volatile delivery (prior to the Moon forming event, during accretion, or just after lunar formation) is still unclear (e.g. Marty, 2012). The similar but slightly offset values of terrestrial mantle and indigenous lunar nitrogen isotopic compositions does not help to clarify this; the difference could be caused by separate mantle evolutions in the two bodies, pulling values away from a common nitrogen composition acquired before the Moon formed, or it could represent a slight difference in the relative proportions of different chondrite sources delivering volatiles to both bodies immediately after lunar formation.

What the abundance and isotopic composition of indigenous lunar nitrogen do demonstrate clearly is that volatiles in the lunar interior are heterogeneous; variations in measured

indigenous $\delta^{15}N$ values cannot be explained by factors such as crystallisation age, CRE age, mineralogy, sample location, depths of melting, or possible contamination, suggesting that the lunar mantle is heterogeneous. This conclusion is in agreement with those of other recent studies concerned with different volatiles derived from the lunar interior (e.g. hydrogen/water (Barnes, 2014); fluorine and chlorine (McCubbin et al., 2011); oxygen (Hallis et al., 2010)), and with the results of trace element modelling (Hallis et al., 2014), building up a picture of a complex history of lunar mantle evolution.

6.2: Volatiles formed on the Moon

Once lunar melts have crystallised at or near to the lunar surface, radiogenic noble gas isotopes (e.g. ^{4}He and ^{40}Ar) are produced within lunar materials as their respective parent isotopes decay over time and remain trapped within samples (subject to loss by diffusion out of the samples at peak temperatures of 500 ºC and 600-700 ºC, respectively (Mortimer et al., 2015)). Therefore, radiogenic isotope abundances are controlled by both the initial composition of samples (U and Th abundances for ^{4}He, and K abundance for ^{40}Ar), and by how much time has elapsed since the formation of the sample in question, with samples containing greater abundances of parent isotopes and older crystallisation ages producing a greater abundance of radiogenic isotopes. In mare basalts, this work demonstrates the correlation between measured abundances of radiogenic noble gas isotopes and literature values for sample compositions and crystallisation ages (Mortimer et al., 2015). Such radiogenic isotopes are volume-correlated, and so this relationship between composition, age, and measured abundances of ^{40}Ar is not observed in lunar soil samples (releases from these samples being dominated by surface-correlated volatiles from non-radiogenic source(s)). Also, the relationship between ^{40}Ar abundances, age, and composition of grains in soils is complicated by the presence of a 'parentless' ^{40}Ar component released at low

temperatures, thought to represent argon that is liberated into the lunar atmosphere during impact events and subsequently reimplanted back down onto the surfaces of grains, or representing ^{40}Ar adsorbed from the terrestrial atmosphere (Assonov et al., 2002; Wieler, 2002). Therefore, not all of the measured ^{40}Ar abundances in soils can be unambiguously attributed to a lunar radiogenic source.

Cosmogenic isotopes are produced in all samples exposed at, or near (within the upper two metres) to, the lunar surface, and are produced when incident cosmic rays cause spallation reactions to occur in target nuclides (Hohenberg et al., 1978). For the production of cosmogenic ^{15}N, the target nuclide is predominantly ^{16}O (Mathew and Marti, 2001; Reedy, 1981), whereas cosmogenic ^{21}Ne is produced by spallation of major elements (Na, Mg, Al, Si, Ca, and Fe) (Hohenberg et al., 1978), and cosmogenic ^{38}Ar by spallation of K, Ca, Fe, and Ti (Turner and Burgess, 2014). As a sample resides at or near to the lunar surface, its abundance of cosmogenic volatiles is positively correlated with exposure age (e.g. Mortimer et al., 2015), making abundances of cosmogenic volatiles important methods for dating samples and planetary surfaces.

After calculating the cosmogenic abundances from the measured total abundances of these isotopes in mare basalts, cosmogenic production rates were calculated; for $^{21}Ne_{cosm}$ and $^{38}Ar_{cosm}$, these production rates appear to be in good agreement with previously published production rates, taking into account the spread of values displayed by different basalts. Therefore, using these calculated production rates, it was possible to calculate CRE ages for two samples (12016 and 12047) for which exposure ages had not previously been established, giving ages of 150 Ma and 70 Ma (respectively) from $^{21}Ne_{cosm}$, and 160 Ma and 55 Ma (respectively) from $^{38}Ar_{cosm}$. However, in the case of cosmogenic ^{15}N, the calculated production rate (based on the calculated abundances from the measured totals in

the basalt samples) is highly variable between samples, although the average rate is similar to that proposed for samples which have experienced a high degree of shielding from cosmic rays (Mathew and Murty, 1993). The $^{15}N_{cosm}$ production rate calculated using data from this present study gives slightly shorter exposure ages for 12016 and 12047 (50 Ma and 40 Ma, respectively) than the cosmogenic noble gas isotopes more commonly used to date samples.

Binary mixing between a cosmogenic neon component and a component with a terrestrial atmospheric composition is observed in powdered mare basalt samples; by contrast, virtually all of the neon measured in an unpowdered chip of 12064 comes from a cosmogenic source. From this observation, the conclusion must be that the powdering process, being carried out under atmospheric conditions in a clean room suite, causes terrestrial atmospheric neon to be trapped within the samples, which, when released, is mixed with the cosmogenic neon component produced at the lunar surface (Mortimer et al., 2015).

As with radiogenic trapped species, cosmogenic volatiles are volume-correlated, and thus only contribute a negligible amount to the total volatile abundances measured in lunar soils (which have much larger surface area to volume ratios than lunar rocks). Nevertheless, a minor cosmogenic neon component is observed in several soil samples analysed by stepped combustion, only being released at temperatures above 1000 ºC, and mixed with the dominant surface-correlated solar neon component (e.g. Füri et al., 2014) also present in soils.

6.3: Volatiles delivered to the Moon

The mare basalt samples analysed in this work all come from the interiors of the main sample masses, and so do not show any evidence for the presence of solar volatiles, despite their often lengthy exposure ages in the order of hundreds of millions of years.

By contrast, noble gases released from lunar soils are predominantly from a solar wind source. This is most clearly observed in neon releases; at temperature steps up to ~ 1000 ºC, neon isotope ratios are mostly similar to a solar value ($^{21}Ne/^{22}Ne_{SW}$ = 0.0328, $^{20}Ne/^{22}Ne_{SW}$ = 13.8 (Lupton et al., 2012); $^{21}Ne/^{22}Ne_{SW}$ = 0.0333 ± 0.0003, $^{20}Ne/^{22}Ne_{SW}$ = 13.81 ± 0.08 (Pepin et al., 1999)), with isotope ratios fractionated away from a true solar value during implantation into regolith (Füri et al., 2014). Above 1000 ºC, neon releases are mixtures of this solar wind neon (implanted into the lunar surface) with cosmogenic neon (produced *in situ* at the lunar surface).

Whilst the majority of noble gases released from lunar soils are of solar origin, nitrogen measured in soils shows a more complex signature. The main source for nitrogen at the lunar surface was long thought to be solar wind (Kerridge, 1993; Mathew et al., 1998), with the widely-observed variations in isotopic compositions of nitrogen from soils attributed to either secular changes in the composition of solar wind (e.g. Kerridge, 1993), or to lunar soil nitrogen being delivered to the Moon from a mixture of both solar and non-solar sources (e.g. Kerridge and Marti, 2001; Wieler et al., 1999). Recent direct measurements of solar wind nitrogen, where $\delta^{15}N_{SW}$ = -407 ± 7 ‰ (Marty et al., 2011), favour the argument that nitrogen in soils is derived from a mixture of solar and non-solar sources (Becker, 2000; Füri et al., 2012; Kerridge and Marti, 2001), since even the most ^{15}N-depleted nitrogen releases measured in soils are significantly more enriched in ^{15}N in comparison to this solar wind signature. In this work, weighted average $\delta^{15}N$ values for

soils 12070, 14141, 15040, 69921, and 72501 can be reconciled with nitrogen from a solar source mixing with non-solar end-members of variable isotopic composition, from +87 ‰ to +140 ‰. This assumes that there has been no loss of solar wind ^{36}Ar from any of the soils, with between 13 % and 23 % of the total nitrogen derived from the solar source, and 77 % to 87 % of the total nitrogen coming from non-solar source(s). Alternatively, measured $\delta^{15}N$ values could represent the mixing of between 14 % and 26 % solar nitrogen with 74 % to 86 % non-solar nitrogen, assuming one non-solar end-member signature of +140 ‰ and losses of $^{36}Ar_{SW}$ of between 4 % and 42 %. A third possibility, taking a non-solar end-member composition of +160 ‰ (following the conclusions of Füri et al., 2012) and assuming $^{36}Ar_{SW}$ losses of between 18 % and 48 %, is that average nitrogen isotopic compositions in these soils represents mixing of between 17 % and 28 % solar wind nitrogen with between 72 % and 83 % non-solar nitrogen. Whichever scenario is chosen, the common theme from all is that the majority of nitrogen present in lunar soils is derived from a non-solar source, which has an end-member isotopic composition at least as enriched in ^{15}N as +87 ‰. Therefore, this study confirms the conclusions of Füri et al. (2012), who suggest that micro-impactors (Interplanetary Dust Particles, with average $\delta^{15}N$ values of +140 ‰) are the main source of non-solar nitrogen delivered to the lunar surface, although it must be noted that CR chondrites are also likely candidates, with average $\delta^{15}N$ values of +130 ‰ (Pearson et al., 2006).

6.4: Future Considerations

The techniques used in this work, involving the simultaneous measurement of abundances and isotopes of five different volatile elements (C, N, He, Ne, and Ar) across a wide range of temperatures (down to a temperature step resolution of 50 ºC), permit the characterisation of many different volatile components from several separate sources, and

thus this work represents one of the more in-depth and wide-ranging single studies of lunar volatiles to date. However, the data obtained here are only a small part of the wider effort within the lunar scientific community to fully understand the Moon's volatile inventory, efforts which have experienced something of a renaissance within the last decade.

From the perspective of enhancing the specific foci of this study, it seems necessary to expand the sample types used to characterise indigenous lunar nitrogen. Analysing more mare basalts will provide better constraints on the abundance and isotopic composition of indigenous nitrogen, given the wide range of $\delta^{15}N$ values measured to date, and this may help to answer questions about the extent of the heterogeneity of the lunar mantle. Whilst mare basalts are derived from mantle melts and thus have undergone considerable processing prior to eruption and crystallisation, anorthositic samples from the lunar highlands may represent a less processed glimpse of nitrogen isotopic composition and distribution from the earliest phases of lunar evolution. However, since the indigenous nitrogen measured in mare basalts comes from an unknown phase within the samples, in highlands samples with a much less diverse mineralogy, it may be the case that far less nitrogen can be incorporated into the rocks upon formation, thereby making nitrogen extremely challenging to detect and characterise.

Whether considering volatiles from the lunar interior, or volatiles delivered to the surface of the Moon, all sample studies to date are hampered by the relatively restricted sampling sites of the Apollo and Luna mission programmes, leading to a lack of sample diversity in returned samples compared to the results of lunar-wide orbital spectroscopic studies. To overcome this bias, lunar meteorites could be used to expand the volatiles dataset; in theory, lunar meteorites should be derived from random locations all over the Moon, not just sampling the same spatially-restricted regions as the sample return missions of the

1970s. Further, lunar breccias (both from the Apollo and lunar meteorite collections), containing a range of clasts of diverse lithologies, ages, and processing histories, will retain a record of surface-correlated volatiles delivered to the Moon at various points in lunar history and locked into breccia samples when they form, providing 'time-capsule' snapshots of volatile delivery to the lunar surface over time. A complicating factor when considering the use of lunar meteorite samples is the possibility of volatile loss and associated fractionation during ejection from the Moon and entry into the terrestrial atmosphere, which may result in the masking of true lunar volatile signatures with terrestrial values.

Ultimately, all lunar sample studies would benefit from a renewed programme of lunar landing missions; future sample return missions would be the most ideal option, enabling the targeting of regions of the Moon not sampled by previous Apollo and Luna missions, with all the benefits in terms of enhanced precision, accuracy, reproducibility, and technological capabilities associated with laboratory analysis back on Earth. Alternatively, *in situ* analyses of volatiles at the lunar surface would provide much needed ground truth about the nature of volatiles delivered to the Moon without any of the risks of terrestrial contamination that result from analysing even the most carefully curated returned samples.

Thus, although much ground-breaking work has been conducted in recent years, collectively, it forms but a small part of the overall work which must be performed if we are to fully comprehend the volatile inventory and history of the Earth-Moon system, leaving the field of lunar volatile research wide open for further advancements and discoveries in the near future.

References:

Abernethy, F. A. J. (2014) Carbon and Nitrogen in the Angrites and their Relationship with Achondrites from Mars and Vesta, *PhD Thesis*, The Open University.

Abernethy, F. A. J., Verchovsky, A. B., Starkey, N. A., Anand, M., Franchi, I. A., Grady, M. M. (2013) Stable isotope analysis of carbon and nitrogen in angrites, *Meteoritics and Planetary Science*, **48**, Nr. 9, 1590-1606.

Albarède, F. (2009) Voaltile accretion history of the terrestrial planets and dynamic implications, *Nature* **461**, 1227-1233.

Anand, M., Tartèse, R., Barnes, J. J. (2014) Understanding the origin and evolution of water in the Moon through lunar sample studies, *Phil. Trans. R. Soc. A* **372**, 20130254.

Anders, E., Grevesse, N. (1989) Abundances of the elements: Meteoritic and solar, *Geochim. Cosmochim. Acta* **53**, 1353-1373.

Antonenko, I., Head III, J. W., Mustard, J. F., Hawke, B. R. (1995) Criteria for the detection of lunar cryptomaria, *Earth, Moon and Planets* **69**, 141-172.

Armytage, R. M. G., Georg, R. B., Williams, H. M., Halliday, A. N. (2012) Silicon isotopes in lunar rocks: Implications for the Moon's formation and the early history of the Earth, *Geochim. Cosmochim. Acta* **77**, 504-514.

Aronowitz, L., Koch, F., Scanlon, J. H., Sidran, M. (1968) Contamination of Lunar Surface Samples by the Lunar Module Exhaust, *J. Geophys. Res.* **73** (10), 3231-3238.

Assonov, S. S., Franchi, I. A., Pillinger, C. T., Semenova, A. S., Shukolyukov, Y. A., Verchovsky, A. B., Iassevitch, A. N. (2002) Nitrogen and argon release profiles in Luna 16 and Luna 24 regolith samples: The effects of regolith reworking. *Meteoritics and Planetary Science* **37**, 27-48.

Barnes, J. J. (2014) Water in the Moon: A Geochemical Approach, *PhD Thesis*, The Open University.

Barnes, J. J., Tartèse, R., Anand, M., McCubbin, F. M., Franchi, I. A., Starkey, N. A., Russell, S. S. (2014) The origin of water in the primitive Moon as revealed by the lunar highlands samples, *Earth Planet. Sci. Lett.* **390**, 244-252.

Barry, P.H., Hilton, D.R., Marti, K., Taylor, L.A. (2013) Indigenous lunar nitrogen, **44th***Lunar Planet. Sci. Conf.*, Abstract 2160.

Becker, R. H. (1980) Evidence for a secular variation in the $^{13}C/^{12}C$ ratio of carbon implanted in lunar soils, *Earth Planet. Sci. Lett*. **50**, 189-196.

Becker, R. H. (2000) Nitrogen on the Moon, *Science* **290**, 1110-1111.

Becker, R. H., Clayton, R. N. (1975) Nitrogen abundances and isotopic compositions in lunar samples. *Proc. Lunar Planet. Sci. Conf.* **6th**, 2131-2149.

Becker, R. H., Clayton, R. N., Mayeda, T. K. (1976) Characterization of lunar nitrogen components, *Proc. Lunar Sci. Conf.* ***7th***, 441-458.

Bogard, D.D., Funkhouser, J.G., Schaeffer, O.A., Zähringer, J. (1971). Noble gas abundances in lunar material- cosmic-ray spallation products and radiation ages from the Sea of Tranquility and the Ocean of Storms. *J. Geophys. Res.* **76** (11), 2757–2779.

Bottke, W. F., Walker, R. J., Day, J. M., Nesvorny, D., Elkins-Tanton, L. (2010) Stochastic late accretion to Earth, the Moon, and Mars, *Science* **330 (6010),** 1527-1530.

Boyd, S. R., Wright, I. P., Franchi, I. A., Pillinger, C. T. (1988) Preparation of sub-nanomole quantities of nitrogen gas for stable isotopic analysis, *J. Phys. E: Sci. Instrum*. **21**, 876-885.

Boyd, S., Wright, I. P., Pillinger, C. T., (1997) Stepped-heating of carbonates and carbon-bearing quartz grains, *Chemical Geology* **134**, 303-310.

Brilliant, D. R., Franchi, I. A., Pillinger, C. T. (1994) Nitrogen components in lunar soil 12023: Complex grains are not the carrier of isotopically light nitrogen. *Meteoritics and Planetary Science* **29**, 718-723.

Brown, G.M., Peckett, A., Emeleus, C. H., Phillips, R., Pinsent, R. H. (1975) Petrology and mineralogy of Apollo 17 mare basalts, *Proc. Lunar Sci. Conf.* **6**, 1–13.

Burnett, D. S., Drozd, R. J., Morgan, C. J., Podosek, F. A. (1975) Exposure histories of Bench Crater rocks, *Proc. Lunar Sci. Conf.* **6th**, 2219-2240.

Cadogan, P. H., Eglinton, G., Maxwell, J. R., Pillinger, C. T. (1971) Carbon Chemistry of the Lunar Surface, *Nature* **231**, 29-31.

Cameron, A. G. W., Ward, W. R. (1976) The origin of the Moon, *Proc.* ***7th*** *Lunar Sci. Conf.*, 120.

Canup, R. M., Asphaug, E. (2001) Origin of the Moon in a giant impact near the end of the Earth's formation, *Nature* **412 (6848)**, 708-712.

Carrier, W. D., Olhoeft, G. R., Mendell, W. (1993) Physical Properties of the Lunar Surface. *In*: Heiken, G. H., Vaniman, D. T., French, B. M. (Eds.) *The Lunar Sourcebook*, 2nd edition, Cambridge, Press Syndicate of the University of Cambridge, 475-594.

Carrier, W. D. (2005) The four things you need to know about the Geotechnical Properties of Lunar Soil, *LPI online report* (http://www.lpi.usra.edu/lunar/surface/carrier_lunar_soils.pdf) -accessed 10th May 2012.

Cartigny, P., Jendrzejewski, N., Pineau, F., Petit, E., Javoy, M. (2001) Volatile (C, N, Ar) variability in MORB and the respective roles of mantle source heterogeneity and degassing: The case of the Southwest Indian Ridge. *Earth Planet. Sci. Lett*. **194**, 241–257.

Chang, S., Lawless, J., Romiez, M., Kaplan, I. R., Petrowski, C., Sakai, H., Smith, J. W. (1974) Carbon, nitrogen and sulfur in lunar fines 15012 and 15013: abundances, distributions and isotopic compositions, *Geochim. Cosmochim. Acta* **38**, 853-872.

Chappell, B.W., Compston, W., Green, D.H., Ware, N.G. (1972) Chemistry, geochronology and petrogenesis of lunar sample 15555. *Science* **175**, 415-416.

Chappell, B.W., Green, D.H. (1973) Chemical compositions and petrogenetic relationships in Apollo 15 mare basalts. *Earth Planet. Sci. Lett*. **18**, 237–246.

Clark, R. N. (2009) Detection of Adsorbed Water and Hydroxyl on the Moon, *Science* **326**, 562-564.

Clayton, R. N., Thiemens, M. H. (1980) Lunar nitrogen: Evidence for secular change in the solar wind. In *The Ancient Sun* (eds. Pepin, R. O., Eddy, J. A., Merrill, R. B.), pp. 463-473. Pergamon Press, New York, New York, USA.

Colaprete, A., Schultz, P., Heldmann, J., Wooden, D., Shirley, M., Ennico, K., Hermalyn, B., Marshall, W., Ricco, A., Elphic, R. C., Goldstein, D., Summy, D., Bart, G. D., Asphaug, E., Korycansky, D., Landis, D., Solitt, L. (2010) Detection of Water in the LCROSS Ejecta Plume, *Science* **330,** 463-468.

Compston, W., Berry, H., Vernon, M. J., Chappell, B.W., Kay, M. J. (1971) Rubidium-strontium chronology and chemistry of lunar material from the Ocean of Storms. *Proc. **2nd** Lunar Sci. Conf.*, 1471-1485.

Compston, W., Chappell, B.W., Arriens, P.A., Vernon, M.J. (1970) The chemistry and age of Apollo 11 lunar material. Proc. Apollo 11 Lunar Sci. Conf. 1007-1027.

Crider, D. H., Vondrak, R. R. (2002) Hydrogen migration to the lunar poles by solar wind bombardment of the Moon, *Advances in Space Research* **30** (8), 1869-1874.

Dale, C. W., Burton, K .W., Greenwood, R. C., Gannoun, A., Wade, J., Wood, B. J., Pearson, D. G. (2012) Late Accretion on the Earliest Planetesimals Revealed by the Highly Siderophile Elements, *Science* **336**, 72-75.

Darwin, G. H. (1879) A tidal theory of the evolution of satellites, *The Observatory* **3**, 79-84.

Delano, J. W. (1986) Pristine lunar glasses: Criteria, data, and implications, *Journal of Geophysical Research Solid Earth (1978–2012)* **91 (B4)**, 201-213.

de Meijer, R. J., Anisichkin, V. F., van Westrenen, W. (2013) Forming the Moon from terrestrial silicate-rich material, *Chemical Geology* **345**, 40-49.

Des Marais, D.J. (1978) Carbon, nitrogen and sulfur in Apollo 15, 16 and 17 rocks, *Proc. 9th Lunar Sci. Conf.*, 2451-2467.

Des Marais, D. J. (1983) Light element geochemistry and spallogenesis in lunar rocks, *Geochim. Cosmochim. Acta* **47**, 1769-1781.

Des Marais, D. J., Basu, A., Hayes, J. M., Meinschein, W. G. (1975) Evolution of carbon isotopes, agglutinates, and the lunar regolith, *Proc.**6th** Lunar Sci. Conf.***,*** 2353-2374.

DesMarais, D. J., Hayes, J. M., Meinschein, W. G. (1973) Accumulation of carbon in lunar soils, *Nature Physical Science,* **246**, 65-68.

Duncan, A. R., Erlank, A. J., Sher, M. K., Abraham, Y. C., Willis, J. P., & Ahrens, L. H. (1976) Some trace element constraints on lunar basalt genesis, Proc. 7th Lunar Sci. Conf. 1659-1671.

Duncan, A.R., Erlank A.J., Willis J.P., Sher M.K. and Ahrens L.H. (1974) Trace element evidence for a two-stage origin of some titaniferous mare basalts. *Proc. 5th Lunar Sci. Conf.* 1147-1157.

Dungan, M. A., Brown, R. W. (1977) The petrology of the Apollo 12 basalt suite. *Proc. Lunar Sci. Conf.* **8**, 1339–1381.

Dymek, R. F., Albee, A. L., Chodos, A. A. (1975a) Comparative petrology of lunar cumulate rocks of possible primary origin: Dunite 72415, troctolite 76535, norite 78235, and anorthosite 62237, *Proc.**3rd** Lunar Sci. Conf.*, 301-341.

Dymek R.F., Albee A.L. and Chodos A.A. (1975b) Comparative mineralogy and petrology of Apollo 17 mare basalts: Samples 70215, 71055, 74255, and 75055. Proc. 6th Lunar Sci. Conf. 49-77.

Eberhardt, P., Geiss, J., Graf, H., Grogler, N., Krahenbuhl, U., Schwaller, H., Schwarzmuller, J., Stettler, A. (1970) Correlation between rock type and irradiation history of Apollo 11 igneous rocks, *Earth and Planet. Sci. Lett.* **10**, 67-72.

Eberhardt, P., Geiss, J., Graf, H., Grogler, N., Krahenbuhl, U., Schwaller, H., Stettler, A. (1974) Noble gas investigations of lunar rocks 10017 and 10071, *Geochim. Cosmochim. Acta* **38**, 97-120.

Elardo, S. M., Draper, D. S., Shearer Jr., C. K. (2011) Lunar magma ocean crystallization revisited: Bulk composition, early cumulate mineralogy, and the source regions of the highlands Mg-suite, *Geochim. Cosmochim. Acta* **75**, 3024-3045.

Elkins-Tanton, L. T., Chatterjee, N., Grove, T. L. (2003) Magmatic processes that produced lunar fire fountains, *Geophys. Res. Lett.* **30** (10), 1513.

Epstein, S., Taylor, H. P. (1970) The concentration and isotopic composition of hydrogen, carbon and silicon in Apollo 11 lunar rocks and minerals, *Proceedings of the Apollo 11 Lunar Science Conference*, **2,** 1085-1096.

Epstein, S., Taylor, H. P. (1971) O^{18}/O^{16}, Si^{30}/Si^{28}, D/H, and C^{13}/C^{12} ratios in lunar samples, *Proc. Second Lunar Sci. Conf.*, **2**, 1421-1441.

Epstein, S., Taylor, H. P. (1972) O^{18}/O^{16}, Si^{30}/Si^{28}, C^{13}/C^{12}, and D/H studies of Apollo 14 and 15 samples, *Proc. Third Lunar Sci. Conf.*, **2**, 1429-1454.

Epstein, S., Taylor, H. P. (1973) The isotopic composition and concentration of water, hydrogen, and carbon in some Apollo 15 and 16 soils and in the Apollo 17 orange soil, *Proc. Fourth Lunar Sci. Conf.*, **2**, 1559-1575.

Epstein, S., Taylor, H. P. (1974) D/H and $^{18}O/^{16}O$ ratios of H_2O in the 'rusty' breccia 66095 and the origin of 'lunar water', *Proc. Lunar Sci. Conf.* **5th**, 1839-1854.

Epstein, S., Taylor, H. P. (1975) Investigation of the carbon, hydrogen, oxygen, and silicon isotope and concentration relationships on the grain surfaces of a variety of lunar soils and in some Apollo 15 and 16 cores samples, *Proc. Lunar Sci. Conf.* **6th**, 1771-1798.

Eugster, O., Eberhardt, P., Geiss, J., Grögler, N., Jungck, M., Meier, F., Mörgeli, M., Niederer, F. (1984b). Cosmic ray exposure histories of Apollo 14, Apollo 15, and Apollo 16 rocks. *J. Geophys. Res*. **89**, B498–B512 (*Proc. **14th** Lunar Planet. Sci. Conf*.).

Eugster, O., Eberhardt, P., Geiss, J., Grögler, N., Jungck, M., Mörgeli, M. (1977) The cosmic-ray exposure history of Shorty Crater samples; the age of Shorty Crater. *Proc. **8th** Lunar Sci. Conf.* 3059-3082.

Eugster, O., Eberhardt, P., Geiss, J., Grögler, N., Schwaller, H. (1984a) Cosmic Ray Exposure Histories and ^{235}U-^{136}Xe Dating of Apollo 11, Apollo 12, and Apollo 17 Mare Basalts, *Proc. **15th** Lunar Planet. Sci. Conf., Journal of Geophysical Research*, **89**, C171-C181.

Evensen, N.M., Murthy, V.R., Coscio, M.R. (1973) Rb-Sr ages of some mare basalts and the isotopic and trace element systematics in lunar fines, *Proc. **4th** Lunar Sci. Conf.*, 1707-1724.

Feldman, W. C., Maurice, S., Binder, A. B., Barraclough, B. L., Elphic, R. C., Lawrence, D. J (1998) Fluxes of Fast and Epithermal Neutrons from Lunar Prospector: Evidence for Water Ice at the Lunar Poles, *Science* **281,** 1496-1500.

Frick, U., Becker, R. H., Pepin, R. O. (1988) Solar wind record in the lunar regolith: Nitrogen and noble gases. *Proc. Lunar Sci. Conf.* **18,** 87–120.

Friedman, I., Gleason, J. D., Hardcastle, K. G. (1970) Water, hydrogen, deuterium, carbon and C13 content of selected lunar material, *Proc. Apollo 11 Lunar Sci. Conf.*, 1103-1109.

Friedman, I., Hardcastle, K. G., Gleason, J. D. (1974) Isotopic composition of carbon and hydrogen in some Apollo 14 and 15 lunar samples, *J. Res. US Geological Survey*, **2**, 7-12.

Funkhouser, J. G., Schaeffer, O. A., Bogard, D. D., Zähringer, J. (1970) Gas analysis of the lunar surface, *Proc. Apollo 11 Lunar Sci. Conf.*, 1111-1116.

Füri, E., Marty, B., Assonov, S. S. (2012) Constraints on the flux of meteoritic and cometary water on the Moon from volatile element (N–Ar) analyses of single lunar soil grains, Luna 24 core. *Icarus* **218 Issue 1**, 220-229.

Füri, E., Deloule, E., Gurenko, A., Marty, B. (2014) New evidence for chondritic lunar water from combined D/H and noble gas analyses of single Apollo 17 volcanic glasses. *Icarus* **229**, 109–120.

Galilei, G. (1610) Sidereus Nuncius.

Gardiner, L. R., Jull, A. J. T., Pillinger, C. T. (1978) Progress towards the direct measurement of ^{13}C/^{12}C ratios for hydrolysable carbon in lunar soils by static mass spectrometry, *Proc. **9th** Lunar Sci. Conf.*, 2149-2165.

Geiss, J., Bochsler, P. (1982) Nitrogen isotopes in the Solar System. *Geochim. Cosmochim. Acta* **46** (4), 529–548.

Geiss, J., Eberhardt, P., Grogler, N., Guggisbert, S., Maurer, P., Stettler, A. (1977) Absolute time scale of lunar mare formation and filling. *Phil. Trans. Roy. Soc. London* **A285**, 151-158.

Gerstenkorn, H. (1955) Über Gezeitenreibung beim Zweikörperproblem, *Zeitschrift für Astrophysik* **36**, S245-S274.

Gibson, E. K. Jr. (1977) Volatile elements, carbon, nitrogen, sulfur, sodium, potassium and rubidium in the lunar regolith, *Physics and Chemistry of the Earth* **10**, 57-62.

Gibson, E. K., Johnson, S. M. (1971) Thermal analysis-inorganic gas release studies of lunar samples, *Proc. Lunar Sci. Conf.* **2nd**, 1351-1366.

Gibson, E. K., Moore, G. W. (1972) Inorganic gas release and thermal analysis study of Apollo 14 and 15 soils, *Proc. Lunar Sci. Conf.* **3rd**, 2029-2040.

Gibson, E. K., Moore, G. W. (1973) Variable carbon contents of lunar soil 74220, *Earth Planet. Sci. Lett.* **20**, 404-408.

Gopalan, K., Kaushal, S., Lee-Hu, C., Wetherill, G. W. (1970) Rb-Sr and U, Th-Pb ages of lunar materials, *Proc. Apollo 11 Lunar Sci. Conf.,* 1195-1206.

Grady, M. M., Pillinger, C. T. (1990) The carbon and nitrogen stable isotope geochemistry of two lunar meteorites: ALHA-81005 and Y-86032, *Proc. NIPR Symp. Antarct. Meteorites* **3**, 27-39.

Greenwood, J.P., Itoh, S., Sakamoto, N., Warren, P., Taylor, L.A., Yurimoto, H. (2011) Hydrogen isotope ratios in lunar rocks indicate delivery of cometary water to the Moon. *Nat. Geosci.* **4**, 79–82.

Grove, T. L., Krawczynski, M. J. (2009) Lunar mare volcanism: where did the magmas come from? *Elements Magazine* **5**, 29-34.

Guggisberg, S., Eberhardt, P., Geiss, J., Grogler, N., Stettler, A., Brown, G.M., Pecket, A. (1979) Classification of the Apollo-11 basalts according to Ar^{39}-Ar^{40} ages and petrological properties. *Proc. **10th** Lunar Planet. Sci. Conf.* 1-39.

Halliday, A. N. (2003) The origin and earliest history of the Earth, *Treatise on Geochemistry* **1**, 509-557.

Halliday, A. N. (2004) Mixing, volatile loss and compositional change during impact-driven accretion of the Earth, *Nature* **427 (6974)**, 505-509.

Halliday, A. N. (2008) A young Moon-forming giant impact at 70–110 million years accompanied by late-stage mixing, core formation and degassing of the Earth, *Phil. Trans. R. Soc. London A*, **366** (1883), 4163-4181.

Halliday, A.N. (2013) The origins of volatiles in the terrestrial planets. *Geochim. Cosmochim. Acta* **105**, 146–171.

Hallis, L. J. (2010) The Geology of the Moon: Geochemistry and Petrology of Lunar Basalts, *PhD Thesis*, The Open University.

Hallis, L. J., Anand, M., Greenwood, R.C., Miller, M. F., Franchi, I. A., Russell, S. S. (2010) The oxygen isotope composition, petrology and geochemistry of mare basalts: Evidence for large-scale compositional variation in the lunar mantle, *Geochim. Cosmochim. Acta* **74 (23)**, 6885-6899.

Hallis, L. J., Anand, M., Strekopytov, S. (2014) Trace-element modelling of mare basalt parental melts: Implications for a heterogeneous lunar mantle, *Geochim. Cosmochim. Acta* **134**, 289-316.

Hartmann, W. K., Davis, D. R. (1975) Satellite-sized planetesimals and lunar origin, *Icarus* **24**, 504-515.

Hashizume, K., Chaussidon, M., Marty, B., Robert, F. (2000) Solar wind record on the Moon: Deciphering presolar from planetary nitrogen, *Science* **290**, 1142-1145.

Hashizume, K., Marty, B. (2004) Nitrogen isotopic analyses at the sub-picomole level using an ultra-low blank laser extraction technique. *In: deGroot, P.A. (Ed.), Handbook of Stable Isotope Analytical Techniques*, **1**, 361–375.

Hashizume, K., Marty, B., Wieler, R. (2002) Analyses of nitrogen and argon in single lunar grains: towards a quantification of the asteroidal contribution to planetary surfaces, *Earth Planet. Sci.Lett*. **202**, 201–216.

Hauri, E. H., Saal, A. E., Rutherford, M. J., Van Orman, J. A. (2015) Water in the Moon's interior: Truth and consequences, *Earth Planet. Sci. Lett.* **409**, 252-264.

Hauri, E. H., Weinreich, T., Saal, A. E., Rutherford, M. C., Van Orman, J. A. (2011) High pre-eruptive water contents preserved in lunar melt inclusions, *Science* **333**, 213-215.

Hintenberger, H., Weber, H. W., Takaoka, N. (1971) Concentrations and isotopic abundances of the rare gases in lunar matter, *Proc. **2nd** Lunar Sci. Conf.*,1607-1625.

Heber, V. S., Baur, H., Wieler, R. (2003) Helium in lunar samples analysed by high-resolution stepwise etching: Implications for the temporal constancy of solar wind isotopic composition, *Astrophysical Journal* **597**, 602-614.

Hess, P.C. (1991) Diapirism and the origin of high TiO_2 mare glasses, *Geophys. Res. Lett.* **18**, 2069-2072.

Hess, P. C., Parmentier, E. M. (1995) A model for the thermal and chemical evolution of the Moon's interior: Implications for the onset of mare volcanism, *Earth Planet. Sci. Lett.* **134 (3)**, 501-514.

Hohenberg, C. M., Davis, P. K., Kaiser, W.A., Lewis, R. S., Reynolds, J. H. (1970) Trapped and cosmogenic rare gases from stepwise heating of Apollo 11 samples. *Proc Apollo 11 Lunar Sci. Conf.*, 1283-1309.

Hohenberg, C.M., Podosek, F.A., Shirck, J.R., Marti, K., Reedy, R.C. (1978) Comparisons between observed and predicted cosmogenic noble gases in lunar samples. *Proc. **9th** Lunar Planet. Sci. Conf.*, 2311-2344.

Horn, P., Kirsten, T., Jessberger, E. K. (1975) Are there Apollo 12 basalts younger than 3.1 b.y.? Unsuccessful search for A12 mare basalts with crystallization ages below 3.1 b.y., *Meteoritics* **10**, 417-418.

Hubbard, N. J., Gast, P. W., Rhodes, J. M., Bansal, B. M., Wiesmann, H., Church, S. E. (1972) Nonmare basalts: Part II. Proc. 3rd Lunar Sci. Conf. 1161-1179.

Huneke, J.C., Jessberger, E.K., Podosek, F.A., Wasserburg, G.J. (1973) $^{40}Ar/^{39}Ar$ measurements in Apollo 16 and 17 samples and the chronology of metamorphic and volcanic activity in the Taurus Littrow region. *Proc. **4th** Lunar Sci. Conf.* 1725-1756.

Huneke, J.C., Podosek, F.A., Burnett, D.S., Wasserburg, G.J. (1972). Rare gas studies of the galactic cosmic ray irradiation history of lunar rocks. *Geochim. Cosmochim. Acta* **36**, 269–301.

Husain, L., Schaeffer, O. A., Funkhouser, J., Sutter, J. (1972) The ages of lunar material from Fra Mauro, Hadley Rille and Spur Crater, *Proc. **3rd** Lunar Sci. Conf.*, 1557-1567.

James, O.B., Jackson, E.D. (1970) Petrology of the Apollo 11 ilmenite basalts. *J. Geophys. Res.* **75**, 5793-5824.

Javoy, M. (1997) The major volatile elements of the Earth: Their origin, behaviour, and fate, *Geophys. Res. Lett*. **24** (2), 177-180.

Joy, K. H., Zolensky, M. E., Nagashima, K., Huss, G. R., Ross, D. K., McKay, D. S., Kring, D. A. (2012) Direct detection of projectile relics from the end of the lunar basin–forming epoch, *Science* **336 (6087)**, 1426-1429.

Kaplan, I. R., Kerridge, J. F., Petrowski, C. (1976). Light element geochemistry of the Apollo 15 site, *Proc.**7th** Lunar Sci. Conf.*, 481-492.

Kaplan, I. R., Petrowski, C. (1971) Carbon and sulfur isotope studies on Apollo 12 lunar samples, *Proc. **2nd** Lunar Sci. Conf.*, 1397-1406.

Kaplan, I. R., Smith, J. W. (1970) Concentration and isotopic composition of carbon and sulfur in Apollo 11 lunar samples, *Science* **167**, 541-543.

Kaplan, I. R., Smith, J. W., Ruth, E. (1970) Carbon and sulphur concentration and isotopic composition in Apollo 11 lunar samples, *Proc. Apollo 11 Lunar Sci. Conf.*, 1317-1329.

Kerridge, J. F. (1975) Solar nitrogen: Evidence for a secular increase in the ratio of nitrogen-15 to nitrogen-14, *Science* **188** (4184), 162–164.

Kerridge, J.F. (1985) Carbon, hydrogen and nitrogen in carbonaceous chondrites: Abundances and isotopic compositions in bulk samples. *Geochim. Cosmochim. Acta* **49** (8), 1707-1714.

Kerridge, J. F. (1989) What has caused the secular increase in solar nitrogen-15? *Science* **245**, 480-486.

Kerridge, J. F. (1993) Long-term compositional variation in solar corpuscular radiation: Evidence from nitrogen isotopes in the lunar regolith. *Rev. Geophys*. **31** (4), 423–437.

Kerridge, J. F., Eugster, O., Kim, J. S., Marti, K. (1991) Nitrogen isotopes in the 74001/74002 double-drive tube from Shorty Crater, Apollo 17, *Proc. Lunar Planet Sci. Conf.* **21**, 291-299.

Kerridge, J. F., Kaplan, I. R., Lesley, F. D. (1974) Accumulation and isotopic evolution of carbon on the lunar surface, *Proc. **5th** Lunar Conf.*, 1855-1868.

Kerridge, J. F., Kaplan, I. R., Kung, C. C., Winter, D. A., Friedman, D. L. (1978) Light element geochemistry of the Apollo 12 site, *Geochim. Cosmochim. Acta* **42**, 391-402.

Kerridge, J. F., Marti, K. (2001) Solar nitrogen measurement and records of past radiations, *Lunar Planet. Sci. Conf.* **32**, Abstract #1246.

Kring, D. A., Cohen, B. A. (2002) Cataclysmic bombardment throughout the inner solar system 3.9–4.0 Ga., *J. Geophys. Res.* **107, No. E2**, 5009.

Langevin, Y., Arnold, J. R. (1977) The Evolution of the Lunar Regolith, *Annual Review of Earth and Planetary Sciences* **5**, 449-489.

Libourel, G., Marty, B., Humbert, F. (2003) Nitrogen solubility in basaltic melt. Part I. Effect of oxygen fugacity. *Geochim. Cosmochim. Acta* **67** (21), 4123–4135.

Lindsay, J. F. (1976) Lunar Stratigraphy and Sedimentology. *In*: Kopal, Z., Cameron, A. G. W (Eds.) *Developments in Solar System and Space Science 3*, Amsterdam, Elsevier, 1-283.

Longhi, J. (1992) Experimental petrology and petrogenesis of mare volcanics, *Geochim. Cosmochim. Acta* **56 (6)**, 2235-2251.

Lucey, P., Korotev, R. L., Gillis, J. J., Taylor, L. A., Lawrence, D., Campbell, B. A., Elphic, R., Feldmann, B., Hood, L. L., Hunten, D., Mendillo, M., Noble, S., Papike, J. J., Reedy, R. C., Lawson, S., Prettyman, T., Gasnault, O., Maurice, S. (2006) Understanding the Lunar Surface and Space-Moon Interactions. *In:* Jolliff, B.L., Wieczorek, M.A., Shearer, C.K., and Neal, C.R. (eds.), New Views of the Moon. *Reviews in Mineralogy and Geochemistry* **60**, 83-219.

Lupton, J. E., Arculus, R. J., Evans, L. J., Graham, D. W. (2012) Mantle hotspot neon in basalts from the Northwest Lau Back-arc Basin. *Geophys. Res. Lett.* **39**, L08308.

Marti, K., Lightner, B. D. (1972) Rare gas record in the largest Apollo 15 rock, *Science* **175** (4020), 421-422.

Marti, K., Lugmair, G. W., Urey, H. C. (1970) Solar wind gases, cosmic-ray spallation products and the irradiation history of Apollo 11 samples, *Proc. Apollo 11 Lunar Sci. Conf.*, 1357-1367.

Marty, B., Hashizume, K., Chaussidon, M., Wieler, R. (2003) Nitrogen isotopes on the Moon: Archives of the solar and planetary contributions to the inner Solar System.*Space Sci. Rev.* **106** (1), 175–196.

Marty, B. (2012) The origins and concentrations of water, carbon, nitrogen and noble gases on Earth. *Earth Planet. Sci. Lett.* **313**, 56-66.

Marty, B., Chaussidon, M., Wiens, R. C., Jurewicz, A. J. G., Burnett, D. S. (2011) A ^{15}N-poor isotopic composition for the Solar System as shown by Genesis solar wind samples. *Science* **332** (6037), 1533–1536.

Marty, B., Zimmermann, L. (1999) Volatiles (He, C, N, Ar) in mid-ocean ridge basalts: Assessment of shallow-level fractionation and characterization of source composition. *Geochim. Cosmochim. Acta* **63** (21): 3619-3633.

Mathew, K. J., Kerridge, J. F., Marti, K. (1998) Nitrogen in solar energetic particles: Isotopically distinct from solar wind. *Geophys. Res. Lett.* **25**, 4293-4296.

Mathew, K. J., Marti, K. (2001) Lunar nitrogen: indigenous signature and cosmic-ray production rate, *Earth Planet. Sci. Lett.***184**, 659-669.

Mathew, K. J., Murty, S. V. S. (1993) Cosmic ray produced nitrogen in extra terrestrial matter, *Proc. Indian. Acad. Sci. (Earth Planet. Sci.)* **102** (3), 415-437.

Maxwell, J.A., Peck, L.C., Wiik, H.B. (1970) Chemical composition of Apollo 11 lunar samples 10017, 10020, 10072, and 10084, *Proc. Apollo 11 Lunar Sci. Conf.*, 1369-1374.

McCord, T. B., Taylor, L. A., Combe, J. P., Kramer, G., Pieters, C. M., Sunshine, J .M., Clark, R. N. (2011) Sources and physical processes responsible for OH/H_2O in the lunar soil as revealed by the Moon Mineralogy Mapper (M^3), *Journal of Geophysical Research*, **116** (E00G05).

McCubbin, F.M., Joliff, B.L., Nekvasil, H., Carpenter, P.K., Zeigler, R.A., Steele, A., Elardo, S.M., Lindsley, D.H. (2011) Fluorine and chlorine abundances in lunar apatite: Implications for heterogeneous distributions of magmatic volatiles in the lunar interior. *Geochim. Cosmochim. Acta* **75**, 5073-5093.

McCubbin, F. M., Steele, A., Hauri, E. H., Nekvasil, H., Yamashita, S., Hemley, R. J. (2010) Nominally hydrous magmatism on the Moon, *Proc. Natl. Acad. Sci.* **107** (25), 11223-11228.

McCubbin, F. M., Vander Kaaden, K. E., Tartèse, R., Klima, R. L., Liu, Y., Mortimer, J., Barnes, J. J., Shearer, C. K., Treiman, A. H., Lawrence, D. J., Elardo, S. M., Hurley, D. M., Boyce, J. W., Anand, M. (In Press) Magmatic volatiles (H, C, N, F, S, Cl) in the lunar mantle, crust, and regolith: Abundances, distributions, processes, and reservoirs, *American Mineralogist.*

McKay, D. S., Heiken, G., Basu, A., Blanford, G., Simon, S., Reedy, R., French, B. M., Papike, J. (1993) The Lunar Regolith. In: Heiken, G. H., Vaniman, D. T., French, B. M. (Eds.) *The Lunar Sourcebook*, 2nd edition, Cambridge, Press Syndicate of the University of Cambridge, 285-356.

Merlivat, L., Lelu, M., Nief, G., Roth, E. (1974) Deuterium, hydrogen, and water content of lunar material, *Proc. Lunar Conf.* **5th**, 1885-1895.

Mikhail, S. (2011) Stable isotope fractionation during diamond growth and the Earth's deep carbon cycle. Ph.D. thesis, University College London, UK.

Mitrofanov, I. G., Sanin, A. B., Boynton, W. V., Chin, G., Garvin, J. B., Golovin, D., Evans, L. G., Harshman, K., Kozyrev, A. S., Litvak, M. L., Malakhov, A., Mazarico, E.,

McClanahan, T., Milikh, G., Mokrousov, M., Nandikotkur, G., Neumann, G. A., Nuzhdin, I., Sagdeev, R., Shevchenko, V., Shvetsov, V., Smith, D. E., Starr, R., Tretyakov, V. I., Trombka, J., Usikov, D., Varenikov, A., Vostrukhin, A., Zuber, M. T. (2010) Hydrogen Mapping of the Lunar South Pole Using LRO Neutron Detector Experiment LEND, *Science*, **330,** 483-486.

Moore, C. B., Gibson, E. K., Larimer, J. W., Lewis, C. F., Nichiporuk, W. (1970) Total carbon and nitrogen abundances in Apollo 11 lunar samples and selected achondrites and basalts, *Proc. Apollo 11 Lunar Sci. Conf.*, 1375-1382.

Morbidelli, A., Marchi, S., Bottke, W. F., Kring, D. A. (2012) A sawtooth-like timeline for the first billion years of lunar bombardment, *Earth Planet. Sci. Lett*. **355**, 144-151.

Morris R.V. (1978) The surface exposure (maturity) of lunar soils: Some concepts and Is/FeO compilation. *Proc. **9th** Lunar Sci. Conf.* 2287-2297.

Mortimer, J., Verchovsky, A. B., Anand, M., Gilmour, I., Pillinger, C. T. (2015) Simultaneous analysis of abundance and isotopic composition of nitrogen, carbon, and noble gases in lunar basalts: Insights into interior and surface processes on the Moon. *Icarus* **255**, 3-17.

Müller, O (1974) Solar wind nitrogen and indigenous nitrogen in Apollo 17 lunar samples, *Proceedings of the Fifth Lunar Conference* (**Supplement 5**, *Geochimica et Cosmochimica Acta*), **2**, 1907-1918.

Murthy, V. R., Coscio, C. (1977) Rb-Sr isotopic systematics and initial Sr considerations for some lunar samples (abs). *Lunar Sci.* **VIII**, 706-708. Lunar Planetary Institute, Houston.

Murty, S. V. S., Goswami, J. N. (1992) Nitrogen, Noble Gases, and Nuclear Tracks in Lunar Meteorites MAC88104/105, *Proc. Lunar Planet. Sci. Conf.* **22**, 225-237.

Niedermann, S., Eugster, O. (1992) Noble gases in lunar anorthositic rocks 60018 and 65315: Acquisition of terrestrial krypton and xenon indicating an irreversible adsorption process. *Geochim. Cosmochim. Acta* **56**, 493–509.

Norris, S. J., Swart, P. K., Wright, I. P., Grady, M. M., Pillinger, C. T. (1983) A search for correlatable, isotopically light carbon and nitrogen components in lunar soils and breccias, *Proc. **14th** Lunar Planet. Sci. Conf.*, B200-B210.

Nozette, S., Lichtenberg, C. L., Spudis, P., Bonner, R., Ort, W., Malaret, E., Robinson, M., Shoemaker, E. M. (1996) The Clementine Bistatic Radar Experiment, *Science*, **274,** 1495-1498.

Nyquist, L. E., Bansal, B. M., Wiesmann, H., Jahn, B. M. (1974) Taurus-Littrow chronology: some constraints on early lunar crustal development. Proc. 5th Lunar Sci. Conf., 1515-1539.

Nyquist, L. E., Bansal B. M., Wiesmann, H. (1975) Rb-Sr ages and initial $^{87}Sr/^{86}Sr$ for Apollo 17 basalts and KREEP basalt 15386. *Proc. **6th** Lunar Sci. Conf.* 1445-1465.

Nyquist, L. E., Shih, C. Y. (1992) The isotopic record of lunar volcanism, *Geochim. Cosmochim. Acta* **56 (6)**, 2213-2234.

O'Kelley, G.D., Eldridge, J.S., Schonfeld, E., Bell, P.R (1970) Primordial radionuclide abundances, solar proton and cosmic ray effects and ages of Apollo 11 lunar samples by non-destructive gamma-ray spectrometry. *Proc. Apollo 11 Lunar Sci. Conf*. 1407-1424.

O'Neill, H. St. C. (1991) The origin of the Moon and the early history of the Earth—A chemical model. Part 2: The Earth, *Geochim. Cosmochim. Acta* **55**, 1159-1172.

Owen, T., Mahaffy, P. R., Niemann, H. B., Atreya, S., Wong, M. (2001) Protosolar nitrogen. *Astrophys. J.* **553** (2000), L77–L79.

Ozima, M., Seki, K., Terada, N., Miura, Y. N., Podosek, F. A., Shinagawa, H. (2005) Terrestrial nitrogen and noble gases in lunar soils. *Nature***436** (7051), 655–659.

Pahlevan, K., Stevenson, D. J. (2007) Equilibration in the aftermath of the lunar-forming giant impact, *Earth Planet. Sci. Lett.* **262 (3)**, 438-449.

Papanastassiou, D. A., DePaolo, D. J., Wasserburg, G. J. (1977) Rb-Sr and Sm-Nd chronology and geneology of mare basalts from the Sea of Tranquillity. *Proc. **8th** Lunar Sci.Conf.*, 1639-1672.

Papanastassiou, D. A., Wasserburg, G. J., Burnett, D. S. (1970) Rb-Sr ages of lunar rocks from the Sea of Tranquillity. *Earth Planet. Sci. Lett*. **8**, 1

Papike, J.J., Hodges, F.N., Bence, A.E., Cameron, M., Rhodes, J.M. (1976) Mare basalts: Crystal chemistry,mineralogy and petrology.*Rev. Geophys. Space Phys.***14**,475-540.

Papike, J. J., Simon, S. B., Laul, J. C. (1982) The Lunar Regolith: Chemistry, Mineralogy, and Petrology, *Reviews of Geophysics and Space Physics*, **20** (4), 761-826.

Pearson, V.K., Sephton, M.A., Franchi, I.A., Gibson, J.M., Gilmour, I. (2006) Carbon and nitrogen in carbonaceous chondrites: Elemental abundances and stable isotopic compositions. *Met. Planet. Sci.* **41** (12), 1899-1918.

Pepin, R. O., Becker, R. H., Schlutter, D. J. (1999) Irradiation records in regolith materials. I: Isotopic compositions of solar-wind neon and argon in single lunar mineral grains. *Geochim. Cosmochim. Acta* **63** (13/14), 2145-2162.

Phinney, W. C. (1991) Lunar anorthosites, their equilibrium melts and the bulk Moon, *Proc. **21st** Lunar Planet. Sci. Conf.*, 29-49.

Phinney, D., Kahl, S. B., Reynolds, J. H. (1975) ^{40}Ar-^{39}Ar dating of Apollo 16 and 17 rocks. *Proc. **6th** Lunar Sci. Conf*., 1593-1608.

Pieters, C. M., Goswami, J. N., Clark, R. N., Annadurai, M., Boardman, J., Buratti, B., Combe, J. P., Dyar, M. D., Green, R., Head, J. W., Hibbitts, C., Hicks, M., Isaacson, P., Klima, R., Kramer, G., Kumar, S., Livo, E., Lundeen, S., Malaret, E., McCord, T., Mustard, J., Nettles, J., Petro, N., Runyon, C., Staid, M., Sunshine, J., Taylor, L. A., Tompkins, S., Varanasi, P. (2009) Character and Spatial Distribution of OH/H_2O on the Surface of the Moon seen by M^3 on Chandrayaan-1, *Science*, **326,** 568-572.

Pillinger, C. T., Gardiner, L. R., Jull, A. J. T. (1976) Preferential sputtering as a method of producing metallic iron, inducing major element fractionation and trace element enrichment, *Earth and Planetary Science Letters*, **33**, 289-299.

Pillinger, C. T. (1979) Solar wind carbon chemistry as revealed by lunar sample analysis, *In: Origin and distribution of the elements*, **34**, *Proc. 2nd Symposium*, 61-72.

Pillinger, C. T. (1979) Solar wind exposure effects in the lunar soil, *Reports on Progress in Physics*, **42**, 897-932.

Ray, D., Misra, S. (2014) Depth-dependent mantle sources for high- and low-Ti mare basalts- an investigation through trace element geochemistry. **45th** *Lunar Planet. Sci. Conf.*, Abstract 1091.

Reedy, R. C. (1981) Cosmic-ray produced stable nuclides: various production rates and their implications. *Proc. Lunar Planet. Sci. Conf.* **12th**, 1809- 1823.

Rhodes, J.M., Blanchard, D.P. (1980) Chemistry of Apollo 11 low-K mare basalts. *Proc. Lunar Planet. Sci. Conf.* **11**, 49-66.

Rhodes, J.M., Blanchard, D.P., Dungan, M.A., Brannon, J.C., Rodgers, K.V. (1977) Chemistry of Apollo 12 mare basalts: Magma types and fractionation processes. *Proc. **8th** Lunar Sci. Conf.* 1305-1338.

Rhodes, J. M., Hubbard, N. J. (1973) Chemistry. Classification, and petrogenesis of Apollo 15 mare basalts. Proc. 4th Lunar Sci. Conf. 1127-1148.

Rhodes, J. M., Hubbard, N. J., Wiesmann, H., Rodgers, K. V., Brannon, J. C., Bansal, B. M. (1976) Chemistry, classification, and petrogenesis of Apollo 17 mare basalts. Proc. 7th Lunar Sci. Conf. 1467-1489.

Ringwood, A. E. (1960) Some aspects of the thermal evolution of the earth, *Geochim. Cosmochim. Acta* **20 (3)**, 241-259.

Robinson, K. L., Taylor, G. J. (2014) Heterogeneous distribution of water in the Moon, *Nat. Geosci.* **7**, 401-408.

Saal, A. E., Hauri, E. H., Cascio, M. L., Van Orman, J. A., Rutherford, M. C., Cooper, R. F. (2008) Volatile content of lunar volcanic glasses and the presence of water in the Moon's interior, *Nature* **454**, 192-195.

Saal, A.E., Hauri, E.H., Van Orman, J.A., Rutherford, M.J. (2013) Hydrogen isotopes in lunar volcanic glasses and melt inclusions reveal a carbonaceous chondrite heritage. *Science* **340**, 1317–1320.

Salmon, J., Canup, R. M. (2012) Lunar accretion from a Roche-interior fluid disk, *The Astrophysical Journal* **760 (1)**, 83.

Schmidt, O. Y. (1959) A Theory of the Origin of the Earth, *Lawrence and Wishart, London*, 1-139.

Shearer, C. K., Hess, P. C., Wieczorek, M. A., Pritchard, M. E., Parmentier, E. M., Borg, L. E., Longhi, J., Elkins-Tanton, L. T., Neal, C. R., Antonenko, I., Canup, R. M., Halliday, A. N., Grove, T. L., Hager, B. H., Lee, D-C., Wiechert, U. (2006) Thermal and magmatic evolution of the Moon, *Reviews in Mineralogy and Geochemistry* **60**, 365-518.

Shearer, C. K., Papike, J. J. (1999) Magmatic evolution of the Moon, *American Mineralogist* **84**, 1469-1494.

Shearer, C. K., Papike, J. J. (2005) Early crustal building processes on the Moon: models for the petrogenesis of the magnesian suite, *Geochim. Cosmochim. Acta* **69**, 3445-3461.

Shoemaker, E. M., Hait, M. H., Swann, G. A., Schleicher, D. L., Schaber, G. G., Sutton, R. L., Dahlem, D. H., Goddard, E. N., Waters, A. C. (1970) Origin of the lunar regolith at Tranquility Base, *Proceedings of the Apollo 11 Lunar Science Conference*, **3,** 2399-2412.

Signer, P., Baur, H., Derksen, U., Etique, P., Funk, H., Horn, P., Wieler, R. (1977) Helium, neon, and argon records of lunar soil evolution, *Proc. **8th** Lunar Sci. Conf*., 3657-3683.

Simoneit, B. R., Wszolek, P. C., Christiansen, P., Jackson, R. F., Burlingame, A. L. (1973) Carbon chemistry of Luna 16 and Luna 20 samples, *Geochim. Cosmochim. Acta*, **37**, 1063-1074.

Smith, J. W., Kaplan, I. R., Petrowski, C. (1973) Carbon, nitrogen, sulfur, helium, hydrogen, and metallic iron in Apollo 15 drill stem fines, *Proc. Lunar Sci. Conf*. **4th**, 1651-1656.

Stettler, A., Eberhardt, P., Geiss, J., Grogler, N., Maurer, P. (1973) Ar^{39}/Ar^{40} ages and Ar^{37}/Ar^{38} exposure ages of lunar rocks, *Proc. **4th** Lunar Sci. Conf*., 1865-1888.

Sunshine, J. M., Farnham, T. L., Feaga, L. M., Groussin, O., Merlin, F., Milliken, R. E., A'Hearn, M. F. (2009) Temporal and Spatial Variability of Lunar Hydration as Observed by the Deep Impact Spacecraft, *Science*, **326,** 565-568.

Tartèse, R., Anand, M., Barnes, J.J., Starkey, N.A., Franchi, I., Sano, Y. (2013) The abundance, distribution, and isotopic composition of Hydrogen in the Moon as revealed by basaltic lunar samples: implications for the volatile inventory of the Moon, *Geochim. Cosmochim. Acta* **122**, 58-74.

Tartèse, R., Anand, M., Delhaye, T. (2013) NanoSIMS Pb/Pb dating of tranquilityite in high-Ti lunar basalts: Implications for the chronology of high-Ti volcanism on the Moon, *Am. Min.*, **98**, 1477-1486.

Tartèse, R., Anand, M., McCubbin, F. M., Elardo, S. M., Shearer, C. K., Franchi, I. A. (2014) Apatites in lunar KREEP basalts: The missing link to understanding the H isotope systematics of the Moon, *Geology* **42** (4), 363-366.

Taylor, L. A., Pieters, C., Patchen, A., Taylor, D-H. S., Morris, R. V., Keller, L. P., McKay, D. S. (2010) Mineralogical and chemical characterization of lunar highland soils: Insights into the space weathering of soils on airless bodies, *Journal of Geophysical Research*, **115** (E02002).

Terada, K., Anand, M., Sokol, A. K., Bischoff, A., Sano, Y. (2007) Cryptomare magmatism at 4.35 Ga recorded in Kalahari 009, *Nature* **450 (7171)**, 849-852.

Thiemens, M. H., Clayton, R. N. (1980) Solar and cosmogenic nitrogen in the Apollo 17 deep drill core, Proc. Lunar Planet. Sci. Conf. 11th, 1435-1451.

Thiemens, M. H., Clayton, R. N. (1983) Nitrogen contents and isotopic ratios of clasts from the enstatite chondrite Abee, *Earth Planet. Sci. Lett.* **62**, 165–168.

Touboul, M., Kleine, T., Bourdon, B., Palme, H., Wieler, R. (2007) Late formation and prolonged differentiation of the Moon inferred from W isotopes in lunar metals, *Nature* **450**, 1206-1209.

Trinquier, A., Birck, J. L., Allegre, C. J., Göpel, C., Ulfbeck, D. (2008) ^{53}Mn–^{53}Cr systematics of the early Solar System revisited, *Geochim. Cosmochim. Acta* **72 (20)**, 5146-5163.

Turner, G., Burgess, R. (2014) The other isotopes: research avenues based on ^{36}Ar, ^{37}Ar, and ^{38}Ar. In: *Advances in ^{40}Ar/^{39}Ar dating: From Archaeology to Planetary Sciences* (eds. Jourdan, F., Mark, D. F., Verati, C.), *The Geological Society of London Special Publication* **378**, The Geological Society Publishing House, Bath.

Verchovsky, A.B., Fisenko, A.V., Semjonova, L.F., and Pillinger, C.T. (1997) Heterogeneous Distribution of Xenon-HL Within Presolar Diamonds, Meteoritics and Planetary Science, **32**, A131–A132.

Verchovsky, A. B., Wright, I. P., Pillinger, C. T. (2003) Ion Implantation into Presolar Grains: A Theoretical Model, *Publications of the Astronomical Society of Australia* **20**, 329-336.

Vinogradov, A. P. (1972) Preliminary data on lunar soil collected by the Luna 20 unmanned spacecraft, *Geochimica et Cosmochimica Acta*, **37,** 721-729.

Wänke, H., Palme, H., Baddenhausen, H., Dreibus, G., Jagoutz, E., Kruse, H., Spettel, B., Teschke, F., Thacker, R. (1974) Chemistry of Apollo 16 and 17 samples: bulk composition, late-stage accumulation and early differentiation of the Moon. *Proc. **5th** Lunar Sci. Conf.* 1307-1335.

Wänke, H., Wlotzka, F., M., Rieder, R. (1971) Apollo 12 samples: Chemical composition and its relation to sample locations and exposure ages, the two component origin of the various soil samples and studies on lunar metallic particles. *Proc. **2nd** Lunar Sci. Conf.* 1187-1208.

Wasserburg, G. J., Papanastassiou, D. A. (1971) Age of an Apollo 15 mare basalt: lunar crust and mantle evolution, *Earth Planet. Sci. Lett*.**13**, 97-104.

Wasson, J.T., Kallemeyn, G.W. (1988) Compositions of chondrites. *Phil. Trans. R. Soc. London* **A325**, 535–544.

Wetzel, D. T., Rutherford, M. J., Jacobsen, S. D., Hauri, E. H., Saal, A. E. (2013) Degassing of reduced carbon from planetary basalts, *Proc. Natl. Acad. Sci.* **110** (20), 8010-8013.

Wiechert, U., Halliday, A. N., Lee, D. C., Snyder, G. A., Taylor, L. A., Rumble, D. (2001) Oxygen isotopes and the Moon-forming Giant Impact, *Science* **294**, 345-348.

Wieczorek, M. A., Jolliff, B. L., Khan, A., Prithchard, M. E., Weiss, B. P., Williams, J. G., Hood, L. L., Righter, K., Neal, C. R., Shearer, C. K., McCallum, I. S., Tompkins, S.,

Hawke, B. R., Peterson, C., Gillis, J., Bussey, D. B. (2006) The constitution and structure of the lunar interior, *Reviews in Mineralogy and Geochemistry* **60**, 221-364.

Wieler, R. (1998) The Solar Noble Gas Record in Lunar Samples and Meteorites, *Space Science Reviews* **85** (1-2), 303-314.

Wieler, R. (2002) Noble gases in the Solar System. In: *Noble Gases in Geochemistry and Cosmochemistry*. (eds. Porcelli, D.; Ballentine, C.; Wieler, R.), pp. 21-70, *Rev. Mineral. Geochem.* **47**. *Mineral. Soc. Am.*, Washington, DC.

Wieler, R., Humbert, F., Marty, B. (1999) Evidence for a predominantly non-solar origin of nitrogen in the lunar regolith revealed by single grain analyses, *Earth and Planetary Science Letters*, **167**, 47-60.

Willbold, M., Elliott, T., Moorbath, S. (2011) The tungsten isotopic composition of the Earth's mantle before the terminal bombardment, *Nature* **477**, 195-198.

Wilson, L., Head III, J. W. (1981) Ascent and Eruption of Basaltic Magma on the Earth and Moon, *J. Geophys. Res.* **86**, 2971-3001.

Wise, D. U. (1969) Origin of the Moon from the Earth: some new mechanisms and comparisons, *J. Geophys. Res.* **74 (25)**, 6034-6045.

Wood, B. J., Halliday, A. N., Rehkämper, M. (2010) Volatile accretion history of the Earth, *Nature* **467**, E6-E7.

Wood, J. A. (1986) Moon over Mauna Loa - A review of hypotheses of formation of Earth's moon, *Origin of the Moon* **1**, 17-55.

Wright, I.P., Boyd, S.R., Franchi, I.A., and Pillinger, C.T. (1988) Determination of High Precision N Stable Isotope Ratios at the Sub-nanomole Level, *J. Phys. E: Sci. Instrum.***21**, 865–875.

Wright, I.P. and Pillinger, C.T. (1989) C Isotopic Analysis of Small Samples by Use of Stepped-Heating Extraction and Static Mass Spectrometry, In *New Frontiers in Stable Isotopic Research: Laser Probes, Ion Probes and Small Sample Analysis*, (eds. Shanks, W.C. and Criss, R.E.), *U.S. Geolog. Surv. Bull.***1890**, 9–34.

York, D., Kenyon, W.J., Doyle, R.J. (1972). ^{40}Ar–^{39}Ar ages of Apollo 14 and 15 samples. *Proc. Lunar Sci. Conf.* **3**, 1613–1622.

Zhang, J., Dauphas, N., Davis, A. M., Leya, I., Fedkin, A. (2012) The proto-Earth as a significant source of lunar material, *Nature Geoscience* **5 (4)**, 251-255.

Blank Correction and Error Propagation Calculations

Despite the low and stable system blanks associated with the Finesse mass spectrometer system, the relatively low abundances of carbon and nitrogen in lunar samples (but especially so in mare basalts) leads to an otherwise negligible blank having an impact on the measured abundances and isotopic compositions obtained during analyses.

Correcting the abundances of carbon and nitrogen is very straightforward; the abundance measured during a blank run is subtracted from the 'raw' abundance measured during sample analysis. If a blank experiment has been run both before and after a sample has been analysed, then the average of the two measured blank abundances can be used instead:

(Eq. 1) $$M_C = M_E - M_B$$

where M_C = the corrected abundance/yield; M_E = the uncorrected measured abundance; and M_B = the measured blank abundance (Abernethy, 2014; Mikhail, 2011).

To correct the isotopic composition of the sample, the following equation is used:

(Eq. 2) $$\delta_C = \frac{(M_E \times \delta_E) - \left(\left(\frac{(M_{B1} \times \delta_{B1}) + (M_{B2} \times \delta_{B2})}{(M_{B1} + M_{B2})}\right) \times \left(\frac{M_{B1} + M_{B2}}{2}\right)\right)}{M_C}$$

where δ_C = the corrected isotopic composition; M_E = the uncorrected yield; δ_E = the uncorrected isotopic composition; M_{B1} and δ_{B1} = the yield and isotopic composition of the first blank experiment (respectively); M_{B2} and δ_{B2} = the yield and isotopic composition of the second blank experiment (respectively); and M_C = the corrected yield (see Eq. 1) (Abernethy, 2014; Mikhail, 2011).

Error calculations take into account several variables, such as the proportion of the total abundance belonging to the blank, any variations in blank isotopic compositions over both the temperature range used and the duration of the analysis, and the measurement error associated with the Finesse mass spectrometer system itself.

To take all of these variables into account, errors are calculated using the following error propagation equation:

(Eq. 3) $$\Delta\delta_C = \frac{1}{(M_C)^2} \times \sqrt{X + Y}$$

where $\Delta\delta_C$ = the calculated propagated error of the corrected isotopic composition of the sample; M_C = the blank-corrected yield; and terms X and Y are defined thus:

$$X = \left[(1 - \delta_E)^2 \times (\Delta M_E)^2 + \left(1 - \delta_{B(avg)}\right)^2 \times (\Delta M_B)^2\right]$$

$$Y = \left[(M_C)^2 \times \left((M_E)^2 \times (\Delta\delta M_{tot})^2 \times \left(M_{B(avg)}\right)^2 \times (\Delta\delta_B)^2\right)\right]$$

where $\delta_{B(avg)}$ = the weighted average isotopic composition of the blank; ΔM_E = the standard deviation of the uncorrected yield; ΔM_B = the standard deviation of the blank yield; $\Delta\delta M_{tot}$ = the weighted average of the measurement errors for the range of temperature steps used; $M_{B(avg)}$ = the weighted average yield of the blank; and $\Delta\delta_B$ = the standard deviation across the two blank analyses (see Eq. 2) for the temperature steps used (Abernethy, 2014; Mikhail, 2011).

When I look at the Moon I do not see a hostile, empty world. I see the radiant body where man has taken his first steps into a frontier that will never end.

— David R. Scott, Commander (Apollo 15).